

Hydrothermal Organic Reduction and Deoxygenation

by

Christiana Bockisch

A Dissertation Presented in Partial Fulfillment  
of the Requirements for the Degree  
Doctor of Philosophy

Approved April 2018 by the  
Graduate Supervisory Committee:

Ian Gould, Chair  
Hilairy Hartnett  
Everett Shock

ARIZONA STATE UNIVERSITY

May 2018

## ABSTRACT

Organic reactions in natural hydrothermal settings have relevance toward the deep carbon cycle, petroleum formation, the ecology of deep microbial communities, and potentially the origin of life. Many reaction pathways involving organic compounds under geochemically relevant hydrothermal conditions have now been characterized, but their mechanisms, in particular those involving mineral surface catalysis, are largely unknown. The overall goal of this work is to describe these mechanisms so that predictive models of reactivity can be developed and so that applications of these reactions beyond geochemistry can be explored. The focus of this dissertation is the mechanisms of hydrothermal dehydration and catalytic hydrogenation reactions. Kinetic and structure/activity relationships show that elimination occurs mainly by the E1 mechanism for simple alcohols via homogeneous catalysis. Stereochemical probes show that hydrogenation on nickel occurs on the metal surface. By combining dehydration with and catalytic reduction, effective deoxygenation of organic structures with various functional groups such as alkenes, polyols, ketones, and carboxylic acids can be accomplished under hydrothermal conditions, using either nickel or copper-zinc alloy. These geomimetic reactions can potentially be used in biomass reduction to generate useful fuels and other high value chemicals. Through the use of earth-abundant metal catalysts, and water as the solvent, the reactions presented in this dissertation are a green alternative to current biomass deoxygenation/reduction methods, which often use exotic, rare-metal catalysts, and organic solvents.

To all the teachers I had throughout my life.

Without your support and encouragement, I would have never come this far.

## ACKNOWLEDGMENTS

There are many people who helped me get to this point in my career; more than can be listed here. First and most importantly, I thank Dr. Ian Gould for his support, expertise, and direction as my advisor. I am eternally grateful for his dedication to helping me with difficult research problems, in the lab and in the computer, and challenges I encountered as a teaching assistant. I also acknowledge the Hydrothermal Organic Geochemistry group – Dr. Everett Shock, Dr. Hilairy Harnett, Dr. Lynda Williams, Dr. Ziming Yang, Dr. Kristopher Fecteau, Dr. Charlene Estrada, Dr. Kirtland Robinson, Dr. Kristin Johnson, and Joshua Nye. The stimulating discussions we had in HOG meetings were infinitely valuable to my progress. Each of you helped me in so many ways, and I thank each of you for your support. I also thank Dr. Ted Lorange for his remote support as a collaborator from Vanguard University, his expertise as a theoretician, and for running many of my samples on his GC/MS. I thank NSF and NASA for funding so much of this work.

There were many others who helped me with my projects in the laboratory, and on a professional level. I thank Dr. Natasha Zolatova for help with GC/MS early on in my graduate career. Dr. Brian Cherry helped me with the numerous challenges I encountered with NMR. I also acknowledge David Wright, Karl Weiss, and Shreya Bhattacharyya for their support on the surface science side of my project. I also am deeply indebted to Dr. Chelsea Brown and Dr. Iolanda Klein for helping me with my job search.

On a more personal note, I thank my parents, David and Joni Bockisch, for their love and support. Without you, I would not be where I am today. Graduate school had more downs than ups sometimes, and you were there for me. My grandparents, Sharon and Robert Bockisch, also had an important role in my life. Sharon encouraged me to be curious about the world around me, from a young age. I am sure this helped me become a scientist today. The support from my friends, both in and outside of the graduate program was infinitely beneficial. I thank all my graduate student friends, and the happy hour crew for all the good times we've had together. I thank Josh for being a good, drama-free roommate. Finally, I thank all my soccer friends; A.S.H. and the staff of Brewers Connection who helped me with a hobby that kept me sane all this time; and my dog friends, Bear, Tig, and Jemma.

## TABLE OF CONTENTS

	Page
LIST OF TABLES.....	viii
LIST OF FIGURES.....	xii
CHAPTER	
1. INTRODUCTION .....	1
Overview.....	1
Introduction to Hydrothermal Conditions.....	2
Hydrothermal Organic Geochemistry.....	5
Geomimicry .....	9
Mechanisms of Hydrogenation on Metal Surfaces.....	10
Biomass Reduction .....	12
2. METHODS .....	14
Hydrothermal Reaction Vessel Preparation.....	14
Hydrothermal Reaction Heating .....	15
Reaction Work-up – Water Only .....	16
Reaction Work-up – with Metal Powders.....	17
Gas Chromatography Analysis .....	17
Metal Powder Characterization.....	19

CHAPTER	Page
3. KINETICS AND MECHANISMS OF DEHYDRATION OF SECONDARY ALCOHOLS UNDER HYDROTHERMAL CONDITIONS .....	20
Introduction.....	20
Methods.....	25
Results and Discussion .....	26
Implications for Hydrothermal Dehydration Under Laboratory and Geologic Conditions.....	49
Summary .....	52
4. SELECTIVE, GREEN, NICKEL-CATALYZED HYDROTHERMAL REDUCTIONS .....	53
Introduction.....	53
Methods.....	55
Results and Discussion .....	57
Conclusion .....	69
5. HYDROTHERMAL REDUCTION AND DEOXYGENATION OF CARBONYLS .....	70
Introduction.....	70
Methods.....	76

CHAPTER	Page
Results and Discussion .....	77
Conclusion .....	95
<b>6. HYDROTHERMAL DEHYDRATION AND HYDROGENOLYSIS OF POLYOLS</b>	
.....	97
Introduction.....	97
Methods.....	100
Results and Discussion .....	101
Summary and Future Work.....	123
<b>7. CONCLUSION.....</b>	<b>125</b>
<b>REFERENCES .....</b>	<b>129</b>
<b>APPENDIX</b>	
<b>A. METAL SURFACE CHARACTERIZATION. ....</b>	<b>148</b>
<b>B. GAS CHROMATOGRAPHY AND MASS SPECTROMETRY .....</b>	<b>159</b>
<b>C. DATA TABLES.....</b>	<b>189</b>



## LIST OF TABLES

Table	Page
1. GC Method Parameters.....	18
2. GC Oven Temperature Program – Volatile Analytes.....	18
3. GC Method Parameters – Phenyl Rings/Higher Boiling Points.....	18
4. GC Oven Temperature Program – Phenyl Rings/Higher Boiling Points.....	18
5. First Order Rate Constants For The Disappearance Of Alcohols, Percent Conversion To Alkenes At Equilibrium, And Rate Constants For Alcohol Dehydration At 250°C And 40 Bar.....	30
6. Best-Fit Elementary Rate Constants For Hydrothermal Dehydration Of T- Butylcyclohexanols At 250°C And 40 Bar.....	37
7. Selective Reductions.....	68
8. Summary Of Carbonyl Reductions With Nickel And Iron.....	74
9. Summary Of Carbonyl Reductions With Cu-Zn Alloy And Iron, 250°C.....	75
10. Ketone Reduction Stereochemistry – Nickel And Iron (250°C).....	87
11. Ketone Reduction Stereochemistry – Cu-Zn Alloy And Iron (250°C).....	88
12. Control Experiments For All Metal Powders, Using Cyclohexanone And Octanoic Acid As Substrate.....	94
13. The Products From Starting With Cis-1,4-Cyclohexanediol (A) And Trans-1,4- Cyclohexanediol (B).....	118
14. Cyclohexanol Conversion At 250°C And 40 Bar In Water.....	190

Table	Page
15. Abundances Of Products With Time Starting With <i>Cis</i> -4- <i>Tbu</i> -Cyclohexanol At 250°C And 40 In Water.....	190
16. Abundances Of Products With Time Starting With <i>Trans</i> -4- <i>Tbu</i> -Cyclohexanol At 250°C And 40 Bar In Water.....	191
17. Conversion of benzene to cyclohexane with time at 250°C and 40 bar in the presence of nickel and iron.....	191
18. Abundances Of Products From Starting With Diphenylacetylene At 250°C And 40 Bar In The Presence Of Nickel And Iron.....	192
19. Abundances Of Styrene With Time, 250°C And 40 Bar In The Presence Of Nickel And Iron.....	192
20. Abundances Of 4-OCH <sub>3</sub> -Styrene With Time, 250°C And 40 Bar In The Presence Of Nickel And Iron.....	192
21. Abundances Of 3-CF <sub>3</sub> -Styrene With Time, 250°C And 40 Bar In The Presence Of Nickel And Iron.....	193
22. Abundances Of Products From Cyclohexanone With Time, 250°C And 40 Bar In The Presence Of Nickel And Iron.....	193
23. Abundances Of Products From Cyclohexanone With Time, 250°C And 40 Bar In The Presence Of Cu-Zn And Iron.....	193
24. Abundances Of Products From Octanoic Acid With Time 250c And 40 Bar In The Presence Of Nickel And Iron.....	194

Table	Page
25. Abundances Of Products From Octanoic Acid With Time, 250°C And 40 Bar In The Presence Of Cu-Zn And Iron.....	194
26. Abundances Of Products From Acetophenone With Time, 250°C And 40 Bar In The Presence Of Nickel And Iron.....	194
27. Abundances Of Products From 4-OCH <sub>3</sub> -Acetophenone With Time, 250°C And 40 Bar In The Presence Of Nickel And Iron.....	195
28. Abundances Of Products From 3-CF <sub>3</sub> -Acetophenone With Time, 250°C And 40 Bar In The Presence Of Nickel And Iron.....	195
29. Abundances Of Products From 3,5-Di-CF <sub>3</sub> -Acetophenone With Time, 250°C And 40 Bar In The Presence Of Nickel And Iron.....	195
30. Abundances Of Products From The Dehydration Of <i>Cis</i> -1,2-Cyclohexanediol With Time, 250°C And 40 Bar In Water.....	196
31. Abundances Of Products From The Dehydration Of <i>Trans</i> -1,2-Cyclohexanediol With Time, 250°C And 40 Bar In Water.....	196
32. Abundances Of Products From The Disproportionation Of <i>Trans</i> -1,2-Cyclohexanediol And Cyclopentylformaldehyde With Time, 250°C And 40 Bar In Water.....	196
33. Abundances Of <i>Cis</i> -1,2-Cyclohexanediol And Cyclohexane In The Presence Of Nickel And Iron, 250°C And 40 Bar.....	197

Table	Page
34. Abundances Of Minor Products From The Reduction Of Cis-1,2-Cyclohexanediol With Time, In The Presence Of Nickel And Iron, 250°C And 40 Bar.....	197
35. Summary Of Yields Of Cyclohexane And Benzene From Polyols Reduced With Nickel And Iron.....	198
36. Mol% of <sup>13</sup> C labeled methanol with time, measured by <sup>13</sup> C NMR.....	198

## LIST OF FIGURES

Figure	Page
Figure 1. Log K Of Solubility Of Benzene In Water With Increasing Temperature.....	3
Figure 2. The Water Autoionization Constant, $K_w$ , As A Function Of Temperature .....	4
Figure 3. Water Vapor Saturation Pressure As A Function Of Temperature .....	4
Figure 4. The Temperature Dependence Log K Values For The Dissociation Of Hydrochloric Acid, Sodium Hydroxide, And Acetic Acid In Water, Obtained Using HKF.....	5
Figure 5. The Organic Redox Reaction Pathway Of Alkanes To Acids In Hydrothermal Conditions.....	6
Figure 6. Two Possible Mechanisms For Alcohol Dehydration In Acidic Aqueous Media .....	8
Figure 7. The Step-Wise Hydrogen Insertion Mechanism Proposed By Horiuti And Polanyi 1934 .....	12
Figure 8. This Dissertation Summarized As The Culmination Of Multiple Techniques To Improve Upon Current Biomass Deoxygenation/Reduction Methods. ....	13
Figure 9. Functional Group Interconversions That Connect Alkanes And Carboxylic Acids Under Hydrothermal Conditions .....	21
Figure 10. Equilibrium Constants (Log $K_{eq}$ ) For Dehydration Of 1-Propanol As A Function Of Temperature At The Saturated Water Vapor Pressure .....	22

Figure	Page
Figure 11. Comparison Of The E1 And E2 Mechanisms For Hydrothermal Dehydration Of 4-Heptanol, As A Representative Secondary Alcohol .....	24
Figure 12. Cyclohexanol Conversion (Mol %) As A Function Of Time, For Hydrothermal Dehydration At 250°C And 40 Bar.....	27
Figure 13. Kinetic Scheme Of Hydrothermal Dehydration Of Cyclohexanol In Water ..	28
Figure 14. Cis- And Trans-4-T-Butylcyclohexanol (C-4OH And T-4OH) In Their Lowest-Energy Chair Conformations. ....	31
Figure 15. Kinetic Scheme For Hydrothermal Dehydration Of Substituted Cyclohexanols, <i>Cis</i> -4- <i>T</i> -Butylcyclohexanol And <i>Trans</i> -4- <i>T</i> -Butylcyclohexanol .....	32
Figure 16. Time Dependence Of Reactant Loss And Product Formation (Mol Fraction) For Hydrothermal Dehydration Of (A) <i>Cis</i> -4- <i>T</i> -Butylcyclohexanol And (B) <i>Trans</i> -4- <i>T</i> -Butylcyclohexanol. ....	37
Figure 17. Rate Constants For Dehydration Of Linear Secondary Alcohols With Carbon Chains From Six To Eleven, Compared To The Corresponding Rate Constants For The Indicated Cyclohexanols.....	45
Figure 18. Reduction Of Cyclohexene.....	58
Figure 19. Reduction Of Diphenylacetylene To Bibenzyl.....	58
Figure 20. Percent Conversion Of Cyclohexene In Metal Control Experiments. Including Iron With Nickel Increases Catalytic Activity.....	58

Figure	Page
Figure 21. Cyclohexane Yield As A Function Of Time At 250°C In The Presence Of Ni And Fe.....	60
Figure 22. The Hydrogenation Pathway Of 1,2-Dimethylcyclohexene After 30 Min For Ni, And 5 Min For Pd/C .....	61
Figure 23. The Ratio Of Decalins Obtained From The Reduction Of Naphthalene.....	62
Figure 24. Abundances Of Diphenyl Acetylene, Stilbenes, And Bibenzyl With Time, In The Presence Of Ni And Fe At 250°C .....	63
Figure 25. Hydrogenation Pathway Of Diphenylacetylene .....	63
Figure 26. Reduction Of 3-Hexyne.....	65
Figure 27. Reduction Rates Of Styrene, 4-OCH <sub>3</sub> -Styrene, And 3-CF <sub>3</sub> -Styrene, As Well As The Abundance Of The Ethylbenzene Product After 1 Hour .....	67
Figure 28. The General Reaction Of Ketones To Alkanes In The Presence Of Nickel, Or Cu-Zn Alloy At Longer Times. ....	78
Figure 29. A Time Series Of Measured Products From The Cyclohexanone Reduction Pathway, In The Presence Of Nickel And Iron, 250°C .....	79
Figure 30. A Time Series Of Measured Products From The Cyclohexanone Reduction Pathway, In The Presence Of Cu-Zn And Iron, 250°C .....	80
Figure 31. The Reduction Of Octanoic Acid In The Presence Of Nickel And Iron At 250°C, In H <sub>2</sub> O.....	81

Figure	Page
Figure 32. Time Series Of Octanoic Acid Reduction With Nickel And Iron At 250°C. .	82
Figure 33. <sup>13</sup> C Labeled Methanol Hydrogenolysis, With Nickel And Iron, 250°C.....	83
Figure 34. The Reaction Pathway Of Octanoic Acid Reduction, Using Cu <sub>2</sub> Zn+Fe At 250°C. ....	84
Figure 35. Time Series Of Products Formed In The Reduction Of Octanoic Acid, Using Cu-Zn And Iron, At 250°C .....	85
Figure 36. The Three Possible Mechanisms Of Ketone Reduction On A Metal Surface That We Considered In This Study.....	86
Figure 37. The Natural Log Of Mole Fraction Of Each Substituted Acetophenone With Time, With Nickel And Iron At 250°C.....	92
Figure 38. <i>Cis</i> And <i>Trans</i> -1,2-Cyclohexanediols Produce Different Ratios Of Cyclohexanone And Cyclopentylformaldehyde At 250°C And 40 Bar In Water (At All Times) .....	103
Figure 39. Possible Mechanisms For <i>Cis</i> -1,2-Cyclohexanediol Dehydration.....	103
Figure 40. The Reaction Pathway Used For The Kinetic Modelling Of <i>Cis</i> -1,2-Cyclohexanediol Dehydrating To Cyclohexanone And Cyclopentylformaldehyde. ....	104
Figure 41. Kinetic Analysis Of <i>Cis</i> -1,2-Cyclohexanediol. Pseudo-First Order Rate Constants Calculated In COPASI Using The Pathway In Figure 40.....	104



Figure	Page
Figure 42. Time Series For <i>Trans</i> -1,2-Cyclohexanediol, With First Order Kinetic Fitting Of The Diol, Cyclopentylformaldehyde, And Cyclohexanone .....	105
Figure 43. Cyclopentanemethanol And 2-Hydroxycyclohexanone Second-Order Fits .	105
Figure 44. The Kinetic Model Used To Fit The <i>Trans</i> -1,2-Cyclohexanediol Data.....	106
Figure 45. The Products Made From Reaction Of 1,2-Epoxy cyclohexane At 250°C, 40 Bar For 1 Hour.. .....	108
Figure 46. The Ratio Of Cyclopentylformaldehyde To Cyclohexanone Formation .....	108
Figure 47. The Proposed Mechanism Of <i>Trans</i> -1,2-Cyclohexanediol To Its Major Product, Cyclopentylformaldehyde .....	109
Figure 48. Proposed Mechanism For The Disproportionation Of <i>Trans</i> -1,2-Cyclohexanediol And Cyclopentylformaldehyde.....	111
Figure 49. Yields Of Major Deoxygenation And Reduction Products Of <i>Cis</i> And <i>Trans</i> -1,2-Cyclohexanediols In The Presence Of Ni And Fe At 250°C In Water. ....	112
Figure 50. Time Dependence Of <i>Cis</i> -1,2-Cyclohexanediol And Cyclohexane/Benzene Production (250°C, 40 Bar, Ni+Fe) .....	113
Figure 51. Time Dependencies Of Minor Products From The Reduction And Deoxygenation Of <i>Cis</i> -1,2-Cyclohexanediol With Ni And Fe, 250°C/40 Bar. ....	114
Figure 52. Reductive Deoxygenation Of <i>Cis</i> -1,2-Cyclohexanediol With Nickel And Iron 250°C .....	115

Figure	Page
Figure 53. Reaction Pathway For The Dehydration Of <i>Cis</i> And <i>Trans</i> -1,4-Cyclohexanediols In Water At 250°C And 40 Bar .....	117
Figure 54. Structures And Energy Differences Between Protonated Axial (A) And Equatorial (B) Hydroxyls And The Protonated Twist-Boat Of <i>Cis</i> -1,4-Cyclohexanediol (C), Calculated At The M06-2x/Aug-Cc-PVTZ Level Of Theory .....	119
Figure 55. Deoxygenation And Reduction Of <i>Cis</i> And <i>Trans</i> -1,4-Cyclohexanediols In The Presence Of Ni And Fe At 250°C In Water.....	121
Figure 56. Reduction And Deoxygenation Of <i>Myo</i> -Inositol To Cyclohexane In The Presence Of Ni And Fe At 350°C In Water.....	122
Figure 57. Fused Silica Tube Containing The Post-Reaction Mixture Of <i>Myo</i> -Inositol In Water Alone (250°C, 48h).....	122
Figure 58. A Map Of Aqueous Hydrothermal Reactions Involving Mono-Ols And Diols .....	128
Figure 59. A Map Of Aqueous And Nickel-Catalyzed Reactions Involving Alcohols That Occur Under Hydrothermal Conditions.....	128
Figure 60. Nickel Nanopowder 5000x Magnification. ....	149
Figure 61. Cu-Zn Alloy, Pre-Experiment, 1200x. ....	150
Figure 62. Cu-Zn Alloy, Pre-Experiment, 15000x. ....	151
Figure 63. Cu-Zn Alloy, Reacted (48h, 250°C, H <sub>2</sub> O, No Organic), 6500x.....	152

Figure	Page
Figure 64. Cu-Zn Alloy, Reacted, 500x.....	153
Figure 65. Cu-Zn Alloy, Reacted, 12000x.....	154
Figure 66. XRD Spectra Of Unreacted Ni, Ni+Fe, And Reacted Ni+Fe (1h, 250°C, H <sub>2</sub> O) .....	155
Figure 67. XRD Spectra Of Unreacted And Reacted Cu-Zn (48h, 250°C, H <sub>2</sub> O).....	155
Figure 68. The Stability Fields Of Nickel, Iron, Magnetite, And Bunsenite, With Respect To Temperature And Activity Of Aqueous Hydrogen. ....	157
Figure 69. Cyclohexanol, 118h (250°C) .....	161
Figure 70. <i>Cis</i> -4- <i>Tbu</i> -Cyclohexanol, 8h (250°C).....	161
Figure 71. <i>Cis</i> -4- <i>Tbu</i> -Cyclohexanol, 8h (250°C).....	162
Figure 72. Mass Spectrum Of 3- <i>Tert</i> -Butylcyclohex-1-Ene.....	163
Figure 73. Mass Spectrum Of 1- <i>Tert</i> -Butylcyclohex-1-Ene.....	164
Figure 74. Mass Spectrum Of 4- <i>Tert</i> -Butylcyclohex-1-Ene.....	165
Figure 75. Mass Spectrum Of <i>Trans</i> -3- <i>Tert</i> -Butylcyclohexanol .....	167
Figure 76. Mass Spectrum Of <i>Cis</i> -3- <i>Tert</i> -Butylcyclohexanol .....	168
Figure 77. 3-Hexanol 48h (250°C).....	169
Figure 78. 6-Undecanol 48h (250°C) .....	169
Figure 79. Cyclohexene 135min, Ni+Fe (250°C) .....	170

Figure	Page
Figure 80. <sup>1</sup> H NMR Spectrum Of The Cyclohexene Reaction Mixture, In CDCl <sub>3</sub> . (135 Min, 250°C, Ni+Fe) .....	171
Figure 81. 1,2-Dimethylcyclohexene 30 Min, Ni+Fe (250°C) .....	171
Figure 82. Mass Spectrum Of A Representative Methylcyclohexanol Isomer. ....	172
Figure 83. Mass Spectrum Of A Second Representative Methylcyclohexanol Isomer..	173
Figure 84. Mass Spectrum Of 1-Methyl-1-Cycloheptanol. This Alcohol Results From Protonation Of 1,2-Dimethylcyclohexene, Ring-Opening To Form The Cycloheptane Ring, And Then Hydration .....	174
Figure 85. 5-Hexen-2-One, 1h Ni+Fe (250°C) .....	175
Figure 86. <i>Trans</i> -Cinnamic Acid, 15 Min Ni+Fe (250°C) .....	175
Figure 87. Benzoic Acid, 70h Ni+Fe (250°C) .....	176
Figure 88. Cyclohexanone, 24h Ni+Fe (250°C) .....	176
Figure 89. Cyclohexanone, 4h Cu-Zn+Fe (250°C) .....	177
Figure 90. Octanoic Acid, 24h Ni+Fe (250°C) .....	177
Figure 91. Benzoic Acid 24h Cu-Zn+Fe (250°C) .....	178
Figure 92. <i>Cis</i> -1,2-Cyclohexanediol 24h (250°C) .....	178
Figure 93. <i>Trans</i> -1,2-Cyclohexanediol 480h (250°C) .....	179
Figure 94. <i>Cis</i> -1,2-Cyclohexanediol 72h Ni+Fe (250°C) .....	179

Figure	Page
Figure 95. <sup>1</sup> H NMR Spectrum Of The <i>Cis</i> -1,2-Cyclohexanediol Reaction Mixture, In CDCl <sub>3</sub> . (72h, 250°C, Ni+Fe).....	180
Figure 96. <i>Trans</i> -1,2-Cyclohexanediol Ni+Fe 70h (250°C).....	180
Figure 97. <sup>1</sup> H NMR Spectrum Of The <i>Trans</i> -1,2-Cyclohexanediol Reaction Mixture, In CDCl <sub>3</sub> . (70h, 250°C, Ni+Fe).....	181
Figure 98. <i>Cis</i> -1,4-Cyclohexanediol 1 Week (250°C), H <sub>2</sub> O.....	181
Figure 99. Partial Chromatogram From GC/MS Analysis Of <i>Cis</i> -1,4-Cyclohexanediol (1 Week, 250°C).....	182
Figure 100. Mass Spectrum Of The Largest Diels-Alder Product, From <i>Cis</i> -1,4-Cyclohexanediol .....	183
Figure 101. Mass Spectrum Of Cyclohexylbenzene, The Result Of EAS Between Benzene And Cyclohexene In The Reaction Of <i>Cis</i> -1,4-Cyclohexanediol.....	184
Figure 102. <i>Cis</i> -1,4-Cyclohexanediol 24h Ni+Fe (250°C).....	185
Figure 103. <sup>1</sup> H NMR Spectrum Of The <i>Cis</i> -1,4-Cyclohexanediol Reaction Mixture, In CDCl <sub>3</sub> . (24h, 250°C, Ni+Fe).....	185
Figure 104. <i>Trans</i> -1,4-Cyclohexanediol 24h Ni+Fe (250°C).....	186
Figure 105. <sup>1</sup> H NMR Spectrum Of The <i>Trans</i> -1,4-Cyclohexanediol Reaction Mixture, In CDCl <sub>3</sub> . (24h, 250°C, Ni+Fe).....	186

Figure	Page
Figure 106. <i>Myo</i> -Inositol 24h Ni+Fe (350°C) .....	187
Figure 107. <sup>1</sup> H NMR Spectrum Of The <i>Myo</i> -Inositol Reaction Mixture, In CDCl <sub>3</sub> . (24h, 350°C, Ni+Fe).....	188

## 1. INTRODUCTION

### Overview

The work discussed in this thesis is a combination of organic mechanistic analyses and investigations of the scope of metal catalysis under hydrothermal conditions. From the perspective of traditional organic chemistry research, this was a rather unusual project. Organic chemistry textbooks do not include any discussion of reactions in high temperature water; most of the reactions covered take place close to ambient temperature and pressure. Traditional organic chemistry reagents are generally toxic, hazardous, exotic, and not found in natural systems. For example, *tert*-butyl lithium will never be mined out of the ground. Never will metal hydride salts be encountered in an environmental setting. Nevertheless, the Earth has been doing organic chemistry for millions of years, but not much is known about how it happens, and none of the usual reagents are used in the process. Buried organic carbon experiences high temperatures, pressures, a variety of mineral surfaces, and water can be present as the solvent.

Over the last 30 years or so, more information has been revealed about the kinds of organic reactions that can happen in high temperature water. Various schemes of reaction pathways have been proposed.<sup>1,2</sup> The reaction pathways are somewhat known, but the mechanisms are still a mystery. Another area of interest is how these reactions can be utilized, and improved upon. Indeed, many pathways are possible, but increasing the kinetics and selectivity of these reactions is necessary for them to have any utility in synthesis. In this project, mechanistic questions about alcohol dehydration under hydrothermal conditions have been addressed. First-row transition metals were also

investigated as selective reduction catalysts, in the perspective of biomass reduction and deoxygenation.

## **Introduction to Hydrothermal Conditions**

Most of the organic reactions occurring on earth are not happening in a round-bottom flask on the benchtop at 25°C and 1 atm (ambient), or even at the surface of the Earth itself. 99.99% of Earth's non-living organic carbon is underground, undergoing processes and transformations that we have yet to fully understand.<sup>3</sup> The reaction conditions encountered there are vastly different from the typical laboratory – high temperatures, high pressures, in the presence of water rather than an organic solvent, and occasionally with extremes in pH and salinity.<sup>4-6</sup> Of particular interest are hydrothermal organic reactions, where the temperatures are between 200-400°C and the pressure is in the range of 2-100MPa.<sup>4,5</sup> The behavior of water under such temperatures and pressures is much different from what we expect at ambient, and a host of organic reaction pathways become available.

Hydrothermal water behaves much differently than liquid water at ambient. The activity of hydronium increases, and the dielectric constant decreases, allowing non-polar compounds to dissolve more readily.<sup>6,7</sup> The solubility of benzene in water increases more than an order of magnitude from 25-300°C; this is supported by both experimental<sup>8</sup> and theoretical data<sup>9</sup> (Figure 1). At 250°C, water has a dielectric constant that is comparable to acetone, and a pH of 5.6 (Figure 2). Heating water in a closed system will increase the water vapor saturation pressure (Figure 3). Water is, in a sense, a tunable solvent.



Multiple properties can be modulated by varying the temperature and pressure. With increased solubility of organic molecules, a lower pH, higher pressure, and inherently high thermal energy, many organic synthesis applications exist for hydrothermal water.<sup>10</sup>

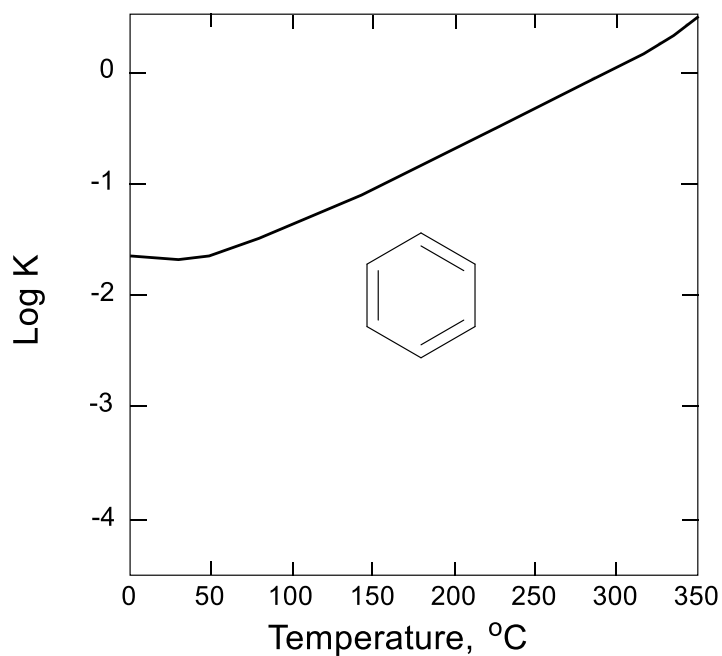


Figure 1. Log K of solubility of benzene in water with increasing temperature. The curve is an adaptation of theoretical thermodynamic calculations made by Plyasunov et al.<sup>9</sup> A review by Shock et al compiled experimental data from various sources, all of which agree strongly with the curve.<sup>8</sup>

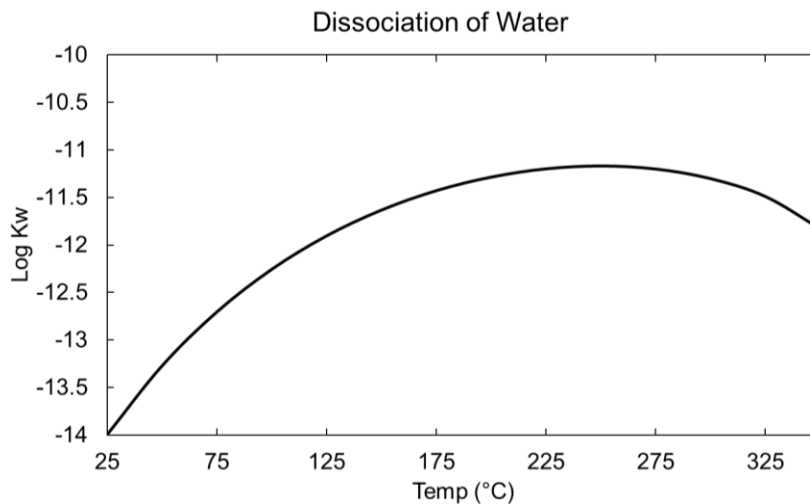


Figure 2. The water autoionization constant,  $K_w$ , as a function of temperature. These values were calculated using the revised Helgeson-Kirkham-Flowers (HKF) equation of state<sup>11</sup>, using data and parameters from Shock and Helgeson 1990<sup>12</sup>

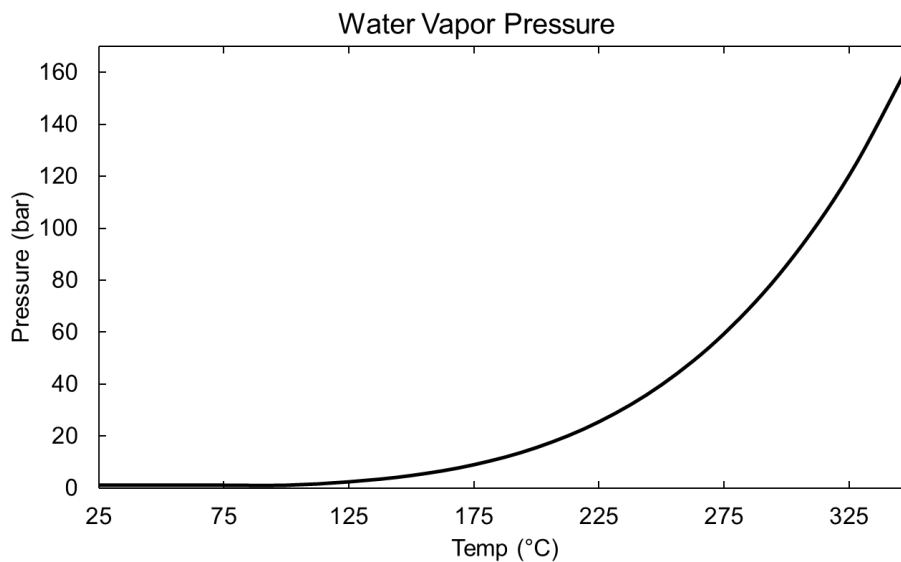


Figure 3. Water vapor saturation pressure as a function of temperature.<sup>13</sup>

Dissociated forms ionic species become less favorable in hydrothermal water. The associated, neutral, forms of ionic compounds become the more stable species (Figure 4). Moderately strong acids, like HCl, become weaker acids. This is attributed to the weakened hydrogen-bonding experienced by water under hydrothermal conditions.<sup>6</sup> It is

important to consider the speciation of dissolved ionic compounds in hydrothermal water, as it can often be much more complex compared to that at ambient.<sup>14</sup>

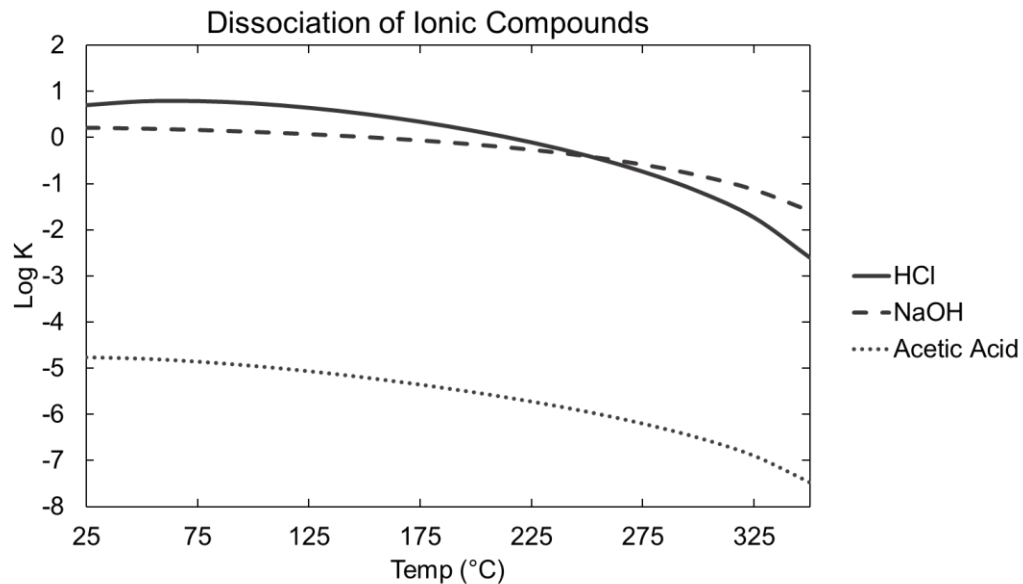


Figure 4. The temperature dependence log K values for the dissociation of hydrochloric acid, sodium hydroxide, and acetic acid in water, obtained using HKF.<sup>11-13</sup> There is a tendency for ionic species to remain associated at higher temperatures. Strong acids become weak, and weak acids become weaker.

### Hydrothermal Organic Geochemistry

Hydrothermal conditions are encountered in volcanic systems, sedimentary basins on land and below the seafloor, often occur as hydrothermal vents. Temperatures and pressures in these systems are elevated. As an example, the Guayamas basin in the Gulf of California has temperatures ranging 350 to 400°C, and pressures of 200-300 bar.<sup>15</sup> Organic matter can be deposited into these systems, and subsequently undergo transformation. It has been estimated that 10 million years, the entire ocean's volume is

cycled through hydrothermal vents.<sup>15</sup> The organic compounds that emerge from hydrothermal vents can serve as nutrients for microbes at the sea floor.<sup>16</sup> The types of organic compounds commonly found in hydrothermal systems are usually oxidized carbon, in the form of carboxylic acids, or reduced carbon, in the form of alkanes.<sup>17</sup>

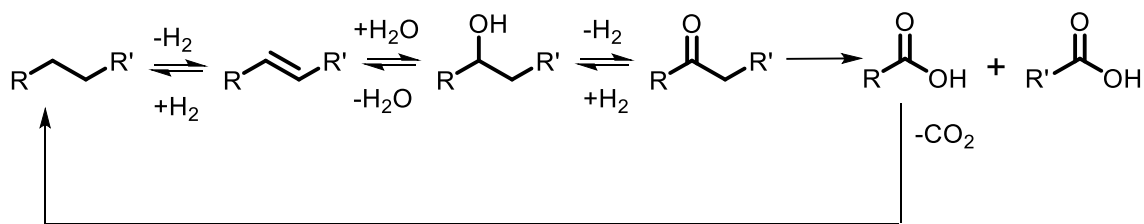


Figure 5. The organic redox reaction pathway of alkanes to acids in hydrothermal conditions. This model was first proposed by Seewald.<sup>17</sup>

An abiotic redox pathway from alkanes to carboxylic acids has been proposed and experimentally observed for organic transformations in hydrothermal systems. Alkenes and alkanes undergo reversible oxidation and reduction; alkenes are hydrated to alcohols, and alcohols are dehydrated to alkenes; alcohols are oxidized to ketones, and ketones are reduced to alcohols; other oxidation pathways result in carboxylic acids, that can decarboxylate, back to alkanes (Figure 5).<sup>1,17</sup> These are fundamental organic chemistry reactions that have been performed and characterized on the benchtop for over a century. The hydrothermal pathway, however, is much less understood. Typical organic chemistry reagents and catalysts are not used by the Earth in these reactions. In the lab, rare metals, such as palladium, are typically used to make alkanes from alkenes.<sup>18</sup> Strong acids have classically been used to dehydrate an alcohol,<sup>19</sup> and mercuric acetate to hydrate an alkene.<sup>20</sup> To reduce a ketone, hydrides of various types are employed, e.g. sodium borohydride or lithium-aluminum hydride;<sup>21</sup> for oxidations, chromium (VI).<sup>22</sup> The earth

does not use these harsh, toxic, and expensive reagents. Nearly all the reactions in Figure 5 have been experimentally observed to occur reversibly, in high temperature water alone.<sup>23,24</sup>

There is still much to learn about hydrothermal organic reactions. While the pathways have been characterized to some extent, most of the mechanisms remain unknown. Obtaining mechanistic insights can help make predictions about the fate of organic molecules in specific hydrothermal systems. It has been proposed that the origin of life began in a hydrothermal system. Reducing conditions, such as those found in serpentinizing systems, have been experimentally shown to have a stabilizing effect on biologically-derived compounds.<sup>25-27</sup> The available thermal energy may have also allowed critical organic transformations to occur.<sup>25-27</sup> While it has also been suggested that organic molecules are merely broken down into simpler structures under hydrothermal conditions, thus making a hydrothermally-based origin of life impossible, evidence to the contrary continues to build. Radical couplings and electrophilic aromatic substitution reactions to form multi-ring structures have been characterized experimentally.<sup>2,28</sup> Minerals have also been demonstrated to promote formation of larger organic structures from smaller, simpler ones.<sup>29-31</sup> Understanding of organic mechanisms in these systems can provide system constraints, and potentially, a scope of what chemistry may have been possible on prebiotic Earth.

The dehydration mechanism of alcohols under hydrothermal conditions was examined here. While there are multiple reports on the dehydration of various alcohols under hydrothermal conditions, there has not been any in-depth mechanistic studies to

determine the dehydration mechanism.<sup>32-34</sup> The dehydration of an alcohol in water is unfavorable enthalpically at ambient. However, with increasing temperature, entropy begins to have a more dominant role in the equilibrium, and a subsequent shift in equilibrium is observed.<sup>35</sup> Thus, alkenes + water are favored at higher temperatures, despite the solvent being water. In this reaction, water is both a solvent and a catalyst. In order for the alcohol to dehydrate, it must become protonated (Figure 6). Hydrothermal water has increased hydronium activity, accelerating this process. We have found that E1 elimination is the dominant mechanism, and competes with E2, even in the most ideal structure. In addition, some of the dehydration reactions reported here are very clean reactions compared to the usual benchtop method of using strong acids.<sup>19</sup> If the mechanism of a reaction is understood, it may then be possible to optimize the reaction conditions for a specific application.

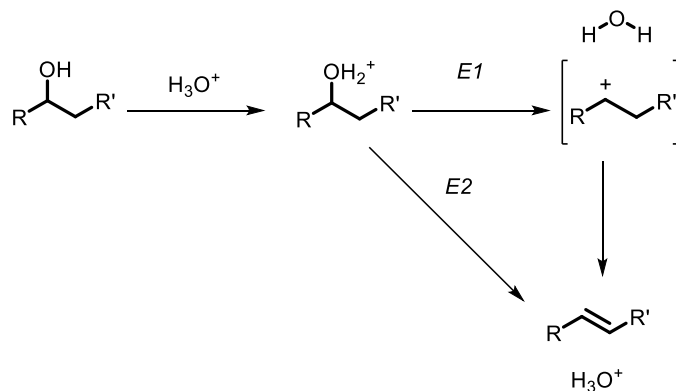


Figure 6. Two possible mechanisms for alcohol dehydration in acidic aqueous media. Both begin with protonation of the alcohol functional group. E1 elimination results in a carbocation intermediate, which can lead to alkene rearrangement.

## Geomimicry

While many hydrothermal organic transformations can happen in water alone, not all of them are selective, and the timescales can be geologic.<sup>23,28,36</sup> The bulk of this reported work is *geomimicry* – reactions that are hydrothermal in nature, that have been optimized (to some extent) for a specific purpose. Geomimicry, or the term “geomimetic” has been used to describe the synthesis of minerals or mineral-like materials, made for a specific application.<sup>37-41</sup> Some of the hydrothermal organic reactions we have performed also fit this criteria – a natural process that has been applied or optimized. The intent of our geomimetic experiments was not necessarily to explain reactions and abundances of products in natural hydrothermal systems, but to take known hydrothermal reactions and improve upon them, in the perspective of developing new organic synthetic methods. In a previous study, the mineral Sphalerite (ZnS) has been shown to selectively activate C-H bonds in 1,2-dimethylcyclohexanes under hydrothermal conditions.<sup>42</sup> Copper (II) chloride was demonstrated to be a selective oxidant, oxidizing a primary alcohol to an aldehyde.<sup>14</sup> These studies attest that increased thermal energy does not necessarily result in a loss of selectivity, or in total decomposition of the organic starting material, as has often been assumed.<sup>15</sup>

Nickel has proved to be an excellent reduction catalyst under hydrothermal conditions. While not very common, Awaruite, a metallic nickel-iron mineral, can be found in serpentinizing systems.<sup>43</sup> Since nickel is a highly active catalyst, even a small amount could have an impact on the fate of organic matter in one of these systems. Iron sulfides, which are commonly found in reducing hydrothermal systems, usually contain

traces of nickel as well.<sup>6</sup> Nickel is also found in bitumen, and could have a role in coal formation. It is possible, if the origin of life did indeed begin in a hot spring or hydrothermal system, that nickel could have had a role in the formation of the necessary organic compounds.<sup>6</sup> It was found that alkenes and aromatics can be reduced in the presence of other oxygen-containing functional groups. Reactions involving simple alkenes reach completion after one hour, or less. At longer timescales, carbonyl compounds have been reduced. Hydrogenolysis reactions, in which C-C and C-O bonds are cleaved, have also been observed. Nickel has also shown potential as a catalyst in biomass reduction processes. Compounds containing multiple oxygen atoms can be reduced to alkanes. Cu-Zn alloy was also investigated. Cu-Zn alloy is known as a selective reductant of CO and CO<sub>2</sub> to methanol, but no reports exist for it as an organic carbon reductant.<sup>44</sup> Excellent activity of Cu-Zn as a reductant of carbonyl compounds was observed. However, its role in the reaction as either a reagent or a catalyst remains unclear and varies among different substrates.

### **Mechanisms of Hydrogenation on Metal Surfaces**

Much is known about heterogeneous metal catalysis, and major advances have been made over the last century in understanding the mechanisms of reactions on metal surfaces. The field has been very active since the 1930s, and continues to this day. One of the earliest proposed mechanisms, by Horiuti and Polanyi, is still supported (Figure 7).<sup>45</sup> While this mechanism was originally a kinetic observation, experiments and imaging techniques have validated it. Over the last eight decades, numerous studies have found



evidence for this mechanism of step-wise H-insertion on the surface of the metal catalyst.<sup>46-48</sup>

Many techniques have been employed to elucidate this mechanism on metal surfaces, under a variety of conditions. The use of stereochemical probes remains a useful method for confirming the Horiuti-Polanyi mechanism on the surface.<sup>48,49</sup> 1,2-Dimethylcyclohexene was used as a stereochemical probe in this study of nickel reductions, and the results align well to the literature and the Horiuti-Polanyi mechanism. Raman and infrared spectroscopy techniques have detected partial hydrogenation intermediates and hydrogen/deuterium atoms on metal surfaces.<sup>46,50</sup> Thermochemistry techniques, such as temperature programmed desorption, have been used to calculate bond strengths between the adsorbate and the surface.<sup>51,52</sup> In-depth kinetic analyses, both in single-collision-single-crystal conditions and under saturation conditions, have been used to determine rate limiting steps and rate orders of the elementary hydrogenation steps on the metal surface.<sup>47</sup> More advanced surface analyses, such as scanning-tunneling microscopy, have uncovered the conformations of molecules adsorbed to the surface.<sup>51</sup>

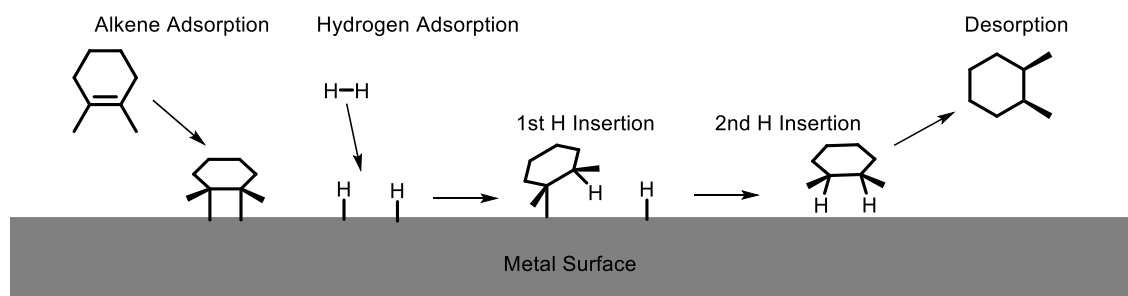


Figure 7. The Step-wise hydrogen insertion mechanism proposed by Horiuti and Polanyi 1934. The catalytic cycle begins with chemisorption of the alkene and hydrogen. Hydrogen atoms add to the alkene one at a time. The physisorbed alkane then desorbs from the surface. 1,2-dimethylcyclohexene, a common stereochemical probe, is shown here as the reactant

## Biomass Reduction

Another aim of this catalysis study is to determine the scope and applicability of nickel and Cu-Zn as Earth-abundant catalysts, for biomass reduction. Current methods for biomass reduction are generally of two types – catalytic, or hydrothermal processing. Hydrothermal processing lacks the redox drive toward more reduced material, and is chemically and/or energetically inefficient, and unselective.<sup>53</sup> Typical reduction catalysts are rare metals, such as palladium, platinum, rhodium, rhenium, and ruthenium, even for simple dehydrations which can be completed with water alone.<sup>54-56</sup> Additionally, despite catalysts being reusable, all catalysts are eventually degraded, poisoned, or lose surface area.<sup>51</sup> In large scale productions, it would be ideal to use cheaper, more readily-available materials for catalysis for this reason.

With the added benefit of water as a benign solvent, the methods presented here are of great interest for safer, more environmentally-friendly, industrial processes. After cooling the reaction, the organic products conveniently separate from the water solvent,

simplifying the work-up. Using nickel or Cu-Zn alloy, this work combines three known methods to generate alkanes from oxygenated organics: hydrothermal processing, geomimicry, and surface catalysis; all without the use of expensive metals. Petroleum is a finite resource, and it will eventually be necessary to seek alternative sources of its fine chemical products – solvents, synthetic starting materials, oils, and many more. It would be ideal to start with non-edible biomass, use inexpensive and safe reagents, and maximize the efficiency of these reactions. The work presented here is a step in that direction.

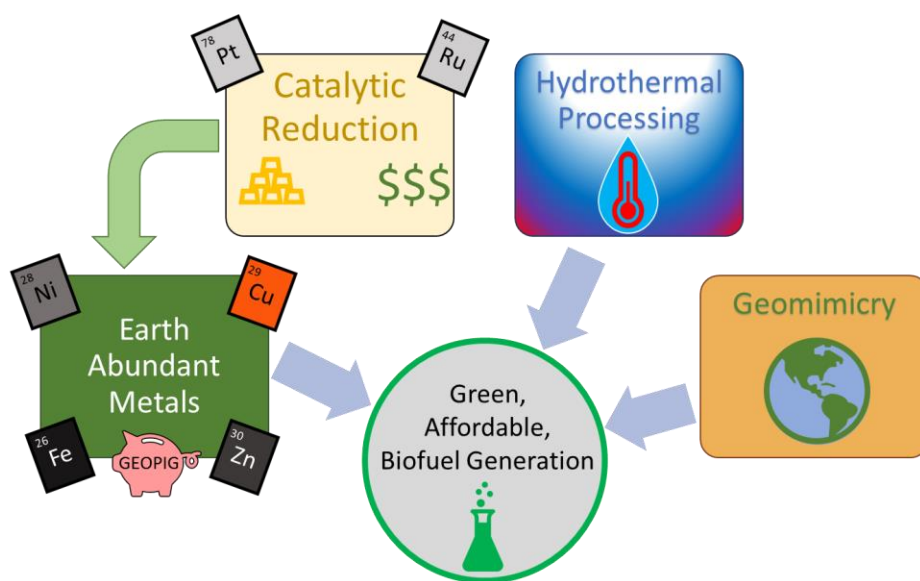


Figure 8. This dissertation summarized as the culmination of multiple techniques to improve upon current biomass deoxygenation/reduction methods.

## 2. METHODS

### **Hydrothermal Reaction Vessel Preparation**

All hydrothermal reactions presented here were performed in sealed quartz/fused-silica tubes. The tubing was purchased from GM Associates or Technical Glass Products. The tubes had inner diameters of 2 mm and outer diameters of 6 mm. They were cut into 9.5” lengths, sealed at one end, and annealed overnight at 1140°C before loading. No attempt was made to “clean” the tubing, as this could potentially introduce more contaminants.

Water for all reactions was 18.2 MΩ·cm, obtained from a Barnstead Diamond purification system. To eliminate oxygen, all water, and all solutions of soluble organics in water, were purged with ultra-high purity Argon for 1 hour before adding to tubes. The organic reactants and water added to each tube were measured by mass. 0.2 g of water was added to each tube. The concentration of organic reactant was 0.2 molal for water-only experiments, and 0.1 molal for experiments using metal catalysts.

Chapters 4-6 discuss experiments which utilize Ni, Fe, and/or Cu-Zn alloy powders as catalysts/reagents. These metal powders were purchased from Sigma-Aldrich as nickel nanopowder, iron powder (micron sized) and Copper-Zinc Alloy Nanopowder. Amounts of nickel and Cu-Zn were added on a surface area basis. The surface areas per mol organic for each experiment were  $5 \times 10^{-4} \text{ m}^2 \text{ Ni}/\mu\text{mol}$  and  $7 \times 10^{-3} \text{ m}^2 \text{ Cu-Zn}/\mu\text{mol}$ . Iron was added on the basis of hydrogen formation, and oxidation of iron to magnetite, enough to create a 6-fold excess of H<sub>2</sub> per mole organic. This amount was 116 μmol iron

per 20  $\mu\text{mol}$  organic. For these tubes, half of the water volume was added after the organic, followed by the metals, and then the rest of the water, in order to prevent air bubbles from becoming trapped in the metal powders.

Quartz tubes were sealed with a hydrogen torch. Before sealing, the headspace of each tube was purged with UHP Argon for 10 minutes. The tubes were then submerged in liquid nitrogen to freeze them, and clamped in place such that the top of the frozen water layer inside the tube sat just below the liquid nitrogen surface. The tubes were evacuated to 60-70 mtorr. At this pressure, tubes were sealed with the hydrogen torch. Each tube was given approximately 1:1 liquid to headspace ratio.

### **Hydrothermal Reaction Heating**

For reactions longer than 2 hours, tubes were heated in a repurposed, preheated, Shimadzu GC oven. For temperatures below 300°C, the tubes were placed in metal pipes with vented screw-cap ends for heating. This container was used only to contain glass shards in case of tube failure. For reactions shorter than 2 hours, a brass block, equipped with internal heating elements, was utilized. A brass insert was used to hold the tubes. Upon completion, reactions were rapidly quenched by plunging the tube and the insert into room temperature water.

For temperatures above 300°C, Swagelok pressure vessels were used. These pressure vessels were 9" long, with swaged end caps (home-built). 3.5 mL deionized water was added to Swagelok tube, along with the reaction vessel. This provided enough

back-pressure to prevent shattering. No reactions above 300°C were run in the brass heating block.

### **Reaction Work-up – Water Only**

Each reaction analyzed by gas chromatography was extracted with dichloromethane (DCM). Experiments analyzed by nuclear magnetic resonance (NMR) were extracted with chloroform-D. Decane, dodecane, or biphenyl were used as internal GC standards for quantification. Prior to extraction, the tubes were scored approximately 2 cm above the liquid level, using a pipe cutter. 1 mL of DCM was added to a 4 mL silanized vial. Another 1 mL DCM was kept in the syringe. The tubes were then snapped open, and DCM was quickly added to each end from the syringe. The DCM in the open tube end was pipetted out first, into the vial containing the 1 mL DCM. This open end was rinsed two more times with more DCM from the syringe. The tube end containing the water, organic reactants, and more DCM, was then pipetted into the vial. This end was rinsed two more times with DCM from the syringe. Any remaining DCM in the syringe after this step was added to the vial, making the total extraction volume 2 mL. If any carboxylic acids were reacted or produced in the experiment, 2-3 drops of concentrated HCl were added at this time. The vial was shaken for vigorously for 20 seconds. An aliquot of the DCM layer was added to a 1.5 mL Agilent amber autosampler Vial, containing a 400  $\mu$ L glass insert. The sample was then analyzed by flame ionization detection (FID) GC and/or GC mass spectrometry (MS).

### **Reaction Work-up – with Metal Powders**

Experiments that used metal powders generally produced hydrogen gas during heating. To prevent total loss of liquid due to hydrogen escaping when tubes were opened, tubes were frozen in liquid nitrogen after scoring (as described in the previous section). 1 mL of DCM was added to a 4 mL silanized vial. Another 1 mL DCM was kept in a syringe. The frozen tube was snapped open, and the end containing the frozen liquid and metal powder was quickly up-ended into the DCM in the vial, so that the open end of the tube was submerged in the DCM. The other open end was filled with DCM from the syringe, and allowed to warm to room temperature. Due to escaping hydrogen gas, the tube containing the liquid often partially or fully emptied itself into the DCM. Once thawed, any remaining liquid/metal powder was pipetted out. Both ends of the tube were rinsed twice with more DCM. The remaining steps were the same as in water-only section.

### **Gas Chromatography Analysis**

A Bruker-Scion 456 gas chromatograph equipped with a Supelco Equity-5 column (Bonded matrix poly(5% diphenyl / 95% dimethyl siloxane) phase) and a flame ionization detector was used for analysis and quantification of the reactants and products.

Table 1. GC Method Parameters – Volatile Analytes

Injection Volume	1 $\mu$ L
Split Ratio	20
Injector Temperature	275°C
FID Temperature	300°C
Flow Rate	1 mL/min

Table 2. GC Oven Temperature Program – Volatile Analytes

Rate (°C/min)	Temperature (°C)	Time (min)	Total Time (min)
Initial	35	3.00	3.00
5.0	80	0.00	12.00
20.0	300	15	38.00
Total Time (min)			38.00

Table 3. GC Method Parameters – Phenyl Rings/Analytes with Higher Boiling Points

Injection Volume	1 $\mu$ L
Split Ratio	20
Injector Temperature	275°C
FID Temperature	300°C
Flow Rate	1.5 mL/min

Table 4. GC Oven Temperature Program – Phenyl Rings/Analytes with Higher Boiling Points

Rate (°C/min)	Temperature (°C)	Time (min)	Total Time (min)
Initial	40	0.00	0.00
10.0	140	0.00	10.00
5.0	240	0.00	30.00
20.0	300	2.00	35.00
Total Time (min)			35.00

A Thermo Electron Trace gas chromatograph 1300-ISQ with a TG-SQC column was used for GC/MS analyses. The same oven temperature programs as in Tables 2 and 4 were used as needed.



## **Metal Powder Characterization**

The surface areas of the nickel nanopowder and Cu-Zn alloy nanopowder were measured in the Goldwater Center at Arizona State University using the Brunauer, Emmett, and Teller (BET) nitrogen adsorption method.<sup>57</sup> The surface area of the first nickel purchased was measured to be  $0.9422 \pm 0.0074$  m<sup>2</sup>/g. A later batch of nickel, from the same supplier (Sigma Aldrich) was found to have a surface area of  $3.5198 \pm 0.0191$  m<sup>2</sup>/g. The surface areas/mol organic were kept constant for each experiment. Only one batch of Cu-Zn alloy powder was used, and its surface area was  $11.0826 \pm 0.0399$  m<sup>2</sup>/g.

The Nickel powder and Cu-Zn alloy powder, pre-reaction and post-reaction, was analyzed with X-ray diffraction (XRD) to determine if any bulk oxidation occurred during the experiment. The Powder X-ray diffractometer in the Leroy Eyring Center for Solid State Science at Arizona State University was used for the analysis. The samples were scanned from 10-90 2 $\theta$ . XRD Spectra are found in Appendix A.

The nickel, iron, and Cu-Zn alloy powders were all imaged using Scanning Electron Microscopy (SEM). Each sample was sputtered with gold to achieve 3-5 nm coating prior to analysis. The XL30 ESEM-FEG in the John M. Cowley Center for High Resolution Electron Microscopy at Arizona State University was used for the imaging. SEM images of each metal powder are found in Appendix A.

### 3. KINETICS AND MECHANISMS OF DEHYDRATION OF SECONDARY ALCOHOLS UNDER HYDROTHERMAL CONDITIONS

#### **Introduction**

Organic reactions commonly occur under hydrothermal conditions in a wide variety of geochemically relevant processes, from petroleum generation to the deposition of minerals, and as part of the deep carbon cycle.<sup>3,16,17,58,59</sup> A wide range of hydrothermal organic chemical reaction types have been surveyed.<sup>10,33,60,61</sup> Of particular interest are a series of reversible functional group interconversions described by Seewald that connect simple alkanes to carboxylic acids, Figure 9.<sup>17</sup> Although product distributions of many hydrothermal reactions have been investigated, kinetic and mechanistic studies of organic transformations under these conditions have received much less attention. Understanding mechanisms and kinetics is important in order to build theoretical geochemical models of the deep subsurface.<sup>23,36</sup>

Dehydration of alcohols to form alkenes is unusual in that it is relatively well understood in both thermodynamic and mechanistic terms at both hydrothermal and ambient conditions.<sup>35,62-65</sup> At ambient, addition of water to an alkene to form an alcohol, the reverse of dehydration, is favorable due to formation of a stronger  $\sigma$ -bond at the expense of a weaker  $\pi$ -bond, although Brønsted or Lewis acid catalysis is required.<sup>64,65</sup> Under these conditions, the favorable enthalpic contribution to the free energy of formation of the alcohol is larger than the unfavorable entropic contribution associated with the conversion of two molecules (alkene and water) into one molecule (alcohol), and equilibrium favors the alcohol rather than the alkene and water.<sup>8,35</sup> Under hydrothermal

conditions at elevated temperatures, however, entropic effects become more important, and the equilibrium shifts so that it lies on the side of alkene and water. Propanol is a simple representative example. As shown in Figure 10, the equilibrium constant for dehydration of this alcohol increases with temperature until the corresponding alkene and water are favored at temperatures above ca. 155°C.<sup>8,12</sup> The result is that in the temperature range of ca. 200 - 350°C (and at the relevant associated confining pressures), alcohols can undergo quite rapid dehydration to form alkenes, even though they are in the presence of a high concentration of water as the solvent.<sup>8,35,62,63</sup>

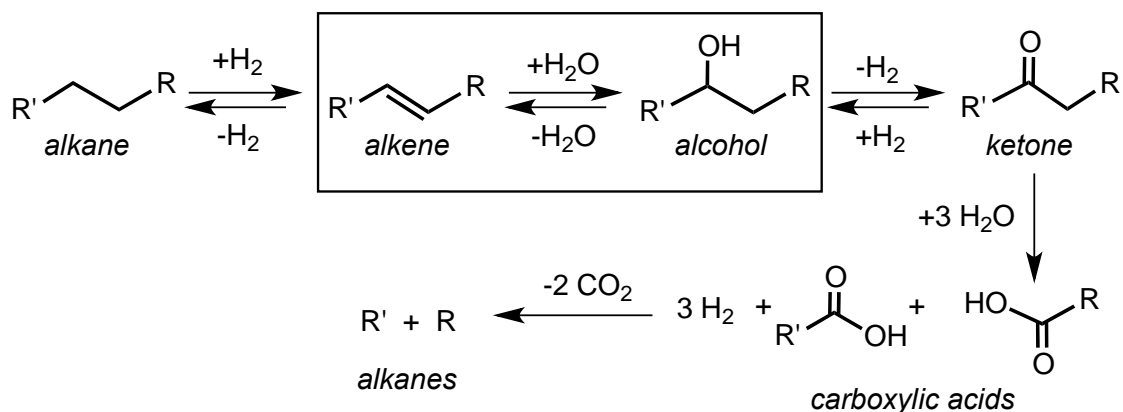


Figure 9. Functional group interconversions that connect alkanes and carboxylic acids under hydrothermal conditions.<sup>17</sup> Alcohol dehydration and the reverse reaction, alkene hydration, are indicated by the box.

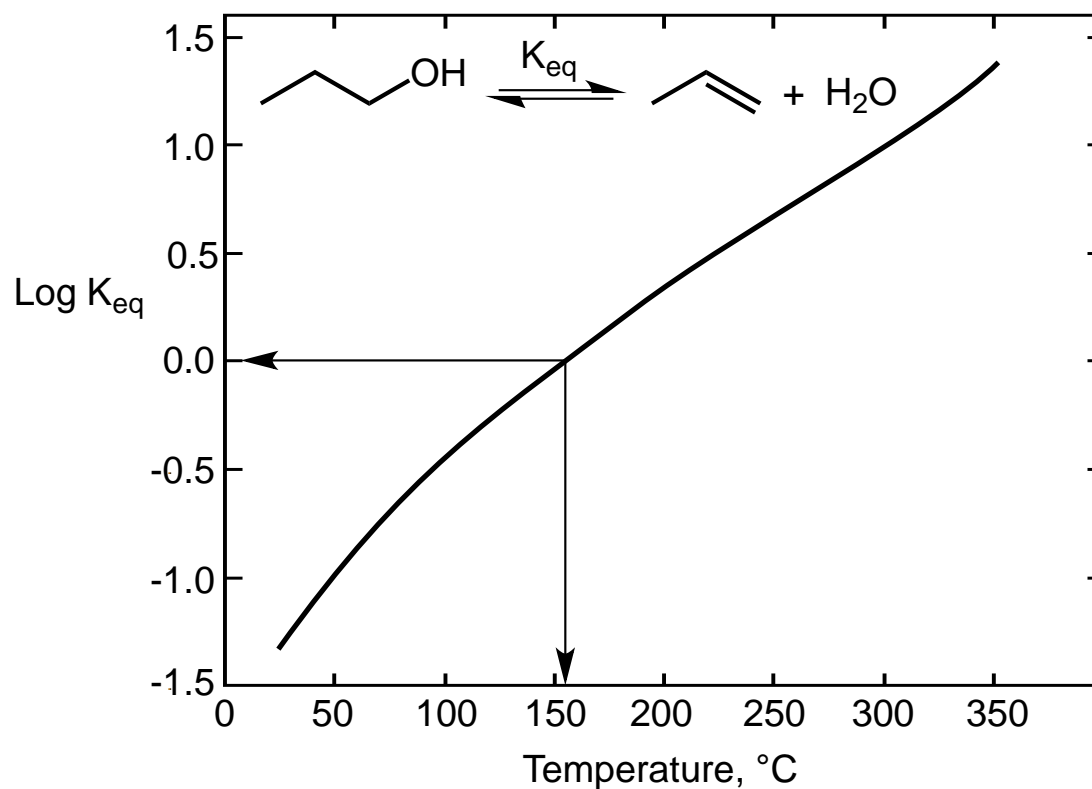


Figure 10. Equilibrium constants (Log  $K_{eq}$ ) for dehydration of 1-propanol as a function of temperature at the saturated water vapor pressure. Above ca. 155°C Log  $K_{eq}$  is positive and the equilibrium favors alkene and water rather than the alcohol. The values for Log  $K_{eq}$  were calculated with the revised Helgeson-Kirkham-Flowers equation of state,<sup>11</sup> using data and thermodynamic parameters from Shock et al 2013<sup>8</sup> and 1990.<sup>12</sup>

The mechanism of hydrothermal alcohol dehydration has been the subject of several previous studies.<sup>32,62,66-73</sup> Previous work suggests that in hot pressurized water the mechanism proceeds *via* conventional, homogeneous, Brønsted acid-catalyzed elimination.<sup>32,66-73</sup> Autoionization of water under hydrothermal conditions is characterized by a larger  $K_w$  compared to ambient.<sup>74-76</sup> The hydronium ions formed by autoionization can protonate the alcohol oxygen to form an oxonium cation that can then undergo elimination with water as the leaving group, Figure 11.<sup>32,71-76</sup> Two different mechanisms are normally considered for elimination of alcohols, E1 and E2, Figure 11.<sup>77,78</sup> Both include protonation of the hydroxyl group of the alcohol as the first step. In the E1 mechanism, the protonated oxygen leaves as a water molecule to generate a cationic intermediate that subsequently undergoes deprotonation to form the alkene. In the E2 mechanism, loss of water and deprotonation occur simultaneously, and no intermediates are involved. Primary alcohols almost certainly dehydrate *via* an E2 mechanism, since the primary carbocation intermediate that would be formed *via* E1 elimination is too unstable.<sup>67-69</sup> For tertiary alcohols, formation of a tertiary carbocation intermediate is facilitated as a consequence of the increased stability of the more substituted cation, and dehydration by an E1 mechanism seems to dominate in these cases.<sup>79,80</sup> For secondary alcohols the mechanism is much less clear and it is possible that E1 and E2 mechanisms are competitive, Figure 11.<sup>32,62,70</sup>

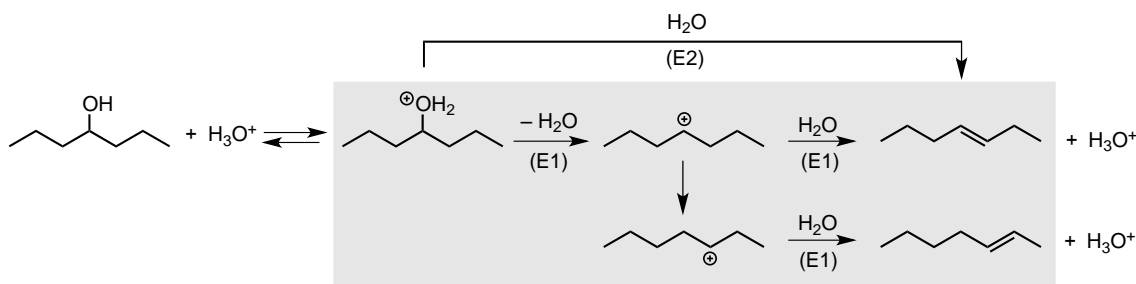


Figure 11. Comparison of the E1 and E2 mechanisms for hydrothermal dehydration of 4-heptanol, as a representative secondary alcohol. The E1 mechanism (grey box) involves a carbocation intermediate that can undergo rearrangement, whereas the E2 mechanism is concerted. Not all of the possible isomeric alkene products are included in this scheme. The results described in this work suggest that for this particular alcohol, E1 is the major elimination mechanism, see text.

Understanding the mechanism and kinetics of dehydration is important in order to build models for organic reaction pathways under geologically relevant conditions. As discussed in detail below, the E1 mechanism is associated with a positive entropy of activation, whereas the E2 mechanism is associated with a negative entropy of activation. This suggests that E2 elimination may become less favorable compared to other possible competing reactions at higher temperatures whereas the E1 mechanism may become more competitive.

Hydrothermal dehydration of alcohols is also of interest as an alternative to conventional dehydration of alcohols at ambient. Alcohol dehydrations performed at ambient require concentrated acids and the use of forcing conditions, such as physical separation of reactants and products *via* distillation.<sup>77,78</sup> Hydrothermal dehydration, however, proceeds with high chemical yield, without the need for external reagents or catalysts, and product isolation is exceedingly simple because the non-polar organic

products simply float on top of the water after quenching to ambient temperature. The lack of reagents, the use of water as the solvent, and the simple product isolation procedures mean that this reaction conforms to many of the standard principles of green chemistry.<sup>81</sup> Hydrothermal reactions of organic chemicals in general are of increasing interest for green chemistry applications,<sup>82-86</sup> and also in the broader context geomimicry, the geochemical analog of biomimicry.<sup>87</sup>

Here we describe a detailed study of the mechanism of dehydration of a series of secondary cyclic and acyclic alcohols. Conformationally locked cyclohexanols are used so that stereoelectronic effects can be used to probe the elimination mechanism, together with a detailed analysis of the minor products at early reaction times. The results of these studies suggest that a Brønsted-acid-catalyzed E1 mechanism dominates over the corresponding E2 mechanism for most secondary alcohols under hydrothermal conditions.

## Methods

Cyclohexanol and 5-nonanol were purchased from Fisher Scientific. The *cis*- and *trans*-4-*t*-butylcyclohexanols and 4-octanol were purchased from TCI America. The remaining alcohols were purchased from Sigma Aldrich. All chemicals were assessed for purity by GC, then used as purchased without further purification.

The mass balances for the reactions of the three cyclohexanols were 95 - 100%. The corresponding values for the linear alcohols were 70 - 100%, with most being greater

than 85%. Kinetic fitting of the time-course data was performed using the COPASI software package, version 4.15 (Build 95).<sup>88</sup>

## Results and Discussion

### *Cyclohexanol*

Hydrothermal dehydration of cyclohexanol has been studied previously by Akiya and Savage.<sup>32</sup> In agreement with this previous work, hydrothermal dehydration of cyclohexanol at 250°C and 40 bar forms cyclohexene as essentially the only product. 1-Methylcyclopentene is detected as a very minor product, at less than 0.1% of the cyclohexene at all times.

Studies as a function of time show that, as described previously,<sup>32</sup> the kinetics of dehydration are pseudo-first order (Figure 12). Several different kinds of rate constants are discussed in this work (see Figure 13). The pseudo-first order rate constant for disappearance of the alcohol and formation of the alkene is directly related to the experimental observables of reactant and product concentrations as a function of time; thus, we indicate this rate constant as  $k_{\text{obs}}$ . Under the current experimental conditions of 250°C and 40 bar,  $k_{\text{obs}}$  for cyclohexanol is 0.20 hr<sup>-1</sup> (Table 5). After 20 hours under these conditions, this reaction reaches an apparent equilibrium consisting of 12% starting alcohol and 88% cyclohexene (Figure 12). Observation of an equilibrium allows  $k_{\text{obs}}$  to be further decomposed into the rate constants for dehydration ( $k_{-\text{H}_2\text{O}}$ ) and hydration ( $k_{+\text{H}_2\text{O}}$ ), by combining  $k_{\text{obs}}$  and the equilibrium constant  $K_{\text{eq}}$ , Figure 13. The rate constant for dehydration of cyclohexanol obtained this way,  $k_{-\text{H}_2\text{O}}$ , is 0.17 hr<sup>-1</sup> (Table 5). This rate



constant also includes any other reaction that forms a product; however, the yield of the only other detectable product (1-methylcyclopentene, <0.1%) is so small that this process can safely be ignored in this case.

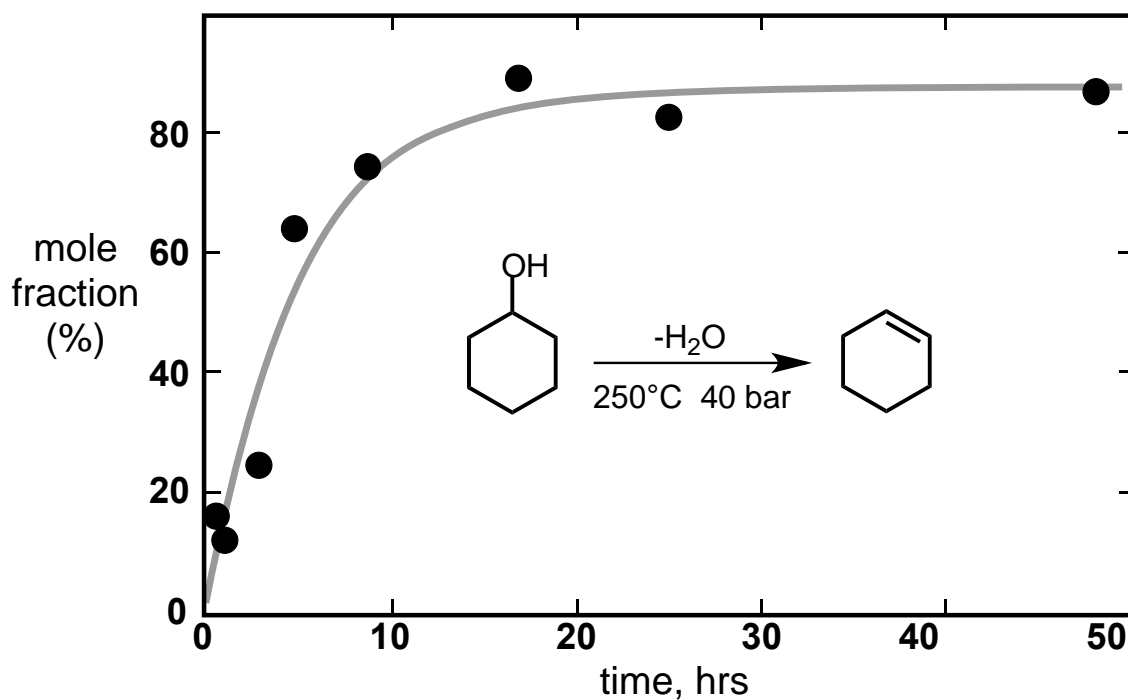


Figure 12. Cyclohexanol conversion (mol %) as a function of time, for hydrothermal dehydration at 250°C and 40 bar. The solid curve is a first-order fit to the data with an observed rate constant,  $k_{\text{obs}}$ , of  $0.196 \pm 0.038 \text{ hr}^{-1}$  for 88% alcohol conversion at infinite time.

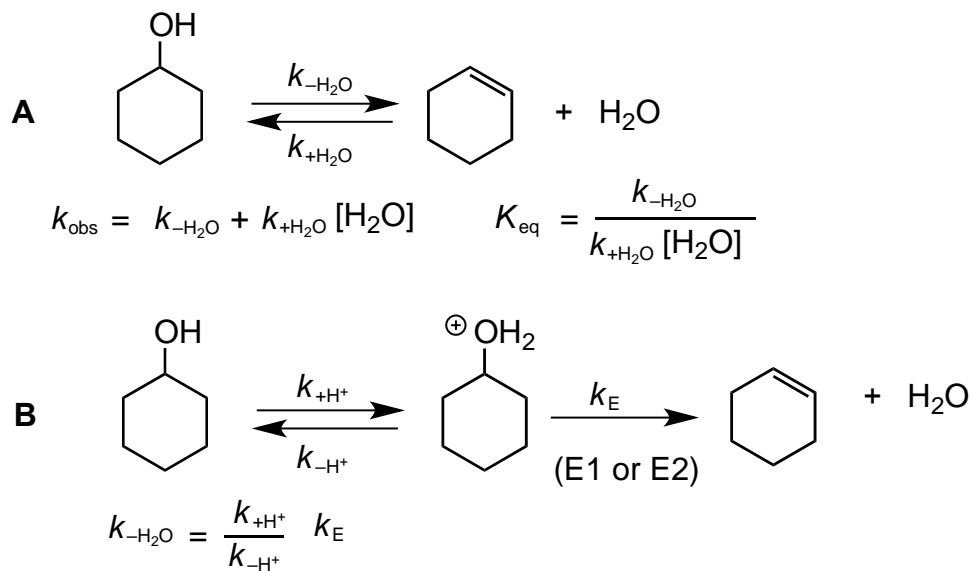


Figure 13. Kinetic scheme of hydrothermal dehydration of cyclohexanol in water showing (A) interpretation of the observed rate constant for loss of alcohol (and formation of alkene products),  $k_{\text{obs}}$ , in terms of the rate constants for the alcohol dehydration ( $k_{-\text{H}_2\text{O}}$ ) and alkene hydration ( $k_{+\text{H}_2\text{O}}$ ) steps; and (B) interpretation of  $k_{-\text{H}_2\text{O}}$  in terms of a rapid pre-equilibrium to form an oxonium ion that eliminates ( $k_{\text{E}}$ ) *via* either an E1 or E2 mechanism. For the *t*-butylcyclohexanols studied here,  $k_{\text{E}}$  can be further decomposed into more elementary steps, (see for example, Figure 15).

The rate constant  $k_{-\text{H}_2\text{O}}$  can, in principle, be further described in terms of more elementary kinetic steps as shown in Figure 13B. Protonation to form the oxonium ion and deprotonation are almost certainly much faster than loss of water by either the E1 or E2 mechanisms.<sup>32,71-76</sup> When the rate constants for the pre-equilibrium steps are larger than the rate constant for the elimination reaction, *and* the ratio of the pre-equilibrium rate constants is not known, extraction of the individual rate constants  $k_{+\text{H}^+}$ ,  $k_{-\text{H}^+}$  and  $k_{\text{E}}$  from  $k_{-\text{H}_2\text{O}}$  is difficult, and therefore is not attempted here. For the rest of this discussion,

the dehydration rate constants are assumed to include the elementary protonation/deprotonation pre-equilibrium steps presented in Figure 13B.

As discussed above, an E1 dehydration mechanism involves a cation intermediate that can rearrange under our experimental conditions. The formation of rearranged primary products, therefore, indicates an E1 mechanism. For the specific case of cyclohexanol, looking for cation rearranged products is not very useful mechanistically. This is because hydride shifts do not generate new isomeric alkene products, and the only rearrangements that generate new isomeric products involve breaking carbon-carbon bonds. Therefore, we investigated substituted cyclohexanols that can generate new alkene isomers with simple hydride shifts, and that also allow a stereoelectronic probe of reaction mechanism.

Table 5. First Order Rate Constants for the Disappearance of Alcohols, Percent Conversion to Alkenes at Equilibrium, and Rate Constants for Alcohol Dehydration at 250°C and 40 bar.

Alcohol	$k_{\text{obs}}$ (hr <sup>-1</sup> ) <sup>a</sup>	Conversion to alkene (%)	$k_{-\text{H}_2\text{O}}$ (hr <sup>-1</sup> ) <sup>a</sup>	# of Isomers <sup>b</sup>
cyclohexanol	0.196 ± 0.038	88 ± 5	0.172 ± 0.040	1
<i>cis</i> -4- <i>tert</i> -butylcyclohexanol	0.160 ± 0.016	98 ± 3	0.157 ± 0.019	2
<i>trans</i> -4- <i>tert</i> -butylcyclohexanol	0.067 ± 0.025	99 ± 13	0.067 ± 0.031	2
3-hexanol	0.067 ± 0.021	91 ± 9	0.061 ± 0.024	8
4-heptanol	0.203 ± 0.013	99 ± 2	0.201 ± 0.015	5
4-octanol	0.032 ± 0.012	100 ± 15	0.032 ± 0.020	5
5-nonanol	0.107 ± 0.023	96 ± 6	0.103 ± 0.035	2
5-decanol	0.113 ± 0.045	100 ± 14	0.113 ± 0.056	2
6-undecanol	0.099 ± 0.019	91 ± 4	0.090 ± 0.019	2

<sup>a</sup> See Figure 13 for definitions of these rate constants. The uncertainties are the standard deviations obtained from the fitting procedure.

<sup>b</sup> The number of alkene isomers observed after dehydration for a 1 hour.

*Substituted Cyclohexanols*

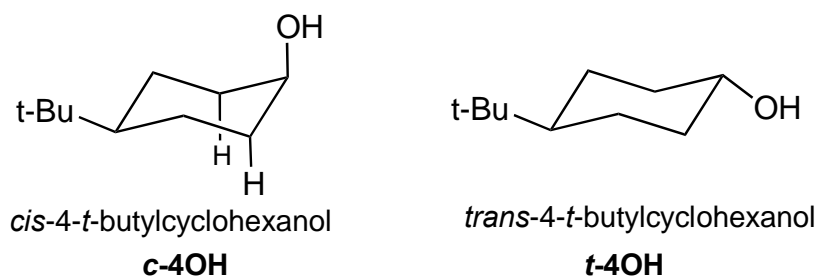


Figure 14. *Cis*- and *trans*-4-*t*-butylcyclohexanol (*c*-4OH and *t*-4OH) in their lowest-energy chair conformations. Note the two hydrogens that are anti-coplanar to the hydroxyl in the *cis*-isomer. In contrast, no hydrogens are anti-coplanar to the hydroxyl in the lowest energy chair for the *trans*-isomer.

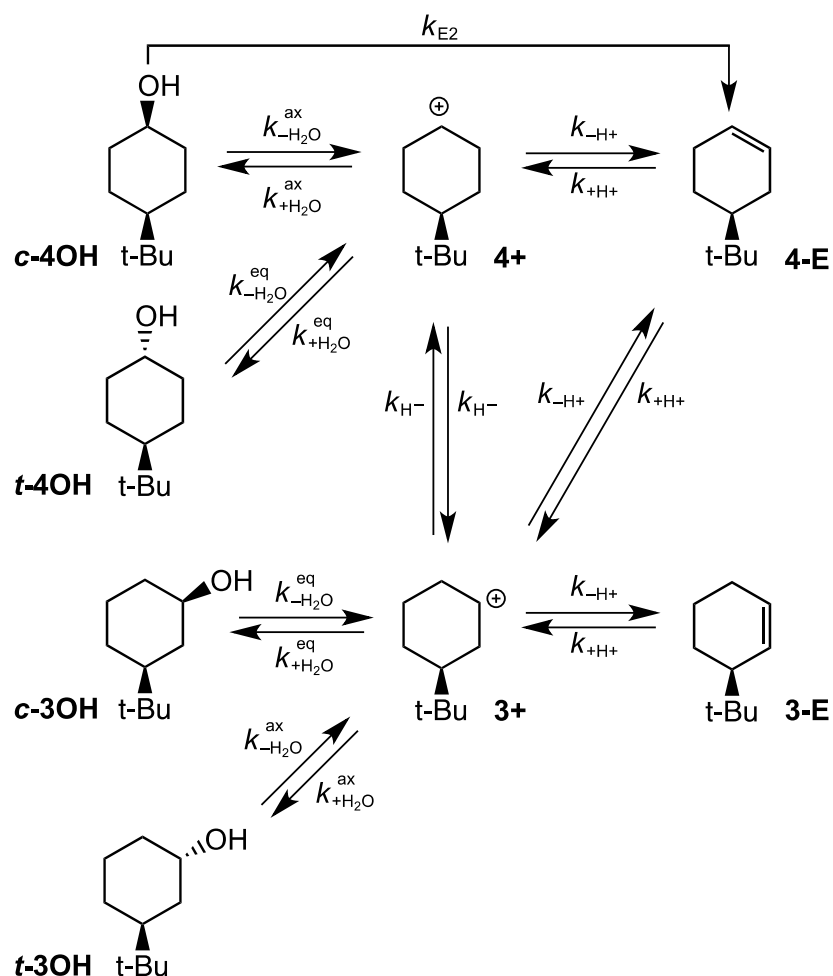


Figure 15. Kinetic scheme for hydrothermal dehydration of substituted cyclohexanols, *cis*-4-*t*-butylcyclohexanol (**c-4OH**) and *trans*-4-*t*-butylcyclohexanol (**t-4OH**), showing formation of the isomeric alkenes: 4- (**4-E**) and 3-*t*-butylcyclohexene (**3-E**), and isomeric alcohols: *cis*- (**c-3OH**) and *trans*-3-*t*-butylcyclohexanol (**t-3OH**) via the cation intermediates: **4+** and **3+**. E2 elimination occurs from **c-4OH**. Each step involving loss ( $k_{E2}$ ,  $k_{-H_2O}^{ax}$ ,  $k_{-H_2O}^{eq}$ ) and addition ( $k_{+H_2O}^{ax}$ ,  $k_{+H_2O}^{eq}$ ) of water includes protonation and deprotonation of the oxygen, respectively, as additional steps that are not shown (see Figure 11). Deprotonation ( $k_{H^+}$ ) is assumed to occur to water and protonation ( $k_{+H^+}$ ) is assumed to occur via the hydronium ion, therefore, these are second-order processes but it is assumed that they are pseudo-first order in the presence of fixed concentrations of water and hydronium ion, respectively.

If dehydration of *cis*- and *trans*-4-*t*-butylcyclohexanol (**c-4OH** and **t-4OH**, respectively; see Figure 14 and 3.7) occurs *via* the E1 mechanism, and is accompanied by a hydride shift in the initial carbocation intermediate (**4+** to **3+** in Figure 15), then two alkene isomers can be formed, 4-*t*-butylcyclohexene and 3-*t*-butylcyclohexene (**4-E** and **3-E**, respectively, see Figure 15). If the carbocation intermediates can be rehydrated by addition of water, both the initial alcohol and its stereoisomer (**c-4OH** or **t-4OH**) and structural isomers of the initial alcohol (**c-3OH** and **t-3OH**; Figure 15) should also be observed as reaction products. In addition, the bulky *t*-butyl substituent locks the cyclohexane into a conformation that can favor one of the elimination mechanisms over the other.<sup>64</sup> The lowest-energy chair conformations for each alcohol that have the bulky *t*-butyl group in the equatorial position are shown in Figure 14. This chair conformation for the *cis*-alcohol is ideal for a concerted E2 elimination, because the hydroxyl substituent is axial and two hydrogens on the  $\sigma$ -carbons are anti-coplanar with respect to the hydroxyl group. E2 elimination in this chair conformation for the *trans*-isomer however, is strongly suppressed, since no hydrogen atoms are anti-coplanar to the hydroxyl in this case. E1 elimination is possible for both alcohol isomers.

Experiments as a function of time reveal that alcohol disappearance is slightly faster for the *cis*-isomer than for the *trans*-isomer (Figure 16 and Table 5), although both appear to react somewhat more slowly than the unsubstituted cyclohexanol. The observed rate constants for removal of the alcohols,  $k_{\text{obs}}$ , are 0.160 hr<sup>-1</sup> and 0.067 hr<sup>-1</sup> for the *cis*- and *trans*-isomers, respectively (Table 5). That  $k_{\text{obs}}$  is larger for the *cis*- compared to the *trans*-isomer is consistent with higher reactivity of the *cis*-isomer due to the additional

possibility of E2 elimination. For these alcohols, decomposition of the observed rate constant into more detailed elementary rate constants as shown in Figure 15 is possible, and is also informative. Although multiple primary and secondary reaction products complicate the analysis, it is these products that allow further insight into the absolute and relative rates of the elementary steps.

The major products of dehydration of the *t*-butylcyclohexanols are given in Figure 15 (identification of the various isomeric alkenes and isomers is described in detail in the supporting information). Starting with either the *cis*- (**c-4OH**) or the *trans*-alcohol (**t-4OH**), the major product is 4-*t*-butylcyclohexene (**4-E**). The isomeric 3-*t*-butylcyclohexene (**3-E**) is also formed, and it is formed with no induction period; *i.e.*, it is a primary elimination product in each case (Figure 16). In addition, the other stereoisomer of the starting alcohol is formed (*i.e.*, *cis*- from *trans*- and *vice versa*). In addition, both the *cis*- and *trans*-isomers of 3-*t*-butylcyclohexanol (**c-3OH** and **t-3OH**) can be detected as minor products on the timescales of the reaction. Other very minor products can also be detected at later reaction times, including 1-*t*-butylcyclohexene and other isomerized alkenes; however, the sum of these products at later times contribute less than 1% to the total product mixture, and are therefore ignored in the kinetic study.

Estimation of the elementary rate constants from Figure 15 is possible by globally simulating the time dependence of the concentrations of the starting alcohols, and of all the primary and secondary products of Figure 15 for both of the dehydration reactions, *i.e.*, the reaction starting with the *cis*-alcohol and the reaction starting with the *trans*-alcohol. As shown in Figure 16, this means that the time-dependence of six different



species (4 alcohols and 2 alkenes) are simulated for each of the reactions, giving 12 different concentration/time datasets consisting of a total of 288 individual concentration/time points. In order to reduce the number of parameters for the kinetic fit, the following simplifications and assumptions were made.

First, as mentioned above and shown in Figure 13, protonation of the oxygen before dehydration achieves a rapid pre-equilibrium and therefore is not explicitly included in the kinetic model. Second, the hydronium ions that provide protons and the water molecules that remove protons in the elementary steps are also not included. Third, we assume that several of the elementary steps of Figure 15 have the same rate constants. Specifically, we assume that deprotonation of both cations has the same rate constant ( $k_{\text{H}^+}$ ), reprotonation of both alkenes has the same rate constant ( $k_{+\text{H}^+}$ ) and that both hydride shifts have the same rate constant ( $k_{\text{H}^-}$ ). It is further assumed that loss of water from the two alcohols with axial hydroxyl substituents (*i.e.*, **c-4OH** and **t-3OH**) have the same rate constant ( $k_{-\text{H}_2\text{O}^{\text{ax}}}$ ), and that hydration of the cations to form these two alcohols also have the same rate constant ( $k_{+\text{H}_2\text{O}^{\text{ax}}}$ ). The same assumption applies to the alcohols with equatorial hydroxyl substituents ( $k_{-\text{H}_2\text{O}^{\text{eq}}}$  and  $k_{+\text{H}_2\text{O}^{\text{eq}}}$ ). We assume that E2 elimination ( $k_{\text{E2}}$ ) only occurs for **c-4-OH**. E2 can, in principle, also occur for **t-3OH**; however, including this step in the kinetic scheme does not improve the fit to the data, presumably because **t-3OH** contributes less than ca. 2% to the total product mixture even at its maximum concentration. All other kinetic processes shown in Figure 15 have to be included in order to obtain satisfactory fits to the experimental data; specifically, the relative yields of the isomeric alkenes **4-E** and **3-E** in the two experiments. Here, we

define a fit as satisfactory when the same values of the variable parameters are obtained using different fitting algorithms and also with different starting values of the variable parameters.

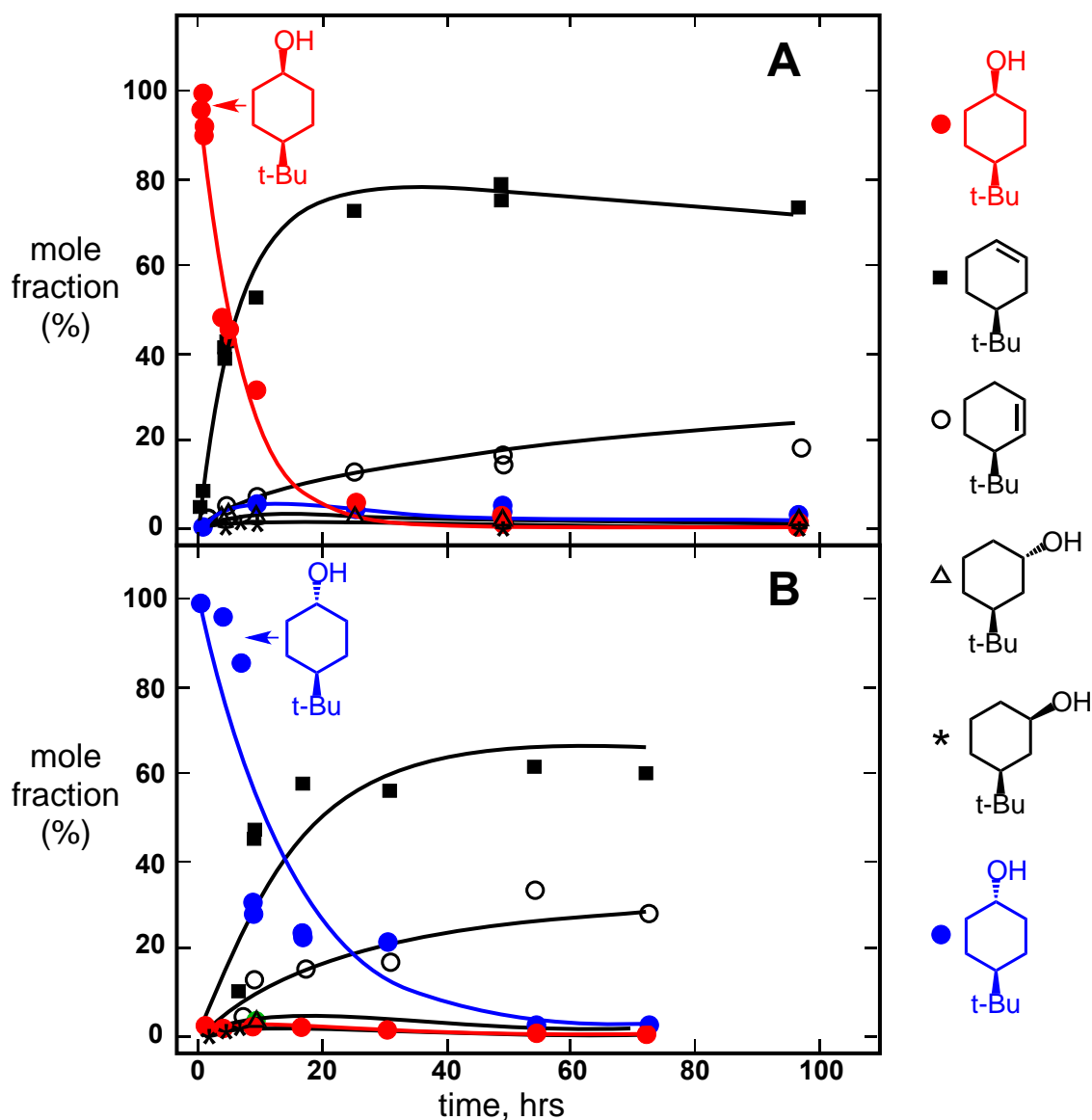


Figure 16. Time dependence of reactant loss and product formation (mol fraction) for hydrothermal dehydration of (A) *cis*-4-*t*-butylcyclohexanol and (B) *trans*-4-*t*-butylcyclohexanol. The curves show the best fits to the data using the kinetic model shown in Figure 15, and the parameters summarized in Table 6. In A, *cis*-4-*t*-butylcyclohexanol is the reactant (red symbols) and *trans*-4-*t*-butylcyclohexanol (blue symbols) is one of the products. In B, *trans*-4-*t*-butylcyclohexanol is the reactant (blue symbols) and *cis*-4-*t*-butylcyclohexanol (red symbols) is one of the products. Other products of the reactions are indicated using the symbols summarized to the right of the figure.

Table 6. Best-Fit Elementary Rate Constants for Hydrothermal Dehydration of *t*-Butylcyclohexanols at 250°C and 40 bar

Slow Reactions		Fast Reactions	
Rate Constant	Value <sup>a</sup> (hr <sup>-1</sup> )	Rate Constant	Relative Value
$k_{E2}$	$0.081 \pm 0.007$	$k_{H^-}$	1.00 <sup>b</sup>
$k_{-H_2O}^{ax}$	$0.079 \pm 0.009$	$k_{+H_2O}^{ax}$	$0.112 \pm 0.041$
$k_{-H_2O}^{eq}$	$0.086 \pm 0.005$	$k_{+H_2O}^{eq}$	$0.272 \pm 0.075$
$k_{+H^+}$	$0.0043 \pm 0.0007$	$k_{-H^+}$	$0.465 \pm 0.095$

<sup>a</sup> The uncertainties correspond to standard deviations of the rate constants obtained from the fitting procedure.

<sup>b</sup> The absolute value for the rate constant for hydride shift,  $k_{H^-}$ , was fixed at  $10^{14}$  hr<sup>-1</sup> in the kinetic modeling, see text. The other fast rate constants are reported relative to this number, since absolute values of rate constants cannot be obtained for reactions that occur on timescales so much shorter than that of the overall reactions.

Finally, we assume that the two cyclohexanes react only from the lower-energy chair conformations shown in Figure 14, *i.e.*, that contributions from other conformations are negligible. This assumption is based on published conformational energy differences for substituted cyclohexanes from variable temperature NMR experiments.<sup>89</sup> Assuming that the free energy differences found for the two chair conformations obtained this way are valid over a wide temperature range, then they can be used to compute relative populations of the two chairs under our experimental conditions. The Gibbs energy differences for axial versus equatorial hydroxyl and *t*-butyl substituents (the former determined at 22°C in water, the latter determined at –120°C in dichloromethane-*d*<sub>2</sub>) are 0.9 kcal/mol,<sup>90</sup> and 4.9 kcal/mol,<sup>91</sup> respectively, with the axial substituent being higher in energy in both cases. The equatorial *t*-butyl substituent is therefore favored by ca. 4 kcal/mol in the *cis*-alcohol, leading to an axial population of ca. 0.4% for the *cis* alcohol at 250°C and even less for the *trans*-alcohol (where both are equatorial). In addition, rotational hindrance of the *t*-butyl group in the axial versus the equatorial position will contribute to the energy difference in the form of decreased entropy in the axial conformation. Therefore, the energy difference between the axial and equatorial conformers at 250°C might be even greater than at the temperatures of the NMR conformation experiments from the literature. An axial population of 0.4% can therefore be considered an upper limit.

The disappearance of the *cis*- and *trans*-isomers and production of all the primary and secondary products shown in Figure 15 were fitted using the COPASI software package.<sup>88</sup> The best global, kinetic fit is shown in Figure 16 and the corresponding values

for the adjustable parameter rate constants are summarized in Table 6. To determine the best fit to the data, minimization of error was performed using both the Levenberg-Marquardt algorithm and simulated high-temperature annealing; we also used different starting values for the rate constants. The model was allowed to converge until constant values were obtained for the variable parameters using the two error minimization methods and the different starting values. The adjustable parameters were the elementary rate constants included in Figure 15, which correspond to two kinds of reactions that occur on very different timescales. Some occur on the timescale of the reaction (*i.e.*, slow, on the order of hours), whereas others occur on a very fast timescale (*i.e.*, fast, submicrosecond). These fast reactions are the cation deprotonations ( $k_{\text{-H}^+}$ ), the hydride shifts ( $k_{\text{H}^-}$ ) and the cation hydrations ( $k_{+\text{H}_2\text{O}^{\text{ax}}}$  and  $k_{+\text{H}_2\text{O}^{\text{eq}}}$ ). Absolute values for the fast rate constants could not, of course, be obtained from the experimental data since they occur on a timescale that is so much shorter than the experimental one. However, their relative values are critical in determining the relative product distributions. In the kinetic fitting, therefore, the rate constant for the 1,2-hydride shift reaction between secondary carbon atoms, ( $k_{\text{H}^-}$ ), was set to a fixed value of  $10^{14} \text{ hr}^{-1}$  based on the closest literature precedent.<sup>92</sup> The absolute value of this rate constant is irrelevant to the fitting procedure just so long as it is fast (equally good fits were obtained using very different values for  $k_{\text{H}^-}$  from  $10^6 \text{ hr}^{-1}$  to  $10^{15} \text{ hr}^{-1}$ ). The rate constants of the other fast reactions were then determined *relative* to the rate of the hydride shift. Only the relative values of these large rate constants have meaning.

Our kinetic scheme assumes that the cations **4+** and **3+** are true intermediates. Computational studies on the dynamical behavior of carbocations suggest that some secondary cations may not actually be intermediates, but may be part of transition structures on pathways to a more stable rearranged cations.<sup>93-96</sup> Specifically, it has been suggested that elimination of water from protonated pinacolyl alcohol may not form a secondary cation. Instead, alkyl rearrangement to form a more stable tertiary cation may be concerted with the loss of the leaving group.<sup>93</sup> In the current systems, however, equivalent rearrangements to more stable cations are not possible and therefore the cations are almost certainly true intermediates.<sup>92-96</sup>

It is apparent from the data in Figure 16 that the time dependencies of the reactants and the products are similar for the two isomeric alcohols. Because the E2 mechanism is impossible for the *trans*-isomer due to the stereoelectronic constraints of the reactive chair, this immediately suggests that the E1 mechanism plays at least some role in *both* alcohol reactions. From Figure 16 it is also clear that the isomerized **3-E** is formed at a similar rate to that of the alkene **4-E**, and there appears to be no induction period starting with either alcohol. This means that **3-E** is likely to be a primary product of the alcohol reactions (though we note, it can also be a secondary product, see Figure 15). Since formation of **3-E** requires a rearrangement of the initial cation intermediate, both alcohols must dehydrate (at least to some extent) by an E1 mechanism. However, the data in Figure 16 also show that the yield of alkene **4-E** compared to alkene **3-E** is higher at all reaction times when starting with the *cis*-alcohol compared to *trans*-alcohol, *i.e.*, the *cis*-isomer reaction forms more of alkene **4-E**. This observation suggests the *cis*-

alcohol also reacts by an E2 mechanism, since only E2 can form the **4-E** alkene in a concerted reaction. Indeed, the time dependence of **4-E** and **3-E** can only be properly described by including the E2 reaction ( $k_{E2}$ ) in the kinetic model for the *cis*-alcohol. Without the E2 contribution, convergent models either overestimate the yield of the **3-E** alkene from the *cis*-alcohol or underestimate the yield of **4-E**.

We conclude that for the *cis*-isomer, E2 elimination occurs *in competition* with E1 elimination under our reaction conditions. The values of the elementary rate constants for the E1 ( $k_{-H_2O}^{ax} = 0.079 \text{ hr}^{-1}$ ) and the E2 ( $k_{E2} = 0.081 \text{ hr}^{-1}$ ) reactions from the kinetic modeling are coincidentally quite similar under the reaction conditions. This is consistent with suggestions from previous work on the dehydration of secondary alcohols.<sup>32,62,70</sup> However, it is important to note that E1 still competes with E2 for the *cis*-alcohol, even though this structure is constrained in a conformation that should be optimum for E2. In other words, E2 can only *compete* with E1 *even in the most favorable structure*. For unsubstituted cyclohexanol, the lowest energy chair has an equatorial hydroxyl group. Based on the results with the *t*-butylcyclohexanols, we would then expect E1 to be the dominant mechanism for hydrothermal dehydration of cyclohexanol, at least under the experimental conditions studied here since the hydroxyl is equatorial in the lowest energy conformation for this compound.

The relative values of the rate constants obtained from the fitting procedure appear plausible. Although the rate constants for loss of water from the two isomers ( $k_{-H_2O}^{ax}$  and  $k_{-H_2O}^{eq}$ ) are indistinguishable based on the uncertainties in these numbers, rehydration of the primary **4+** cation to give the *trans*-alcohol is faster than rehydration to



give the *cis*-isomer (*i.e.*,  $k_{+H_2O}^{eq}$  is larger than  $k_{+H_2O}^{ax}$  given the uncertainty). This is consistent with the *trans*-isomer being more stable than the *cis*-isomer in the lowest energy chair conformation, since in the *trans*-isomer both substituents are equatorial.<sup>64</sup> Protonation of the alkenes ( $k_{+H^+}$ ) is slower than loss of water from the alcohols ( $k_{-H_2O}^{ax}$  and  $k_{-H_2O}^{eq}$ ), but reprotonation of the alkene is responsible for much of the secondary chemistry, and accounts for the observed decrease in **4-E** concentration over time and the corresponding increase in **3-E** concentration after the alcohols have been consumed, Figure 16. Deprotonation of the cations ( $k_{-H^+}$ ) is faster than rehydration to reform the starting alcohols (*i.e.*,  $k_{-H_2O}^{ax}$  and  $k_{-H_2O}^{eq}$ ), consistent with overall transformation from alcohol to alkene with time, but hydride transfer seems to be the fastest process for the cations, and accounts for formation of **3-E** as a primary product in the E1 reactions.

The elementary rate constants from Table 6 enable a deeper understanding of the observed overall rate constants for dehydration,  $k_{obs}$ , given in Table 5. The elementary E1 elimination rate constants for both *t*-butylcyclohexanols are similar ( $k_{-H_2O}^{eq}$  and  $k_{-H_2O}^{ax}$ , Table 6), and are also somewhat larger than the rate constant for overall loss of the *trans-t*-butylcyclohexanol,  $k_{obs}$ , given in Table 5. This is because the reaction to form the starting alcohol from the primary cation intermediate ( $k_{+H_2O}^{eq}$ ), decreases the overall rate of removal of the starting alcohol, lowering the composite  $k_{obs}$ . The *trans-t*-butylcyclohexanol concentration also decreases more slowly than that of the *cis-t*-butylcyclohexanol because the reverse reaction to the more stable *trans*-alcohol ( $k_{+H_2O}^{eq}$ )

is faster than that to the *cis*-alcohol ( $k_{+H_2O}^{ax}$ ). Of course, the *cis-t*-butylcyclohexanol concentration also decays more rapidly because it can react *via* the E2 mechanism.

It is perhaps not surprising that E2 can only compete with E1 under the most ideal circumstances for dehydration of secondary alcohols. The entropy of activation for E2 elimination is negative because of the stereoelectronic requirements of the anti-coplanar arrangement of the bonds being broken, particularly for unconstrained acyclic structures.<sup>97,98</sup> On the other hand, the entropies of activation for E1 reactions tend to be positive.<sup>99</sup> With increasing temperature, the entropy contribution to the activation energy becomes more important, consistent with E1 being the dominant elimination mechanism at the higher temperatures characteristic of hydrothermal dehydration. This is the explanation for the related observation that when elimination and substitution are competitive, elimination tends to dominate over substitution at higher temperatures.<sup>64,65</sup>

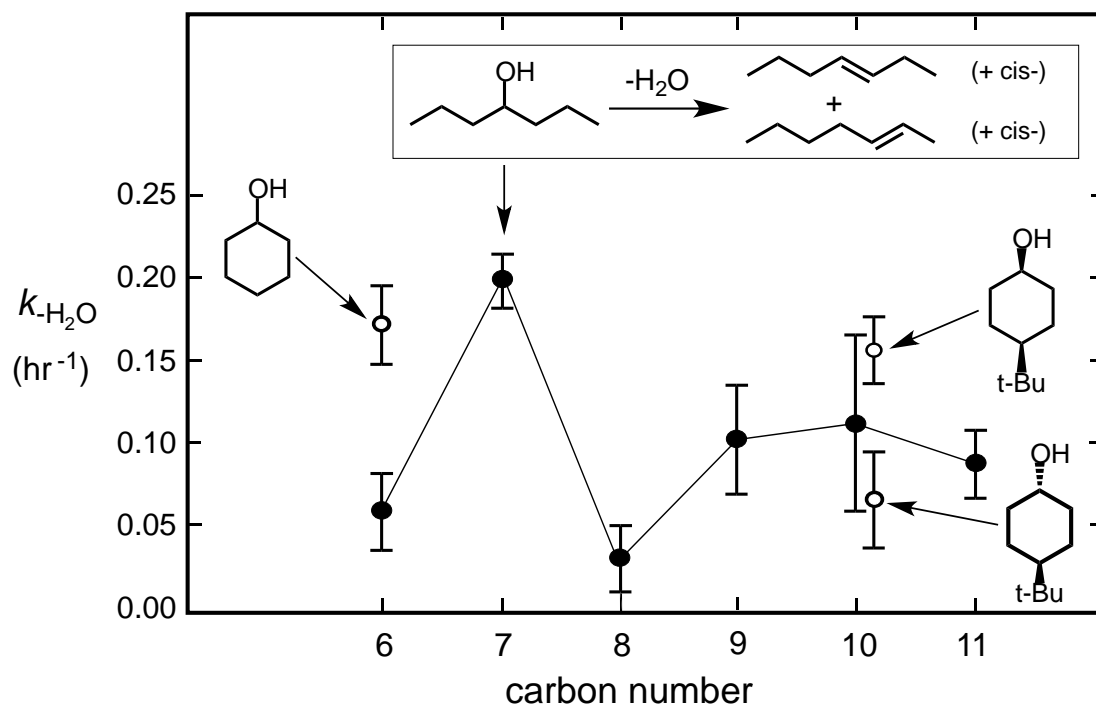


Figure 17. Rate constants for dehydration of linear secondary alcohols with carbon chains from six to eleven, compared to the corresponding rate constants for the indicated cyclohexanols (also positioned in terms of their carbon number content),  $k_{-H_2O}$  (defined in Figure 13). The rate constants for the two *t*-butylcyclohexanols are slightly offset to the right to show the error bars. The data are summarized in Table 5. All reactions are hydrothermal dehydration at 250°C and 40 bar. The line joining the data is intended to guide the eye. The inset gives the products of dehydration of 4-heptanol for a 1 hour reaction time period as the *cis*- and *trans*-stereoisomers of the alkenes 3-heptene and 2-heptene.

We note that the rearranged alkene products could also have been formed *via* other mechanisms in addition to hydride transfer from the initial carbocation. For example, it has been suggested that formation of a hydrogen-bridged ion intermediate can result in the formation of isomeric alkenes in alcohol elimination reactions.<sup>19</sup> However, such bridged ions are still formed *via* an E1 mechanism, and thus the fundamental principle of competition between E1 and E2 mechanisms in our kinetic scheme would be unaltered by consideration of these intermediates. The intermediacy of hydrogen-bridged ions in the reactions cannot be ruled out based on the experimental data, but if they are formed they cannot be the only cationic intermediates, since at longer reaction times, products that involve skeletal rearrangement, including five-membered rings, can be detected, and such products are characteristic of the carbocation intermediates shown in Figure 15.<sup>19,64,65</sup>

Finally, isomerization of one alcohol to the other isomer (e.g., *c*-4OH to *t*-4OH or *vice versa*) could be possible *via* an S<sub>N</sub>2 reaction, with water as the nucleophile and the protonated hydroxyl as the leaving group. However, including such S<sub>N</sub>2 reactions in the kinetic scheme did not lead to any improvement in the fit to the experimental data. Thus, either S<sub>N</sub>2 is not an important mechanism for such isomerization, or kinetic information on this process cannot be extracted from the current experimental data.

### *Acyclic Alcohols*

The kinetics of hydrothermal dehydration of a series of acyclic alcohols were also studied, Table 5. Based on the discussion above, we assume the dominant dehydration mechanism for these alcohols is also E1. The observation of isomeric alkenes as primary products in several of these reactions is consistent with this assumption (see further below). The rate constants for disappearance of the alcohols are summarized in Table 5, and compared graphically to those of the cyclohexanols in Figure 17. The range of the rate constants cover a little less than one order of magnitude, but there is no clear trend with the number of carbon atoms, nor any obvious relationship between the linear alcohols and the substituted cyclohexanol with respect to  $k_{\text{H}_2\text{O}}$ . As the analysis of the kinetics of the *t*-butyl-cyclohexanol reactions discussed above shows, however, decomposition of  $k_{\text{H}_2\text{O}}$  into elementary rate constants would be necessary in order to understand the rate differences in detail.

As indicated in Table 5, different numbers of alkene products are observed, depending upon the alkyl chain length. Experiments were performed for 1 hour duration for each alcohol. After 1 hour, conversion of the alcohols was only 5 - 10%, so that the alkene product distribution should reflect primary rather than secondary products. Dehydration of 3-hexanol for 1 hour formed the most alkene isomers (eight), which included 1-hexene, *cis*- and *trans*-2-hexene and *cis*- and *trans*-3-hexene, as well as three minor alkene isomers with rearranged carbon skeletons (3-hexanol is the only alcohol that produces skeletally rearranged alkenes in significant quantities). In comparison, 4-heptanol forms five alkenes after reaction for 1 hour, and 4-octanol and 5-decanol form

three alkene products in the same time period. 5-nonanol and 6-undecanol produce only two alkene isomers each, which are *cis*- and *trans*-4-nonene and *cis*- and *trans*-5-undecene, from 5-nonanol and 6-undecanol, respectively.

Evidence that these alkenes are primary products, not formed by rearrangement of the primary alkenes, is obtained by examining the products of some of the primary alkenes under the same conditions. Hydrothermal reaction of a 50:50 mixture of *cis*- and *trans*-3-heptenes at 250°C and 40 bar for 1 hour resulted in no detectable change in the ratio of the isomers and no detectable formation of any other structural isomers or other products. Similarly, reaction of *trans*-5-decene at 250°C and 40 bar for 3 hours resulted in no detectable isomerization or other product formation. This suggests alkene isomerization by protonation followed by deprotonation is not important on a 1-hour timescale under the experimental conditions, and that the alkene isomers observed after dehydration of the alcohols are likely to be primary reaction products.

The shorter chain alcohols tend to produce more alkene isomers as a result of rearrangement from the initial cation intermediates of the E1 elimination mechanism. This observation may be consistent with a recent computational study on secondary alkyl cations,<sup>100</sup> where it was found that the preferred conformations for shorter chain cations were those that would facilitate 1,2-hydride transfer, and therefore alkene isomer formation.<sup>100</sup> The preferred conformations for longer chain cations, on the other hand, would inhibit hydride transfer.<sup>100</sup> Alternatively, cation rearrangement requires relocation of the positive charge in the primary cation intermediate, which in turn requires reorganization of the solvent molecules to solvate the charge at the new location on the

chain.<sup>101,102</sup> However, solvation of carbocations by water is more difficult in the middle of longer alkyl chains, especially if aggregation or coiling occurs to exclude the polar solvent molecules. These two effects will decrease the likelihood of positive charge migration *via* a hydride shift as the chain length increases, and therefore decrease the likelihood of alkene isomer formation. Decreased solvation in the middle of longer chains will also inhibit protonation of the initial alkene products, which will also decrease the likelihood of isomer formation due to follow-up protonation and deprotonation reactions.

### **Implications for Hydrothermal Dehydration Under Laboratory and Geologic Conditions**

Dehydration reactions of alcohols under laboratory conditions are of interest since they represent potential routes to the formation of ethylene,<sup>103</sup> other alkenes,<sup>104</sup> and ethers.<sup>71</sup> As mentioned above, the historical method of using concentrated acids often results in low yields, and many different reagents/conditions to improve alcohol dehydration are described in the literature.<sup>105-113</sup> An important application for alcohol dehydration is the deoxygenation of biomass for bioproduct production (including fuels).<sup>114</sup> Again, many methods for effecting deoxygenation of alcohols and polyols have been described in the literature.<sup>115-121</sup> With these considerations, hydrothermal dehydration could find application in a wide range of processes, within the constraints imposed by the reaction mechanisms. The observation that E2 elimination can only compete with E1 under the most favorable stereoelectronic conditions implies that, with the exception of primary alcohols, essentially all hydrothermal dehydrations will proceed

*via* the E1 mechanism, which in turn means that rearranged products can be expected, especially for secondary alcohols.

The chemical yields of alkenes in the hydrothermal dehydrations are remarkably high, certainly compared to the traditional methods using concentrated acids. Cyclohexanol itself represents a good example.<sup>32</sup> The conversion to alkene at 250°C is 88% (the equilibrium value under these conditions), the yield of isomeric alkenes is negligible and the mass balance for the reaction is essentially 100%. In comparison, dehydration of cyclohexanol with concentrated sulfuric acid using a standard procedure<sup>122</sup> formed alkene products with less than 20% chemical yield.

Dehydration with dilute HCl at 225°C gives cyclohexene, but also methylcyclopentenes as 14% of the product mixture.<sup>123</sup> However, hydrothermal dehydration gives cyclohexene and only 0.1% methylcyclopentene. Isomerization can occur both as a result of partition in the initially formed cation intermediate and also by protonation/deprotonation of the primary alkene products. The extent to which these two processes compete will depend upon the acid concentration and reactivity. As the rate constants summarized in Table 6 indicate, alkene protonation under hydrothermal conditions is considerably slower than alcohol dehydration, which may be the reason for the simpler product distribution for the hydrothermal reactions.

That E2 is in general much slower than E1 for secondary alkenes in the absence of specialized stereoelectronic effects is readily understood in terms of the temperature dependence of the entropy of activation for the E2 reaction. However, primary alcohols cannot dehydrate *via* the E1 mechanism, which suggests that hydrothermal dehydration



of primary alcohols could be quite slow, and indeed, literature studies of primary alcohol dehydration are most often performed in supercritical water at the associated very high temperatures.<sup>67</sup> This suggests that hydrothermal deoxygenation of primary alcohols at moderate temperatures around 200 - 250°C may be impractical using simple Brønsted acid catalysis. Work to circumvent reluctant dehydration of primary alcohols under these conditions using alternate catalytic routes is currently under investigation in our labs.

The mechanistic results have implication for the dehydration of alcohols and subsequent alcohol reactions in geochemically relevant environments including seafloor and terrestrial hydrothermal systems, and deep sedimentary basins. A mixture of primary, secondary, and tertiary alcohols would undergo hydrothermal dehydration with significantly different rates; i.e., with primary alcohols being considerably slower than secondary or tertiary alcohols. Although these differences may be mitigated by other reaction mechanisms,<sup>124,125</sup> the prediction would be that primary alcohols should persist in natural system longer than secondary or tertiary alcohols. This may be important since this might allow other reactions of primary alcohols to compete with dehydration. For example, oxidation of primary alcohols can generate carboxylic acids, one of the most abundant functional groups found in natural systems.<sup>126-130</sup>

## Summary

Detailed kinetic analysis of the dehydration reactions of *cis*- and *trans*-4-*tert*-butylcyclohexanol under hydrothermal conditions has shown that the E1 and E2 elimination mechanisms are competitive only for those secondary alcohols where E2 is stereoelectronically favored. We conclude that, in general, the E1 mechanism dominates for hydrothermal dehydration of secondary alcohols. Reaction rate constants do not depend systematically on hydrophobicity or on chain length for linear secondary alcohols. In fact, the rate constants for disappearance of all of the alcohols,  $k_{\text{obs}}$ , are remarkably similar, and fall within the same order of magnitude. The E2 reaction is not competitive with E1 presumably because the transition state for E2 is quite constrained and at higher temperatures the activation entropy becomes unfavorable. This implies that hydrothermal dehydration of primary alcohols, which can only undergo E2 elimination, should be slow. The reactions are inherently green in the sense that they use only water with no additional reagents, the reactions proceed with high chemical yield, and isolation of the organic products is trivial due to their insolubility in the solvent at ambient conditions.

## 4. SELECTIVE, GREEN, NICKEL-CATALYZED HYDROTHERMAL REDUCTIONS

### **Introduction**

Petroleum is a finite resource, and eventually it may be necessary to synthesize petroleum-derived solvents, organic precursors, and fuels.<sup>55</sup> As the world population increases, so will the demand for these products. Additionally, our ability to produce synthetic petroleum products will reduce the need for drilling and fracking, which are potentially harmful to the environment and groundwater supply.<sup>131</sup> Ideally, these synthetic products would be prepared from biomass, using green chemistry methods and inexpensive materials. Current processes for biomass reduction often require the use of expensive catalysts, such as platinum and rhenium.<sup>54,132</sup> Water in industrial processes is gaining attention as a non-toxic, non-flammable solvent, with physical properties that can be modulated by varying the temperature, i.e. the pKa, density, and dielectric constant.<sup>133,134</sup> We report a green pathway from alkenes and alkynes to alkanes, using geomimicry – hydrothermal conditions, water as a solvent, and an earth-abundant metal catalyst, nickel.

There are many organic reaction pathways that can be accessed with high temperatures and pressures using water as the solvent.<sup>1,17,23,36</sup> The organic transformations presented here will occur in water alone under hydrothermal conditions, but are often kinetically slow, or have limited selectivity.<sup>23</sup> One of our research goals is to enhance the rate and selectivity of these reactions with the use of earth-abundant catalysts. Under hydrothermal conditions, the water dissociation constant increases and

the dielectric constant decreases, allowing the complete dissolution of non-polar aliphatic moieties that would be insoluble at room temperature.<sup>6,7</sup> Once the hydrothermal reaction is quenched at room temperature, the organics conveniently separate from the aqueous phase. Nickel is an excellent catalytic surface in our aqueous phase reduction method, that can reduce alkynes and alkenes to alkanes. Numerous reports on nickel and nickel alloy-catalyzed reductions of carbon-carbon  $\pi$ -bonds exist.<sup>48,49,135,136</sup>

Active first-row transition metal catalysts are preferred over the usual platinum and palladium catalysts due to their abundance and lower cost. While these rare metals are very active catalysts, the methods associated with their use require vast excesses of hydrogen, and toxic or flammable solvents. Raney nickel, and other nickel-aluminum alloys are often used as well, however these are quite toxic and require molten aluminum for their manufacture.<sup>137</sup> Green reduction methods have become of greater interest in recent years.<sup>138-143</sup> However, reports of green reductions often utilize expensive metals that carry a high risk of depletion. Some methods which use earth-abundant metals also employ organic solvents and high temperatures.<sup>141</sup> Other frequently used green reducing agents include enzymes and biological systems.<sup>142,143</sup> While these systems reduce waste, they are less robust than heterogeneous catalysts. Nickel is a very active catalyst. Iron is used as a sacrificial electron donor in these reactions to generate hydrogen *in-situ*. In this system, earth abundant metals and a benign solvent are used, while molecular hydrogen is avoided. Molecular hydrogen is explosive, and carries a high energy cost to produce industrially.<sup>138</sup> Cheaper and safer alternatives should be used in its place. The nickel nanopowder used in these experiments requires no additional preparation, and can be

used as purchased. The temperature of these experiments is 250°C, but this is a relatively moderate temperature on an industrial scale, and compared to similar reductions. A majority of the reductions reported here reach completion in an hour or less. We have analyzed the kinetics of reduction, probed the mechanisms of hydrogen addition, and have demonstrated alkene and aromatic reduction selectivity in the presence of other functional groups.

## **Methods**

### *Chemicals Used*

All reagents were purchased from Sigma-Aldrich, apart from 1,2-dimethylcyclohexene, which was purchased from ChemSampCo. The 1,2-dimethylcyclohexene was purified by microscale distillation.

### *Reduction with Pd/C*

The reduction of 1,2-dimethylcyclohexene using Pd/C was performed according to a method described in *Organic Experiments, 8<sup>th</sup> Ed.*<sup>122</sup>

### *NMR Analysis*

Experiments starting with cyclohexene, benzene and 3-hexyne were analyzed by <sup>1</sup>H NMR. The same extraction method (as in Chapter 2) was used, except with CDCl<sub>3</sub> and no decane. This was done since benzene and cyclohexane are not separable by GC without the use of a specialized column, and it was difficult to separate the hexane isomers that result from reduction of 3-hexyne. A Bruker 400 MHz NMR instrument in

the Magnetic Resonance Research Center at Arizona State University was used. A standard, 8-scan proton protocol was used.

### *Hydrogen Measurements*

The amount of hydrogen generated from iron oxidation at 250°C was measured. The sample tube for the hydrogen generation measurement was loaded with nickel, iron, and water, as per a typical experiment. No organic was added. The tube was heated for 1 hour at 250°C in a brass heating block. The tube was scored and placed inside a piece of 1" ID tygon tubing. The tubing was capped with a rubber septum at each end. The volume of the tygon tubing with the glass tube inside was determined by massing the entire apparatus with and without water. After the volume was determined and the apparatus was fully dried, the tube was opened by bending the tygon tubing where the tube was scored. 10  $\mu\text{L}$  of the headspace inside the tygon tubing was injected on a reducing compound photometer-GC (Peak Labs) in triplicate using a gas-tight syringe. Blanks of the air within the tygon tubing prior to opening the tube were also injected in triplicate. Negligible  $\text{H}_2$  was detected. The  $\text{H}_2$  in the headspace (ppmv) was quantified using a calibration curve of 50 ppm  $\text{H}_2$  standard with nitrogen balance (Praxair). The volume of the tygon tubing, and the equilibrium constant of dissolved hydrogen in water degassing at 25°C (HKF)<sup>11-13</sup> were used to calculate the total mass of hydrogen generated by iron oxidation.

## Results and Discussion

### *Nickel Catalyst*

The reductions presented here employ a nickel catalyst, and iron as a sacrificial donor. The iron produces hydrogen from water, forming iron oxide. Production of in-situ hydrogen is more convenient and safer than addition of molecular hydrogen. These reactions take place at elevated temperature and pressure: 250°C and 40 bar (water vapor pressure) with water as the solvent. While iron was intended to oxidize, produce hydrogen, and thus protect the nickel surface from oxidation, it was critical to prove that this was the case. Nickel and iron were heated in water alone for 1h at 250°C. This was a typical time point for many of the reductions presented here. Also, short heating times would be the point in the reaction where oxidation of nickel would be most likely to occur, since the kinetics of H<sub>2</sub> generation from iron are not known. The post-reaction nickel was confirmed to have undergone no bulk oxidation using XRD analysis (Appendix A). Characteristic signals for nickel oxide were not present. There is also no evidence of decreased activity with long time points (>7 days). In addition, the amount of iron used in these experiments should generate enough hydrogen to preserve the nickel surface, according to calculations using the Helgeson-Kirkham-Flowers equation of state<sup>11-13</sup> and thermodynamic parameters for each species.<sup>144-146</sup> Since there is sufficient hydrogen produced at a typical reaction time of 1h, no evidence of bulk oxidation, and no decreased activity at long reaction times, we conclude that the nickel in these experiments remains Ni<sup>0</sup>. This is not unexpected, as other researchers using nickel as a catalyst under

similar conditions also noted no oxidation of the nickel, with zinc as a sacrificial donor.<sup>147</sup> Iron has the advantage of being more earth-abundant.<sup>148</sup>

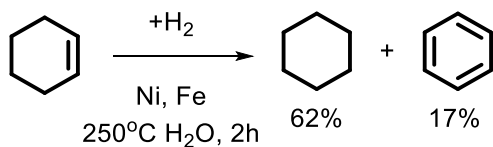


Figure 18. Reduction of cyclohexene.

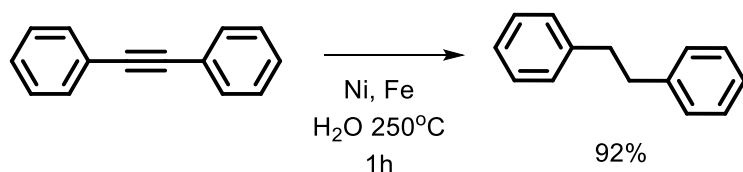


Figure 19. Reduction of diphenylacetylene to bibenzyl.

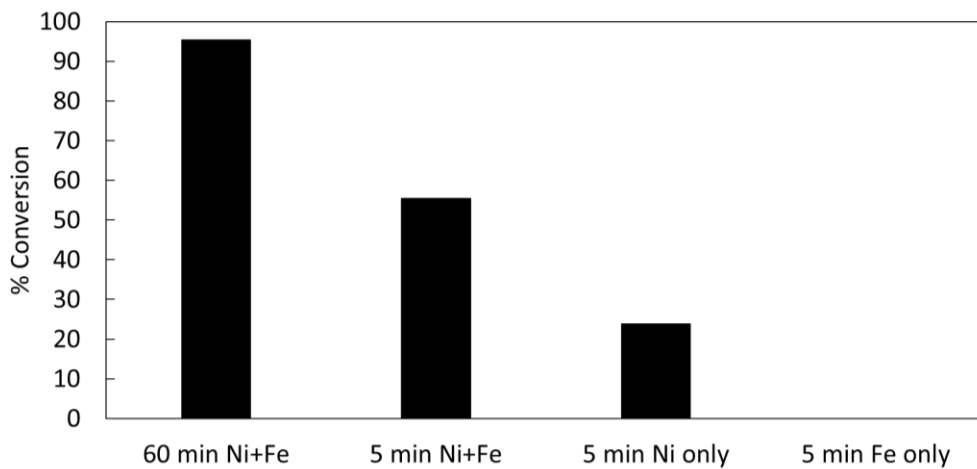


Figure 20. Percent conversion of cyclohexene in metal control experiments. Including iron with nickel increases catalytic activity. Cyclohexene does not react in the presence iron.



Cyclohexene reacts rapidly in the presence of nickel and iron. 95% conversion is obtained after 1 hour at 250°C with nickel as the catalyst, and iron as the sacrificial H<sub>2</sub> generator (Figure 20). After 2 hours, 62% yield of cyclohexane was obtained, with 17% benzene as a side product (Figure 18). The oxidation product, benzene, is not entirely unexpected, as many hydrogenation catalysts are also dehydrogenation catalysts. Dehydrogenation of cyclohexene has also been observed with nickel in other studies.<sup>149,150</sup> Control experiments were run in order to determine the role of nickel and iron in the reaction (Figure 20). Cyclohexene was reacted with nickel alone and iron alone at 250°C for 5 minutes. In the control reaction with nickel only, about two-fold less conversion is observed. In the control reaction with iron alone, no reaction occurred. Diphenylacetylene (DPA) was reduced to bibenzyl after 1 hour (Figure 19). The alkyne and intermediate alkenes can be reduced to an alkane on a short timescale.

The phenyl rings on diphenylacetylene remain unreduced after 1 hour of reaction time. To determine if aromatic reduction was possible on nickel under hydrothermal conditions, benzene was reduced over a much longer timescale. This reduction is slow due to the stability of the aromatic compound, and cyclohexadiene may be formed as an intermediate species. Cyclohexadiene is a well-known hydrogen donor, and will release H<sub>2</sub> to form benzene, due to the stabilizing effect of aromaticity.<sup>151,152</sup> Cyclohexyl dienes were also shown to dehydrogenate quickly under hydrothermal conditions.<sup>23</sup> 99% cyclohexane is obtained in 9 days at 250°C (Figure 21).

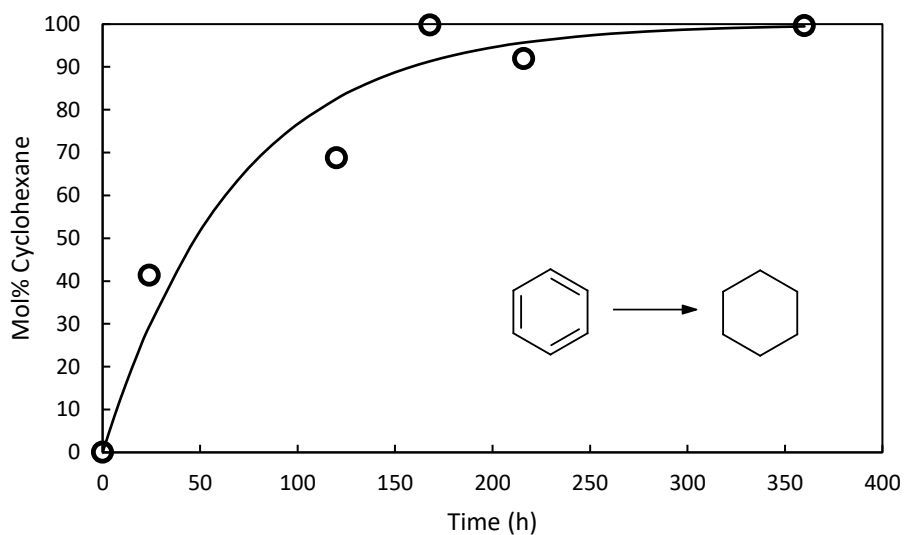


Figure 21. Cyclohexane yield as a function of time at 250°C in the presence of Ni and Fe.

#### *Mechanisms of Alkene and Alkyne Reduction*

Reduction of cyclohexene and complete reduction of DPA does not provide mechanistic information about  $\pi$ -bond reductions on nickel under hydrothermal conditions. 1,2-dimethylcyclohexene was selected as a stereochemical probe for alkene reductions. By observing the ratio of *cis* and *trans*-1,2-dimethylcyclohexane, it can be determined whether *syn* or *anti*-addition is dominant. 30-minute timepoints of 1,2-dimethylcyclohexene reduction were performed to observe the primary products of the reaction. After 30 minutes at 250°C, a ratio of 58:42 *cis* : *trans*-1,2-dimethylcyclohexane are formed (Figure 22). Nickel and nickel alloys have exhibited preferential formation for *cis* isomers in the reduction of 1,2-dimethyl cyclo-alkenes at milder conditions.<sup>48,49,135,136</sup> There is an alkene rearrangement which occurs more rapidly than reduction which affects the stereochemistry of the products. 1,2-dimethylcyclohexene tends to rearrange to 2-

methyl-1-methylenecyclohexane. *Syn* addition is the preferred mechanism, but is inhibited by the rearrangements that occur prior to reduction. The *trans* isomer is a primary product, and not the result of isomerization of the *cis*. *Cis*-1,2-dimethylcyclohexane was reacted with nickel and iron at 250°C for 90 minutes, and only 1% isomerization to the *trans* occurred in that time. This is not enough to account for the amount of the *trans* product that is observed in the reduction.

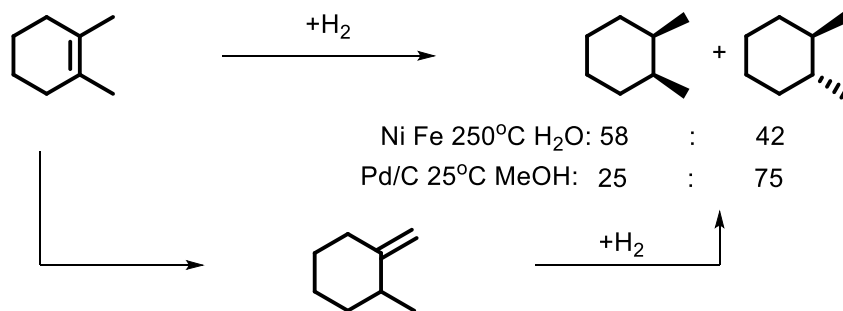


Figure 22. The hydrogenation pathway of 1,2-dimethylcyclohexene after 30 min for Ni, and 5 min for Pd/C. Ratios of each isomer are relative to one another.

The reduction of 1,2-dimethylcyclohexene was also performed at ambient conditions in methanol with 5% Pd on carbon as a comparison. While the reduction 1,2-dimethylcyclohexene has been studied extensively at ambient conditions, many of the studies report the ratio of *cis* and *trans* at 100% conversion rather than at early times. Organic chemistry textbooks often report that mainly the *cis* isomer is produced in this reduction on Pd/C; however, this was not what was observed in this experiment.<sup>153</sup> A 75:25 *trans* to *cis* isomers are obtained from the reduction of 1,2-dimethylcyclohexene

after 5 minutes (Figure 22). This reaction was incredibly rapid, and 100% conversion was observed on that timescale.

After 5 seconds, 4% conversion was obtained. Interestingly, there was still 75:25 *trans* to *cis*. 2-methyl-1-methylenecyclohexane was observed. The reaction proceeds through the exocyclic alkene intermediate and then is reduced to mainly the *trans*. This is analogous to observations of isomerization in the hydrothermal reduction with nickel. Isomerization is more prevalent in the ambient reduction with Pd/C than at hydrothermal conditions with nickel. This was shown before with 1,2-dimethylcyclohexene and palladium.<sup>154</sup> Hydrated products are produced at early times. These hydrated products will also result numerous alkene isomers as the alcohol dehydrates back to an alkene.

The reduction of naphthalene yielded 1,2,3,4-tetrahydronaphthalene as the major product (discussed in a later section), and both *cis* and *trans*-decalins as very minor products. The absolute abundances of these were <1 mol%, but their ratio was mechanistically informative. 70:30 *cis* to *trans*-decalin was obtained (Figure 23). This also indicates *syn* addition of hydrogen, in a more constrained structure than 1,2-dimethylcyclohexene. Rearrangement would be expected to happen less, leading to more *cis* product than what was observed from 1,2-dimethylcyclohexene.

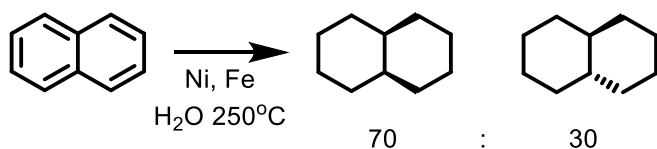


Figure 23. The ratio of decalins obtained from the reduction of naphthalene.

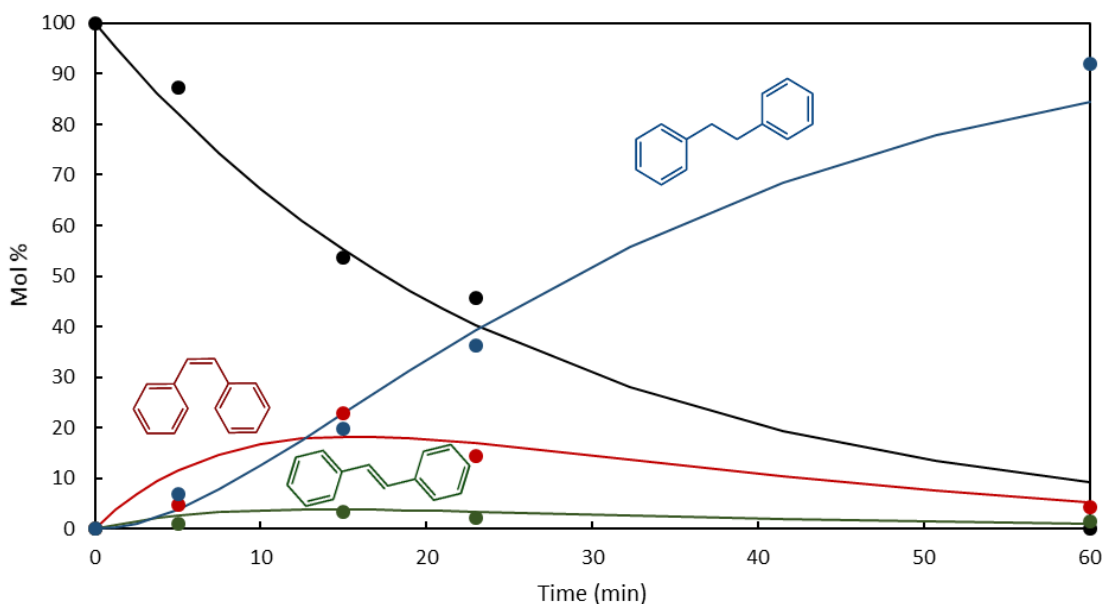


Figure 24. Abundances of diphenyl acetylene, stilbenes, and bibenzyl with time, in the presence of Ni and Fe at 250°C. The reaction is complete after 1 hour at 250°C with nickel and iron. Copasi was used to fit the data. The rate constants are shown in Figure 25, which also represent the model used in the fitting.

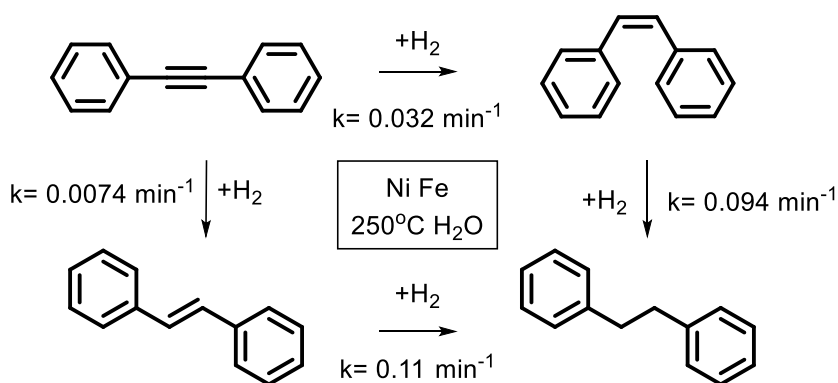


Figure 25. Hydrogenation pathway of diphenylacetylene. This pathway was used as a model to obtain a kinetic fit. First-order rates are shown in each reduction step. 10% error is associated with these values, based on repeated measurements.

Diphenylacetylene was reduced as a model alkyne, in order to determine whether the addition of H<sub>2</sub> to the carbon triple bond is syn or anti-addition. The kinetics of the

reaction and minor products were analyzed (Figure 24). As most heterogeneous catalysts reduce alkynes to the corresponding *cis*-alkene, it was not surprising that nickel produces mainly *cis*-stilbene as the first reduction product. More than 82% *cis*-stilbene relative to the *trans* is produced at all times during the reduction of DPA. The amount of *trans*-stilbene in the reaction cannot be accounted for via isomerization of the *cis*-stilbene. *Cis*-stilbene was reacted in the same conditions for 5 minutes, and less than 1% isomerization was observed. Therefore, the *trans* isomer is a primary product of the reduction. The alkene products of this reaction are eventually reduced to bibenzyl in 1 hour, at which full conversion is achieved. Many reduction catalysts will reduce the alkyne as well as alkenes; generally, a poisoning agent is generally required to prevent further reduction.<sup>155</sup> Copasi analysis of the kinetics was performed to determine the rates of alkyne and alkene reduction (Figures 24 and 25).<sup>88</sup> The reduction of DPA to both stilbenes is generally slower than the reduction of the stilbenes to bibenzyl (Figure 25). In this reaction, alkene reduction is faster than alkyne reduction. It would be difficult to determine the absolute difference in reduction rate between *cis*-stilbene and *trans*-stilbene from these data, as the rate constants for these two reactions are similar.

3-hexyne was also reduced as a stereochemical comparison (Figure 26). The smaller ethyl groups around the alkyne were expected to have a decreased steric effect compared to DPA. After 5 minutes at 250°C in the presence of nickel and iron, 7% 3-hexyne remained. The reduction products included 72% alkenes and 21% hexane. Of the alkenes, there was 68% *cis*-3-hexene, 6% *trans*-3-hexene, and 26% *trans*-2-hexene. Relative to one another, there was 92:8 *cis* to *trans*-3-hexene. The preference for *cis* is

still high, but some isomerization in the alkyl chain occurs. This type of isomerization is not possible for the stilbenes due to the phenyl substituents. The smaller ethyl substituents did not have a large effect on the stereochemistry of the alkenes. Addition of H<sub>2</sub> occurs *syn* for alkyne reduction.

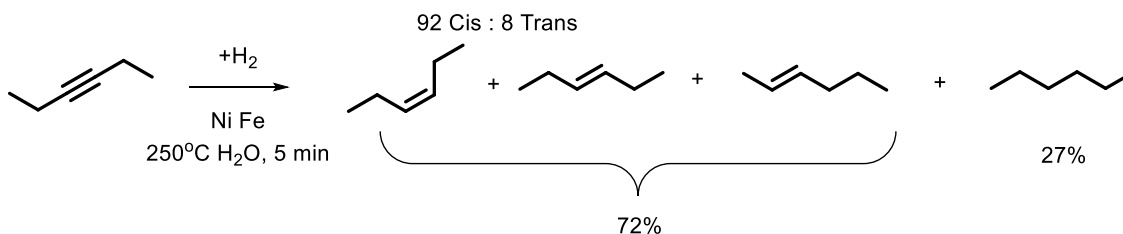


Figure 26. Reduction of 3-hexyne.

Few studies of substituent effects on heterogeneous catalytic reductions exist. Kw increases under hydrothermal conditions, so it was reasonable to consider protonation of the alkene in the reaction mechanism. Electron-transfer could also be invoked on the surface. Using styrene as the parent compound, a substituent effect study of the reduction of the vinyl group on nickel was performed (Figure 27). 4-Methoxy (4-OCH<sub>3</sub>) and 3-trifluoromethyl (3-CF<sub>3</sub>) substituents were used as electron-donating and withdrawing groups, respectively. The pseudo first-order rates of vinyl reduction to the ethylbenzene derivatives were compared. The rate of 4-OCH<sub>3</sub>-styrene reduction is nearly two-fold higher than that of the parent. 3-CF<sub>3</sub>-styrene also reduces faster than the parent, but slightly slower than 4-OCH<sub>3</sub>-styrene.

In terms of substituent effects, the differences in rates among the substituted styrenes are not large, suggesting there is no highly-charged transition state during the reaction. Another styrene reduction substituent effects study was performed with a

homogeneous catalyst, and the results indicated that there was a protonation/hydride transfer mechanism.<sup>156</sup> Hydride transfer is not likely in water, however, a Clemmensen-like protonation/electron transfer could have been a possibility since there is significant hydronium activity under hydrothermal conditions.<sup>157</sup> Since there is no evidence of a charged intermediate from these results, the mechanism does not likely involve proton/electron transfer. The mechanism is also not radical in character. The results of Dust and Arnold 1983 in analyzing the stability of benzyl radicals with respect to substitution show that a 3-CF<sub>3</sub> substituent should be destabilizing.<sup>158</sup> If this were the case, 3-CF<sub>3</sub>-styrene would reduce slower than the parent, which it does not. There are no coupling products observed in this reaction, which is another piece of evidence against a radical mechanism. The reduction rates of the substituted styrenes are no more than a factor of two larger than the parent. Generally, a true substituent effect causes larger than two-fold differences in rate.

It has been shown that the elementary hydrogenation steps in the Horiuti-Polanyi mechanism<sup>45</sup> can be characterized kinetically in the reduction of styrene on palladium nanoparticles.<sup>47</sup> The rate limiting step is insertion of the first hydrogen atom. Since the addition of substituents to styrene did not indicate a charged intermediate or radical, our findings suggest that the Horiuti-Polyani mechanism may be invoked. This is an area of heterogeneous catalysis mechanistic studies that should be expanded in the future.



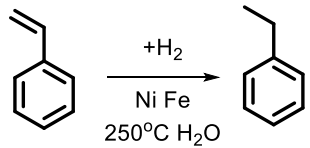
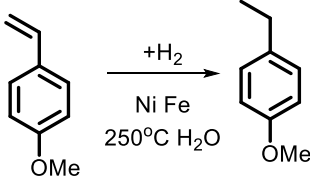
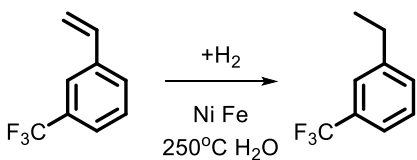
	$k$ ( $\text{min}^{-1}$ )	% Alkane
	$0.44 \pm 0.0060$	99%
	$0.75 \pm 0.0060$	99%
	$0.67 \pm 0.028$	93%

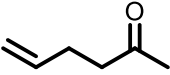
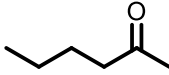
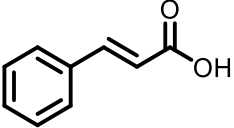
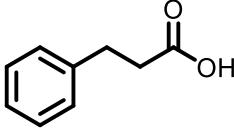
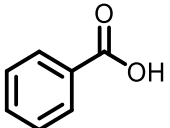
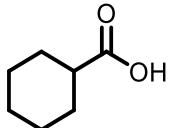
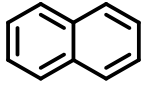
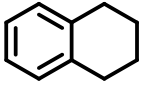
Figure 27. Reduction rates of styrene, 4-OCH<sub>3</sub>-styrene, and 3-CF<sub>3</sub>-styrene, as well as the abundance of the ethylbenzene product after 1 hour. Statistical errors calculated in Copasi.

### *Alkene and Aromatic Selectivity*

Nickel exhibited excellent selectivity for the reduction of alkenes over ketones and carboxylic acids with the reduction of 5-hexen-2-one, cinnamic acid (Table 7). After 1h at 250°C, 5-hexen-2-one reduced to 95% 2-hexanone, and 5% 2-hexanol, a follow-up reduction product of 2-hexanone. *Trans*-cinnamic acid was reduced to 83% hydrocinnamic acid in 15 minutes at 250°C, but with high selectivity, 97%. This is a particularly interesting reduction, because the alkene is conjugated to the ring and the carboxylic acid. One aromatic ring can be reduced in the presence of another in the case of naphthalene. 1,2,3,4-tetrahydronaphthalene (94%) was produced after 24 hours.

Benzoic acid was reduced to 49% cyclohexanecarboxylic acid, after 70 hours, demonstrating that an aromatic ring can be reduced in favor of a carboxylic acid. The yield of this reaction is less than the others. Nonetheless, the reduction of benzoic acid on nickel is noteworthy, as this particular ring reduction is generally observed only on Ru, Pd, and Rh catalysts.<sup>159-161</sup>

Table 7. Selective reductions. Starting compounds and the favored reduction product at 250°C in water, with nickel and iron.

Starting Compound	Major Product	Reaction Time	Selectivity <sup>a</sup> (%)	Yield <sup>b</sup> (%)
		1 hour	95	95
		15 min	97	83
		70h	70	49
		24h	98	94

<sup>a</sup> Defined as moles desired product out of all products.

<sup>b</sup> Moles of product collected out of moles starting material.

## Conclusion

Nickel is a useful catalytic surface for reduction of alkenes and alkynes under hydrothermal conditions. Simple alkenes and alkynes can be reduced on short time scales. The mechanism of hydrogen additions is mainly *syn*, but some *trans* isomers are made as primary products in all cases. The reduction of aromatic compounds is slow, but may be improved with a higher surface-area catalyst. There is no charged intermediate in the reduction, nor is it a radical mechanism. The reduction likely proceeds via a typical heterogeneous catalysis of hydrogen addition, and may follow the Horiuti-Polyani mechanism. Nickel is also a selective alkene reducing catalyst, and can effectively reduce an alkene in the presence of a ketone or a carboxylic acid. Increased reactivity and decreased selectivity are often observed at higher temperatures. Using an active, selective, catalyst, undesired side reactions can be avoided. These experiments have demonstrated the potential of green, aqueous reductions on Earth-abundant nickel, which has a low risk of shortage. Water is a non-toxic solvent which conveniently allows non-polar organics to separate post-reaction, making the work-up facile.

## 5. HYDROTHERMAL REDUCTION AND DEOXYGENATION OF CARBONYLS

### **Introduction**

Reduction of carbonyls to alcohols or alkanes is an important transformation in both industrial synthetic pathways, and the production of biofuels.<sup>162</sup> Typical methods for reduction of a ketone, aldehyde, or carboxylic acid, use hydride as the reductant.<sup>153,163-166</sup> Hydride compounds can be dangerous to handle, are not reusable, and produce large amounts of salts as waste.<sup>162</sup> Other reduction methods include Wolff-Kischner type reductions, and reductions using metals with liquid ammonia, both of which carry significant hazards.<sup>167</sup> Recent advances have been made in heterogeneous catalysis for carbonyl reduction, through the use of transition-metal nanoparticles and supported catalysts.<sup>168-172</sup> Nickel, and various nickel alloys, are well-known catalytic surfaces, and have been documented in numerous reports to reduce carbonyl compounds.<sup>147,167,169,173</sup> Nickel has the benefit of being cheaper and more Earth-abundant than the more rare transition metals that are often used as catalysts, such as palladium, platinum, rhenium and rhodium. Still, these expensive metals are frequently encountered as reduction catalysts.<sup>168,174-176</sup>

In this report, nickel nano powder, and Cu-Zn alloy nano powder, were used to reduce carbonyl compounds to alkanes or alcohols. Unlike supported catalysts or nanoparticles, the metal nano powders used in this study are commercially available and require no preparation prior to use. Furthermore, there is no ambiguity as to what role the support plays in the reduction. Cu-Zn alloy and materials comprised of Cu deposited on ZnO are known to reduce carbon monoxide and carbon dioxide.<sup>44</sup> Neither metal on its

own reduces carbon dioxide quite as well as the two combined.<sup>177-180</sup> We also find this to be true as well for carbonyl reduction in this study. This effect has been dubbed the “copper zinc synergy” in the literature.<sup>178,179</sup> There is evidence to suggest that copper on zinc oxide enhances the catalytic activity of the zinc oxide. By making oxygen vacancies even more electron-poor, the zinc oxide can accept electrons from an adsorbed species to form a strong bond.<sup>177</sup> Carbon monoxide has been observed to adsorb most strongly on Cu/ZnO/Zn, compared to Cu or Zn alone.<sup>181</sup> Cu-Zn reagents have been used in the past for other types of reactions aside from reduction; for example, the Simmons-Smith reaction.<sup>182</sup> This is the first report of this alloy as a reductant of ketones and carboxylic acids.

The reductions investigated here are performed under hydrothermal conditions in water, at 250°C, and 40 bar. There are numerous advantages of this technique. Water is a green solvent. Under hydrothermal conditions, organic compounds become more soluble in water as the dielectric constant decreases.<sup>6,7</sup> The organic products also separate from the water at room temperature, simplifying the isolation step. Since metallic iron is used as a water reductant, no molecular hydrogen is handled in the set-up of the reaction. Use of a sacrificial hydrogen donor for reduction reactions is common in the literature.<sup>147,183,184</sup> We have shown, in the previous chapter and in published results, that organics do not simply decompose under hydrothermal conditions, and that the reactions can be selective in the presence of certain metals and minerals.<sup>14,42</sup>

Nickel is applicable to biofuel generation, since it tends to reduce carbonyls all the way to alkanes. Cu-Zn alloy is more alcohol-selective, and could be used for

synthesis applications. This is not an unexpected result; in the reduction of carbon monoxide, nickel will produce methane, whereas Cu-Zn alloy will produce methanol.<sup>44</sup> Nickel reduces certain ketones more slowly than Cu-Zn alloy, and since the reactions are under hydrothermal conditions, dehydration of the resulting secondary alcohol begins to occur.<sup>32,60,62</sup> In the case of carboxylic acids, nickel will cleave the primary alcohol product to produce methanol, which undergoes further hydrogenolysis to methane. Nickel has been reported to reduce fatty acids to alkanes with zinc as the sacrificial donor in water at elevated temperatures,<sup>147</sup> but the mechanism is more thoroughly investigated in this report. Hydrogenolysis does not occur on Cu-Zn. This alloy can reduce acids to primary alcohols without secondary reactions decreasing the yield, including dehydration. E1 is the dominant mechanism of dehydration under hydrothermal conditions, so primary alcohols are quite stable.

The scope and behavior of nickel and Cu-Zn alloy in reduction of a range of carbonyl compounds are presented here. The mechanisms of ketone reduction on each metal were also investigated. Unlike reduction of alkenes, the mechanism of carbonyl reduction on metal surfaces is not well-understood, and multiple mechanisms have been proposed. The two-step hydrogenation mechanism proposed by Horiuti and Polanyi has been invoked in one case,<sup>168</sup> but has been refuted in another.<sup>185</sup> Some studies have demonstrated that solvent pH has a direct affect on the stereochemistry of the alcohol products from substituted cyclic ketones.<sup>157</sup> Radical-anion intermediates have also been invoked, particularly on Raney nickel, due to the formation of coupling products in significant quantities from phenyl ketones.<sup>157,185</sup> By using stereochemical probes, varying

the pH, and investigating substituent effects, this study finds that ketone reduction on nickel does not proceed via enol reduction and does not involve a charged intermediate. The ketone reduction mechanism agrees most with a hydrogenation mechanism like Horiuti-Polanyi.<sup>45</sup> Radical coupling products are not observed in any of our experiments. The ketone reduction mechanism on Cu-Zn is less clear, but could involve electron transfer. Summaries of yields of various carbonyl reductions are provided in Tables 8 and 9.

Table 8. Summary of carbonyl reductions with nickel and iron at 250°C.

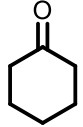

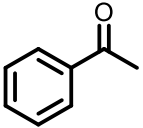
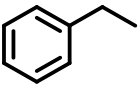
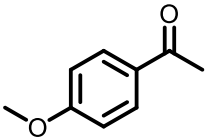
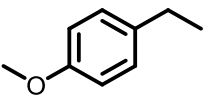
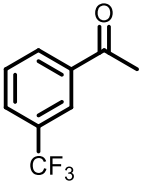
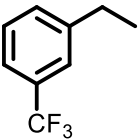
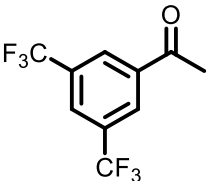
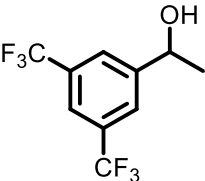
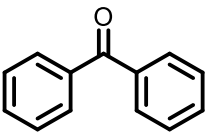
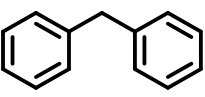
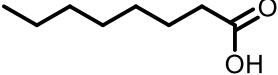

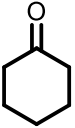
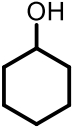
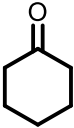
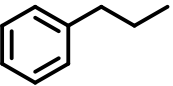
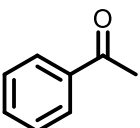
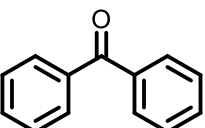
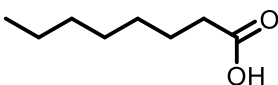
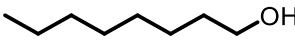
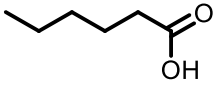
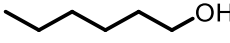
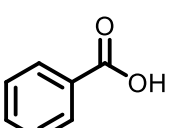
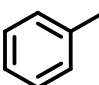
Starting Material	Major Product	Mol% Major Product	Reaction Time
		96	96h
		97	26h
		82	24h
		96	24h
		79	24h
		77	7h
		82	72h



Table 9. Summary of carbonyl reductions with Cu-Zn alloy and iron at 250°C.

Starting Material	Major Product	Mol% Major Product	Reaction Time
		86	4h
 	No Reaction	-	1h
	No Reaction	-	8h
	No Reaction	-	7h
		90	48h
		85	47h
		78	24h

## Methods

### *Chemicals Used*

For general methods of reaction preparation, extraction, and GC analysis, refer to Chapter 2. Nickel nano powder ( $\geq 99\%$  Ni basis) and Cu-Zn Alloy nano powder (56-60% Cu basis, 37-41% Zn basis) were purchased from Sigma-Aldrich. No further preparation, purification, or cleaning was performed for these metal powders.

### *NMR Experiments*

The Bruker 400 MHz NMR instrument in the Magnetic Resonance Research Center at Arizona State University was used for all NMR measurements. The NMR spectra, for the  $^{13}\text{C}$  labeled methanol Hydrogenolysis experiment were obtained using a custom  $^{13}\text{C}$  protocol. Locking was turned off for this experiment, as the solvent was  $\text{H}_2\text{O}$  (to avoid  $^{13}\text{C}$ -D coupling complications). The field strength,  $Z_0$ , was set to 0 for each experiment. The probe was tuned on  $^{13}\text{C}$ , then on  $^1\text{H}$ .  $^1\text{H}$  coupling was set to “Decoupled – NOE (Nuclear Overhauser Effect).” 256 scans with 120 second relaxation delay were performed.

Standard  $^1\text{H}$  NMR was used to analyze benzene from the cyclohexanone reduction. Samples were extracted into  $\text{CDCl}_3$  and analyzed on a Bruker 400MHz NMR. A standard 8-scan proton protocol was run.

### *Cavity Ring-Down Spectroscopy*

As a qualitative test,  $^{13}\text{C}$  labeled methane was measured by cavity ring-down Spectroscopy from the  $^{13}\text{C}$  labeled methanol hydrogenolysis experiment with nickel and iron. A piece of tygon tubing, plugged at both ends with rubber septa, was used for both

opening the tube and containing the gas. The volume of the silica tube headspace was estimated to be 200  $\mu\text{L}$ . The volume of the tygon tubing was 47 mL. Opening the tube resulted in a dilution by a factor of approximately 235. After snapping opening the tube inside the tygon tubing, the gas inside (assumed to be equilibrated between the water phase and gas phase) was diluted 0.5 mL into 20 mL before injecting on the Picarro G2201-i CRDS Analyzer (Goldwater Environmental Laboratory at Arizona State University). Blanks consisting of the gas inside the tygon tubing without the opened tube were also analyzed. A trace amount of methane was detected in the blanks, and it was mostly  $^{12}\text{C}$ . The instrument was calibrated using 500 ppm  $\text{CH}_4$ /2010 ppm  $\text{CO}_2$  standards (Air Liquide, Inc.) with  $^{13}\text{C}$  ratios of methane  $-69\pm 1\%$ ,  $-36\ 1\%$ , and  $+5\pm 1\%$ .

## **Results and Discussion**

### *Ketone Reduction*

As a simple model ketone, cyclohexanone was reduced in the presence of nickel and iron, and Cu-Zn alloy and iron, at 250°C and 40 bar in water. The general pathway of this reduction is shown in Figure 28. The ketone is first hydrogenated to an alcohol, then the alcohol dehydrates to an alkene. Although the reaction takes place in 55 molal water, entropy has a greater impact at elevated temperatures, and dehydration occurs readily. We demonstrated in previous work that secondary alcohols under hydrothermal conditions dehydrate primarily E1 (See Ch. 3). Once the alkene is formed, it is reduced to an alkane. The reduction of cyclohexanone all the way to cyclohexane takes 96 hours for nickel and iron, and 125 hours for Cu-Zn alloy and iron. In the case of nickel, the limiting

step in the reduction is the reduction of the carbonyl. Once cyclohexene forms, it is rapidly reduced to cyclohexane. Benzene, which can elute at the same GC retention time as cyclohexane, was not detected by NMR at 96 hours. If benzene is formed at earlier times, it is fully consumed by 96 hours. Cyclohexene does not build up in concentrations larger than 10 mol% at all times (Figure 29). By contrast, Cu-Zn alloy reduces the ketone faster than it can reduce the alkene. Cyclohexanol reaches a maximum of 86 mol% after 4 hours (Figure 30). In principle, the reaction could be stopped at this time if an alcohol were the desired product. The yield of cyclohexanol in the reduction with nickel is never high enough for it to be a synthetically useful pathway to form an alcohol from a ketone. Cyclohexene does build up as the dehydration of cyclohexanol proceeds, demonstrating that Cu-Zn alloy does not reduce alkenes as fast as nickel.

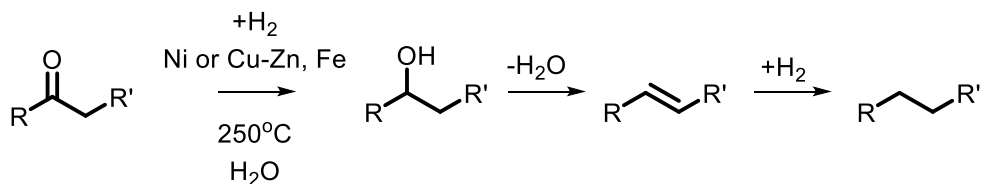


Figure 28. The general reaction of ketones to alkanes in the presence of nickel, or Cu-Zn alloy at longer times.

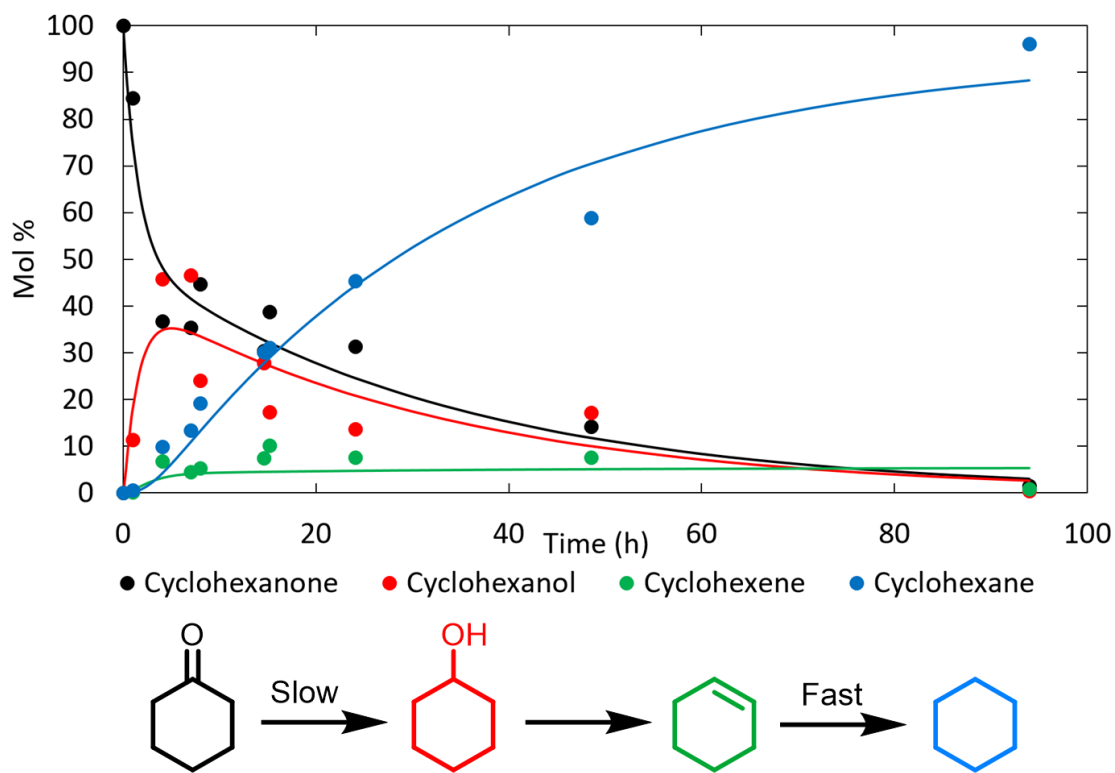


Figure 29. A time series of measured products from the cyclohexanone reduction pathway, in the presence of nickel and iron, 250°C. Cyclohexanone is first reduced to cyclohexanol. Cyclohexanol dehydrates to cyclohexene, which is reduced to cyclohexane. The fast step in this pathway is the alkene reduction, as indicated by the constant low abundance of cyclohexene. Curves drawn through the data points are included to guide the eye.

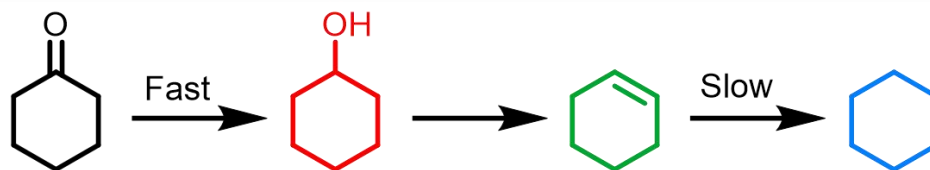
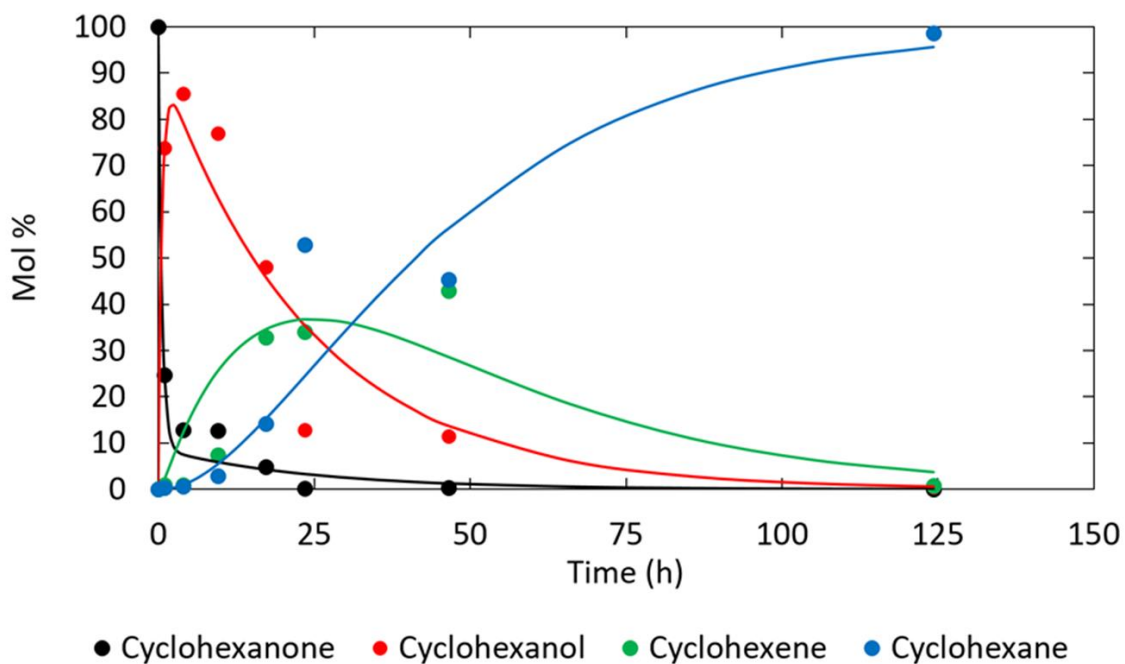


Figure 30. A time series of measured products from the cyclohexanone reduction pathway, in the presence of Cu-Zn and iron, 250°C. Cyclohexanone reduction on Cu-Zn alloy follows the same general pathway as the reduction on nickel, but the carbonyl reduction step is much faster, while the alkene reduction is slower. Curves drawn through the data points are included to guide the eye.

### *Carboxylic Acid Reduction - Nickel*

Octanoic acid was used as a model fatty acid. Nickel reduced the acid to 1-octanol, which is eventually consumed to produce heptane as the major product (Figure 31 and 32). The pathway from 1-octanol to heptane is C-C hydrogenolysis, a surface-catalyzed reduction which has been observed on metal surfaces.<sup>186,187</sup> A recent report also observed loss of a carbon atom in the reduction of fatty acids on nickel.<sup>147</sup> C-O hydrogenolysis to form octane also occurs, but to a lesser extent. Octane concentrations remain less than 5 mol% at all times. By observing the time dependencies of the products of octanoic acid, it was determined that heptane forms exclusively from hydrogenolysis, and not decarboxylation.

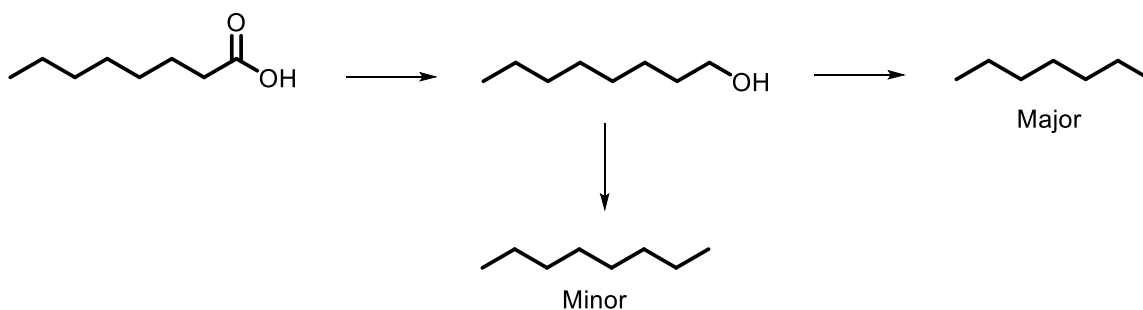


Figure 31. The reduction of octanoic acid in the presence of nickel and iron at 250°C, in H<sub>2</sub>O. The reduction of octanoic acid on nickel, produces 1-octanol as a transient species, and heptane and octane as hydrogenolysis products.

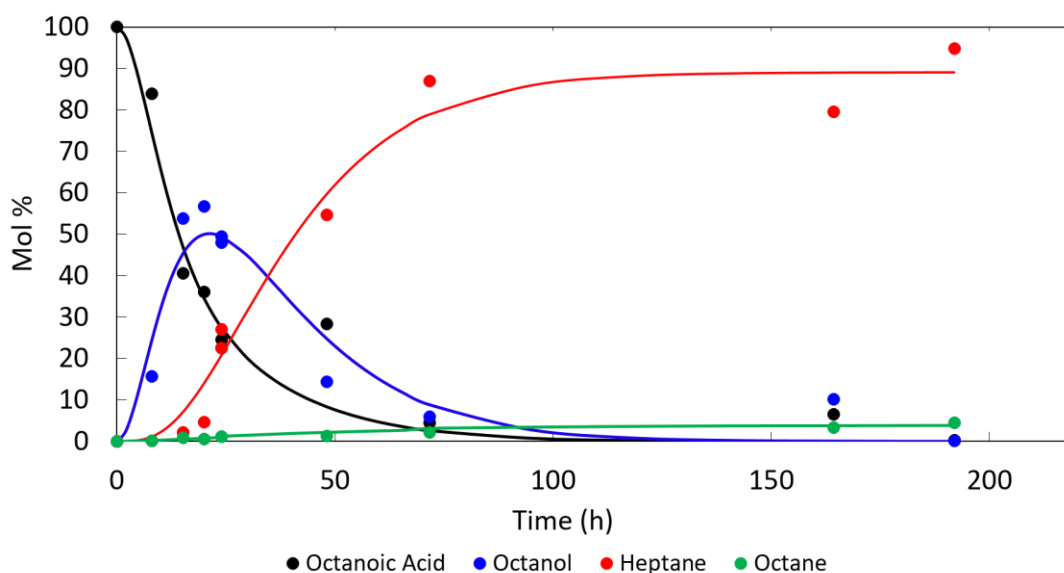


Figure 32. Time series of octanoic acid reduction with Nickel and Iron at 250°C. Octanoic acid reduced to octanol, which reached a maximum abundance near 24h. Heptane exhibits an induction period before becoming the major reduction product. Octane remains a minor product throughout the reaction. Drawn curves included to guide the eye.

1-Octanol was found to reach a maximum concentration at approximately 24 hours before decaying. Heptane has a distinct induction period lasting about the same time scale. If heptane were the result of decarboxylation, the induction period would be nonexistent. Heptane is the major hydrogenolysis product at all times. A C-C sigma bond is weaker than a C-O sigma bond in terms of homolytic bond dissociation energy.<sup>188</sup> The  $\sigma$ -bond between carbons 1 and 2 in 1-octanol is also expected to be the weakest, since electron density is pulled toward the oxygen atom. Therefore, it is the most likely to dissociate and make bonds to the metal surface during the hydrogenolysis step.



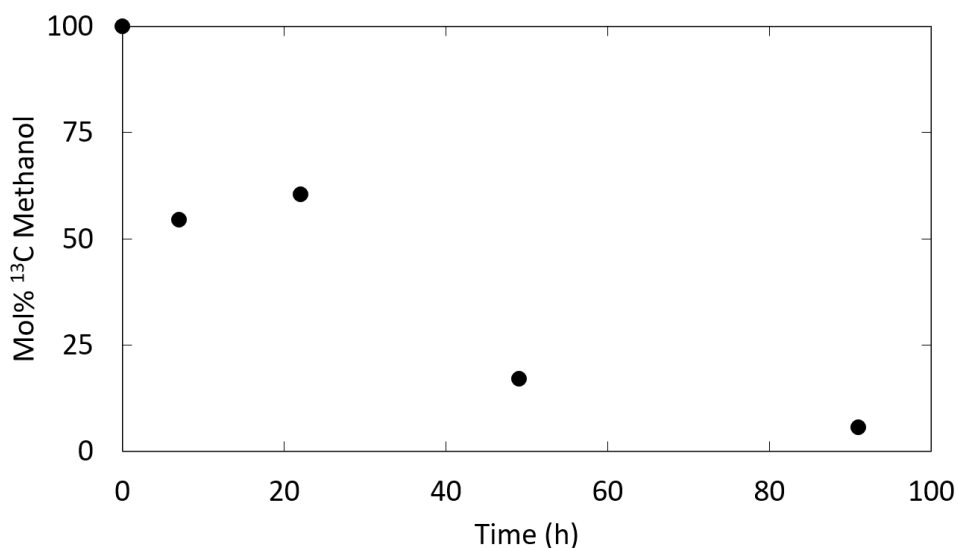


Figure 33. <sup>13</sup>C labeled methanol hydrogenolysis, with nickel and iron, 250°C. Methanol decays with time as it undergoes hydrogenolysis to methane.

Methanol was expected to be a hydrogenolysis product from 1-octanol. However, since methanol is miscible with water, it is difficult to extract with DCM and analyze by GC. A separate experiment starting with <sup>13</sup>C-labeled methanol, using the same conditions and reagents, was performed, and analyzed by <sup>13</sup>C NMR. Indeed, methanol decreases with time (Figure 33). No other signals appeared in the NMR spectra with time, so it was likely that methanol was undergoing hydrogenolysis to methane. As a qualitative test, the gases from an 18 hour <sup>13</sup>C methanol/Ni experiment were analyzed with cavity ring-down spectroscopy, to measure the amount of <sup>13</sup>C methane vs <sup>12</sup>C methane. Methane measured in the gas inside the silica reaction vessel was  $1.2 \times 10^5$  ‰  $\delta^{13}\text{C}$ , providing strong evidence for hydrogenolysis of labeled methanol to labeled methane.

### Carboxylic Acid Reduction – Cu-Zn Alloy

Cu-Zn alloy can reduce carboxylic acids on timescales similar to those of nickel, but C-C hydrogenolysis of the primary alcohol product does not occur. Octanoic acid was reduced to 1-octanol, with octyloctanoate formed as a minor product (Figure 34). This ester is not observed in the nickel reduction, since 1-octanol does not exist long enough for it to react with octanoic acid. Hexanoic acid was also reduced to 1-hexanol (Table 9). The only hydrogenolysis occurring in experiments using Cu-Zn was with benzoic acid (Table 9). Benzoic acid reduces to benzyl alcohol, which is then reduced to toluene via C-O hydrogenolysis. This is likely a special case, as the substrate is benzylic.

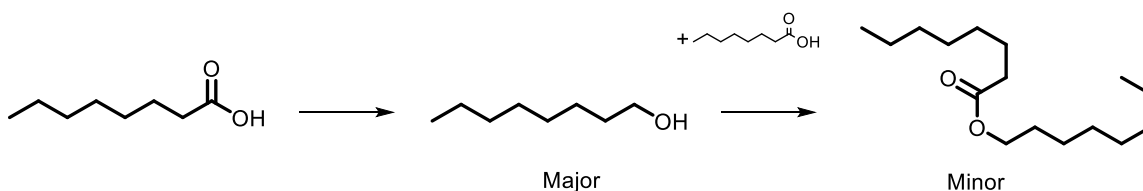


Figure 34. The reaction pathway of octanoic acid reduction, using CuZn+Fe at 250°C. 1-Octanol is the major product, with minor amounts of octyloctanoate.

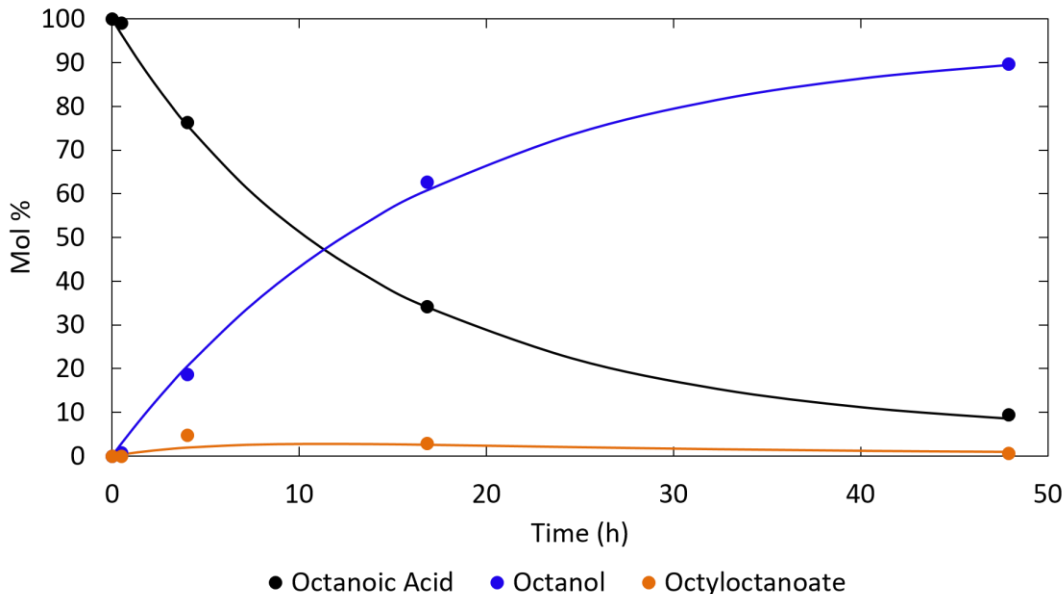


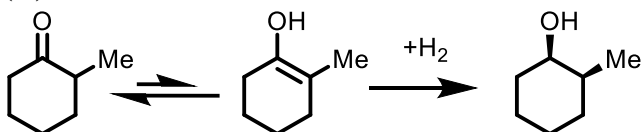
Figure 35. Time series of products formed in the reduction of octanoic acid, using Cu-Zn and Iron, at 250°C. No hydrogenolysis products were observed. Since the acid and alcohol are present at all times, some octyloctanoate forms. Curves included to guide the eye.

### *Mechanistic Considerations*

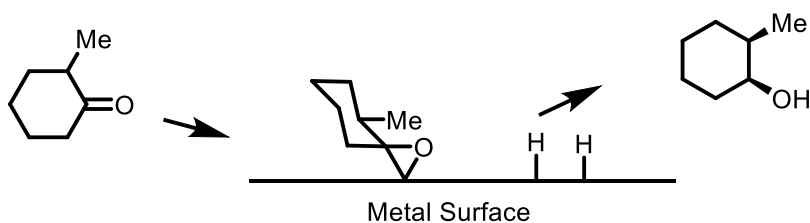
The mechanisms of carbonyl reduction were examined for both nickel and Cu-Zn alloy. Stereochemical probes were used to determine the nature of hydrogen addition to the carbon-oxygen double bond, and a substituent effect study was performed to determine if any build-up of charge occurred during the reduction. Possible mechanisms that were considered were enol reduction, the Horiuti-Polanyi mechanism, and a radical-anion mechanism (often invoked for Clemmensen-like reductions). The mechanisms probed are shown in Figure 36.

Figure 36. The three possible mechanisms of ketone reduction on a metal surface that we considered in this study. Shown are three possible mechanisms that were explored in this study. (A) Reduction of the enol form of 2-methylcyclohexanone should yield *cis*-2-methylcyclohexanol as the major product, since it is an analogue for 1,2-dimethylcyclohexene. Similarly, in the Horiuti-Polanyi mechanism (B), the *cis* should also be favored as a *syn* addition product.<sup>48</sup> The substituent is held in the equatorial conformation, while the carbonyl preferentially binds in the axial position. The result is the *cis* isomer. (C) In the radical anion mechanism, the surface donates a single electron to the partial positive charge in the carbonyl. From there, the intermediate can make a bond to the metal surface and undergo protonation/hydrogenation to form the alcohol.<sup>185</sup> If the ketone is bound to a phenyl ring, radical coupling products can form.

**(A) Enol Reduction:**



**(B) Horiuti-Polanyi:**



**(C) Radical Anion:**

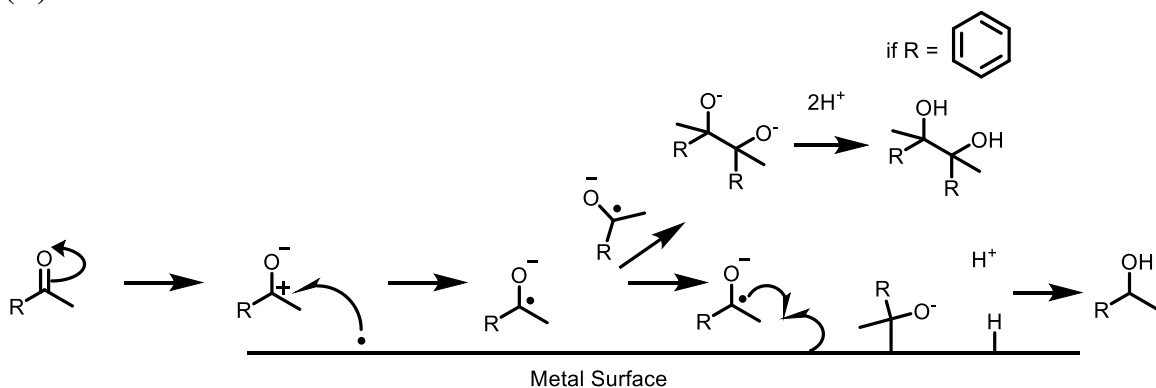


Table 10. A summary of ketone reduction stereochemistry in the presence of nickel and iron (250°C). Isomer quantities reported as a ratio relative to one another.

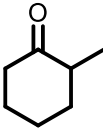
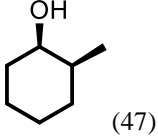
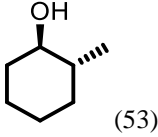
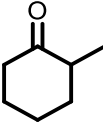
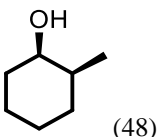
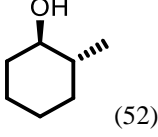
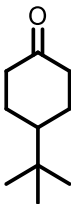
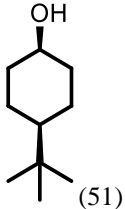
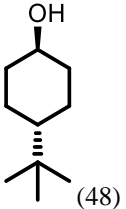
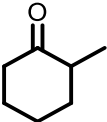
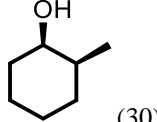
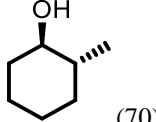
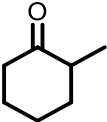
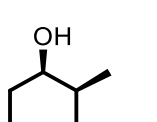
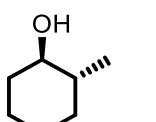
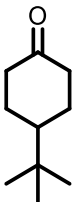
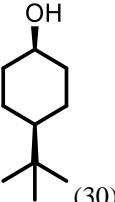
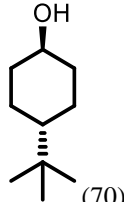
Starting Material	Cis Product (Mol %, rel)	Trans Product (Mol%, rel)	Time	Conversion
	 (47)	 (53)	30 min	26
 (pH 4, HCl)	 (48)	 (52)	30 min	26
	 (51)	 (48)	5 min	14

Table 11. A summary of ketone reduction stereochemistry in the presence of nickel and iron (250°C). Isomer quantities reported as a ratio relative to one another.

Starting Material	Cis Product (Mol %, rel)	Trans Product (Mol%, rel)	Time	Conversion
	 (30)	 (70)	30 min	64
 (pH 4, HCl)	 (22)	 (78)	30 min	10
	 (30)	 (70)	5 min	14

A series of substituted cyclohexanones were used as stereochemical probes to elucidate the mechanism of carbonyl reduction on nickel and on Cu-Zn alloy. Nickel reduces C=C bonds very quickly, but was slower to reduce the C=O bond in cyclohexanone. Therefore, one possibility for the mechanism was enol reduction. Perhaps, nickel was actually reducing the fleeting enol species, and this contributed to the relatively slow carbonyl reduction kinetics. It is known from previous experiments (Chapter 4) with 1,2-dimethylcyclohexene, that nickel adds hydrogen across the double bond in a *syn* fashion, and produces more *cis*-1,2-dimethylcyclohexane than *trans*. Therefore, if reduction of 2-methylcyclohexanone occurred through the enol, *cis*-2-methylcyclohexanol would be the major product. This was not observed, however. Nickel produced nearly 50:50 *cis* and *trans*-2-methylcyclohexanol in a 30 minute experiment at

250°C (Table 10). 26% conversion of the ketone was achieved in this time (Table 10). It was possible that more *cis* was produced at early times, then quickly isomerized to the more stable *trans* product. This was ruled out with a 30 minute experiment starting with *cis*-2-methylcyclohexanol, that only produced 2 mol% *trans* relative to the amount of remaining *cis* – not enough to account for the amount of *trans* generated from 2-methylcyclohexanone. As additional evidence against an enol reduction, benzophenone was reduced to diphenylmethane on nickel, as benzophenone cannot form an enol tautomer (Table 8). 4-*t*bu-Cyclohexanone was also tested as a stereochemical probe. Similar to 2-methylcyclohexanone, nearly equal amounts of *cis* and *trans*-4-*t*bu-cyclohexanol were produced from the ketone experiments using nickel.

Cu-Zn alloy produced a different ratio of *cis* to *trans* isomers in the reduction of the substituted cyclohexanones compared to nickel (Table 11). For both 2-methylcyclohexanone and 4-*t*bu-cyclohexanone, the *trans* product was favored, 70:30 compared to the *cis* (Table 11). The difference in isomer ratios is indicative of different mechanisms on Cu-Zn vs nickel surfaces. The Horiuti-Polanyi mechanism is expected to yield mainly the *cis* isomers from these two ketones.<sup>48</sup> However, the literature does not agree in all cases, or across metal surfaces. For example, the 1973 study Mitsui et al.<sup>48</sup> observed *cis*-4-*t*bu-cyclohexanol as the major product from the reduction of 4-*t*bu-cyclohexanone on Raney Nickel, while a more recent study<sup>189</sup> observed the *trans* isomer as the major product, also on Raney Nickel. It has also been proposed that the stereochemistry of ketone reduction on metal surfaces is affected by the pH of solvent, and that this is evidence against a standard hydrogenation mechanism; specifically, that a

decrease in pH should result in more axial (*cis*) product.<sup>157</sup> Decreasing the pH of the water to pH 4 using HCl (at 250°C; neutral is pH 5.6)<sup>11</sup> did not affect the ratio of *cis* to *trans*-2-methylcyclohexanols in the reduction of 2-methylcyclohexanone on nickel. On Cu-Zn alloy, the ratio changed only slightly, to favor the *trans* isomer. The overall conversion of the reaction was also unchanged on nickel. Conversely, conversion of 2-methylcyclohexanone on Cu-Zn alloy was diminished at pH 4 HCl compared to water alone (pH 5.5 at 250°C). It is possible that the decreased pH resulted in more oxidation of the surface, and subsequent deactivation. Cu-Zn alloy did not reduce benzophenone in 7 hours (Table 9). While this could indicate enol reduction, Cu-Zn was also found to not reduce other ketones when phenyl rings are present. This indicates a difference in adsorption strengths. Two possible reasons for this is the increased number of d-electrons in copper and zinc compared to nickel, and the larger electron density found in an aromatic ring compared to a ketone. These factors could lead to a stronger orbital overlap on the surface, and thus a stronger bond.

Another proposed mechanism for ketone reduction on metal surfaces involves a charged intermediate, possibly a radical anion.<sup>157,185</sup> Evidence for this mechanism includes the formation of radical coupling products, particularly in aromatic ketones. Often, these products are in the form of pinacols. Such products were not found in any of the ketone reductions on nickel or on Cu-Zn alloy. To determine if a similar mechanism involving a charged intermediate was occurring, a substituent effect study was performed using acetophenone as the parent compound. Unfortunately, Cu-Zn alloy did not reduce acetophenone at all in a 24 hour timescale. A substituent effects study was not performed



for Cu-Zn as a result. The lack of acetophenone reduction was attributed to the phenyl ring having a stronger affinity for the surface than the carbonyl, i.e., cyclohexanone cannot be reduced on Cu-Zn alloy if an aromatic compound, such as propyl benzene, is present (See table 9). A substituent effect study using substituted benzoic acids with Cu-Zn was performed instead, since benzoic acid can be reduced. Benzoic acid, p-Toluic acid and 3-fluorobenzoic acid were reduced on a 4.5h timescale, and conversions were compared. 28%, 20% and 20% conversion were observed for each compound, respectively. Therefore, no significant substituent effect was observed, thus, there is no charged intermediate in the rate limiting step of the carboxylic acid reduction on Cu-Zn. Substituted benzoic acids were not reduced on nickel, since nickel was observed to reduce the benzene ring of rather than the carboxylic acid functional group (Chapter 4).

Several substituted acetophenones were reduced on nickel, in the presence of iron and water, at 250°C and 40 bar. The reductions generally followed the pathway in Figure 28. It was found that both electron donating (4-OCH<sub>3</sub>) and withdrawing groups (3-CF<sub>3</sub>, 3,5-di-CF<sub>3</sub>) decreased the rate of ketone reduction (Figure 37). If a negatively charged intermediate had formed, as proposed in the literature, electron withdrawing substituents should have enhanced the reduction rate. This was not the case. Since the unsubstituted acetophenone reduced the fastest, it was concluded that the decrease in rate across all substituted acetophenones may simply be a steric effect. In a previous study of the reduction of substituted styrenes on nickel under hydrothermal conditions, there was no evidence of a charged intermediate (Chapter 4). Based on results from stereochemical probes in that study, it was determined that a standard surface-catalyzed hydrogenation

mechanism can be invoked. Therefore, the same could be true for the reduction of carbonyl compound on nickel under the same conditions. It is interesting to note that the 3,5-di- $\text{CF}_3$ -acetophenone produced 3,5-di- $\text{CF}_3$ -(1-phenylethanol) as the major product, rather than the alkane product, even after 24h (Table 8). The presence of two electron withdrawing groups clearly prevents dehydration of the alcohol.

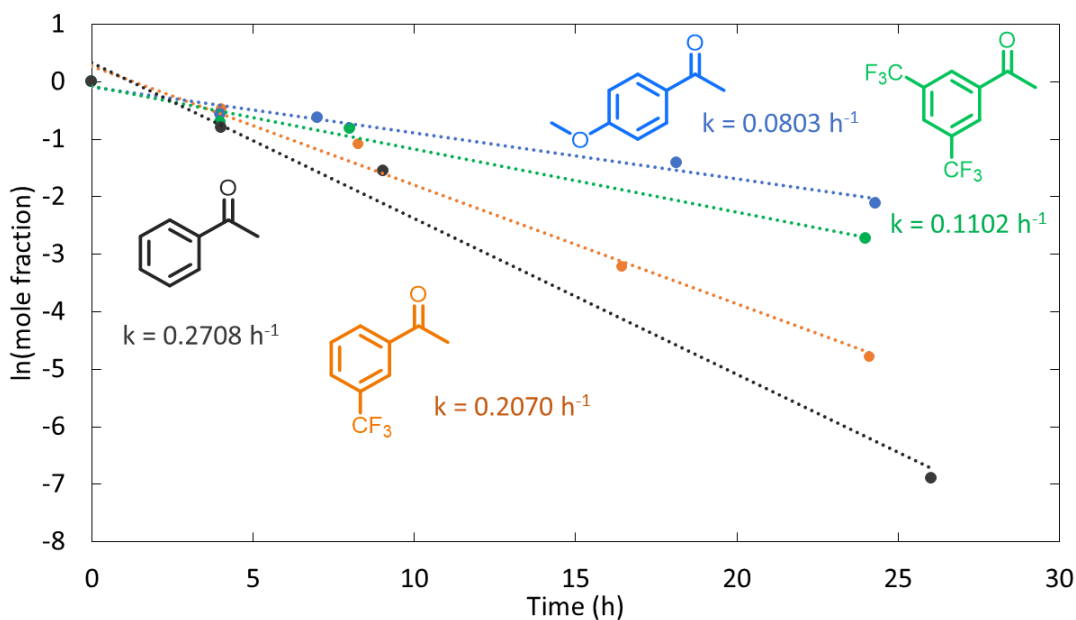


Figure 37. The natural log of mole fraction of each substituted acetophenone with time, with nickel and iron at 250°C. First-order kinetic fitting of the disappearance of substituted acetophenones. No clear substituent effect that would suggest a charged intermediate is involved. A decrease in observed rate relative to the parent across all substituted acetophenones could point to a steric effect.

The results of this mechanistic analysis are not definitive for any of the three mechanisms that were proposed. The enol reduction can be ruled out for nickel, since benzophenone can be reduced on nickel. Nickel also did not produce mainly *cis* product from 2-methylcyclohexanone or 4-*t*bu-cyclohexanone, which is claimed to be expected for a Horiuti-Polanyi like mechanism. However, even this observation is inconsistent in

the literature for different studies using the same metal surfaces. There was also no evidence of charge build-up in the acetophenone substituent effect experiments. Therefore, standard surface catalyzed hydrogenation is most likely for nickel. It is interesting to note that nickel produces nearly 50:50 ratio of *cis:trans* isomers from 2-methylcyclohexanone and 4-*tbu*-cyclohexanone. This could indicate that these ketones are standing upright on the surface, and that hydrogen adds equally from either side of the molecule. If the ring were parallel to the surface, more *cis* product would result from 4-*tbu*-cyclohexanone. Due to the position of the bulky *tert*-butyl group, it would be impossible for the molecule to assume a *trans* configuration, if *syn* addition were occurring.

Enol reduction also seems to be an unlikely pathway on Cu-Zn. While the benzophenone reduction was inconclusive in this regard, Cu-Zn produces mostly *trans* product from both cyclic ketones. *Syn* addition across the enol would result in more *cis*. A different reduction mechanism is occurring on Cu-Zn than nickel, based on the strong preference for *trans* products, rather than the 50:50 mixtures of *cis* and *trans* isomers obtained on nickel. Evidence for a charged intermediate for ketone reduction could not be obtained because aromatic rings tend to prevent the reaction on Cu-Zn. The preference for *trans* product may suggest an intermediate where formation of the lowest energy isomer is favored. Electron transfer could also be occurring, but may not be involved in the rate limiting step. Reduction of substituted benzoic acids revealed that there is no evidence of a charged intermediate that influences reduction rate, at least for the carboxylic acids studied here. Since the Cu-Zn surface oxidizes (Appendix A) during the

experiment, it makes its role as catalyst or reagent rather ambiguous. Cu-Zn can reduce cyclohexanone and octanoic acid without iron present (Table 12), but including iron increases the conversion substantially.

Table 12. Experimental results for all metal powders, using cyclohexanone and octanoic acid as model substrates.

Organic	Metal(s)	Time (h)	% Conversion
Cyclohexanone	Ni+Fe	1	17
	Cu	4	1
	Zn	4	2
	Cu-Zn alloy	1	47
	Cu-Zn alloy + Fe	1	75
Octanoic Acid	Ni+Fe	48	72
	Cu	48	0
	Zn	48	2
	Cu-Zn alloy	48	23
	Cu-Zn alloy + Fe	48	90

## Conclusion

The scope and mechanisms of carbonyl reduction on two metal surfaces under hydrothermal conditions were explored. It was determined that, in the case of ketone reduction on nickel, a standard Horiuti-Polanyi hydrogenation is the most probable mechanism. The ratio of isomers produced was unaffected by pH, and a substituent effect study concluded that a charged intermediate was not present in the mechanism. Nickel is selective for alkanes in the reduction of carboxylic acids. Primary alcohols, which cannot dehydrate easily, are cleaved to make an alkane and methanol. Methanol then reduces to methane. Unlike other biofuel generation methods, that rely on decarboxylation, the lost carbon atom in this case is more useful, and reduction of CO<sub>2</sub> is unnecessary. While hydrogenolysis is an active pathway on nickel, there are surface preparation methods that can be applied to prevent it if a primary alcohol is desired. Hydrogenolysis occur more rapidly on “stepped” crystalline metal surfaces – on edges, and vertices, rather than on flat surface.<sup>44,187</sup> Sulfur atoms can be adsorbed along edges of the metal surface to deactivate those sites.<sup>44</sup> Although a preparation such as that one was not attempted in this study, it is a possible future direction for nickel catalyzed reduction of carboxylic acids.

The carbonyl reduction mechanism on Cu-Zn alloy is still unclear. Its strong preference for *trans* isomers in the reduction of substituted cyclohexanones suggests the mechanism is not standard hydrogenation. Additionally, the ratio of isomers and conversion were slightly affected by decreasing the solvent pH. It is possible that zinc is donating electrons to the organic molecule as the metal oxidizes, much like in the

Clemmensen reduction.<sup>157</sup> In other reports, catalytic activity is observed with unoxidized copper on zinc oxide.<sup>44,178,179</sup> The mechanism and catalytic activity of Cu-Zn alloy, and other Cu-Zn catalysts, are not well understood yet. Alloys in particular, are not well understood as catalysts.<sup>190</sup> Cu-Zn compounds should be further explored as carbonyl reduction catalysts because copper and zinc are less expensive and more earth-abundant than other typical transition metals. Despite zinc becoming oxidized, the reductions presented on Cu-Zn alloy are a good example of a green, hydride-free carbonyl reduction. A green, solar-powered method to reduce the oxidized zinc has been proposed.<sup>191,192</sup> There may also be the possibility for using a Cu/ZnO type catalyst in these conditions, and avoiding oxidation of the zinc entirely, but this would be a supported catalyst rather than a true alloy. It is also possible that a different ratio of copper to zinc, either as an alloy, or a supported catalyst, may have increased activity.

## 6. HYDROTHERMAL DEHYDRATION AND HYDROGENOLYSIS OF POLYOLS

### **Introduction**

With global climate change due to fossil fuel-derived CO<sub>2</sub> becoming an imminent problem, alternative fuels are being sought to replace petroleum products. Petroleum is also in limited supply, which poses a challenge for sourcing solvents and fine chemicals that are typically isolated from oil.<sup>176</sup> Biomass deoxygenation is a possible solution for both problems, since it can be a carbon-neutral process if performed efficiently, and could replace many petroleum products.<sup>193</sup> Ideally, the biomass used for fuel production would be from algae or waste rather than from potential food sources.<sup>194</sup> Biomass processing can go through one of several routes: Gasification to form CO and H<sub>2</sub>, which can be reacted to produce methanol, or undergo Fischer-Tropsch to form alkanes; pyrolysis to form bio-oil, which must then be refined; or hydrolysis to form monosaccharides, which can be fermented to ethanol, or undergo further processing to form alkanes or aromatics.<sup>55</sup>

There is current research interest under hydrothermal liquefaction (HTL) of algae or lignocellulosic biomass.<sup>193,195,196</sup> Hydrothermal processing is an attractive option, as water is an eco-friendly solvent, simplifies the isolation of hydrophobic products, and has properties that can be modulated simply by changing the temperature, such as pH and the dielectric constant.<sup>7,197</sup> Organic carbon, when buried, and exposed to high temperatures and pressures in the presence of water and clay minerals, can eventually form petroleum.<sup>34</sup> Biomass hydrothermal processing research seeks to enhance the rate and efficiency of this natural process. Crude bio-oil can be prepared from biomass HTL,

using only water as a solvent and reagent.<sup>195</sup> High temperature water can hydrolyze cellulose to monosaccharides, dehydrate sugars to form furans, perform retro-Claisen condensation and retro-Michael additions, and produce alkanes from fatty acids.<sup>195-198</sup> However, HTL processing can produce char material, that has limited utility, and can result in the formation of many organic products, some of which still contain oxygen atoms post-processing. Increasing selectivity, and breaking C-O bonds in biomass processing are two major obstacles that must be overcome in order to make biomass HTL a viable option.

The cleavage of C-O bonds under hydrothermal conditions can also be addressed, since alcohols are known to dehydrate readily in high temperature water.<sup>32,35</sup> Alcohols are an abundant functional group in lignocellulosic biomass; saccharides can compose up to 90% of the raw starting material.<sup>55</sup> Sugars, such as glucose, can be dehydrated in high temperature water to form hydroxymethylfurans<sup>197</sup> or aromatic compounds.<sup>55</sup> Many side products can form from dehydrating polyols.<sup>198</sup> Additionally, it is impossible to synthesize alkanes from sugars without a reducing agent. Some studies aim to reduce and deoxygenate sugars as the starting structure,<sup>54,198</sup> while others begin by cleaving the sugar into glycols, and performing a second reduction of the individual glycols to methane, ethane, methanol, or ethanol.<sup>194,199,200</sup> In general, including a metal catalyst and either hydrogen or a sacrificial electron donor in these reactions increases the yield of alkanes or smaller alcohols.<sup>194,195</sup>

Current reduction/deoxygenation catalysts are often composed of exotic, rare, metals or metal alloys.<sup>54,56,186,194,199</sup> Platinum or rhenium catalysts on carbon can convert



sugars into aliphatic carboxylic acids, mono-ols, and ketones.<sup>54</sup> Ruthenium has also produced favorable results as a homogeneous catalyst in reductive deoxygenation reactions.<sup>56,121</sup> Various nickel catalysts, including Raney Nickels,<sup>201</sup> Ni-La,<sup>199</sup> NiMoS<sub>2</sub>,<sup>202,203</sup> and Ni-Si<sup>204</sup> have been employed to perform reduction or deoxygenation reactions. Nickel is less expensive than most second-row transition metals, and has been shown to have comparable activity to platinum in some cases.<sup>55</sup> The best-case scenario for sugar reduction and deoxygenation would be a one-pot method with tandem (a catalyst that can perform more than one type of reaction) or tandem-orthogonal (two catalysts with different utilities) catalysis, using Earth-abundant materials, to limit the number of steps and overall cost.<sup>205</sup>

One focus of this report is the 1,2-cyclohexanediols, that have been commonly used as sugar models in past studies. These represent the vicinal diols found in cellulosic biomass. A current challenge is deoxygenating *trans*-1,2-cyclohexanediol in particular, which has proven to be unreactive in the presence of a variety of catalysts and reaction conditions.<sup>121,132,206-208</sup> This *trans* diol has even been observed to poison a homogeneous rhenium catalyst.<sup>121</sup> Most cases where *trans*-1,2-cyclohexanediol is shown to be unreactive are attempts to dehydrate the diol. Perhaps, a better mechanism would be C-O hydrogenolysis, that can take place on heterogeneous metal catalysts.<sup>194,209,210</sup>

Understanding the mechanisms of deoxygenation and dehydration of smaller “sugar model” compounds can provide necessary insights on potential mechanistic or kinetic challenges when starting from bulk biomass. It is important to consider the reactions that take place in water in absence of a catalyst, as these aqueous phase

reactions can still occur when the catalyst is present. Nickel nanopowder was used as a catalyst in this investigation, with iron as a sacrificial donor for in-situ hydrogen production from water. 1,2 and 1,4-cyclohexanediols of varying stereochemistries were deoxygenated in water alone, and in the presence of nickel, under hydrothermal conditions. 1,4-Cyclohexanediols have been studied much less in regard to biomass deoxygenation, but still represent a relevant functional group in cellulosic biomass. The stereochemistry of the diols, as well as intermolecular hydrogen-bonding, can affect the dehydration rates, mechanisms, and product distributions. *Myo*-inositol, a common sugar model in the literature, was also fully deoxygenated and reduced to cyclohexane using nickel and iron under hydrothermal conditions.

## **Methods**

### *Chemicals Used*

The *cis*-1,2-cyclohexanediol, *trans*-1,2-cyclohexanediol, and *myo*-inositol were purchased from Sigma-Aldrich. 3-Cyclohexen-1-ol was purchased from Aldlab. *cis*-1,4-cyclohexanediol, and *trans*-1,4-cyclohexanediol were purchased from TCI. All were used without further purification. The starting concentrations of these were 0.1-0.15 molal. *Myo*-inositol was purchased from Sigma-Aldrich. The starting concentration of *myo*-inositol was 0.05 molal, to avoid potential bimolecular reactions and polymerization. Quantification of the diols was done using DCM-water extraction calibration curves, to correct for the solubility of these compounds in water.

### *Benzene and Cyclohexane Quantification*

Benzene and cyclohexane are inseparable by GC. To determine how much of the cyclohexane peak observed by GC is really benzene, NMR analysis was performed on a single timepoint for relevant experiments. For these samples, CDCl<sub>3</sub> was used as the extraction solvent. A standard <sup>1</sup>H spectrum was taken. Integrals of the benzene and cyclohexane singlets were used to calculate a ratio. The integrals were normalized to account for the benzene singlet (7.35 ppm) representing 1H while the cyclohexane singlet (1.41 ppm) represents 2H. Benzene that was measured in experiments that were performed in water alone, without any metal powders, was assumed to be 100% benzene, since negligible hydrogen and no metal surface was present, so no cyclohexane was expected.

*Myo*-inositol does not extract from water appreciably, and so only the organic-soluble products were analyzed by GC and NMR.

### **Results and Discussion**

A series of model sugar compounds were reacted under hydrothermal conditions, in water alone, and in the presence of nickel as a catalyst, and iron as a hydrogen donor. Previously, we showed that nickel does not oxidize appreciably and acts as a catalyst, if iron is present under hydrothermal conditions. Reaction conditions were varied to assess aqueous versus surface catalyzed reactions. The stereochemistry of each tends to have a large effect on the reaction rates and product distributions in each case. Intramolecular

hydrogen bonding, and the location of neighboring hydroxyls, can also affect the rates and mechanisms of sugar dehydration.

*Cis and trans-1,2-cyclohexanediols, 250°C/40 bar, H<sub>2</sub>O*

*Cis*-1,2-cyclohexanediol was reacted in water at 250°C and 40 bar. *Cis*-1,2-cyclohexanediol dehydrates to cyclohexanone as the major product, and cyclopentylformaldehyde as a minor product. The kinetics of this dehydration were analyzed (Figures 40 and 41). If E1 dehydration occurs, rearrangement to the ring contracted oxonium intermediate (Figure 39) produces a very stable carbocation. Therefore, it seems safe to assume that the cyclopentylformaldehyde produced from this dehydration results entirely from E1, making E2 elimination the dominant mechanism of this dehydration. Previously, we found that dehydration of secondary mono-alcohols is primarily E1, with E2 only possible in the most ideal structure. *Cis*-1,2-cyclohexanediol has an axial hydroxyl in either chair conformer, making E2 favorable. The E2 rate to form cyclohexanone is six-fold higher than the E1 rate to form cyclopentylformaldehyde (Figure 40). No other products result from this dehydration, including alkenols such as 2-cyclohexen-1-ol. This suggests that when E1 occurs, ring contraction is faster than hydride shifts around the cyclohexane ring.

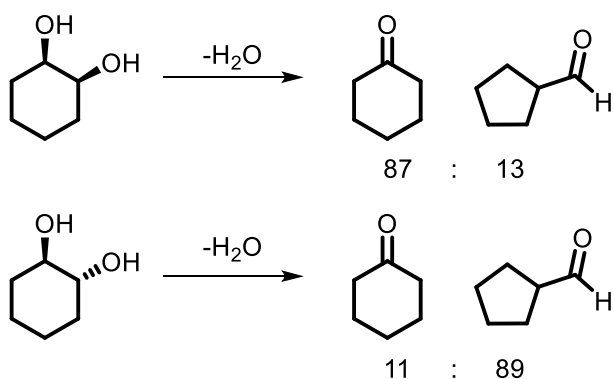


Figure 38. *Cis* and *trans*-1,2-cyclohexanediols produce different ratios of cyclohexanone and cyclopentylaldehyde at 250°C and 40 bar in water (at all times). The *trans* isomer gives more of the ring-contracted cyclopentylaldehyde than the *cis*. The *cis* is able to do E2 elimination, and therefore undergoes less rearrangement.

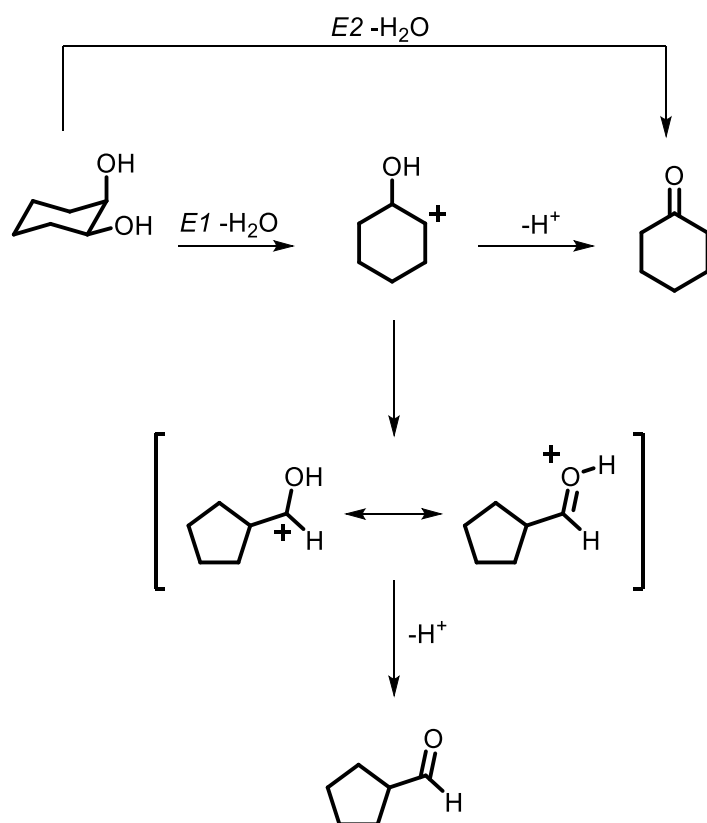


Figure 39. Possible mechanisms for *cis*-1,2-cyclohexanediol dehydration.

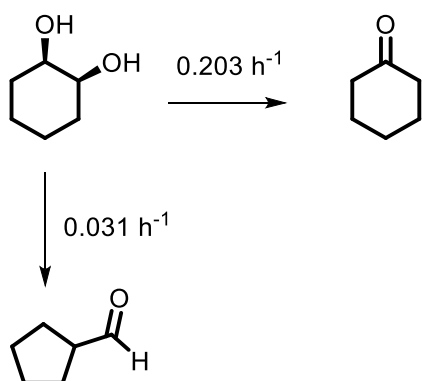


Figure 40. The reaction pathway used for the kinetic modelling of *cis*-1,2-cyclohexanediol dehydrating to cyclohexanone and cyclopentylformaldehyde.

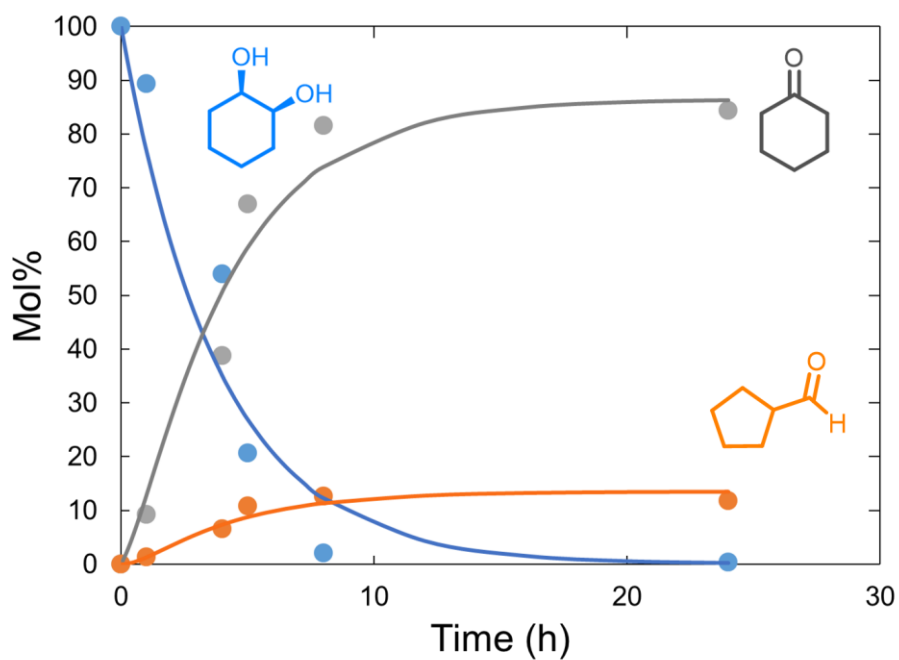


Figure 41. Kinetic analysis of *cis*-1,2-cyclohexanediol. Pseudo-first order rate constants calculated in COPASI using the pathway in Figure 40.

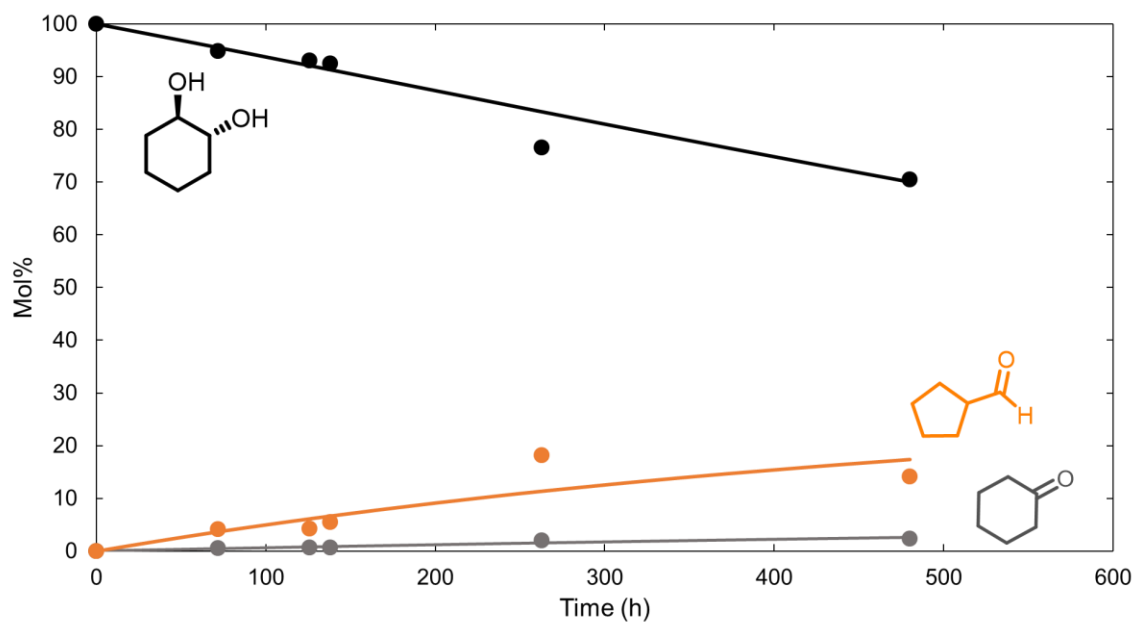


Figure 42. Time series for *trans*-1,2-cyclohexanediol, with first order kinetic fitting of the diol, cyclopentylformaldehyde, and cyclohexanone. This fit was generated from the model in Figure 44. Other minor products are plotted in Figure 43.

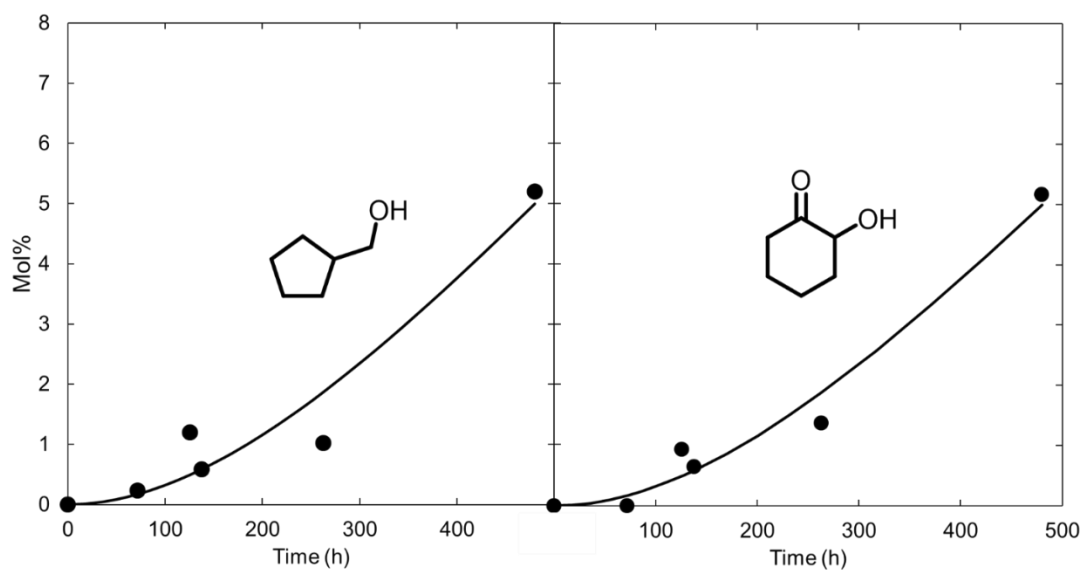


Figure 43. Cyclopentanemethanol and 2-hydroxycyclohexanone second-order fits from Figure 44. These compounds are produced by disproportionation of *trans*-1,2-cyclohexanediol and cyclopentylformaldehyde.

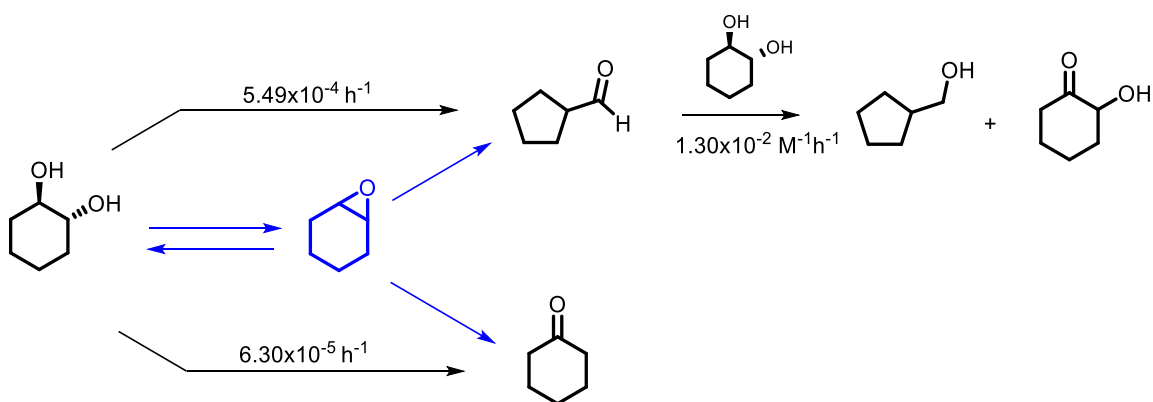


Figure 44. The kinetic model used to fit the *trans*-1,2-cyclohexanediol data. In blue is the anchimeric assistance pathway through the epoxide. While there is evidence for this mechanism, the epoxide is never detected. There is not enough data to properly model this pathway. The aldehyde undergoes an unexpected disproportionation with the *trans* diol to form cyclopentanemethanol and 2-hydroxycyclohexanone.

Unlike *cis*-1,2-cyclohexanediol, *trans*-1,2-cyclohexanediol produces more cyclopentylaldehyde than cyclohexanone. The change in carbonyl product ratio indicates a different dehydration mechanism (Figure 44). The *trans* also dehydrates more than two orders of magnitude more slowly than the *cis* isomer. After 480 hours at 250°C, only 30% of the *trans* diol has reacted (Figure 42). The slow dehydration rate could be attributed to intramolecular hydrogen bonding. Infrared spectroscopy analysis in another study showed that this diol has an intramolecularly-bound O-H stretch.<sup>211</sup> Therefore, it may be difficult for the *trans* to dehydrate if the protonated alcohol is participating in an intramolecular hydrogen bond. An epoxide intermediate for the dehydration of *trans*-1,2-cyclohexanediol has also been cited as a reason for its slow rate of dehydration.<sup>208</sup> Cyclopentanemethanol and 2-hydroxycyclohexanone also appear as minor products.



Kinetic modelling (Figure 43) suggests that they are the result of disproportionation between *trans*-1,2-cyclohexanediol and cyclopentylformaldehyde.

It is possible the dehydration of *trans*-1,2-cyclohexanediol goes through an anchimeric assistance mechanism, rather than standard E1, with 1,2-epoxycyclohexane as an intermediate (Figure 44). If the *trans* adopted a conformation with both alcohol groups axial, it could dehydrate intramolecularly. 1,2-epoxycyclohexane was not detected in any of the *trans*-1,2-cyclohexanediol experiments, but would be expected to react very quickly at 250°C in water. To determine if 1,2-epoxycyclohexane has a role in this dehydration, a 1 hour experiment starting with the epoxide was performed. After 1 hour, all of the epoxide reacted. The epoxide mainly hydrated to produce the *trans*-1,2-cyclohexane diol (and none of the *cis* isomer), and opened to form cyclopentylformaldehyde and cyclohexanone (Figure 45). Alkyl and hydride shifts of opening epoxides are known to occur *via* the Meinwald rearrangement.<sup>212</sup> The ratio of the aldehyde to the ketone in the reaction of the epoxide is the same as the average ratio obtained at all times from the dehydration of *trans*-1,2-cyclohexanediol (Figure 46). These carbonyl products almost certainly came from the epoxide, and not from the *trans* diol; the *trans* diol would not produce the detected concentrations of carbonyl products detected after 1 hour.

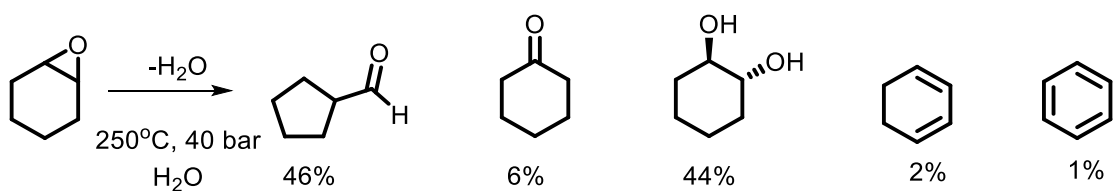


Figure 45. The products made from reaction of 1,2-epoxycyclohexane at 250°C, 40 bar for 1 hour. 1,2-epoxycyclohexane produces mostly cyclopentylformaldehyde and *trans*-1,2-cyclohexanediol, with cyclohexanone, 1,3-cyclohexadiene, and benzene as smaller components.

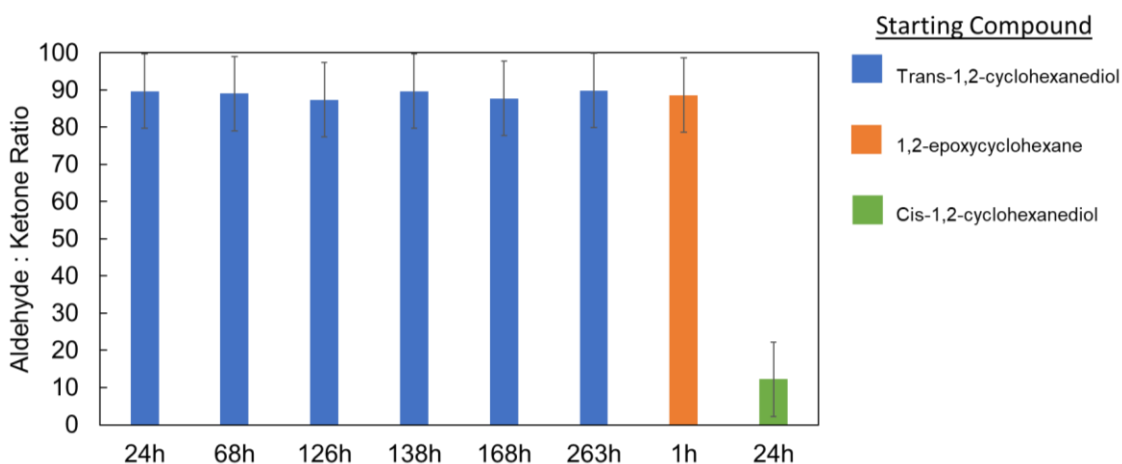


Figure 46. The ratio of cyclopentylformaldehyde to cyclohexanone formation from the *trans*-1,2-cyclohexanediol (blue bars), a 1-hour reaction of 1,2-epoxycyclohexane (orange bar), and for a 24 hour reaction of *cis*-1,2-cyclohexanediol at 250°C and 40 bar in water.

Based on the very similar ratios of aldehyde to ketone obtained from the epoxide opening and from dehydration of *trans*-1,2-cyclohexanediol, it is very likely that the epoxide is a fleeting intermediate in this dehydration reaction. In order for this intramolecular dehydration to the epoxide to take place, the *trans* isomer must adopt an axial conformation (Figure 47). Not only is this sterically unfavorable, the intramolecular hydrogen bond between the two hydroxyls must be broken to do so. This can explain why

the *trans* is extremely slow to dehydrate. The epoxide also rehydrates very quickly, which will also decrease the overall dehydration rate.

While intramolecular hydrogen bonding may cause slow dehydration in the *trans*-1,2-cyclohexanediol, the *cis* also has an intramolecular hydrogen bond, and yet can dehydrate in 24 hours.<sup>211</sup> The *cis* has the advantage of an axial hydroxyl in both chair conformers. It is possible that the nucleophilic attack during E2 dehydration is enough to cause the protonated alcohol to leave, in spite of hydrogen bonding. The wavenumber of the *cis* intramolecular hydrogen bond is lower than that in the *trans*, indicating that it is a slightly weaker bond.<sup>211</sup> Formation of 1,2-epoxycyclohexane from the *cis* is impossible, as the *cis* cannot exist in a conformation where intramolecular backside attack can occur. No *trans*-1,2-cyclohexanediol is formed from *cis*-1,2-cyclohexanediol, which would occur if the epoxide were accessed. Therefore, the *cis* diol does not have the reversibility problem of dehydrating to form the epoxide, only for it to be hydrated back to a diol.

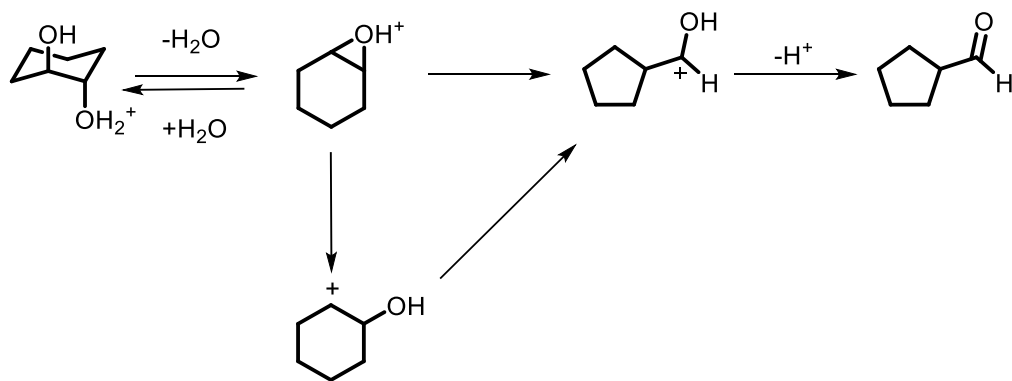


Figure 47. The proposed mechanism of *trans*-1,2-cyclohexanediol to its major product, cyclopentylformaldehyde. The hydroxyls must be axial for backside attack to occur. After the initial dehydration, a Meinwald-like rearrangement occurs to produce cyclopentylformaldehyde

Two other products appear in significant quantities from the *trans*-1,2-cyclohexanediol: 2-hydroxycyclohexanone, and cyclopentanemethanol. Several pathways were tested in COPASI to describe the pathway in which these products form. 2-Hydroxycyclohexanone could have been the result of the diol losing hydrogen. Loss of hydrogen from organics has been observed under hydrothermal experiments, especially at longer reaction times.<sup>23</sup> Cyclopentanemethanol could result from cyclopentylformaldehyde undergoing the Cannizzaro reaction; however, cyclopentanecarboxylic acid is detected only 0.1 mol% and in only the 480 hour timepoint. Therefore, cyclopentanemethanol results from a different pathway. Since hydrogen could be lost from the diol in making 2-hydroxycyclohexanone, cyclopentylformaldehyde could be reducing. However, this pathway produced a poor kinetic fit. Both 2-hydroxycyclohexanone and cyclopentanemethanol have a small induction period, and appear to have a roughly one-to-one ratio to one another at all times (Figure 43). In order for these products to form, the aldehyde must grow in first, which would explain the induction periods. Based on this information, and the kinetic fit, the disproportionation path appears to be feasible. Similar hydride-transfer mechanisms have been observed under hydrothermal conditions involving aldehydes.<sup>28</sup> A proposed mechanism is shown in Figure 48. This is an interesting reaction, since it is an example of a reduction that uses a sacrificial alcohol donor, and is likely catalyzed by water.

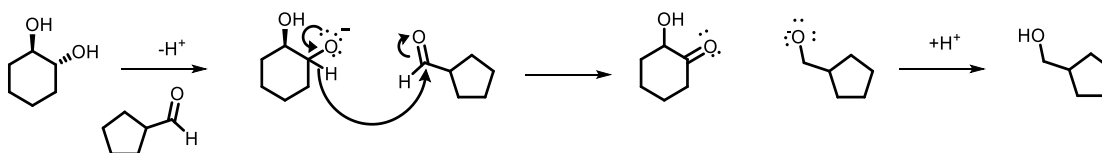


Figure 48. Proposed mechanism for the disproportionation of *trans*-1,2-cyclohexanediol and cyclopentylformaldehyde. The diol loses a proton, and transfers hydride to cyclopentylformaldehyde. The cyclopentanemethoxide is then protonated.

#### *Cis and Trans*-1,2-Cyclohexanediols – Reduction with Nickel and Iron

*Cis* and *trans*-1,2-cyclohexanediols were deoxygenated and reduced in the presence of nickel and iron, at 250°C in water. Both diols produce cyclohexane as the major product, in relatively high yields (Figure 49). *Cis*-1,2-cyclohexanediol follows the reaction pathway in Figure 52. Dehydration of the diol to cyclohexanone was found to occur in conjunction with direct hydrogenolysis to cyclohexanol. Cyclohexanol concentrations increases in concentration from the start of the reaction, without any induction period (Figure 51C). Its maximum abundance is also higher than that of cyclohexanone (Figure 51B). Cyclohexanol is therefore a primary product of C-O hydrogenolysis.

Rapid equilibrium is also observed with two oxidation products, 2-hydroxycyclohexanone, and phenol (Figure 51). While 2-hydroxycyclohexanone was determined to result from disproportionation of the *trans*-1,2-cyclohexanediol and cyclopentylformaldehyde in water alone, this not likely the case here since the nickel surface is involved, and cyclopentanemethanol is not observed in a 1:1 ratio with 2-hydroxycyclohexanone, as it was in the aqueous dehydration (Figure 43). Formation of 2-hydroxycyclohexanone is the result of oxidation of the *cis* on the nickel surface.

Eventually, the oxidation products are reduced. 83% yield of cyclohexane was obtained in 72 hours. Benzene (16% yield) could result from dehydration of the diol to form dienes, which liberate hydrogen; from hydrogenolysis of phenol; or dehydrogenation of cyclohexane on the metal surface. Benzene was only measured by NMR at the 72h timepoint.

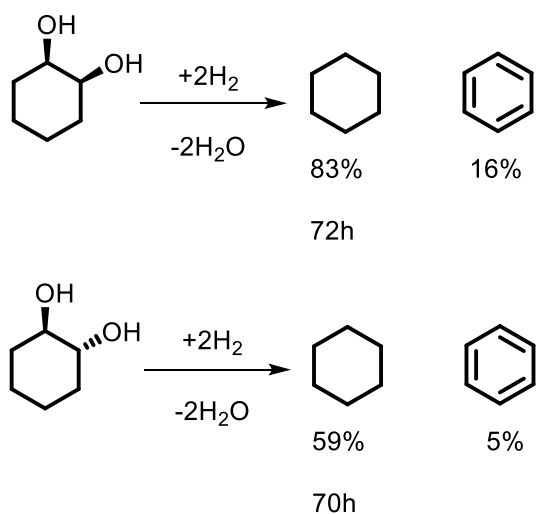


Figure 49. Yields of major deoxygenation and reduction products of *cis* and *trans*-1,2-cyclohexanediols in the presence of Ni and Fe at 250°C in water.

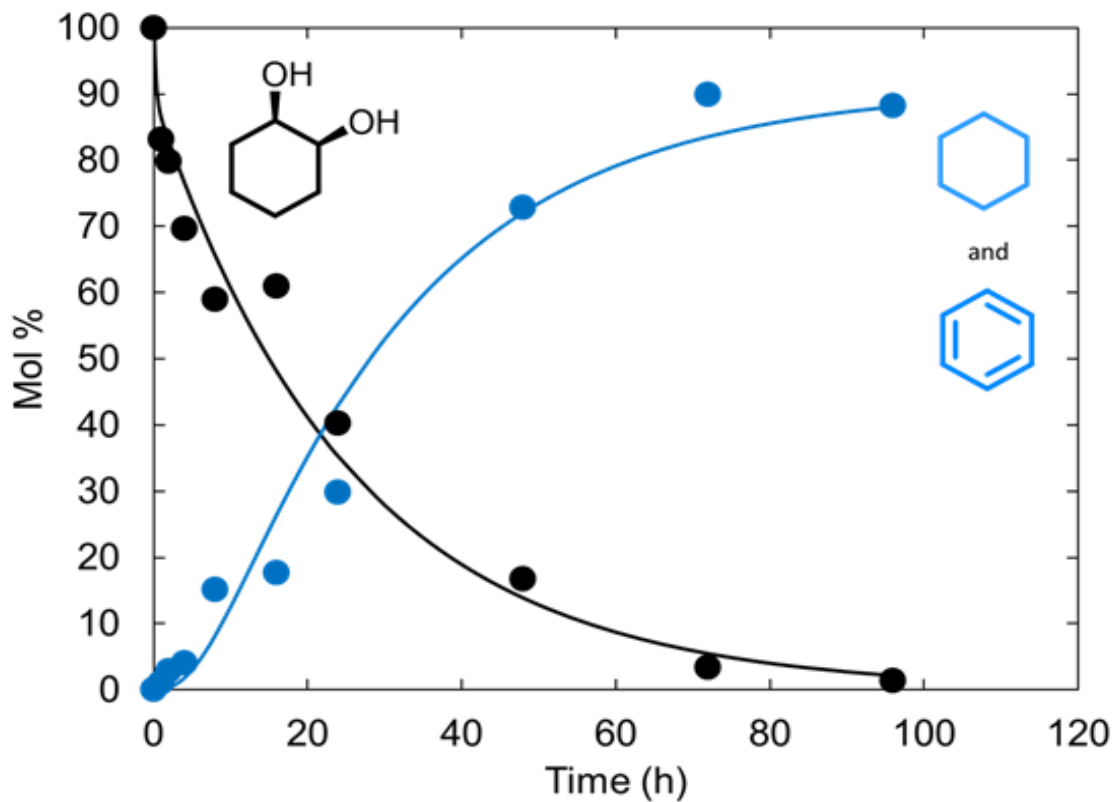
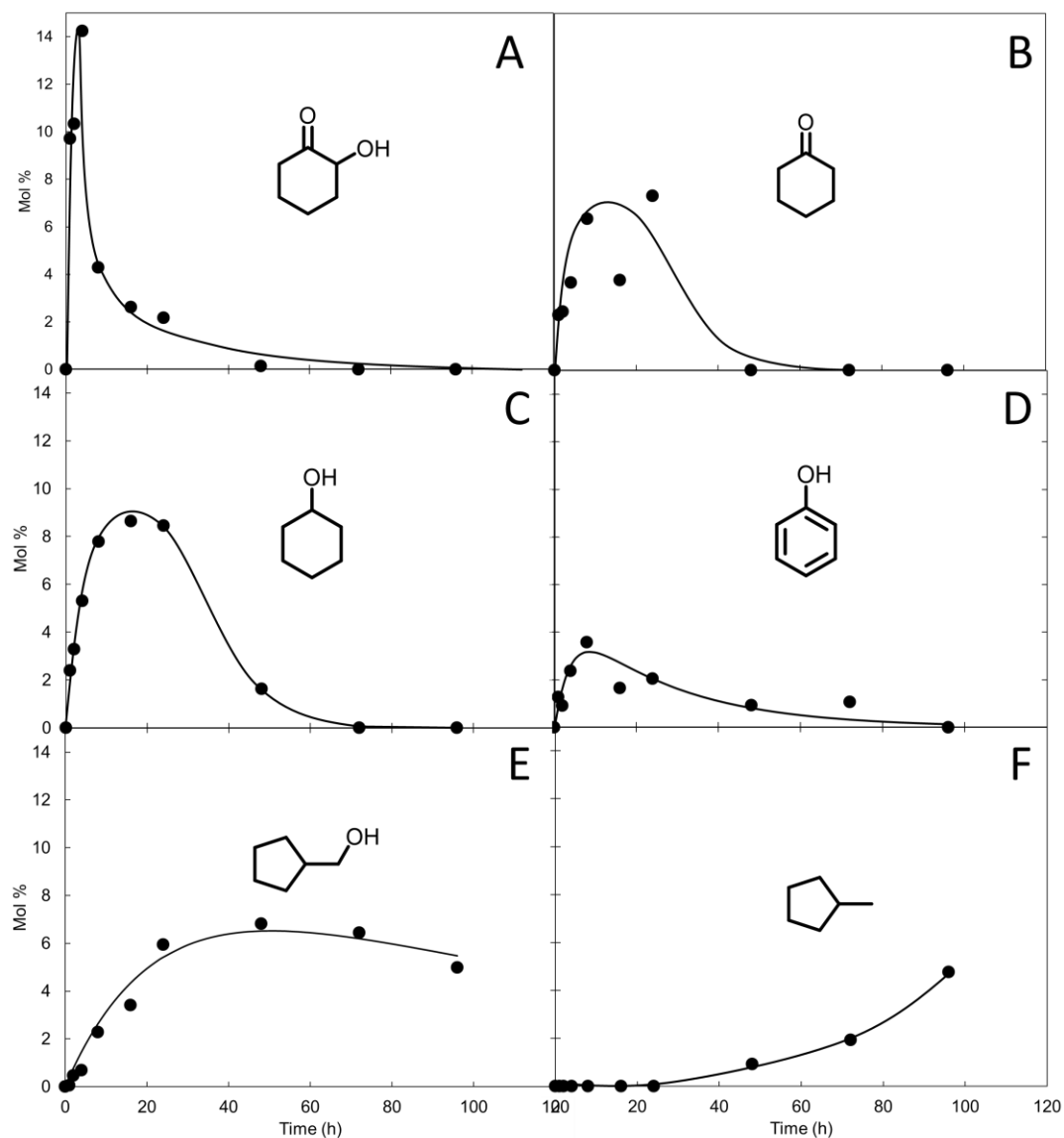


Figure 50. Time dependence of cis-1,2-cyclohexanediol and cyclohexane/benzene production (250°C, 40 bar, Ni+Fe) Minor products of this reaction are plotted in Figs. 51A-F. Lines included to guide the eye. Fraction of cyclohexane GC peak that is benzene is reported in Figure 49.

Figure 51. Time dependencies of minor products from the reduction and deoxygenation of *cis*-1,2-cyclohexanediol with Ni and Fe, 250°C/40 bar. **A.** 2-hydroxycyclohexanone, an early-time oxidation product. **B.** Cyclohexanone, the first major dehydration product, also observed in water-only experiments. **C.** Cyclohexanol, the reduction product of cyclohexanone and hydrogenolysis product of the *cis* diol. **D.** Phenol, an oxidation product of cyclohexanone. **E.** Cyclopentanemethanol, the reduction product of cyclopentylformaldehyde. The aldehyde reacts rapidly on Ni, and is never observed in measurable quantities. **F.** Methylcyclopentane, the hydrogenolysis product of cyclopentanemethanol. Curves included to guide the eye.





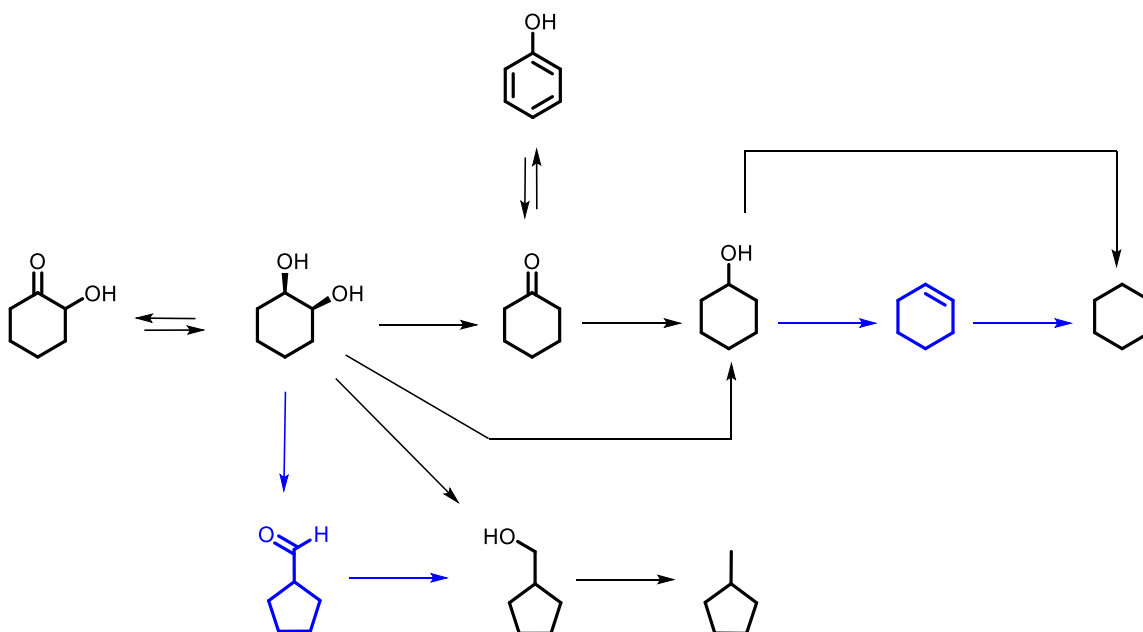


Figure 52. Reductive deoxygenation of *cis*-1,2-cyclohexanediol with nickel and iron 250°C. The pathways in black were determined by observing the time dependencies of each product in the reduction. The pathways in blue could be active pathways, but are too rapid for the intermediate species to build up in concentration. Cyclohexene and cyclopentylformaldehyde are not detected. The time dependent data set can be found in Figs 50 and 51.

A different mechanism for deoxygenation of the *trans*-1,2-cyclohexanediol is accessed on nickel. A large amount of non-ring contracted product is generated from the *trans* when nickel is present (Figure 49), compared to the water-alone experiments. Hydrogenolysis of the diol occurred on the surface instead of dehydration, resulting in less of the ring-contracted aldehyde that is produced via the anchimeric assistance mechanism proposed in Figure 47. As in the reduction of the *cis* diol, the aldehyde rapidly reduced to cyclopentanemethanol. This product was detected in the *trans* reduction, but in less than 5 mol%. The hydrogen bonding between the two alcohols still must be broken for the hydrogenolysis to occur as well. This may explain the decreased

yield of cyclohexane compared to the *cis*-diol reaction. There is also less benzene produced from the *trans* than the *cis*. This is reasonable since the *trans*-diol undergoes hydrogenolysis rather than dehydration, thus decreasing formation of dienes *via* allylic chemistry that can lead to benzene. Cyclohexane was obtained in 59% yield after 70h at 250°C. Optimization of the catalyst and conditions could increase the yield of cyclohexane and decrease the time needed for the reaction to occur.

*Cis and Trans-1,4-cyclohexanediols, 250°C/40 bar, H<sub>2</sub>O*

*Cis* and *trans*-1,4-cyclohexanediol follow similar dehydration pathways, and produce essentially the same products (Figure 53 and Table 13). The *cis* isomer dehydrates slower than the *trans* isomer. This is somewhat unintuitive, as the *cis* isomer has an axial hydroxyl at all times, much like the *cis*-1,2-cyclohexanediol, that dehydrates quickly. However, it is possible for the *cis* to access a hydrogen-bonded twist-boat conformation mid-chair interconversion. Protonated *cis*-1,4-cyclohexanediol was calculated at the M06-2x/aug-cc-PVTZ level of theory in both chair conformers and as a twist-boat. Calculations were carried out with water as the solvent at 250°C and 40 bar, using the Polarizability Continuum Model. The lowest energy structure, in all cases, was the twist-boat conformer, in which a proton is shared by the two hydroxyls. (Figure 54) This conformation would make dehydration less favorable, as the water molecule leaving-group is hydrogen bonded. Both 1,4-cyclohexanediols are slower to dehydrate than *cis*-1,2-cyclohexanediol. After dehydration, the 1,4-cyclohexanediols do not have access to a more stable oxonium cation, unlike the *cis*-1,2-cyclohexanediol.

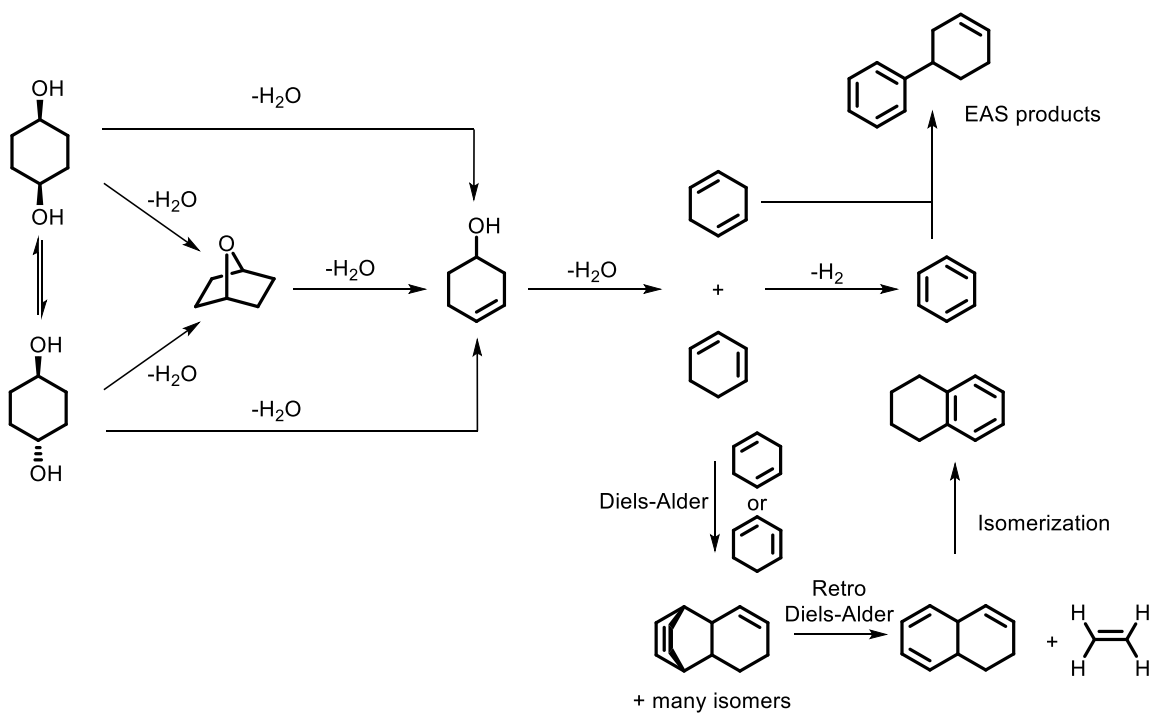
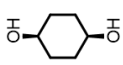
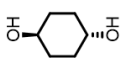
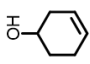



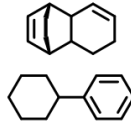
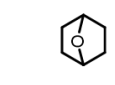
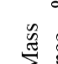
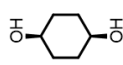
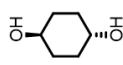
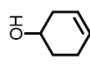
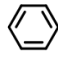
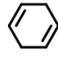
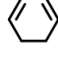
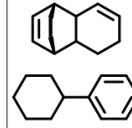
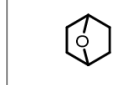
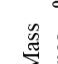


Figure 53. Reaction pathway for the dehydration of *cis* and *trans*-1,4-cyclohexanediols in water at 250°C and 40 bar. Both diols produce similar product distributions. Traces of 1,4-epoxycyclohexane are found in both products, and may be an intermediate during dehydration to 3-cyclohexen-1-ol. 3-Cyclohexen-1-ol dehydrates to 1,3 and 1,4-cyclohexadiene. The dienes can release  $H_2$  to form benzene, or undergo Diels-Alder cyclization. The bridged Diels-Alder dimer releases ethylene via Retro Diels-Alder, and rearranges to 1,2,3,4-tetrahydronaphthalene. Benzene also undergoes electrophilic aromatic substitution (EAS) with alkenes.

Table 13. The products formed from starting with *cis*-1,4-cyclohexanediol (A) and *trans*-1,4-cyclohexanediol (B). Numbers under each species are micromoles measured (GC). Mass balance is the percent extracted post-experiment on a mol basis. The *cis* diol is slower to dehydrate than the *trans* diol. In both cases, the mass balance of the reaction decreases with time, and may be attributed to the formation of dimers that are insoluble in DCM.

A		Cis-1,4-cyclohexanediol - Products (μmol)										Mass Balance - % (μmol lost)
Reaction Time (h)										Mass Balance - % (μmol lost)		
69	0.11	0.005	0.013	0.0008	0.0037	0.0037	0	0.004	0.0001	90% (3.2)		
171	0.051	0.010	0.022	0.011	0.0081	0.010	0.0006	0.0031	0.0001	83% (6.3)		
312	0.0007	0.012	0.0082	0.037	0.0055	0.0071	0.0023	0.0086	0.00004	58% (20)		
B		Trans-1,4-cyclohexanediol - Products (μmol)										Mass Balance - % (μmol lost)
Reaction Time (h)										Mass Balance - % (μmol lost)		
24	0.0045	0.071	0.019	0.0006	0	0.0005	0	0.0003	0.0014	97% (0.6)		
78	0.032	0.01	0.024	0.004	0.012	0.01	0.0002	0.0026	0.012	88% (2.9)		
144	0.0042	0.0023	0.0076	0.018	0.0011	0.0082	0.0016	0.018	0.00007	72% (4.9)		

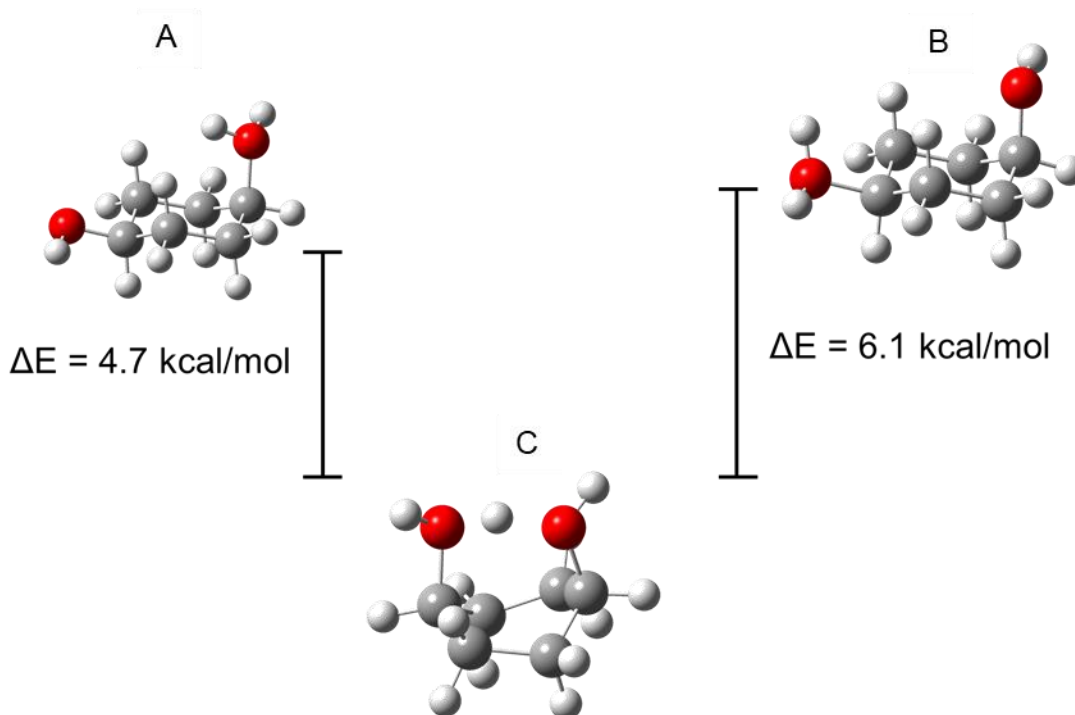


Figure 54. Structures and energy differences between protonated axial (A) and equatorial (B) hydroxyls and the protonated twist-boat of cis-1,4-cyclohexanediol (C), calculated at the M06-2x/aug-cc-PVTZ level of theory, with PCM solvation (250°C/40 bar). The protonated twist-boat is the lowest energy structure; the two hydroxyls share the extra proton.

The first dehydration of both diols yields 3-cyclohexen-1-ol (Figure 53). Both diols also produce small amounts of 1,4-epoxycyclohexane, as an intramolecular dehydration product. When reacted on its own, 1,4-epoxycyclohexane ring-opens rapidly to form 3-cyclohexen-1-ol, and rehydrates to form *trans*-1,4-cyclohexanediol, in the timescale of 1 hour. Unlike the epoxide experiment conducted with the *trans*-1,2-cyclohexandiol, there is not a consistent ratio of products throughout time in the reaction to aid in determining the role of 1,4-epoxycyclohexane. It is possible that the 1,4-diols make 1,4-epoxycyclohexane as a primary product, and 3-cyclohexen-1-ol is a secondary

product. A reasonable kinetic fit of the data could not be obtained due to the continuous loss of mass from dimer/polymer formation, and this pathway could not be proven. 3-Cyclohexen-1-ol then dehydrates to 1,4-cyclohexadiene and 1,3-cyclohexadiene; 1,3-cyclohexadiene can undergo Diels-Alder reactions with either itself, 1,4-cyclohexadiene, or 3-cyclohexen-1-ol. A large number of dimers, in the C<sub>12</sub> mass range, were observed by GC/MS. EAS products and an isomer of the Diels-Alder reaction were identified. These dimers can represent up to 10-20 mol% of the total at long reaction times for both stereoisomers.

The Diels-Alder dimers can undergo retro-Diels-Alder to produce 1,2,3,4-tetrahydronaphthalene (Figure 53). This pathway demonstrates a drive toward aromaticity, and can serve as a model for the formation of polycyclic aromatic hydrocarbons in nature. The Diels-Alder reaction is one of the most fundamental methods for synthesizing polycyclic compounds. The production of 1,2,3,4-tetrahydronaphthalene in this reaction demonstrates that the Diels-Alder reaction could have a role in the formation of kerogen, coal, and possibly C<sub>6</sub>-cyclic hydrocarbons in natural systems. Formation of polycyclic aromatic hydrocarbons (PAHs) is usually expected to occur through the dehydrogenation of sterols,<sup>213</sup> and aromatization has also been observed in prior hydrothermal organic reactions.<sup>23,214</sup> Based on these new observations, the Diels-Alder mechanism should also be considered as an alternative pathway toward PAHs. This method of dehydrating 1,4-cyclohexanediols is not ideal; the reactions are somewhat slow (Table 13) and unselective. Hydrothermal processing of biomass is still heavily used, even for more complex starting materials. This model sugar compound generates

numerous products, and has a simpler structure than a sugar. A catalyst, and reducing conditions, are necessary to avoid the dimerized products made by the dienes.

*Cis-1,4-cyclohexanediol, Trans-1,4-cyclohexanediol, and myo-inositol – Reductions with Nickel and Iron*

Despite the complexity of the aqueous 1,4-cyclohexanediol reactions, the reactions in the presence of nickel and iron are very selective for cyclohexane. Good yields of cyclohexane are obtained from both 1,4-cyclohexanediols in only 24 hours (Figure 55). The conversion of both diols is enhanced compared to the water only experiments, where 100+ hours are required to reach full conversion. This implies an alternative mechanism. Rather than dehydration followed by reduction, hydrogenolysis is the likely pathway. 3-cyclohexen-1-ol is observed in sub-millimolar amounts.

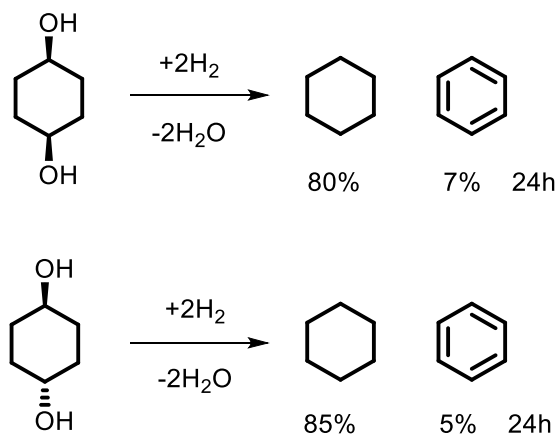


Figure 55. Deoxygenation and reduction of *cis* and *trans*-1,4-cyclohexanediols in the presence of Ni and Fe at 250°C in water. Chemical yields given as %.

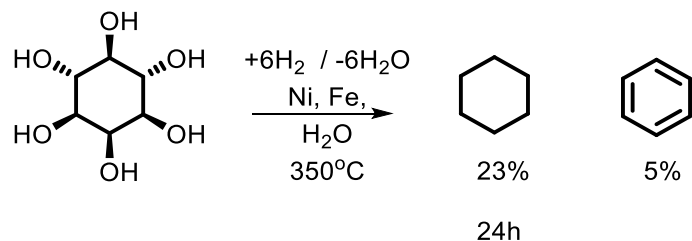


Figure 56. Reduction and deoxygenation of *myo*-inositol to cyclohexane in the presence of Ni and Fe at 350°C in water.

*Myo*-inositol can also be deoxygenated to cyclohexane and benzene using nickel at 350°C (Figure 56). In water alone at 250°C, *myo*-inositol produces a solid, black material resembling char (Figure 57). This material is not observed when nickel is present. This polyol is frequently used as a sugar model in the literature. Typically, products obtained from its deoxygenation are phenols or benzene.<sup>121,132</sup> While the yield is low, cyclohexane is the major product of the reduction with nickel and iron. Mechanistic information was not obtained from this reduction. Any intermediates that exist may be water soluble, and do not extract. It is uncertain how much remaining starting material and other products remained. It is possible that the yield is low due to the number of intramolecular hydrogen bonds *myo*-inositol can form. This reaction is nonetheless impressive, considering that the reaction took place in water, and an earth-abundant catalyst was used in place of the more frequently encountered rare metal catalysts.



Figure 57. Fused silica tube containing the post-reaction mixture of *myo*-inositol in water alone (250°C, 48h). The reaction started out as a clear, colorless, solution.



## Summary and Future Work

Valuable mechanistic insights into deoxygenation of sugars were obtained from this study. Intramolecular hydrogen bonding between neighboring hydroxyls can significantly affect the rate of dehydration. *Trans*-1,2-diol functionalities are likely to be slower to deoxygenate both for this reason, and due to anchimeric assistance being the most dominant mechanism of dehydration (and rehydration). Formation of bridged ethers and epoxides in cyclic polyols can increase reversibility toward the hydrated structure. *Trans*-1,2-cyclohexanediol was shown to be unreactive and slow to deoxygenate in past studies. This kinetic problem must be overcome in order to deoxygenate sugars, since *trans* hydroxyls are more common in nature. Dehydration is not a viable option since the epoxide formation is difficult to avoid. Elevated temperature, and use of a heterogeneous catalyst capable of hydrogenolysis, may be the answer. Hydrogenolysis of all polyols in this study was observed on nickel. Good yields of cyclohexane were obtained from these reductive deoxygenation reactions. Since hydrogenolysis usually occurs on the edges of “stepped” crystalline metal surfaces, using a nickel catalyst that has more of these surface features could promote this mechanism further.<sup>44</sup> Nickel nanoparticles, or a higher surface area nickel powder, should be used in future experiments.

Deoxygenation of 1,4-diols results in dienes that can undergo Diels-Alder reactions. Without reducing conditions and a catalyst, these reactions are a dominant pathway toward polymeric material and aromatic compounds. While this pathway is of interest as a model for kerogen and polycyclic aromatic hydrocarbon formation, it has no

utility for fuels. However, with nickel and iron, 1,4-cyclohexanediols reduce cleanly to cyclohexane, avoiding the Diels-Alder products. Undesired aqueous reaction pathways can be circumvented with the use of a good catalyst. Using nickel as catalyst under hydrothermal conditions, reasonable yields of cyclohexane can be obtained from highly oxygenated organics. In systems where dehydration is slow, hydrogenolysis pathways can be activated on the nickel surface. Characterization of the water soluble products from reacting *myo*-inositol may also be insightful. Further examination of other sugar models, which possess the cyclic ether functional group, should be performed.

## 7. CONCLUSION

The research presented in this dissertation has given insight into hydrothermal transformation of organic matter in natural systems, potential green chemistry methods, and potential future paths for biomass processing. The reactivity and behavior of many functional groups were assessed, under reducing and non-reducing conditions. These observations can aid in making predictions on the fate of organic carbon under hydrothermal conditions in nature. The first three reactions in the scheme proposed by Seewald, showing the pathway between ketone and alkane, have been re-validated by this work.<sup>1</sup> We have been able to expand on this scheme (Figure 58), as well as enhance certain steps and open up new pathways with nickel as a catalyst (Figure 59). The mechanisms of most reactions described in this investigation were probed. Mechanistic information about hydrothermal reactions, that have been largely ignored in the geologic literature, is important for assessing the utility of various reactions in an applied sense, and for analyzing organics found in the environment. For example, it may be assumed that polycyclic aromatic hydrocarbons inherently came from lignin. However, this work has shown that the Diels-Alder reaction can also produce PAHs. There may also be an alternative pathway to carboxylic acids that does not involve ketone oxidation. More plausibly, primary alcohols could oxidize to carboxylic acids, as they cannot dehydrate via E1.

The dehydration mechanism for most alcohols is E1 under hydrothermal conditions. Only in very constrained structures, where E2 is favored, will E2 be observed. Even in those cases, E1 is still a competitive pathway. This dehydration mechanism was

determined for alcohols reacting in water alone. It would be interesting and potentially useful to examine different minerals or heterogeneous catalysts that increase the rate of dehydration. Dehydration is a necessary step in deoxygenating biomass. Dehydration of simple mono-ols results in an alkene, which must be reduced if the end goal of the reaction is fuels.

Nickel was found to be a selective reduction catalyst for alkenes and aromatics. Simple alkenes and aromatic rings can be reduced in the presence of other functional groups. Unsurprisingly, aromatic ring reduction was slower than alkene reduction. It is possible that a more finely-divided nickel powder or nickel nanoparticles could increase the rate of aromatic reduction. Nickel is a cheaper and more earth-abundant alternative to palladium and platinum. We have shown what functional groups nickel can reduce, but optimizing the conditions is still a task that needs to be completed. However, this is more of an engineering problem. There may also be a better sacrificial donor than iron, or a better hydrogen source. Simple alcohols have been used as hydrogen donors in the literature. It may also be possible to generate hydrogen using a solar fuel cell, rather than oxidizing iron metal with water. Iron has not proven to be catalytic in any of the experiments in this dissertation, but this may not always be the case.

Cu-Zn alloy was found to readily reduce carbonyls. However, its ambiguous role as reagent or catalyst adds complication to understanding its effect in the reduction. Further study of this material is needed. Materials including both of these metals should be tested as catalysts. Cu-Zn alloy is an active surface, and both metals are inexpensive compared to rarer transition metals often used as catalysts. There is a need for reduction

of carboxylic acids without the use of hydrides. With some optimization, Cu-Zn may prove to be useful for reducing carbonyls to alcohols on an industrial scale.

Preparation of biofuels requires deoxygenation and reduction. Dehydration of simple cyclic diols was shown to have more complicated behavior and kinetics than the analogous cyclohexanol. *Trans*-1,2-cyclohexanediol proved to be a challenge to deoxygenate. This observation has been noted in the literature many times, and in the presence of different catalysts and conditions.<sup>121,132,206-208</sup> Hydrogenolysis was found to be a solution to the *trans* diol problem. Dehydration is problematic because *trans*-1,2-cyclohexanediol is limited to a very reversible anchimeric assistance mechanism, and it can undergo intramolecular hydrogen bonding. Intramolecular hydrogen bonding was also found to decrease the dehydration rate of *cis*-1,4-cyclohexanediol, that can adopt a twist-boat conformation. Hydrogenolysis on nickel produced good yields of cyclohexane from both isomers of 1,4-cyclohexanediol. Nickel can also fully deoxygenate *myo*-inositol to cyclohexane, which has not been reported before.

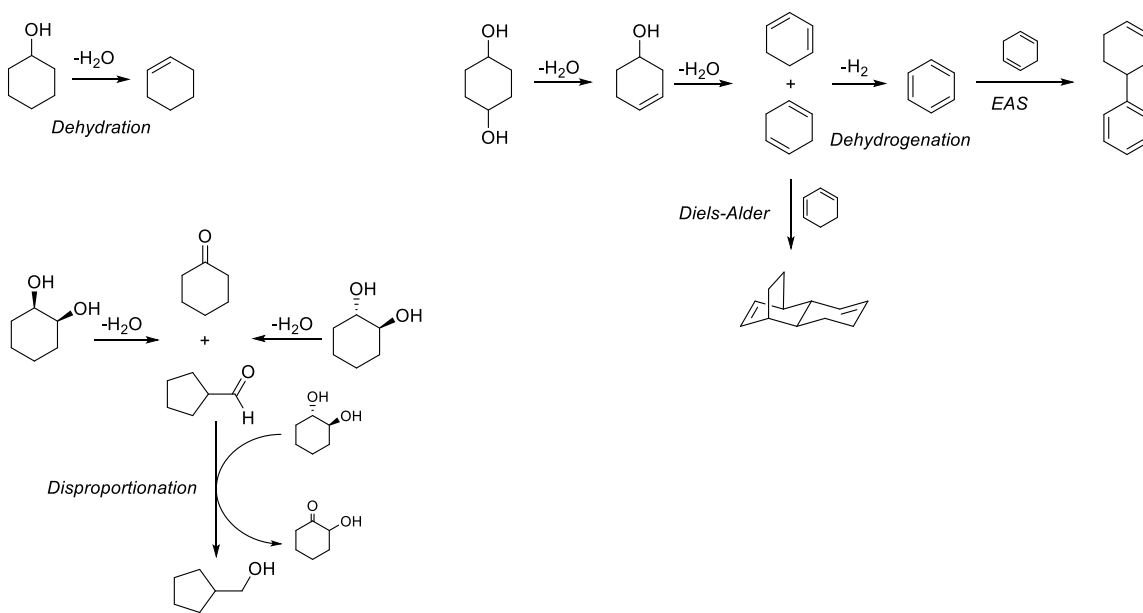


Figure 58. A map of aqueous hydrothermal reactions involving mono-ols and diols.

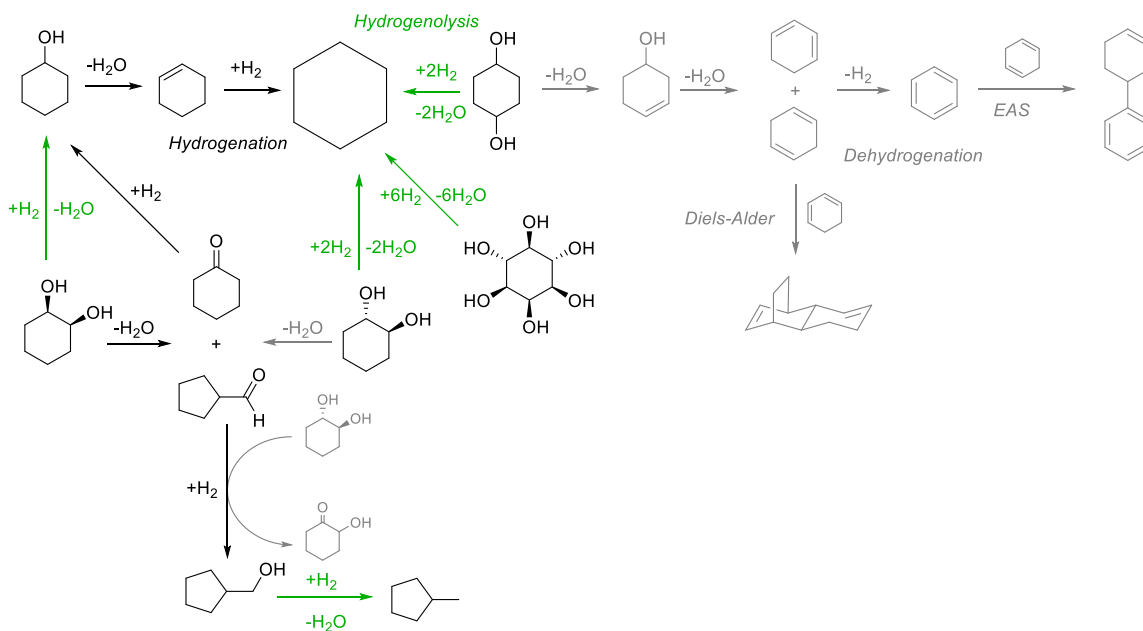


Figure 59. A map of aqueous and nickel-catalyzed reactions involving alcohols that occur under hydrothermal conditions. Cyclohexane becomes the major product of many reactions. Hydrogenolysis emerges as an alternative deoxygenation pathway (Shown in green). Reactions shown in grey are either diminished or do not occur at all in the presence of nickel and iron.

## References

1. Seewald, J. S. Aqueous geochemistry of low molecular weight hydrocarbons at elevated temperatures and pressures: constraints from mineral buffered laboratory experiments. *Geochim. Cosmochim. Acta* **2001**, *65*, 1641-1664.
2. Yang, Z.; Lorance, E. D.; Bockisch, C.; Williams, L. B.; Hartnett, H. E.; Shock, E. L.; Gould, I. R. Hydrothermal Photochemistry as a Mechanistic Tool in Organic Geochemistry: The Chemistry of Dibenzyl Ketone. *J. Org. Chem.* **2014**, *79*, 7861-7871.
3. Falkowski, P.; Scholes, R. J.; Boyle, E.; Canadell, J.; Canfield, D.; Elser, J.; Gruber, N.; Hibbard, K.; Hignier, P.; Linder, S.; Mackenzie, F. T.; Moore, B., III; Pedersen, T.; Rosenthal, Y.; Seitzinger, S.; Smetacek, V.; Steffen, W. The global carbon cycle: A test of our knowledge of Earth as a system. *Science (Washington, D. C. )* **2000**, *290*, 291-296.
4. Franks, F. *Water: A Matrix for Life*; Royal Society of Chemistry: Cambridge, UK, 2000; Vol. 2.
5. Murrell, J.; Jenkins, A. *Properties of Liquids and Solutions*; Wiley & Sons: Chichester, 1994; .
6. Simoneit, B. R. T. Alteration and Migration Processes of Organic Matter in Hydrothermal Systems. In *Organic Matter and Mineralisation: Thermal Alteration, Hydrocarbon Generation, and Role in Metallogenesis*; Glikson, M., Mastalerz, M., Eds.; Kluwer Academic Publishers: Dordrecht, 2000; pp 1-37.
7. Uematsu, M.; Franck, E. U. Static dielectric constant of water and steam. *J. Phys. Chem. Ref. Data* **1981**, *9*, 1291-306.
8. Shock, E. L.; Canovas, P.; Yang, Z.; Boyer, G.; Johnson, K.; Robinson, K.; Fecteau, K.; Windman, T.; Cox, A. Thermodynamics of organic transformations in hydrothermal fluids. *Rev. Mineral. Geochem.* **2013**, *76*, 311-350.
9. Plyasunov, A. V.; Shock, E. L. Correlation strategy for determining the parameters of the revised Helgeson-Kirkham-Flowers model for aqueous nonelectrolytes. *Geochim. Cosmochim. Acta* **2001**, *65*, 3879-3900.
10. Siskin, M.; Katritzky, A. R. Reactivity of organic compounds in hot water: geochemical and technological implications. *Science (Washington, D. C. , 1883-)* **1991**, *254*, 231-7.

11. Shock, E. L.; Oelkers, E. H.; Johnson, J. W.; Sverjensky, D. A.; Helgeson, H. C. Calculation of the thermodynamic properties of aqueous species at high pressures and temperatures: effective electrostatic radii, dissociation constants and standard partial molal properties to 1000°C and 5 kbar. *J. Chem. Soc. , Faraday Trans.* **1992**, *88*, 803-26.
12. Shock, E. L.; Helgeson, H. C. Calculation of the thermodynamic and transport properties of aqueous species at high pressures and temperatures: Standard partial molal properties of organic species. *Geochim. Cosmochim. Acta* **1990**, *54*, 915-45.
13. Johnson, J. W.; Oelkers, E. H.; Helgeson, H. C. SUPCRT92: A Software Package for Calculating the Standard Molal Thermodynamic Properties of Minerals, Gases, Aqueous Species, and Reactions from 1 to 5000 Bar and 0 to 1000°C. *Comp. Geosci.* **1992**, *18*, 899-947.
14. Yang, Z.; Hartnett, H. E.; Shock, E. L.; Gould, I. R. Organic Oxidations Using Geomimicry. *J. Org. Chem.* **2015**, *80*, 12159-12165.
15. Brack, A.; Editor. *Molecular Origins of Life: Assembling Pieces of the Puzzle*; Cambridge Univ Press: 1998; , pp 417 pp.
16. Horsfield, B.; Schenk, H. J.; Zink, K.; Ondrak, R.; Dieckmann, V.; Kallmeyer, J.; Mangelsdorf, K.; Di Primio, R.; Wilkes, H.; Parkes, R. J.; Fry, J.; Cragg, B. Living microbial ecosystems within the active zone of catagenesis: Implications for feeding the deep biosphere. *Earth Planet. Sci. Lett.* **2006**, *246*, 55-69.
17. Seewald, J. S. Organic-inorganic interactions in petroleum-producing sedimentary basins. *Nature (London, U. K. )* **2003**, *426*, 327-333.
18. Hartings, M. Reactions coupled to palladium. *Nat. Chem.* **2012**, *4*, 764.
19. Cawley, J. J.; Lindner, P. E. The acid catalyzed dehydration of an isomeric 2-methylcyclohexanol mixture: a kinetic and regiochemical study of the Evelyn effect. *J. Chem. Educ.* **1997**, *74*, 102-104.
20. Rappoport, Z.; Sleezer, P. D.; Winstein, S.; Young, W. G. Allylic oxidation of olefins by mercuric acetate. *Tetrahedron Lett.* **1965**, 3719-28.
21. Davis, R. E.; Carter, J. Heats of reduction of ketones with sodium borohydride. *Tetrahedron* **1966**, *22*, 495-504.
22. Kwart, H.; Nickle, J. H. Transition states in chromium(VI) oxidation of alcohols. *J. Amer. Chem. Soc.* **1973**, *95*, 3394-6.



23. Shipp, J.; Gould, I. R.; Herckes, P.; Shock, E. L.; Williams, L. B.; Hartnett, H. E. Organic functional group transformations in water at elevated temperature and pressure: Reversibility, reactivity, and mechanisms. *Geochim. Cosmochim. Acta* **2013**, *104*, 194-209.
24. An, J.; Bagnell, L.; Cablewski, T.; Strauss, C. R.; Trainor, R. W. Applications of High-Temperature Aqueous Media for Synthetic Organic Reactions. *J. Org. Chem.* **1997**, *62*, 2505-2511.
25. Corliss, J. B. Hotsprings and the Origin of Life. *Nature* **1990**, *347*, 624.
26. Lee, N.; Foustoukos, D. I.; Sverjensky, D. A.; Hazen, R. M.; Cody, G. D. Hydrogen enhances the stability of glutamic acid in hydrothermal environments. *Chem. Geol.* **2014**, *386*, 184-189.
27. Baross, J. A.; Hoffman, S. E. Submarine hydrothermal vents and associated gradient environments as sites for the origin and evolution of life. *Origins Life* **1985**, *15*, 327-45.
28. Fecteau, K. Organic Carbon in Hydrothermal Systems: From Phototrophy to Aldehyde Transformations, Arizona State University, Tempe, AZ, 2016.
29. Williams, L. B.; Canfield, B.; Voglesonger, K. M.; Holloway, J. R. Organic molecules formed in a primordial womb. *Geology* **2005**, *33*, 913-916.
30. Canfield, B. M. Abiotic organic synthesis in simulated subseafloor hydrothermal vent conditions, 2006.
31. Bell, J. L. S.; Palmer, D. A.; Barnes, H. L.; Drummond, S. E. Thermal decomposition of acetate. III. Catalysis by mineral surfaces. *Geochim. Cosmochim. Acta* **1994**, *58*, 4155-77.
32. Akiya, N.; Savage, P. E. Kinetics and Mechanism of Cyclohexanol Dehydration in High-Temperature Water. *Ind Eng Chem Res* **2001**, *40*, 1822-1831.
33. Katritzky, A. R.; Nichols, D. A.; Siskin, M.; Murugan, R.; Balasubramanian, M. Reactions in High-Temperature Aqueous Media. *Chem. Rev. (Washington, D. C. )* **2001**, *101*, 837-892.
34. Akiya, N.; Savage, P. E. Roles of Water for Chemical Reactions in High-Temperature Water. *Chem. Rev. (Washington, DC, U. S. )* **2002**, *102*, 2725-2750.

35. Shock, E. L. Hydrothermal dehydration of aqueous organic compounds. *Geochim. Cosmochim. Acta* **1993**, *57*, 3341-9.
36. Yang, Z.; Gould, I. R.; Williams, L. B.; Hartnett, H. E.; Shock, E. L. The central role of ketones in reversible and irreversible hydrothermal organic functional group transformations. *Geochim. Cosmochim. Acta* **2012**, *98*, 48-65.
37. Adamiano, A.; Lesci, I. G.; Fabbri, D.; Roveri, N. Adsorption of bovine serum albumin onto synthetic Fe-doped geomimetic chrysotile. *J. R. Soc. Interface* **2015**, *12*, 1-11.
38. Bacsa, R. R.; de Parseval, P.; Martin, F.; Serp, P. Geomimetic catalysis: From volcanic stones to ultra-selective Fe-Mo/Al<sub>2</sub>O<sub>3</sub>-TiO<sub>2</sub> catalysts for few-walled carbon nanotube production. *Carbon* **2013**, *64*, 219-224.
39. Hashimoto, S.; Kusawake, S.; Daiko, Y.; Honda, S.; Iwamoto, Y. Fabrication of pure phase calcium carbonate hardened bodies as a means of creating novel geomimetic ceramics. *Constr. Build. Mater.* **2017**, *135*, 405-410.
40. Nair, B. G.; Zhao, Q.; Cooper, R. F. Geopolymer matrices with improved hydrothermal corrosion resistance for high-temperature applications. *J. Mater. Sci.* **2007**, *42*, 3083-3091.
41. Pierini, F.; Foresti, E.; Fracasso, G.; Lesci, I. G.; Roveri, N. Potential Technological Applications of Synthetic Geomimetic Nanotubes. *Isr. J. Chem.* **2010**, *50*, 484-499.
42. Shipp, J. A.; Gould, I. R.; Shock, E. L.; Williams, L. B.; Hartnett, H. E. Sphalerite is a geochemical catalyst for carbon-hydrogen bond activation. *Proc. Natl. Acad. Sci. U. S. A.* **2014**, *111*, 11642-11645.
43. McCollom, T. M.; Bach, W. Thermodynamic constraints on hydrogen generation during serpentinization of ultramafic rocks. *Geochim. Cosmochim. Acta* **2009**, *73*, 856-875.
44. Somorjai, G. A. *Introduction to Surface Chemistry and Catalysis*; Wiley: 1994; , pp 667 pp.
45. Horiuti, J.; Polanyi, M. Exchange reactions of hydrogen on metallic catalysts. *Trans. Faraday Soc.* **1934**, *30*, 1164-72.
46. Cremer, P. S.; Su, X.; Shen, Y. R.; Somorjai, G. The hydrogenation and dehydrogenation of isobutene on Pt(111) monitored by IR-visible sum frequency

- generation and gas chromatography. *J. Chem. Soc. , Faraday Trans.* **1996**, *92*, 4717-4722.
47. Betti, C.; Badano, J.; Lederhos, C.; Maccarrone, M.; Carrara, N.; Coloma-Pascual, F.; Quiroga, M.; Vera, C. Kinetic study of the selective hydrogenation of styrene over a Pd egg-shell composite catalyst. *React. Kinet. , Mech. Catal.* **2016**, *117*, 283-306.
48. Mitsui, S.; Gohke, K.; Saito, H.; Nanbu, A.; Senda, Y. Stereochemistry and mechanism of the catalytic hydrogenation of substituted methylenecyclohexanes. *Tetrahedron* **1973**, *29*, 1523-30.
49. Mintsá-Eya, V.; Hilaire, L.; Choplin, A.; Touroude, R.; Gault, F. G. The reaction of deuterium with olefins on nickel catalysts: evidence for adsorbed vinylic species. *J. Catal.* **1983**, *82*, 267-78.
50. Guan, S.; Donovan-Sheppard, O.; Reece, C.; Willock, D. J.; Wain, A. J.; Attard, G. A. Structure Sensitivity in Catalytic Hydrogenation at Platinum Surfaces Measured by Shell-Isolated Nanoparticle Enhanced Raman Spectroscopy (SHINERS). *ACS Catal.* **2016**, *6*, 1822-1832.
51. Bond, G. C. *Metal-Catalysed Reactions of Hydrocarbons*; Springer: 2005; , pp 450 pp. (approx.).
52. Christmann, K. The interaction of hydrogen with metal surfaces of two-fold symmetry. *Mol. Phys.* **1989**, *66*, 1-50.
53. Lopez Barreiro, D.; Samori, C.; Terranella, G.; Hornung, U.; Kruse, A.; Prins, W. Assessing microalgae biorefinery routes for the production of biofuels via hydrothermal liquefaction. *Bioresour. Technol.* **2014**, *174*, 256-265.
54. Kunkes, E. L.; Simonetti, D. A.; West, R. M.; Serrano-Ruiz, J.; Gaertner, C. A.; Dumesic, J. A. Catalytic conversion of biomass to monofunctional hydrocarbons and targeted liquid-fuel classes. *Science (Washington, DC, U. S. )* **2008**, *322*, 417-421.
55. Huber, G. W.; Dumesic, J. A. An overview of aqueous-phase catalytic processes for production of hydrogen and alkanes in a biorefinery. *Catal. Today* **2006**, *111*, 119-132.
56. Kalutharage, N.; Yi, C. S. Scope and mechanistic analysis for chemoselective hydrogenolysis of carbonyl compounds catalyzed by a cationic ruthenium hydride complex with a tunable phenol ligand. *J. Am. Chem. Soc.* **2015**, *137*, 11105-11114.

57. Brunauer, S.; Emmett, P. H.; Teller, E. Adsorption of gases in multimolecular layers. *J. Am. Chem. Soc.* **1938**, *60*, 309-19.
58. Helgeson, H. C.; Richard, L.; McKenzie, W. F.; Norton, D. L.; Schmitt, A. A chemical and thermodynamic model of oil generation in hydrocarbon source rocks. *Geochim. Cosmochim. Acta* **2009**, *73*, 594-695.
59. Amend, J. P.; McCollom, T. M.; Hentscher, M.; Bach, W. Catabolic and anabolic energy for chemolithoautotrophs in deep-sea hydrothermal systems hosted in different rock types. *Geochim. Cosmochim. Acta* **2011**, *75*, 5736-5748.
60. Katritzky, A. R.; Allin, S. M.; Siskin, M. Aquathermolysis: Reactions of Organic Compounds with Superheated Water. *Acc. Chem. Res.* **1996**, *29*, 399-406.
61. Siskin, M.; Katritzky, A. R. Reactivity of Organic Compounds in Superheated Water: General Background. *Chem. Rev. (Washington, D. C. )* **2001**, *101*, 825-835.
62. Kuhlmann, B.; Arnett, E. M.; Siskin, M. Classical Organic Reactions in Pure Superheated Water. *J. Org. Chem.* **1994**, *59*, 3098-101.
63. Ott, L.; Bicker, M.; Vogel, H. Catalytic dehydration of glycerol in sub- and supercritical water: a new chemical process for acrolein production. *Green Chem.* **2006**, *8*, 214-220.
64. Gould, E. S. *Mechanism and structure in organic chemistry*; Holt: 1959; .
65. Anslyn, E. V.; Dougherty, D. A. *Modern Physical Organic Chemistry*; University Science: 2005; .
66. Antal, M. J., Jr.; Brittain, A.; DeAlmeida, C.; Ramayya, S.; Roy, J. C. Heterolysis and homolysis in supercritical water. *ACS Symp. Ser.* **1987**, *329*, 77-86.
67. Narayan, R.; Antal, M. J., Jr. Influence of pressure on the acid-catalyzed rate constant for 1-propanol dehydration in supercritical water. *J. Am. Chem. Soc.* **1990**, *112*, 1927-31.
68. Ramayya, S.; Brittain, A.; DeAlmeida, C.; Mok, W.; Antal, M. J., Jr. Acid-catalyzed dehydration of alcohols in supercritical water. *Fuel* **1987**, *66*, 1364-71.
69. Xu, X.; De Almeida, C. P.; Antal, M. J., Jr. Mechanism and kinetics of the acid-catalyzed formation of ethene and diethyl ether from ethanol in supercritical water. *Ind Eng Chem Res* **1991**, *30*, 1478-85.

70. Antal, M. J., Jr.; Carlsson, M.; Xu, X.; Anderson, D. G. M. Mechanism and kinetics of the acid-catalyzed dehydration of 1- and 2-propanol in hot compressed liquid water. *Ind Eng Chem Res* **1998**, *37*, 3820-3829.
71. Hunter, S. E.; Ehrenberger, C. E.; Savage, P. E. Kinetics and Mechanism of Tetrahydrofuran Synthesis via 1,4-Butanediol Dehydration in High-Temperature Water. *J. Org. Chem.* **2006**, *71*, 6229-6239.
72. Changi, S.; Brown, T. M.; Savage, P. E. Reaction kinetics and pathways for phytol in high-temperature water. *Chem. Eng. J. (Amsterdam, Neth. )* **2012**, *189-190*, 336-345.
73. Hietala, D. C.; Savage, P. E. Reaction pathways and kinetics of cholesterol in high-temperature water. *Chem. Eng. J. (Amsterdam, Neth. )* **2015**, *265*, 129-137.
74. Johnson, J. W.; Norton, D. Critical phenomena in hydrothermal systems: state, thermodynamic, electrostatic, and transport properties of water in the critical region. *Am. J. Sci.* **1991**, *291*, 541-648.
75. Palmer, D. A.; Fernandez-Prini, R.; Harvey, A. H. *Aqueous Systems at Elevated Temperatures and Pressures: Physical Chemistry in Water, Steam and Hydrothermal Solutions*; Elsevier: 2004; , pp 753 pp.
76. Wagner, W.; Pruss, A. The IAPWS Formulation 1995 for the Thermodynamic Properties of Ordinary Water Substance for General and Scientific Use. *J. Phys. Chem. Ref. Data* **2002**, *31*, 387-535.
77. Friesen, J. B.; Schretzman, R. Dehydration of 2-Methyl-1-cyclohexanol: New Findings from a Popular Undergraduate Laboratory Experiment. *J. Chem. Educ.* **2011**, *88*, 1141-1147.
78. Streitwieser, A.; Heathcock, C. H.; Kosower, E. M. *Introduction to Organic Chemistry*; Prentice Hall: 1995; .
79. Xu, X.; Antal, M. J., Jr.; Anderson, D. G. M. Mechanism and temperature-dependent kinetics of the dehydration of tert-butyl alcohol in hot compressed liquid water. *Ind Eng Chem Res* **1997**, *36*, 23-41.
80. Xu, X.; Antal, M. J., Jr. Kinetics and mechanism of isobutene formation from T-butanol in hot liquid water. *AIChE J.* **1994**, *40*, 1524-32.
81. Anastas, P. T.; Warner, J. C. *Green Chemistry: Theory and Practice*; Oxford University Press: 1998; .

82. Broll; Kaul; Kramer; Krammer; Richter; Jung; Vogel; Zehner Chemistry in Supercritical Water. *Angew. Chem. Int. Ed Engl.* **1999**, *38*, 2998-3014.
83. Hunter, S. E.; Savage, P. E. Recent advances in acid- and base-catalyzed organic synthesis in high-temperature liquid water. *Chem. Eng. Sci.* **2004**, *59*, 4903-4909.
84. Hunter, S. E.; Felczak, C. A.; Savage, P. E. Synthesis of p-isopropenylphenol in high-temperature water. *Green Chem.* **2004**, *6*, 222-226.
85. Avola, S.; Guillot, M.; da Silva-Perez, D.; Pellet-Rostaing, S.; Kunz, W.; Goettmann, F. Organic chemistry under hydrothermal conditions. *Pure Appl. Chem.* **2013**, *85*, 89-103.
86. Shanab, K.; Neudorfer, C.; Schirmer, E.; Spreitzer, H. Green Solvents in Organic Synthesis: An Overview. *Curr. Org. Chem.* **2013**, *17*, 1179-1187.
87. Yang, Z.; Hartnett, H. E.; Shock, E. L.; Gould, I. R. Organic Oxidations Using Geomimicry. *J. Org. Chem.* **2015**, *80*, 12159-12165.
88. Hoops, S.; Sahle, S.; Gauges, R.; Lee, C.; Pahle, J.; Simus, N.; Singhal, M.; Xu, L.; Mendes, P.; Kummer, U. COPASI - A COMplex PATHway SIMulator. *Bioinformatics* **2006**, *22*, 3067-3074.
89. Smith, M. B.; March, J. Stereochemistry. In *March's Advanced Organic Chemistry, 6th Ed* John Wiley & Sons: New York, NY, 2007; pp 206.
90. Angyal, S. J.; McHugh, D. J. Interaction energies of axial hydroxyl groups. *Chem. Ind. (London, U. K. )* **1956**, 1147-8.
91. Manoharan, M.; Eliel, E. L. Conformation, in solution, of c-4-tert-butyl-1-phenyl-r-1-(N-piperidyl)cyclohexane hydrochloride. The conformational energy of tert-butyl. *Tetrahedron Lett.* **1984**, *25*, 3267-8.
92. Saunders, M.; Kates, M. R. Rates of degenerate 1,2-hydride and 1,2-methide shifts from the carbon-13 nuclear magnetic resonance spectra of tertiary alkyl cations. *J. Am. Chem. Soc.* **1978**, *100*, 7082-3.
93. Ammal, S. C.; Yamataka, H.; Aida, M.; Dupuis, M. Dynamics-Driven Reaction Pathway in an Intramolecular Rearrangement. *Science (Washington, DC, U. S. )* **2003**, *299*, 1555-1557.
94. Hare, S. R.; Tantillo, D. J. Dynamic behavior of rearranging carbocations - implications for terpene biosynthesis. *Beilstein J. Org. Chem.* **2016**, *12*, 377-390.

95. Hong, Y. J.; Tantillo, D. J. How Many Secondary Carbocations Are Involved in the Biosynthesis of Avermitilol? *Org. Lett.* **2011**, *13*, 1294-1297.
96. Hong, Y. J.; Tantillo, D. J. Consequences of Conformational Preorganization in Sesquiterpene Biosynthesis: Theoretical Studies on the Formation of the Bisabolene, Curcumene, Acoradiene, Zizaene, Cedrene, Duprezianene, and Sesquithuriferol Sesquiterpenes. *J. Am. Chem. Soc.* **2009**, *131*, 7999-8015.
97. Bartsch, R. A.; Bunnett, J. F. Kinetics of reactions of 2-hexyl halides and 2-hexyl p-bromobenzenesulfonate with sodium methoxide in methanol. Evidence that orientation of olefin-forming elimination is not determined by the steric requirements of halogen leaving groups. *J. Amer. Chem. Soc.* **1968**, *90*, 408-17.
98. Bunnett, J. F.; Baciocchi, E. Kinetics of olefin-forming elimination from benzyldimethylcarbinyl halides induced by halide ions in acetone. *J. Org. Chem.* **1970**, *35*, 76-9.
99. Winstein, S.; Fainberg, A. H. Correlation of solvolysis rates. IV. Solvent effects on enthalpy and entropy of activation for solvolysis of tert-butyl chloride. *J. Am. Chem. Soc.* **1957**, *79*, 5937-50.
100. East, A. L. L.; Bucko, T.; Hafner, J. On the structure and dynamics of secondary n-alkyl cations. *J. Chem. Phys.* **2009**, *131*, 104314/1-104314/10.
101. Bergsma, J. P.; Gertner, B. J.; Wilson, K. R.; Hynes, J. T. Molecular dynamics of a model SN2 reaction in water. *J. Chem. Phys.* **1987**, *86*, 1356-76.
102. Van, d. Z.; Hynes, J. T. Dynamical polar solvent effects on solution reactions: a simple continuum model. *J. Chem. Phys.* **1982**, *76*, 2993-3001.
103. Zhang, M.; Yu, Y. Dehydration of Ethanol to Ethylene. *Ind Eng Chem Res* **2013**, *52*, 9505-9514.
104. Honkela, M. L.; Ouni, T.; Krause, A. O. Thermodynamics and Kinetics of the Dehydration of tert-Butyl Alcohol. *Ind Eng Chem Res* **2004**, *43*, 4060-4065.
105. Chen, L.; Xin, J.; Ni, L.; Dong, H.; Yan, D.; Lu, X.; Zhang, S. Conversion of lignin model compounds under mild conditions in pseudo-homogeneous systems. *Green Chem.* **2016**, *18*, 2341-2352.
106. Cuesta Zapata, P. M.; Nazzarro, M. S.; Gonzo, E. E.; Parentis, M. L.; Bonini, N. A. Cr/SiO<sub>2</sub> mesoporous catalysts: Effect of hydrothermal treatment and calcination

- temperature on the structure and catalytic activity in the gas phase dehydration and dehydrogenation of cyclohexanol. *Catal. Today* **2016**, 259, 39-49.
107. Xu, S.; Sheng, H.; Ye, T.; Hu, D.; Liao, S. Hydrophobic aluminosilicate zeolites as highly efficient catalysts for the dehydration of alcohols. *Catal. Commun.* **2016**, 78, 75-79.
  108. Yoon, J. S.; Choi, J.; Suh, D. J.; Lee, K.; Lee, H.; Ha, J. Water-Assisted Selective Hydrodeoxygenation of Lignin-Derived Guaiacol to Monooxygenates. *ChemCatChem* **2015**, 7, 2669-2674.
  109. Murru, S.; Nicholas, K. M.; Srivastava, R. S. Ruthenium (II) sulfoxides-catalyzed hydrogenolysis of glycols and epoxides. *J. Mol. Catal. A: Chem.* **2012**, 363-364, 460-464.
  110. Zhao, C.; He, J.; Lemonidou, A. A.; Li, X.; Lercher, J. A. Aqueous-phase hydrodeoxygenation of bio-derived phenols to cycloalkanes. *J. Catal.* **2011**, 280, 8-16.
  111. Zhao, C.; Song, W.; Lercher, J. A. Aqueous Phase Hydroalkylation and Hydrodeoxygenation of Phenol by Dual Functional Catalysts Comprised of Pd/C and H/La-BEA. *ACS Catal.* **2012**, 2, 2714-2723.
  112. Ludmany, A.; Kurek, S. S.; Stoklosa, A.; Wilczynski, G.; Wojtowicz, A.; Zajecki, J. Amorphous titanium hydrogen phosphate - an inorganic sorbent and a catalyst. *Appl. Catal. , A* **2004**, 267, 149-156.
  113. Hiegel, G. A.; Rubino, M. Conversion of alcohols into alkyl chlorides using trichloroisocyanuric acid with triphenylphosphine. *Synth. Commun.* **2002**, 32, 2691-2694.
  114. Gallezot, P. Conversion of biomass to selected chemical products. *Chem. Soc. Rev.* **2012**, 41, 1538-1558.
  115. Mohan, D.; Pittman, C. U., Jr.; Steele, P. H. Pyrolysis of Wood/Biomass for Bio-oil: A Critical Review. *Energy Fuels* **2006**, 20, 848-889.
  116. Zhang, Q.; Chang, J.; Wang, T.; Xu, Y. Review of biomass pyrolysis oil properties and upgrading research. *Energy Convers. Manage.* **2006**, 48, 87-92.
  117. Corma, A.; Iborra, S.; Velty, A. Chemical Routes for the Transformation of Biomass into Chemicals. *Chem. Rev. (Washington, DC, U. S. )* **2007**, 107, 2411-2502.



118. Rinaldi, R.; Schueth, F. Design of solid catalysts for the conversion of biomass. *Energy Environ. Sci.* **2009**, *2*, 610-626.
119. Tong, X.; Ma, Y.; Li, Y. Biomass into chemicals: Conversion of sugars to furan derivatives by catalytic processes. *Appl. Catal. , A* **2010**, *385*, 1-13.
120. Jin, F.; Enomoto, H. Rapid and highly selective conversion of biomass into value-added products in hydrothermal conditions: chemistry of acid/base-catalyzed and oxidation reactions. *Energy Environ. Sci.* **2011**, *4*, 382-397.
121. Shiramizu, M.; Toste, F. D. Deoxygenation of Biomass-Derived Feedstocks: Oxorhenium-Catalyzed Deoxydehydration of Sugars and Sugar Alcohols. *Angew. Chem. , Int. Ed.* **2012**, *51*, 8082-8086, S8082/1-S8082/36.
122. Williamson, F. *Organic Experiments, 8th Ed*; Houghton Mifflin: 1998; .
123. Werstiuk, N. H.; Timmins, G. Protium-deuterium exchange of cyclic and acyclic alkenes in dilute acid medium at elevated temperatures. *Can. J. Chem.* **1985**, *63*, 530-3.
124. Galwey, A. K. Reactions of alcohols adsorbed on montmorillonite and the role of minerals in petroleum genesis. *J. Chem. Soc. D* **1969**, 577-8.
125. Soma, Y.; Soma, M. Chemical reactions of organic compounds on clay surfaces. *Environ. Health Perspect.* **1989**, *83*, 205-14.
126. MacGowan, D. B.; Surdam, R. C. Difunctional carboxylic acid anions in oilfield waters. *Org. Geochem.* **1988**, *12*, 245-59.
127. Hanor, J. S.; Land, L. S.; Macpherson, G. L. Carboxylic acid anions in formation waters, San Joaquin Basin and Louisiana Gulf Coast, U.S.A.-Implications for clastic diagenesis. Critical comment. *Appl. Geochem.* **1993**, *8*, 305-7.
128. Shock, E. L. Application of thermodynamic calculations to geochemical processes involving organic acids. In *The Role of Organic Acids in Geochemical Processes*; Lewan, M., Pittman, E., Eds.; Springer-Verlag: Berlin, 1994; pp 270-318.
129. Lang, S. Q.; Butterfield, D. A.; Schulte, M.; Kelley, D. S.; Lilley, M. D. Elevated concentrations of formate, acetate and dissolved organic carbon found at the Lost City hydrothermal field. *Geochim. Cosmochim. Acta* **2010**, *74*, 941-952.

130. Hubova, P.; Tejnecky, V.; Ash, C.; Boruvka, L.; Drabek, O. Low-Molecular-Mass Organic Acids in the Forest Soil Environment. *Mini-Rev. Org. Chem.* **2017**, *14*, 75-84.
131. Gordalla, B. C.; Ewers, U.; Frimmel, F. H. Hydraulic fracturing: a toxicological threat for groundwater and drinking-water? *Environ. Earth Sci.* **2013**, *70*, 3875-3893.
132. Raju, S.; Moret, M.; Klein Gebbink, Robertus J. M. Rhenium-Catalyzed Dehydration and Deoxydehydration of Alcohols and Polyols: Opportunities for the Formation of Olefins from Biomass. *ACS Catal.* **2015**, *5*, 281-300.
133. Garcia-Verdugo, E.; Liu, Z.; Ramirez, E.; Garcia-Serna, J.; Fraga-Dubreuil, J.; Hyde, J. R.; Hamley, P. A.; Poliakoff, M. In situ generation of hydrogen for continuous hydrogenation reactions in high temperature water. *Green Chem.* **2006**, *8*, 359-364.
134. Kalpala, J.; Hartonen, K.; Huhdanpaa, M.; Riekkola, M. Deuteration of 2-methylnaphthalene and eugenol in supercritical and pressurised hot deuterium oxide. *Green Chem.* **2003**, *5*, 670-676.
135. Alonso, F.; Osante, I.; Yus, M. Highly selective hydrogenation of multiple carbon-carbon bonds promoted by nickel(0) nanoparticles. *Tetrahedron* **2007**, *63*, 93-102.
136. Mitsui, S.; Imaizumi, S.; Nanbu, A.; Senda, Y. Stereochemistry and mechanism of the catalytic hydrogenation of dimethylcyclohexenes. *J. Catal.* **1975**, *36*, 333-7.
137. Wainwright, M. S. 3.2 Skeletal Metal Catalysts. In *Preparation of Solid Catalysts*; Ertl, G., Knozinger, H. and Weitkamp, J., Eds.; Wiley-VCH Verlag: Germany, 1999; pp 28-29.
138. Schafer, C.; Ellstrom, C. J.; Cho, H.; Torok, B. Pd/C-Al-water facilitated selective reduction of a broad variety of functional groups. *Green Chem.* **2017**, *19*, 1230-1234.
139. Cui, X.; Yuan, H.; Junge, K.; Topf, C.; Beller, M.; Shi, F. A stable and practical nickel catalyst for the hydrogenolysis of C-O bonds. *Green Chem.* **2017**, *19*, 305-310.
140. Lucarelli, C.; Lolli, A.; Giugni, A.; Grazia, L.; Albonetti, S.; Monticelli, D.; Vaccari, A. Efficient and ecofriendly route for the solvent-free synthesis of piperonal and aromatic aldehydes using Au/CeO<sub>2</sub> catalyst. *Appl. Catal., B* **2017**, *203*, 314-323.

141. Soni, V. K.; Sharma, P. R.; Choudhary, G.; Pandey, S.; Sharma, R. K. Ni/Co-Natural Clay as Green Catalysts for Microalgae Oil to Diesel-Grade Hydrocarbons Conversion. *ACS Sustainable Chem. Eng.* **2017**, *5*, 5351-5359.
142. Finnigan, W.; Thomas, A.; Cromar, H.; Gough, B.; Snajdrova, R.; Adams, J. P.; Littlechild, J. A.; Harmer, N. J. Characterization of Carboxylic Acid Reductases as Enzymes in the Toolbox for Synthetic Chemistry. *ChemCatChem* **2017**, *9*, 1005-1017.
143. Biermann, M.; Bakonyi, D.; Hummel, W.; Groeger, H. Design of recombinant whole-cell catalysts for double reduction of C=C and C=O bonds in enals and application in the synthesis of Guerbet alcohols as industrial bulk chemicals for lubricants. *Green Chem.* **2017**, *19*, 405-410.
144. Helgeson, H. C.; Delany, J. M.; Nesbitt, H. W.; Bird, D. K. *Summary and critique of the thermodynamic properties of rock-forming minerals*; Kline Geology Laboratory, Yale University: 1978; , pp 229 pp.
145. Robie, R. A.; Hemingway, B. S.; Fisher, J. R. *Thermodynamic Properties of Minerals and Related Substances at 298.15 K and 1 Bar (105 Pascals) Pressure and at Higher Temperatures*; Government Printing Office: 1978; , pp 456 pp.
146. Kelley, K. K. Data on theoretical metallurgy. XIII. High-temperature, heat-capacity, and entropy data for the elements and inorganic compounds. *Bull. - U. S. , Bur. Mines* **1960**, No. 584, 232 pp.
147. Gao, X.; Tong, D.; Zhong, H.; Jin, B.; Jin, F.; Zhang, H. Highly efficient conversion of fatty acids into fatty alcohols with a Zn over Ni catalyst in water. *RSC Adv.* **2016**, *6*, 27623-27626.
148. Cox, P. A. *The Elements: Their Origin, Abundance, and Distribution*; Oxford University Press: New York, 1989; .
149. Son, K.; Gland, J. L. Gas Phase Atomic Hydrogen-Induced Hydrogenation of Cyclohexene on the Ni(100) Surface. *J Phys Chem B* **1997**, *101*, 3540-3546.
150. Corson, B. B.; Ipatieff, V. N. Simultaneous dehydrogenation-hydrogenation of cyclohexene in the presence of nickel. *J. Am. Chem. Soc.* **1939**, *61*, 1056-7.
151. Benson, S. W.; Shaw, R. Kinetics and mechanism of the pyrolysis of 1,3-cyclohexadiene. Thermal source of cyclohexadienyl radicals and hydrogen atoms. Addition of hydrogen atoms to benzene and toluene. *J. Am. Chem. Soc.* **1967**, *89*, 5351-4.

152. Boucher-Jacobs, C.; Nicholas, K. M. Oxo-rhenium-catalyzed deoxydehydration of polyols with hydroaromatic reductants. *Organometallics* **2015**, *34*, 1985-1990.
153. Gorzynski Smith, J. *Organic Chemistry*; McGraw-Hill: Boston, MA, 2010; .
154. Nishimura, S.; Sakamoto, H.; Ozawa, T. Stereoselectivity patterns of the platinum metals in the catalytic hydrogenation of some cycloolefinic compounds. *Chem. Lett.* **1973**, 855-8.
155. Verho, O.; Zheng, H.; Gustafson, K. P. J.; Nagendiran, A.; Zou, X.; Baeckvall, J. Application of Pd Nanoparticles Supported on Mesoporous Hollow Silica Nanospheres for the Efficient and Selective Semihydrogenation of Alkynes. *ChemCatChem* **2016**, *8*, 773-778.
156. Xu, R.; Chakraborty, S.; Bellows, S. M.; Yuan, H.; Cundari, T. R.; Jones, W. D. Iron-Catalyzed Homogeneous Hydrogenation of Alkenes under Mild Conditions by a Stepwise, Bifunctional Mechanism. *ACS Catal.* **2016**, *6*, 2127-2135.
157. Brewster, J. H. Mechanism of reductions at metal surfaces. I. A general working hypothesis. *J. Am. Chem. Soc.* **1954**, *76*, 6361-3.
158. Dust, J. M.; Arnold, D. R. Substituent effects on benzyl radical ESR hyperfine coupling constants. The  $\sigma\alpha\cdot$  scale based upon spin delocalization. *J. Am. Chem. Soc.* **1983**, *105*, 1221-7.
159. Tang, Y.; Miao, S.; Pham, H. N.; Datye, A.; Zheng, X.; Shanks, B. H. Enhancement of Pt catalytic activity in the hydrogenation of aldehydes. *Appl. Catal., A* **2011**, *406*, 81-88.
160. Wei, Y.; Rao, B.; Cong, X.; Zeng, X. Highly Selective Hydrogenation of Aromatic Ketones and Phenols Enabled by Cyclic (Amino)(alkyl)carbene Rhodium Complexes. *J. Am. Chem. Soc.* **2015**, *137*, 9250-9253.
161. Anderson, J. A.; Athawale, A.; Imrie, F. E.; McKenna, F. -.; McCue, A.; Molyneux, D.; Power, K.; Shand, M.; Wells, R. P. K. Aqueous phase hydrogenation of substituted phenyls over carbon nanofibre and activated carbon supported Pd. *J. Catal.* **2010**, *270*, 9-15.
162. Korstanje, T. J.; van, d. V.; Elsevier, C. J.; de Bruin, B. Hydrogenation of carboxylic acids with a homogeneous cobalt catalyst. *Science (Washington, DC, U. S. )* **2015**, *350*, 298-302.

163. Alonso, F.; Riente, P.; Yus, M. Nickel Nanoparticles in Hydrogen Transfer Reactions. *Acc. Chem. Res.* **2011**, *44*, 379-391.
164. Feghouli, A.; Fort, Y.; Vanderesse, R.; Caubere, P. Activation of reducing agents. Sodium hydride-containing complex reducing agents. 28. Stereochemistry of reduction of ketones by complex reducing agents. *Tetrahedron Lett.* **1988**, *29*, 1379-82.
165. Sarkar, A.; Rao, B. R. Montmorillonite-supported (-)-N-dodecyl-N-methylephedrenium borohydride: an efficient reducing agent. *Tetrahedron Lett.* **1991**, *32*, 1247-50.
166. Ramanujam, V. M. S.; Trieff, N. M. Reduction of some ketones using sulfurated sodium borohydride (NaBH<sub>2</sub>S<sub>3</sub>): kinetics and mechanism. *J. Chem. Soc., Perkin Trans. 2* **1976**, 1811-15.
167. Liu, G.; Zhao, H.; Zhu, J.; He, H.; Yang, H.; Thiemann, T.; Tashiro, H.; Tashiro, M. New Method for the Reduction of Benzophenones with Raney Ni-Al Alloy in Water. *Synth. Commun.* **2008**, *38*, 1651-1661.
168. Carrara, N.; Badano, J.; Bertero, N.; Torres, G.; Betti, C.; Martinez-Bovier, L.; Quiroga, M.; Vera, C. Kinetics of the liquid phase selective hydrogenation of 2,3-butanedione over new composite supported Pd catalysts. *J. Chem. Technol. Biotechnol.* **2014**, *89*, 265-275.
169. Kim, D.; Kang, H.; Park, H.; Park, S.; Park, J. C.; Park, K. H. Nickel Nanoparticles Supported on CMK-3 with Enhanced Catalytic Performance for Hydrogenation of Carbonyl Compounds. *Eur. J. Inorg. Chem.* **2016**, *2016*, 3469-3473.
170. Poupart, R.; Le Droumaguet, B.; Guerrouache, M.; Carbonnier, B. Copper nanoparticles supported on permeable monolith with carboxylic acid surface functionality: Stability and catalytic properties under reductive conditions. *Mater. Chem. Phys.* **2015**, *163*, 446-452.
171. Kidwai, M.; Bansal, V.; Saxena, A.; Shankar, R.; Mozumdar, S. Ni-nanoparticles. An efficient green catalyst for chemoselective reduction of aldehydes. *Tetrahedron Lett.* **2006**, *47*, 4161-4165.
172. Kidwai, M.; Mishra, N. K.; Bansal, V.; Kumar, A.; Mozumdar, S. Ni nanoparticles usage for the reduction of ketones. *Catal. Commun.* **2008**, *9*, 612-617.

173. Horikoshi, S.; Tsuzuki, J.; Sakai, F.; Kajitani, M.; Serpone, N. Microwave effect on the surface composition of the Urushibara Ni hydrogenation catalyst and improved reduction of acetophenone. *Chem. Commun. (Cambridge, U. K.)* **2008**, 4501-4503.
174. Brewster, T. P.; Miller, A. J. M.; Heinekey, D. M.; Goldberg, K. I. Hydrogenation of Carboxylic Acids Catalyzed by Half-Sandwich Complexes of Iridium and Rhodium. *J. Am. Chem. Soc.* **2013**, *135*, 16022-16025.
175. Cui, X.; Li, Y.; Topf, C.; Junge, K.; Beller, M. Direct Ruthenium-catalyzed Hydrogenation of Carboxylic Acids to Alcohols. *Angew. Chem., Int. Ed.* **2015**, *54*, 10596-10599.
176. Bernardo, J. R.; Fernandes, A. C. Deoxygenation of carbonyl compounds using an alcohol as an efficient reducing agent catalyzed by oxo-rhenium complexes. *Green Chem.* **2016**, *18*, 2675-2681.
177. Frost, J. C. Junction effect interactions in methanol synthesis catalysts. *Nature (London)* **1988**, *334*, 577-80.
178. Le Valant, A.; Comminges, C.; Tisseraud, C.; Canaff, C.; Pinard, L.; Pouilloux, Y. The Cu-ZnO synergy in methanol synthesis from CO<sub>2</sub>, Part 1: Origin of active site explained by experimental studies and a sphere contact quantification model on Cu + ZnO mechanical mixtures. *J. Catal.* **2015**, *324*, 41-49.
179. Huang, C.; Chen, S.; Fei, X.; Liu, D.; Zhang, Y. Catalytic hydrogenation of CO<sub>2</sub> to methanol: study of synergistic effect on adsorption properties of CO<sub>2</sub> and H<sub>2</sub> in CuO/ZnO/ZrO<sub>2</sub> system. *Catalysts* **2015**, *5*, 1846-1861.
180. Yin, G.; Abe, H.; Kodiyath, R.; Ueda, S.; Srinivasan, N.; Yamaguchi, A.; Miyauchi, M. Selective electro- or photo-reduction of carbon dioxide to formic acid using a Cu-Zn alloy catalyst. *J. Mater. Chem. A* **2017**, Ahead of Print.
181. Harikumar, K. R.; Santra, A. K. A comparative study of the interaction of CO with Cu and Cu-Zn alloy clusters. *Solid State Commun.* **1996**, *99*, 403-406.
182. Simmons, H. E.; Smith, R. D. A new synthesis of cyclopropanes. *J. Am. Chem. Soc.* **1959**, *81*, 4256-64.
183. Braun, F.; Di Cosimo, J. I. Catalytic and spectroscopic study of the allylic alcohol synthesis by gas-phase hydrogen transfer reduction of unsaturated ketones on acid-base catalysts. *Catal. Today* **2006**, *116*, 206-215.

184. Alonso, F.; Riente, P.; Yus, M. Hydrogen-transfer reduction of carbonyl compounds catalyzed by nickel nanoparticles. *Tetrahedron Lett.* **2008**, *49*, 1939-1942.
185. Suceveanu, M.; Raicopol, M.; Enache, R.; Finaru, A.; Rosca, S. I. Selective reductions of the carbonyl compounds and aryl halides with Ni-Al alloy in aqueous alkali medium. *Lett. Org. Chem.* **2011**, *8*, 690-695.
186. Di, L.; Yao, S.; Li, M.; Wu, G.; Dai, W.; Wang, G.; Li, L.; Guan, N. Selective Catalytic Hydrogenolysis of Carbon-Carbon  $\text{C}-\text{C}$  Bonds in Primary Aliphatic Alcohols over Supported Metals. *ACS Catal.* **2015**, *5*, 7199-7207.
187. Gillespie, W. D.; Herz, R. K.; Petersen, E. E.; Somorjai, G. A. The structure sensitivity of n-heptane dehydrocyclization and hydrogenolysis catalyzed by platinum single crystals at atmospheric pressure. *J. Catal.* **1981**, *70*, 147-59.
188. Luo, Y.; Editor. *Comprehensive Handbook of Chemical Bond Energies*; CRC Press: 2007; , pp 1520 pp.
189. Mebane, R. C.; Holte, K. L.; Gross, B. H. Transfer Hydrogenation of Ketones with 2-Propanol and Raney Nickel. *Synth. Commun.* **2007**, *37*, 2787-2791.
190. Hong, H. L.; Wang, Q.; Dong, C.; Liaw, P. K. Understanding the Cu-Zn brass alloys using a short-range-order cluster model: significance of specific compositions of industrial alloys. *Sci Rep* **2014**, *4*, 7065.
191. Steinfeld, A. Solar thermochemical production of hydrogen--a review. *Sol. Energy* **2005**, *78*, 603-615.
192. Xu, L.; Huo, Z.; Fu, J.; Jin, F. Highly efficient conversion of biomass-derived glycolide to ethylene glycol over CuO in water. *Chem. Commun. (Cambridge, U. K.)* **2014**, *50*, 6009-6012.
193. Onwudili, J. A.; Nahil, M. A.; Wu, C.; Williams, P. T. High temperature pyrolysis of solid products obtained from rapid hydrothermal pre-processing of pinewood sawdust. *RSC Adv.* **2014**, *4*, 34784-34792.
194. Delgado, S. N.; Vivier, L.; Especel, C. Polyol hydrogenolysis on supported Pt catalysts: Comparison between glycerol and 1,2-propanediol. *Catal. Commun.* **2014**, *43*, 107-111.
195. Yang, C.; Li, R.; Cui, C.; Liu, S.; Qiu, Q.; Ding, Y.; Wu, Y.; Zhang, B. Catalytic hydroprocessing of microalgae-derived biofuels: a review. *Green Chem.* **2016**, *18*, 3684-3699.

196. Mathieu, Y.; Sauvanaud, L.; Humphreys, L.; Rowlands, W.; Maschmeyer, T.; Corma, A. Production of High Quality Syncrude from Lignocellulosic Biomass. *ChemCatChem* **2017**, *9*, 1574-1578.
197. Jin, F. Water Under High Temperature and Pressure Conditions and Its Applications to Develop Green Technologies for Biomass Conversion. In *Application of Hydrothermal Reactions to Biomass Conversion*; Jin, F., Wang, Y., Zeng, X., Shen, Z. and Yao, G., Eds.; Springer-Verlag: Berlin Heidelberg, 2014; pp 3-28.
198. Deutsch, K. L.; Lahr, D. G.; Shanks, B. H. Probing the ruthenium-catalyzed higher polyol hydrogenolysis reaction through the use of stereoisomers. *Green Chem.* **2012**, *14*, 1635-1642.
199. Sun, R.; Wang, T.; Zheng, M.; Deng, W.; Pang, J.; Wang, A.; Wang, X.; Zhang, T. Versatile Nickel-Lanthanum(III) Catalyst for Direct Conversion of Cellulose to Glycols. *ACS Catal.* **2015**, *5*, 874-883.
200. Wu, C.; Qu, J.; Elliott, J.; Yu, K. M. K.; Tsang, S. C. E. Hydrogenolysis of ethylene glycol to methanol over modified RANEY catalysts. *Phys. Chem. Chem. Phys.* **2013**, *15*, 9043-9050.
201. Wang, K.; Hawley, M. C.; Furney, T. D. Mechanism Study of Sugar and Sugar Alcohol Hydrogenolysis Using 1,3-Diol Model Compounds. *Ind Eng Chem Res* **1995**, *34*, 3766-70.
202. Yoosuk, B.; Tumnantong, D.; Prasassarakich, P. Amorphous unsupported Ni-Mo sulfide prepared by one step hydrothermal method for phenol hydrodeoxygenation. *Fuel* **2012**, *91*, 246-252.
203. Wang, W.; Li, L.; Tan, S.; Wu, K.; Zhu, G.; Liu, Y.; Xu, Y.; Yang, Y. Preparation of NiS<sub>2</sub>/MoS<sub>2</sub> catalysts by two-step hydrothermal method and their enhanced activity for hydrodeoxygenation of p-cresol. *Fuel* **2016**, *179*, 1-9.
204. Meszaros, S.; Halasz, J.; Konya, Z.; Sipos, P.; Palinko, I. Search for a Raney-Ni type catalyst efficient in the transformation of excess glycerol into more valuable products. *Catal. Commun.* **2014**, *43*, 116-120.
205. Lohr, T. L.; Marks, T. J. Orthogonal tandem catalysis. *Nat. Chem.* **2015**, *7*, 477-482.
206. Nalesnik, T. E.; Holy, N. L. Homogeneous catalytic cyclization and oxidation of diols. *J. Org. Chem.* **1977**, *42*, 372-4.



207. Arceo, E.; Ellman, J. A.; Bergman, R. G. Rhenium-Catalyzed Didehydroxylation of Vicinal Diols to Alkenes Using a Simple Alcohol as a Reducing Agent. *J. Am. Chem. Soc.* **2010**, *132*, 11408-11409.
208. Ziegler, J. E.; Zdilla, M. J.; Evans, A. J.; Abu-Omar, M. H<sub>2</sub>-driven deoxygenation of epoxides and diols to alkenes catalyzed by methyltrioxorhenium. *Inorg. Chem.* **2009**, *48*, 9998-10000.
209. Chen, K.; Mori, K.; Watanabe, H.; Nakagawa, Y.; Tomishige, K. C-O bond hydrogenolysis of cyclic ethers with OH groups over rhenium-modified supported iridium catalysts. *J. Catal.* **2012**, *294*, 171-183.
210. Nakagawa, Y.; Mori, K.; Chen, K.; Amada, Y.; Tamura, M.; Tomishige, K. Hydrogenolysis of CO bond over Re-modified Ir catalyst in alkane solvent. *Appl. Catal.* , A **2013**, *468*, 418-425.
211. Moriconi, E. J.; O'Connor, W. F.; Kuhn, L. P.; Keneally, E. A.; Wallenberger, F. T. Intramolecular hydrogen bonding of vicinal diols in cyclic systems. II. OH...O and OH... $\pi$ -electron bonding in cis- and trans-1,2-diaryl-1,2-acenaphthenediols. *J. Am. Chem. Soc.* **1959**, *81*, 6472-7.
212. Meinwald, J.; Labana, S. S.; Chadha, M. S. Peracid reactions. III. The oxidation of bicyclo[2.2.1]-heptadiene. *J. Am. Chem. Soc.* **1963**, *85*, 582-5.
213. McCollom, T. M.; Simoneit, B. R. T.; Shock, E. L. Hydrous Pyrolysis of Polycyclic Aromatic Hydrocarbons and Implications for the Origin of PAH in Hydrothermal Petroleum. *Energy Fuels* **1999**, *13*, 401-410.
214. Venturi, S.; Tassi, F.; Gould, I. R.; Shock, E. L.; Hartnett, H. E.; Lorange, E. D.; Bockisch, C.; Fecteau, K. M.; Capecchiacci, F.; Vaselli, O. Mineral-assisted production of benzene under hydrothermal conditions: Insights from experimental studies on C<sub>6</sub> cyclic hydrocarbons. *Journal of Volcanology and Geothermal Research* **2017**.
215. Glein, C. R. Theoretical and Experimental Studies of Cryogenic and Hydrothermal Organic Geochemistry, Arizona State University, Tempe, AZ, 2012.
216. Linstrom, P. J.; Mallard, W. G. NIST Chemistry WebBook NIST Standard Reference Database Number 69 . (accessed June, 2017).

217. Nishiyama, Y.; Katsuen, S.; Jounen, H.; Hamanaka, S.; Ogawa, S.; Sonoda, N. Selenium-catalyzed debromination of vic-dibromoalkanes and  $\alpha$ -bromo ketones with carbon monoxide and water. *Heteroat. Chem.* **1990**, *1*, 467-74.
218. Dolejs, L.; Hanus, V. Mass spectrometric study of water elimination from tert-butylcyclohexanols. *Collect. Czech. Chem. Commun.* **1968**, *33*, 332-5.
219. Kamata, K.; Yonehara, K.; Nakagawa, Y.; Uehara, K.; Mizuno, N. Efficient stereo- and regioselective hydroxylation of alkanes catalyzed by a bulky polyoxometalate. *Nat. Chem.* **2010**, *2*, 478-483.

## APPENDIX A.

### METAL/SURFACE CHARACTERIZATION

## SEM Images

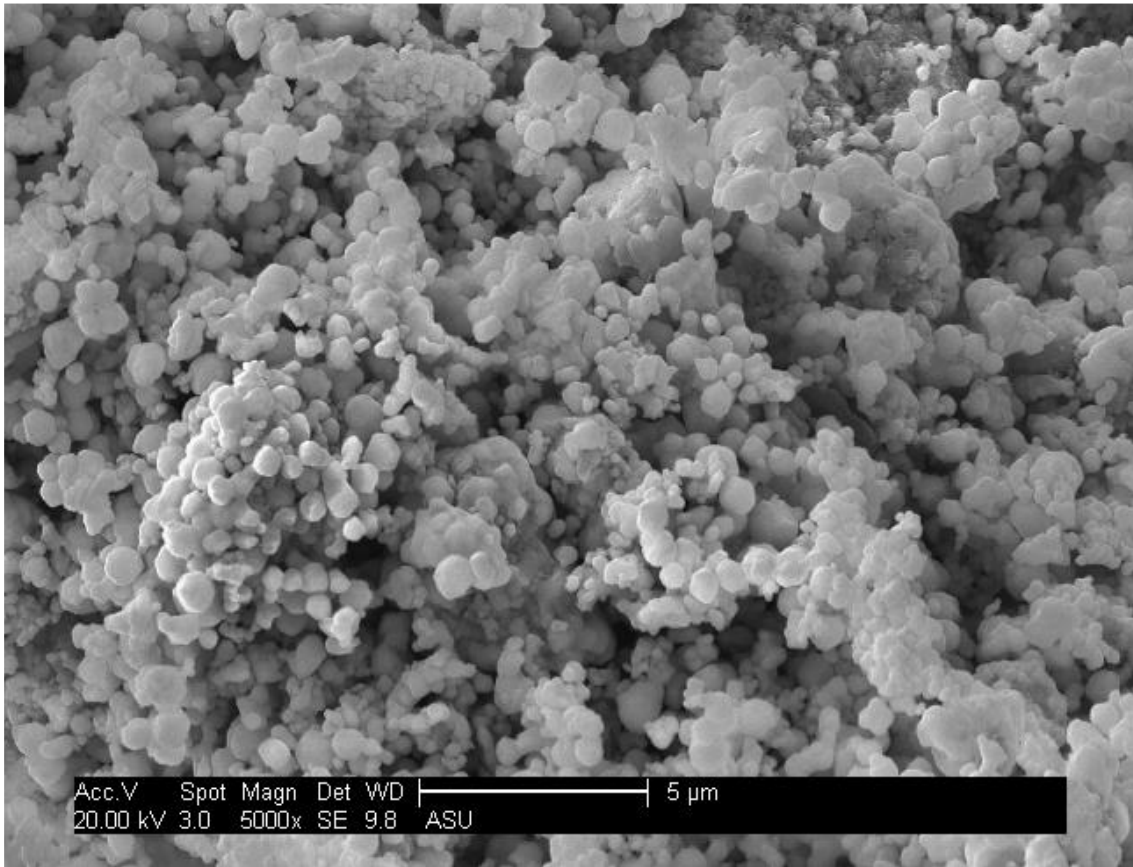


Figure 60. Nickel Nanopowder 5000x magnification.

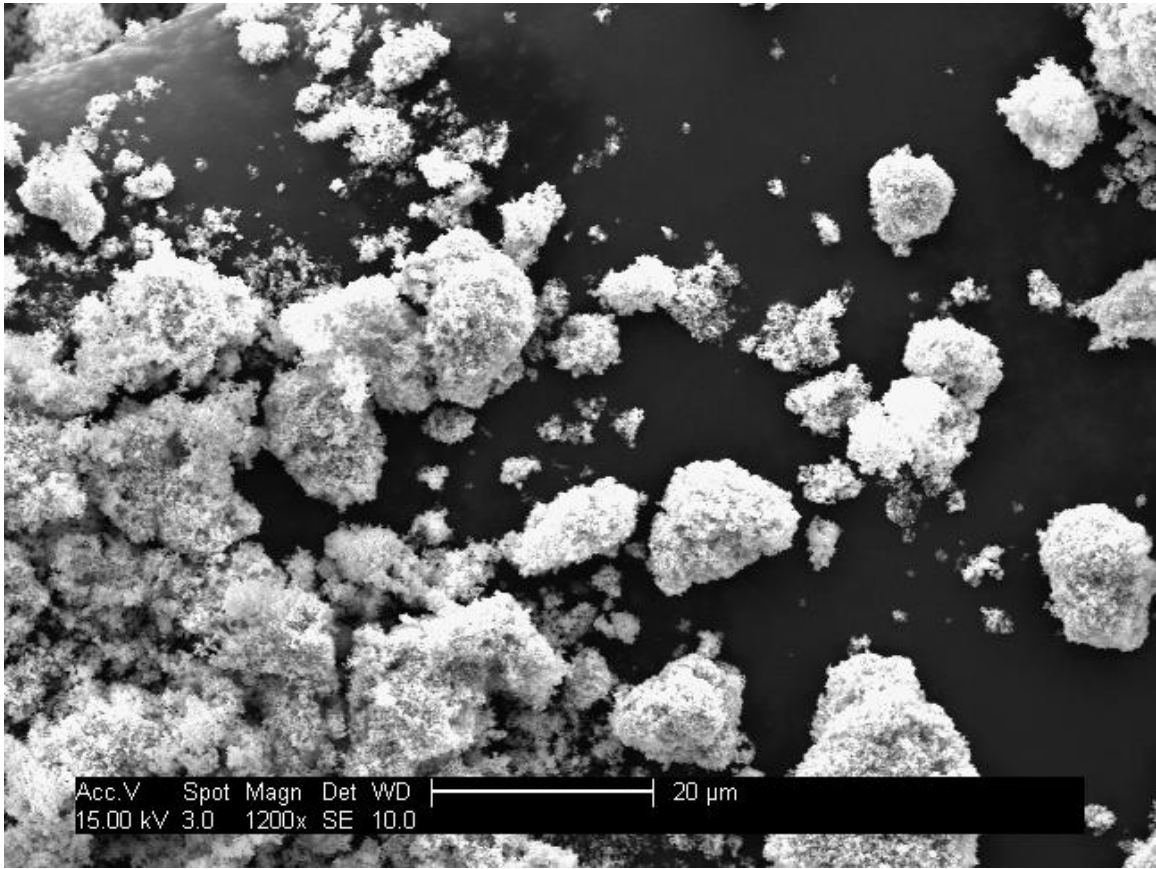


Figure 61. Cu-Zn Alloy, Pre-Experiment, 1200x.

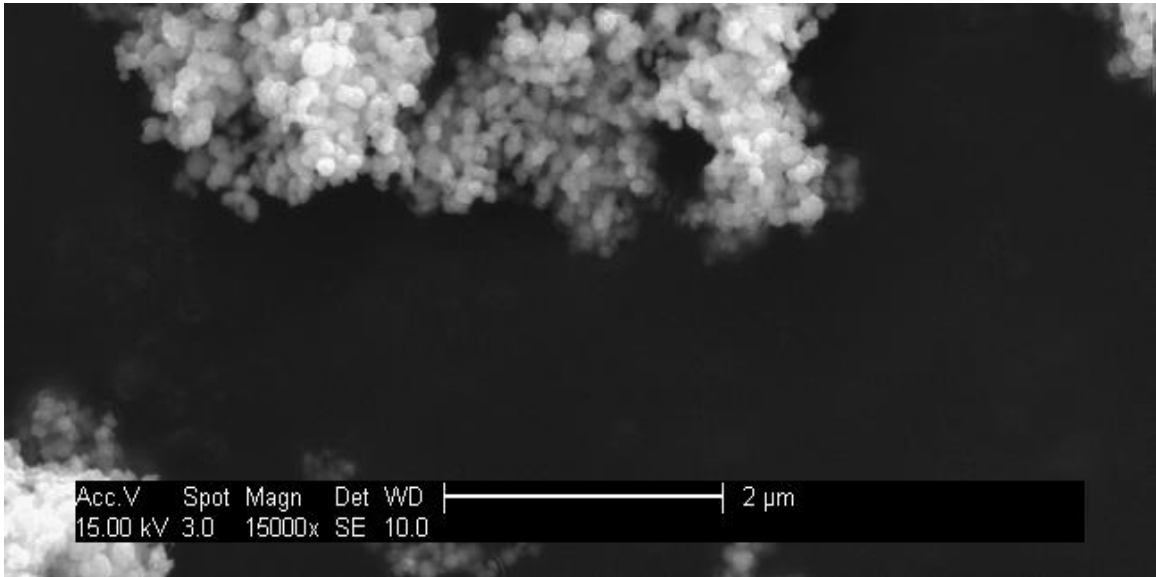


Figure 62. Cu-Zn Alloy, Pre-Experiment, 15000x.

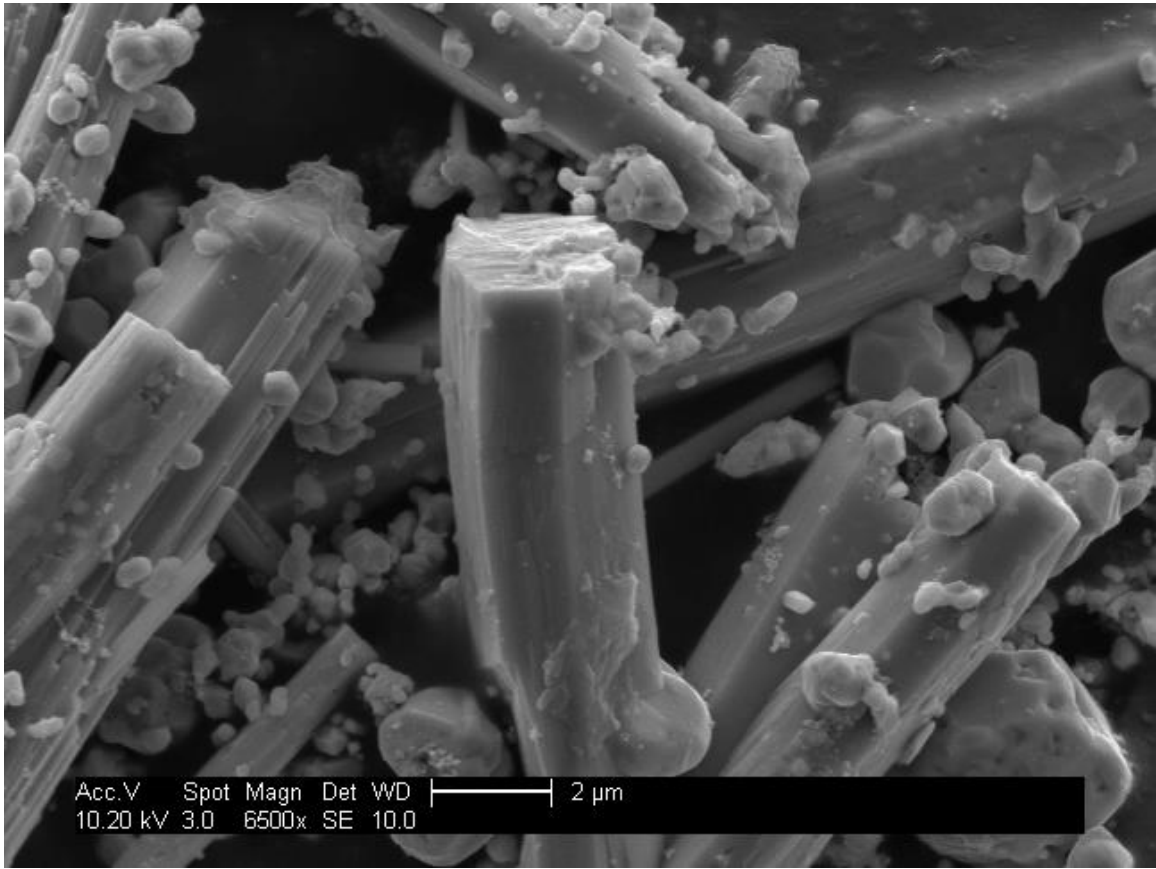


Figure 63. Cu-Zn Alloy, Reacted (48h, 250°C, H<sub>2</sub>O, No Organic), 6500x.



Figure 64. Cu-Zn Alloy, Reacted, 500x.

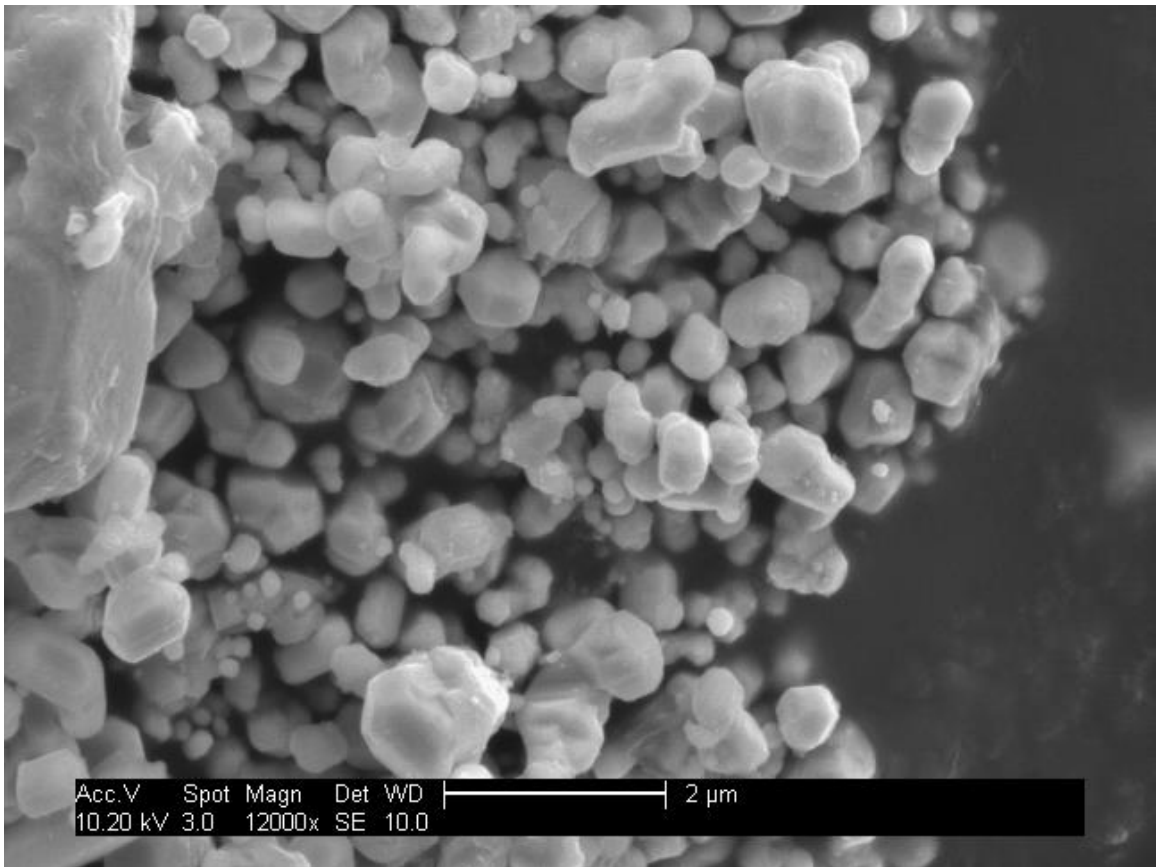


Figure 65. Cu-Zn Alloy, Reacted, 12000x.



## XRD Spectra

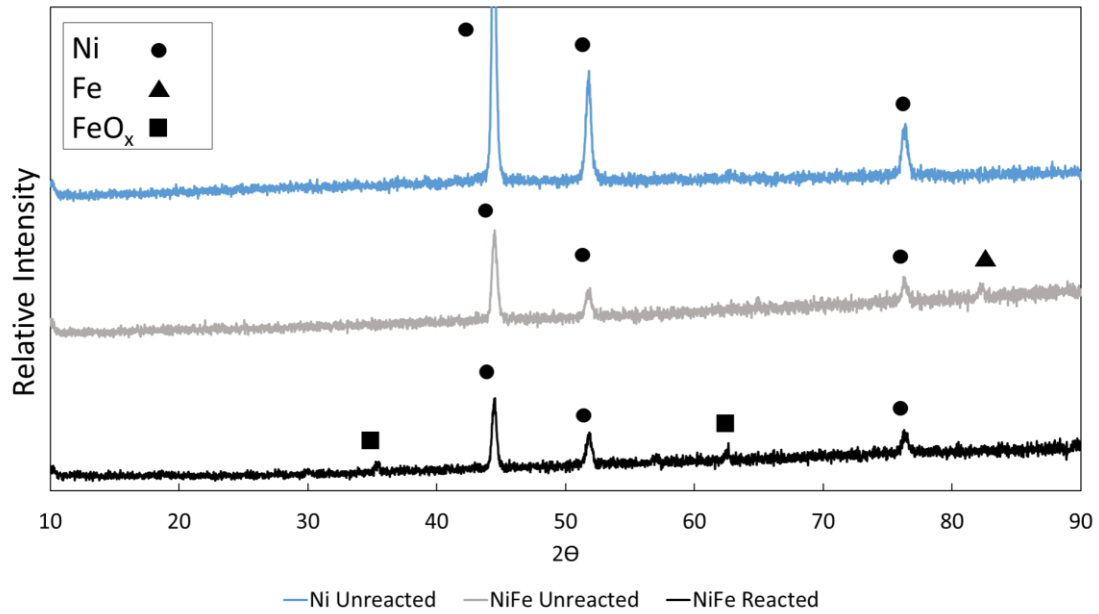


Figure 66. XRD Spectra of unreacted Ni, Ni+Fe, and reacted Ni+Fe (1h, 250°C, H<sub>2</sub>O)

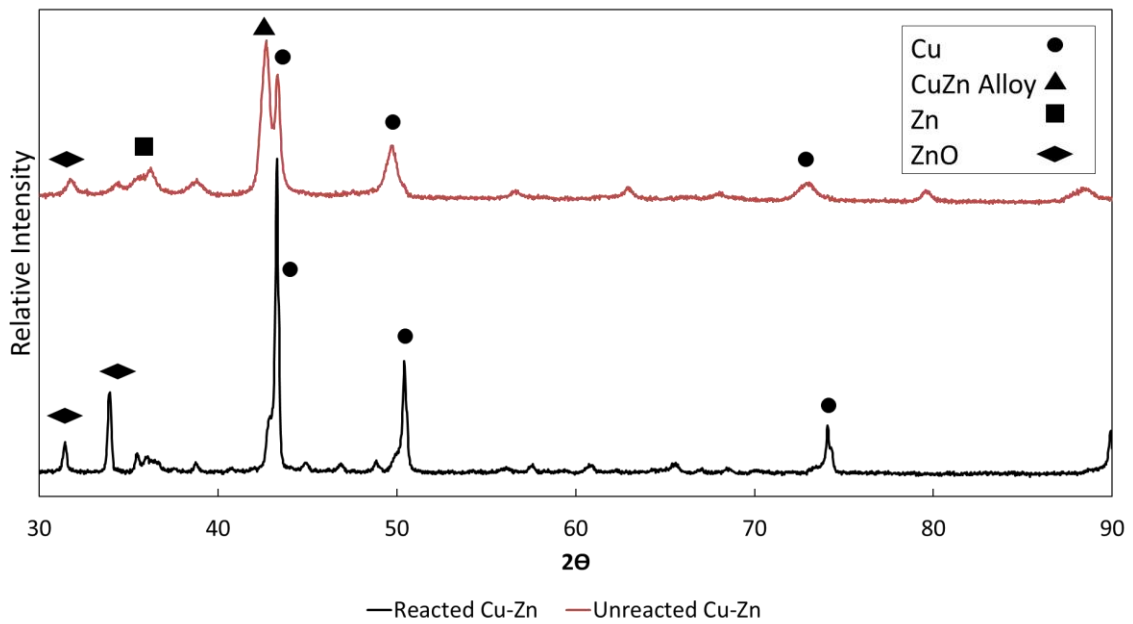


Figure 67. XRD Spectra of unreacted and reacted Cu-Zn (48h, 250°C, H<sub>2</sub>O)

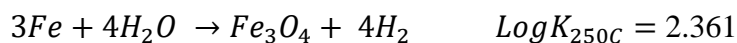
## Calculations, rationale, and experimental results of the hydrogen measurement experiment.

The following redox reactions were considered:

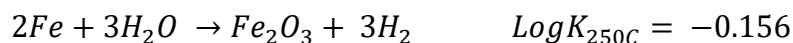
1. Nickel oxidizes to bunsenite (NiO)



2. Iron oxidizes to magnetite (Fe<sub>3</sub>O<sub>4</sub>)



3. Iron oxidizes to hematite (Fe<sub>2</sub>O<sub>3</sub>)



4. Iron oxidizes to ferrous Oxide:



The oxidation of iron to magnetite, in equation 2, was chosen as the major iron oxidation pathway, as it has the largest Log K value at 250°C compared to other pathways, such as oxidation to hematite (Fe<sub>2</sub>O<sub>3</sub>) or ferrous oxide. The oxidation of iron to magnetite and nickel to bunsenite was used to generate a nickel and iron stability field diagram with temperature and activity of aqueous hydrogen (Figure 68).

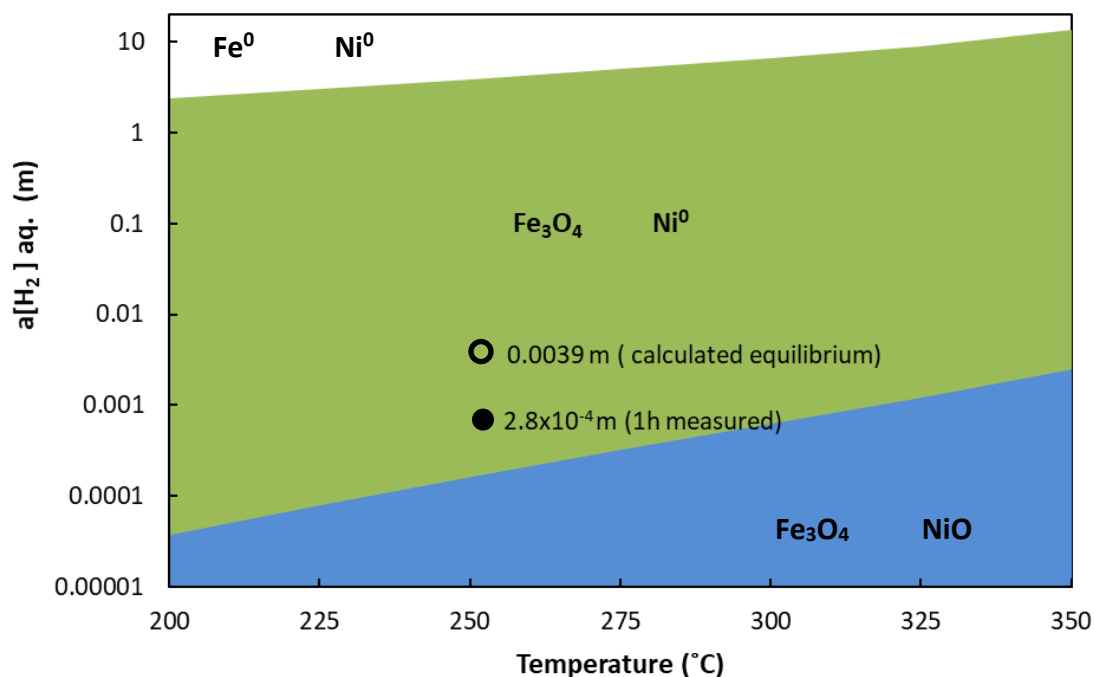


Figure 68. The stability fields of nickel, iron, Magnetite, and Bunsenite, with respect to temperature and activity of aqueous hydrogen. The equilibrium activity of dissolved hydrogen is indicated by the open circle. Measured hydrogen from iron oxidation, after 1 hour at  $250^\circ\text{C}$ , is indicated by the closed circle. This experimental activity of hydrogen is within the safe range for unoxidized nickel.

At the reaction conditions of  $250^\circ\text{C}$ ,  $\text{Log K}$  for oxidation of iron to magnetite is 2.361.

Starting with the typical  $240 \mu\text{mol}$  iron, 100% conversion to magnetite and hydrogen results in approximately  $320 \mu\text{mol}$  of hydrogen, or 1.6 molal given  $200 \mu\text{L}$  water. This will speciate between aqueous and gas phases.  $\text{Log K}$  of  $\text{H}_2(\text{aq}) \rightarrow \text{H}_2(\text{g})$  at  $250^\circ\text{C}$  is 2.631. Beginning with 1.6 molal hydrogen, this results in 0.0039 molal hydrogen in the aqueous phase (open circle in Fig 68). This is within the safe range for nickel metal.

However, the kinetics of iron oxidation are not known, so it may be unsafe to assume that

this equilibrium is reached within the timescale of a typical experiment. Hydrogen was measured in a 1 hour 250°C experiment including water, nickel, and iron, but no organic. Hydrogen was measured by a Reducing Compound Photometer (RCP) GC, and the estimated equilibrium aqueous hydrogen at 250°C was calculated from this value. 0.12 mg H<sub>2</sub> total was measured. This corresponds to 2.8x10<sup>-4</sup> molal aqueous H<sub>2</sub> at experimental conditions. This is within the stability range for unoxidized nickel, and is noted on Figure 68 (filled circle).

APPENDIX B.

GAS CHROMATOGRAPHY AND MASS SPECTROMETRY

Unless otherwise noted in the figure caption, all chromatograms shown in this section are from the Bruker-Scion 456 FID-GC. Mass spectra were obtained using a Thermo Electron TRACE 1310 gas chromatograph with a Thermo Electron ISO mass spectrometer.

### **Gas Chromatography-Mass Spectrometry Method**

The samples were dissolved in dichloromethane and 1  $\mu\text{L}$  was injected (*via* an AS 1310 autosampler). The GC parameters were: 250°C injection chamber, running in split mode (30:1); TG-SQC capillary column (0.25mm  $\times$  0.25 $\mu\text{m}$   $\times$  15m) with 1 mL/min constant flow control; oven program: 5 minutes at 30°C followed by a 5°C/min ramp to 130°C with a final 5 minute hold. The transfer line and ion source were maintained at 250°C. The mass spectra were acquired from 40-400  $m/z$  at a rate of 5 scans/second. Mass spectra for certain compounds were included in this section. Generally, these compounds do not have a commercial supplier. For FID response factors, a calibration curve for a commercially available structural isomer was used.

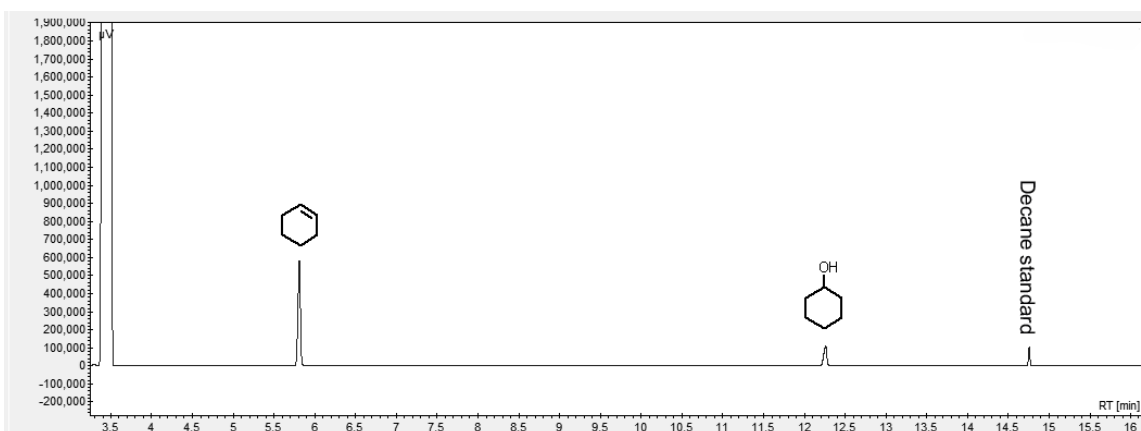


Figure 69. Cyclohexanol, 118h (250°C)

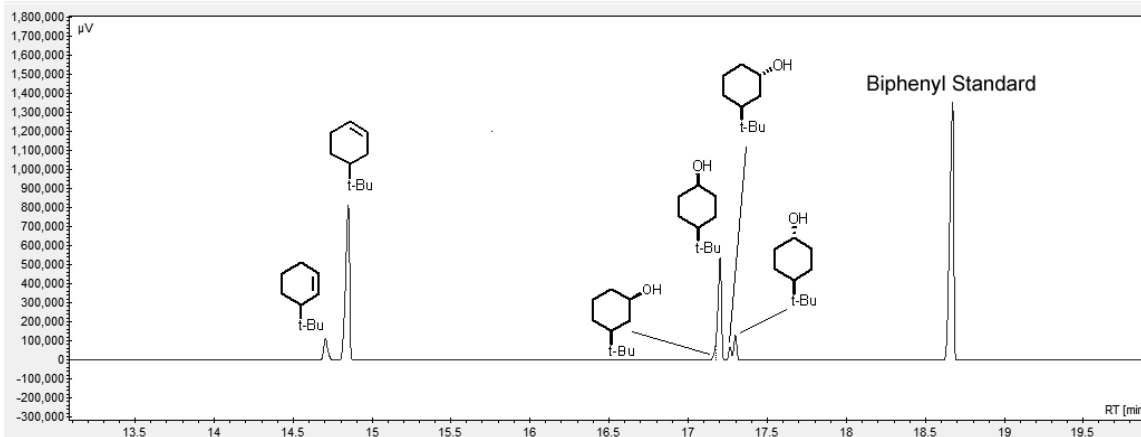


Figure 70. *Cis*-4-*tBu*-cyclohexanol, 8h (250°C). Biphenyl was used as an internal standard because decane and dodecane elute at the same time as the species in this product suite.

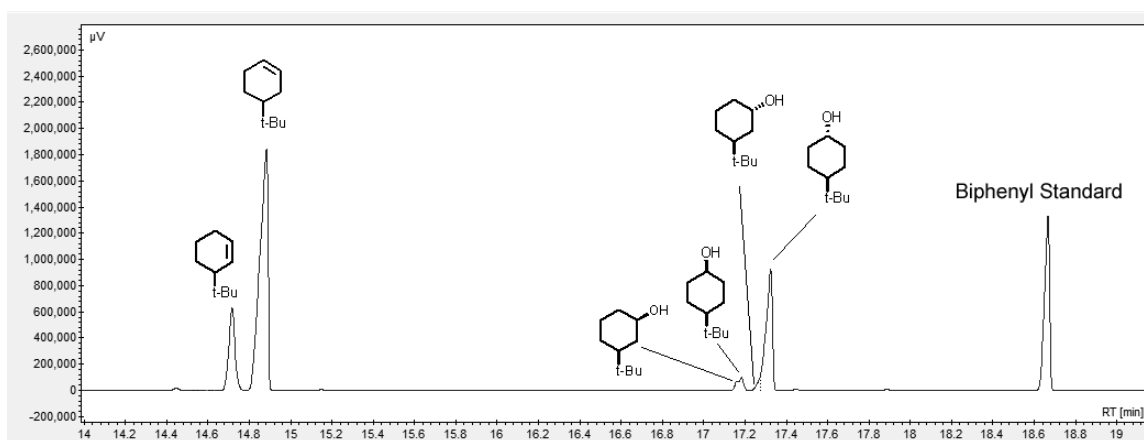


Figure 71. *Cis-4-*t*Bu-cyclohexanol*, 8h (250°C). Biphenyl was used as an internal standard because decane and dodecane elute at the same time as the species in this product suite.

Mass spectral data are not available in the literature except for 4-*tert*-butylcyclohexene,<sup>216,217</sup> which is not available commercially; All runs produced clearly-identifiable matches (in both retention time and mass spectrum) to both the 4- and 1- isomers in a tight (but chromatographically baseline-resolved) cluster which always included a third C<sub>10</sub>H<sub>18</sub> isomer with a very similar mass spectrum: this peak and spectrum have been assigned to 3-*tert*-butylcyclohexene. Both mass spectra of the 3- and the 1- isomers are reported here for the first time. Incidentally, both the 3- and 4- isomers were also present as minor contaminants in the synthesis of 1-*tert*-butylcyclohex-1-ene.



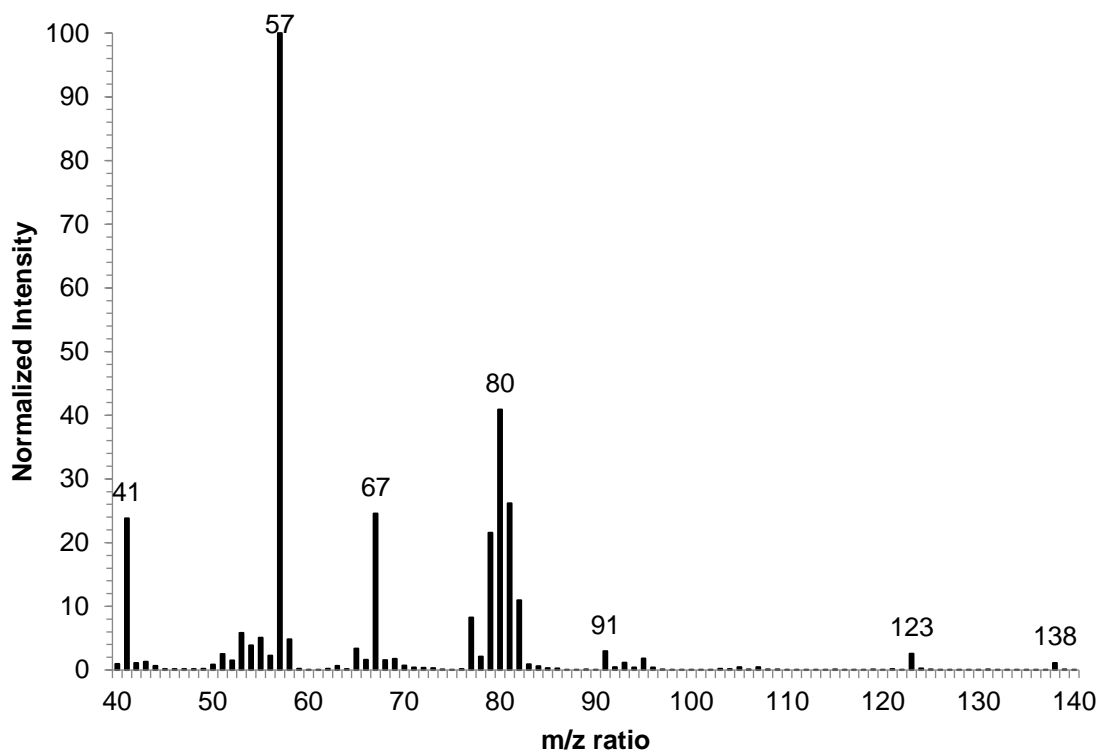


Figure 72. Mass spectrum of 3-*tert*-butylcyclohex-1-ene.

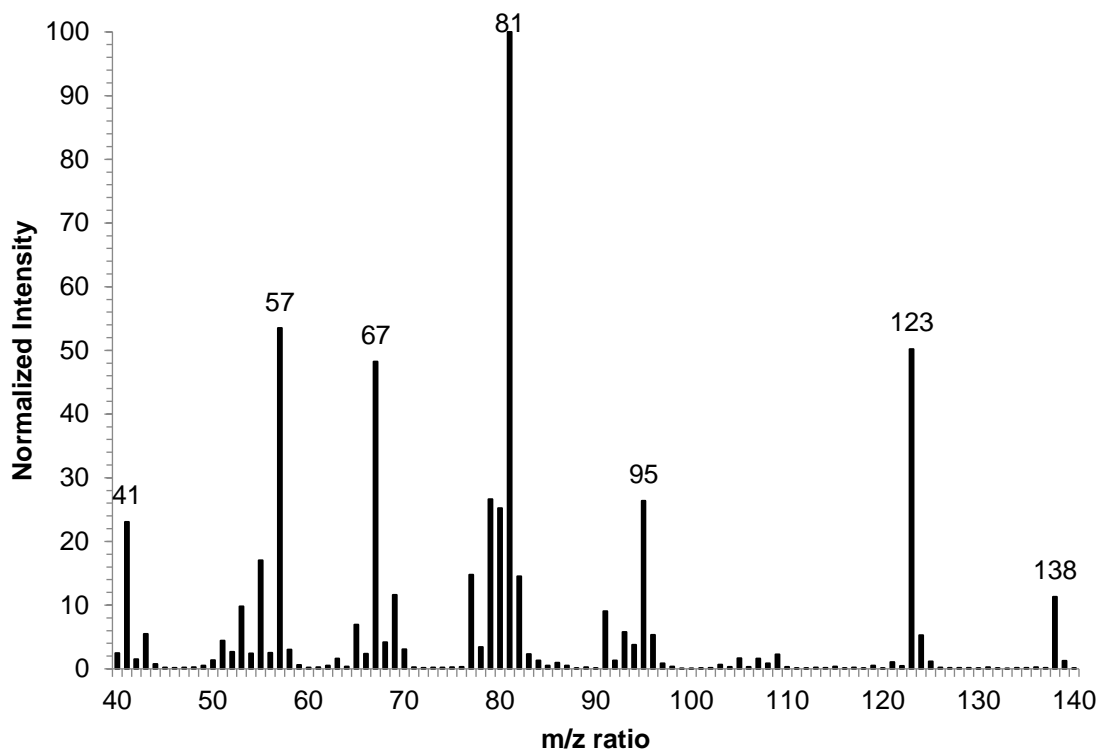


Figure 73. Mass spectrum of 1-*tert*-butylcyclohex-1-ene

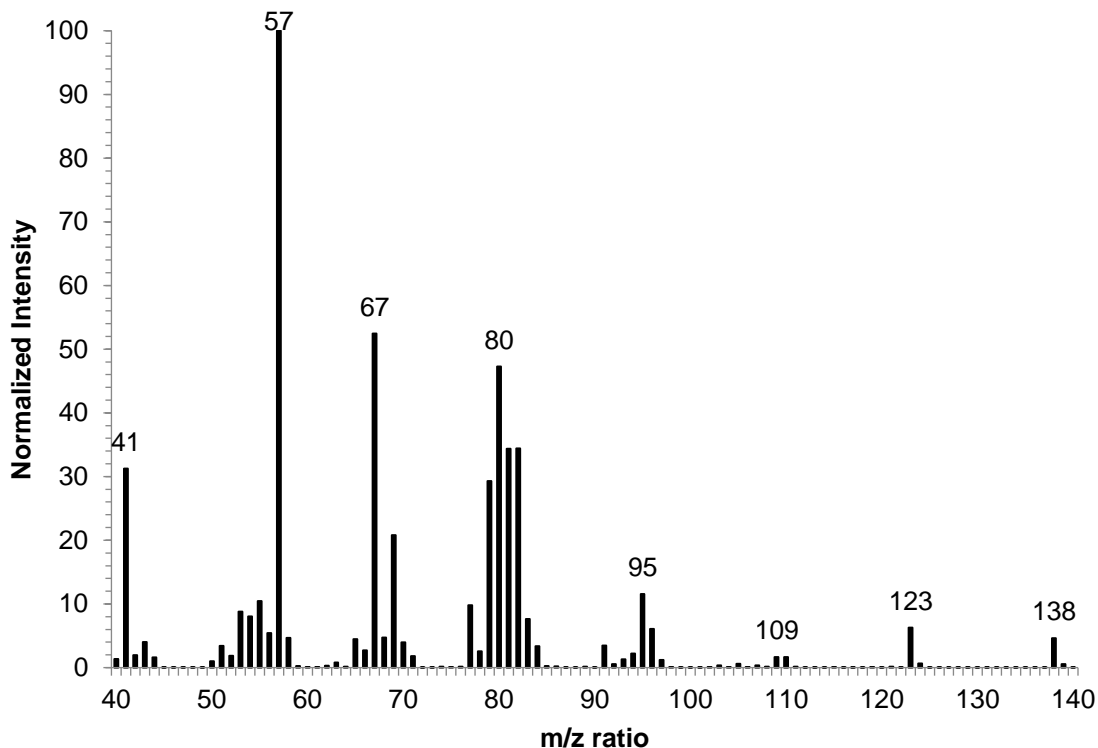


Figure 74. Mass spectrum of 4-*tert*-butylcyclohex-1-ene

#### *Identification of tert-butylcyclohexanols*

The various *tert*-butylcyclohexanols form a tight grouping (17.00, 17.08, 17.34, and 17.42 minutes) (GC/MS). Since only the 4-isomer spectra are in the NIST database, the built-in library function's best guess for all of them is the 4-isomer. Indeed, the mass spectra of the 3-isomers have only been reported twice in the literature<sup>218,219</sup> and the two reports are completely at odds with one another. The results from the older study, which was specifically a mass spectrometry study, are consistent with our results and the mass

spectra of almost every other *tert*-butylcyclohexanol in that they almost all predict the main fragmentation to cleave the bond between the *tert*-butyl group and the ring (although in the case of the 1-isomer, the presence of the 1-hydroxyl reverses the charge/radical distribution).<sup>218</sup> The solitary exception to this cleavage pattern is *cis*-2-*tert*-butylcyclohexanol, to which the mass spectra in the newer study<sup>219</sup> are suspiciously similar. This is unfortunate in that, unlike the newer study, the older study has no digitized data.

We present here the mass spectra of the 3-*tert*-butylcyclohexanols; we have assigned them by retention time in analogy to the 4-isomers and on the basis that, since they must appear *via* the 3-cation in our experiments, the more stable *cis* isomer (which has both substituents equatorial) should be more abundant. We obtained authentic samples of both *cis*- and *trans*-4-*tert*-butylcyclohexanol, so the identity of these peaks was determined by retention time and verified by mass spectral match. In addition to the greater abundance of the *cis*-3 isomer vs. the *trans*-3 isomer, the mass spectrum of the *cis*-3 isomer (Figure 76) has a “triplet” of high-abundance peaks (81-83 *m/z*) as opposed to a “quartet” of moderate-abundance peaks (*see below*: 80-83 *m/z*); this is in agreement with the spectral patterns reported by Dolejš and Hanuš. The only other differentiating feature in the spectrum is that the 67 *m/z* peak should be much smaller in the *trans* (and it is).

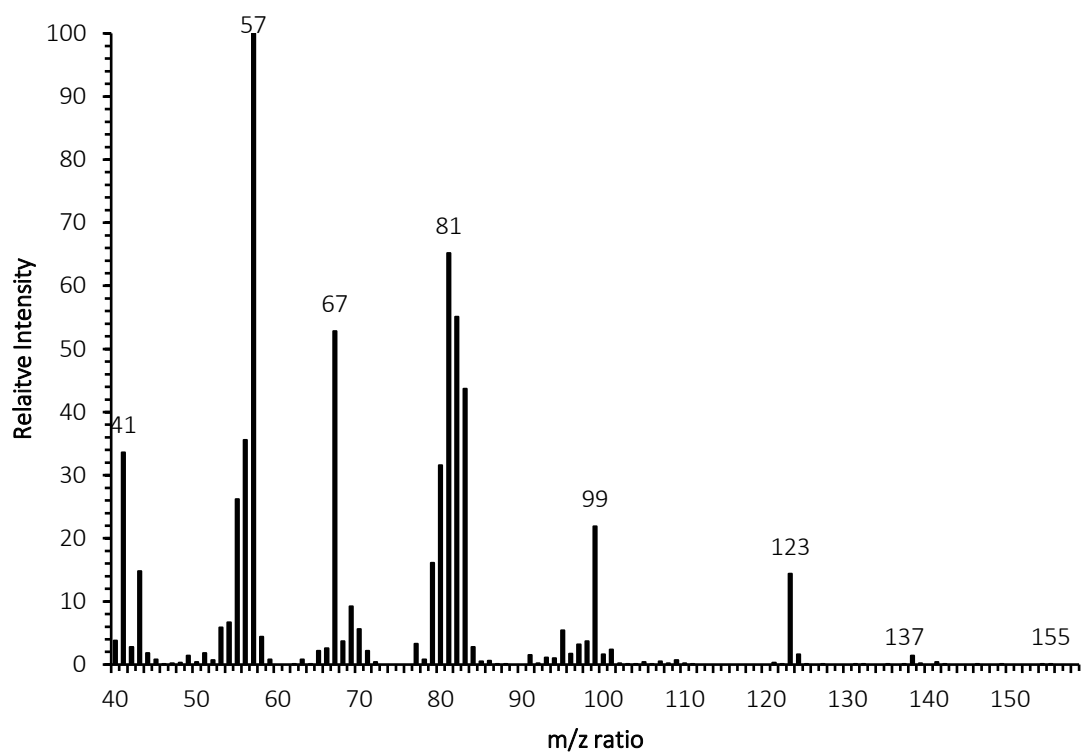


Figure 75. Mass spectrum of *trans*-3-*tert*-Butylcyclohexanol

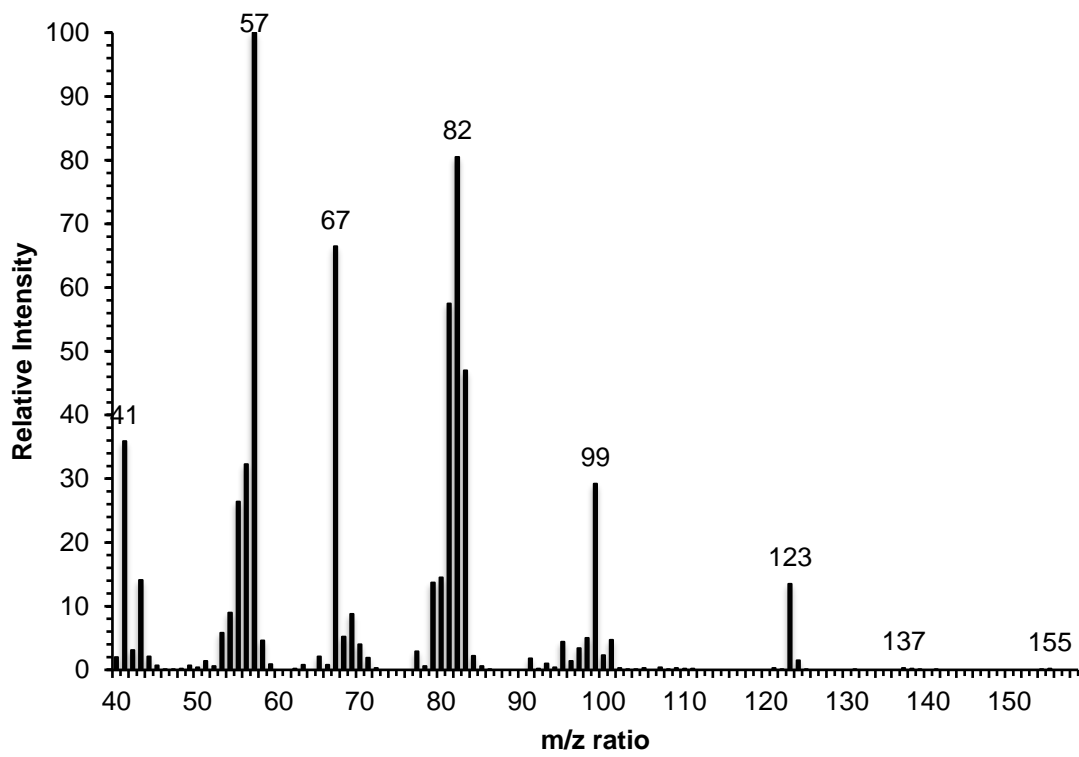


Figure 76. Mass spectrum of *cis*-3-*tert*-Butylcyclohexanol

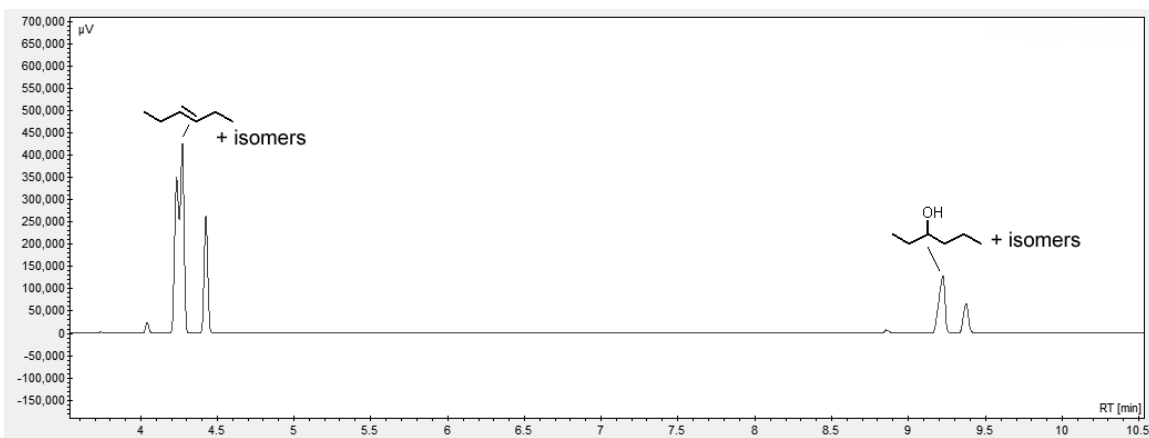


Figure 77. 3-hexanol 48h (250°C)

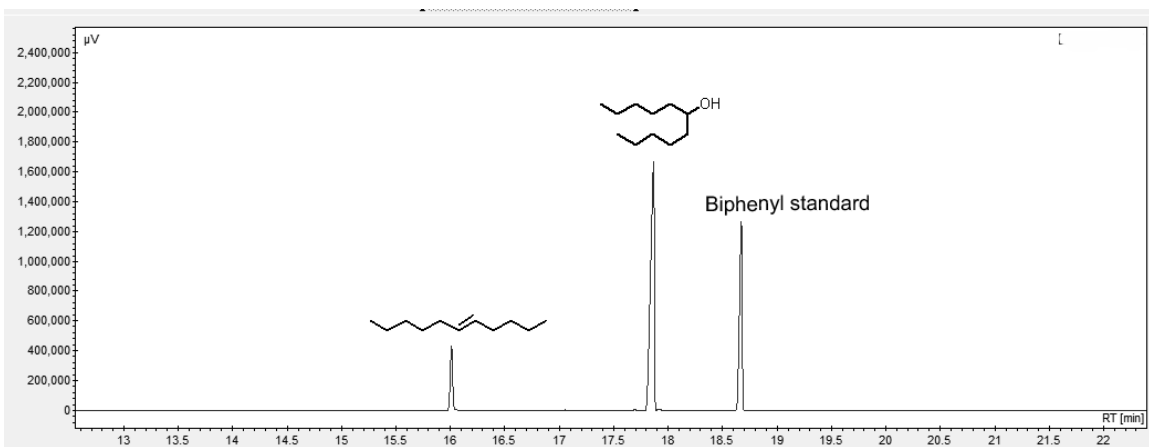


Figure 78. 6-undecanol 48h (250°C)

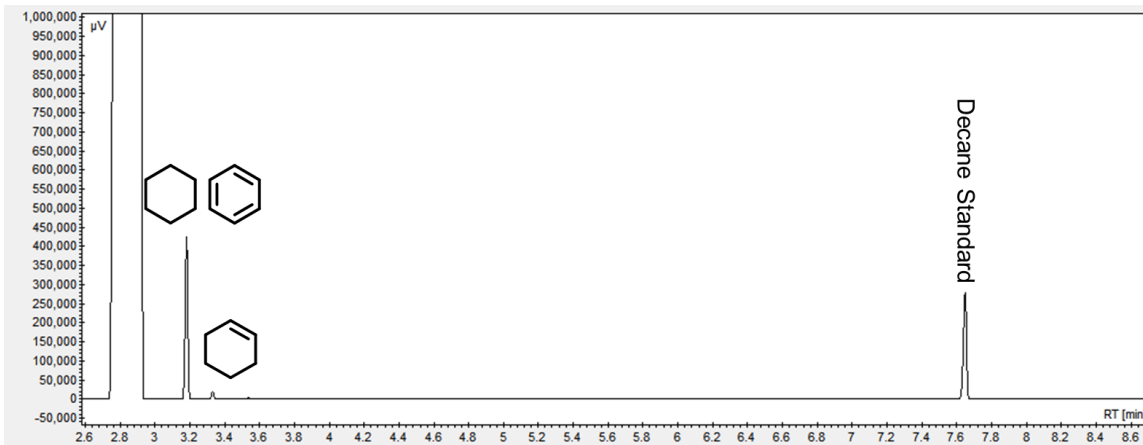


Figure 79. Cyclohexene 135min, Ni+Fe (250°C). Cyclohexane and benzene are inseparable by GC. The peak at 3.19 min represents both species. NMR data provided in Figure 80.



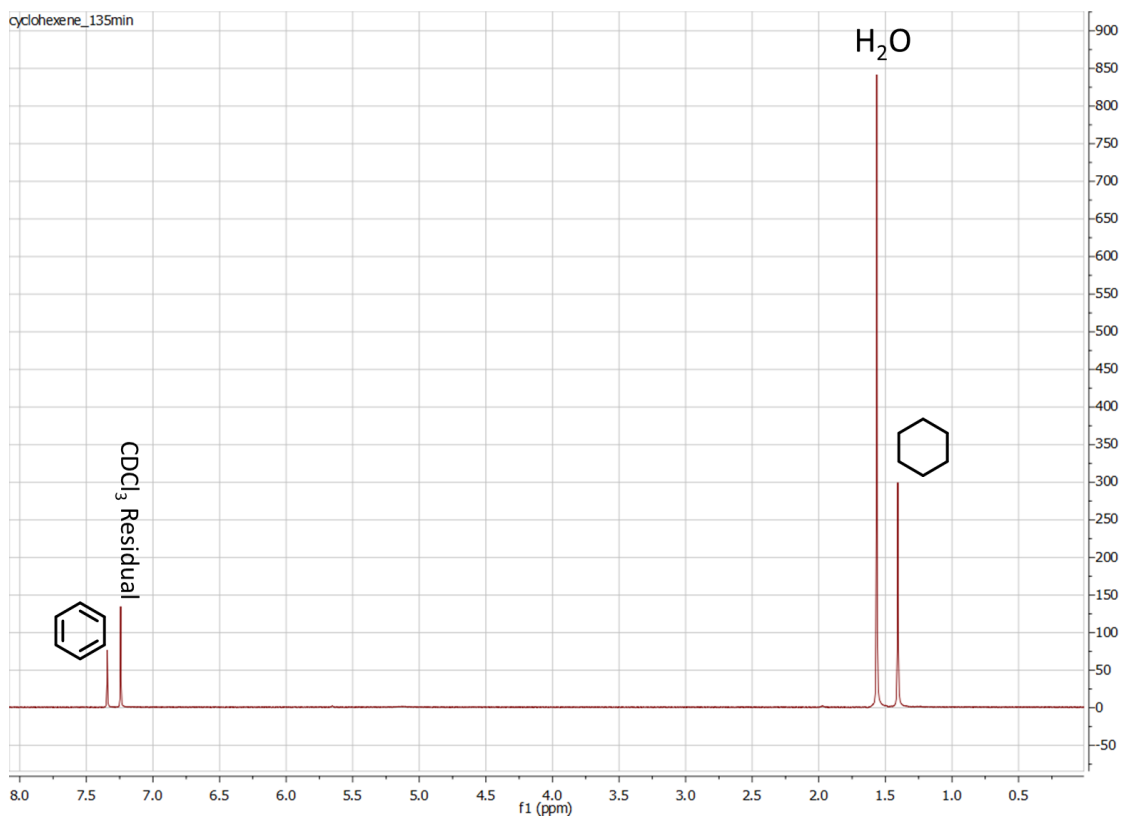


Figure 80.  $^1\text{H}$  NMR spectrum of the cyclohexene reaction mixture, in  $\text{CDCl}_3$ . (135 min,  $250^\circ\text{C}$ , Ni+Fe)

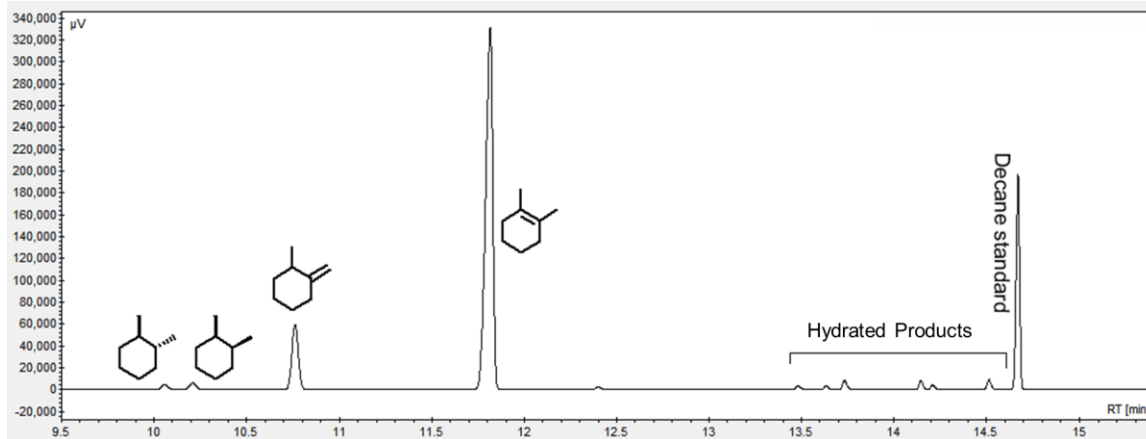


Figure 81. 1,2-dimethylcyclohexene 30 min, Ni+Fe ( $250^\circ\text{C}$ )

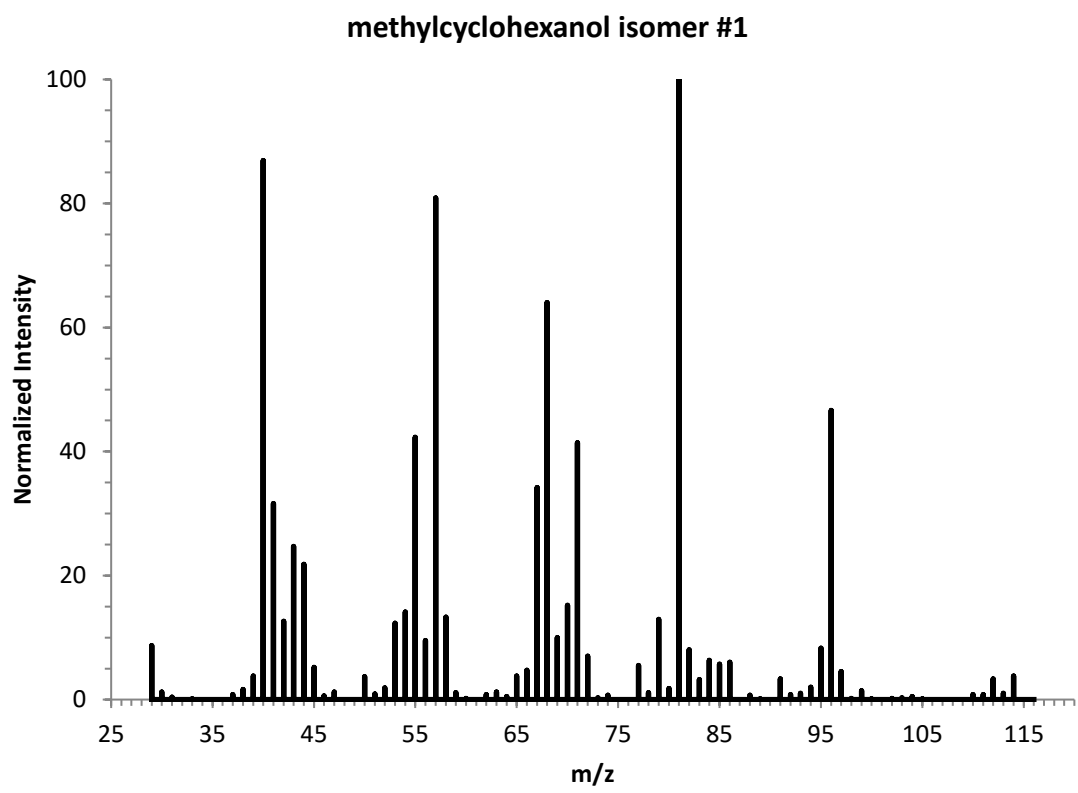


Figure 82. Mass spectrum of a representative methylcyclohexanol isomer.

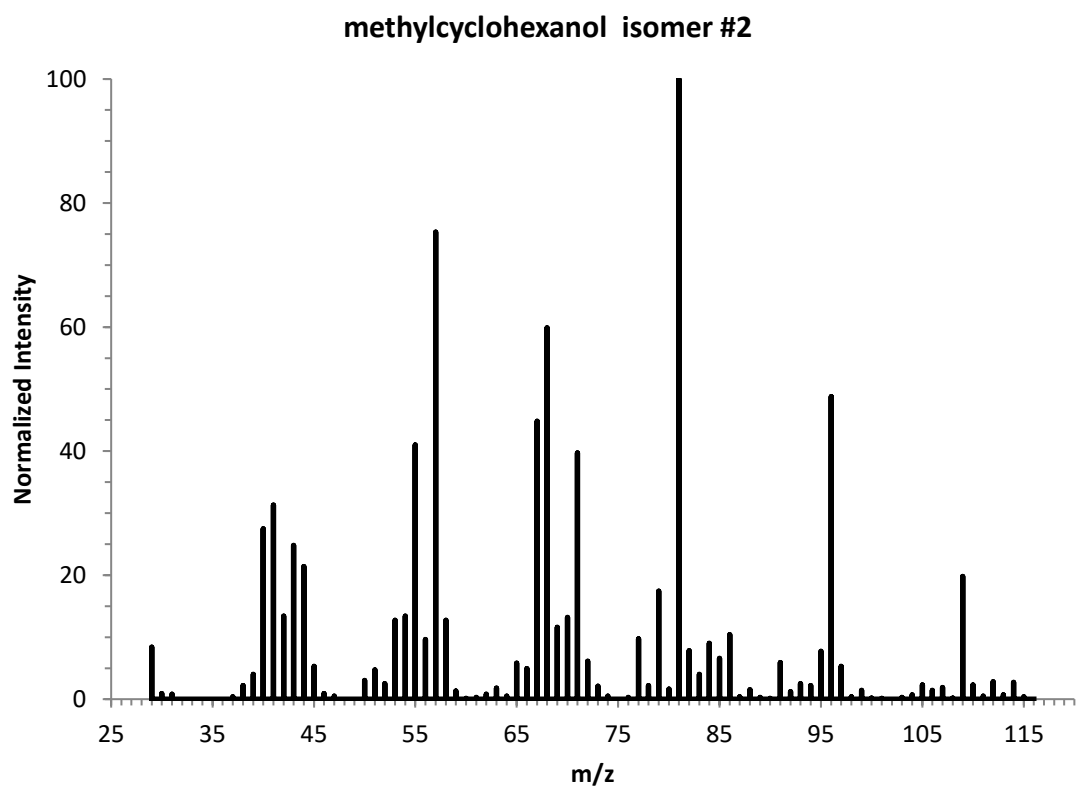


Figure 83. Mass spectrum of a second representative methylcyclohexanol isomer.

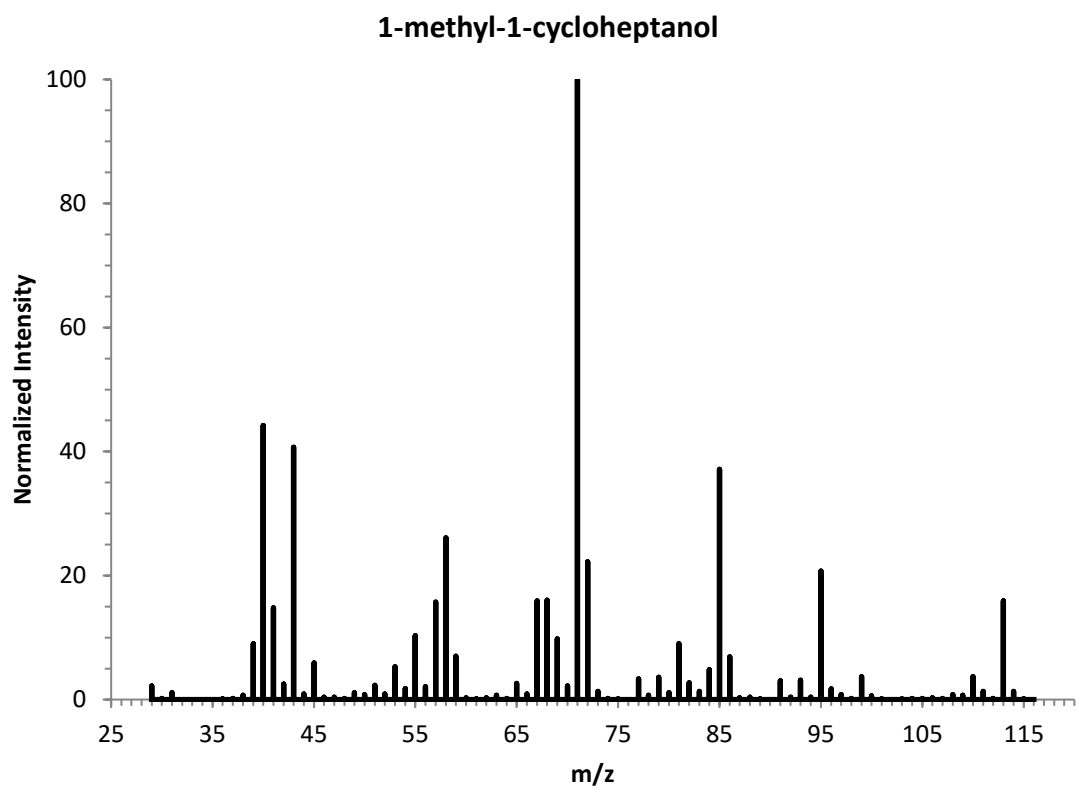


Figure 84. Mass spectrum of 1-methyl-1-cycloheptanol. This alcohol results from protonation of 1,2-dimethylcyclohexene, ring-opening to form the cycloheptane ring, and then hydration.

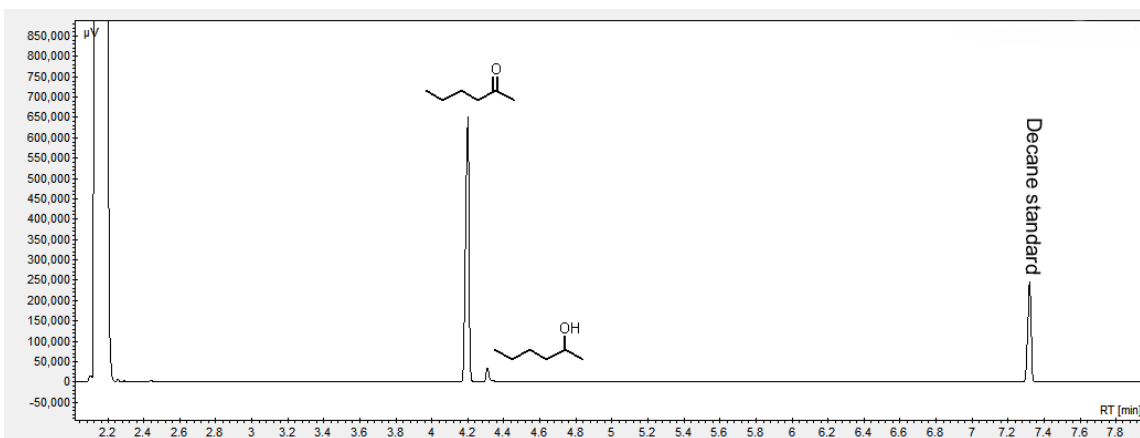


Figure 85. 5-hexen-2-one, 1h Ni+Fe (250°C)

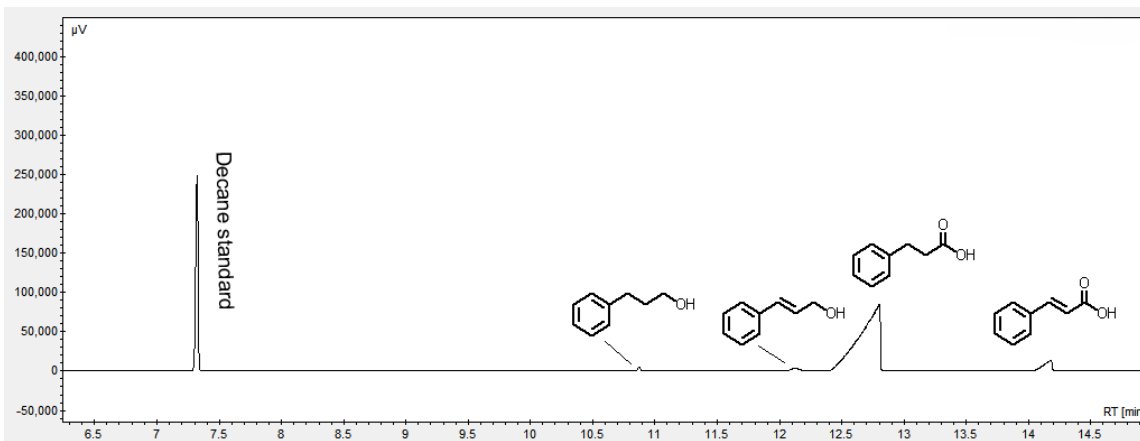


Figure 86. *trans*-cinnamic acid, 15 min Ni+Fe (250°C)

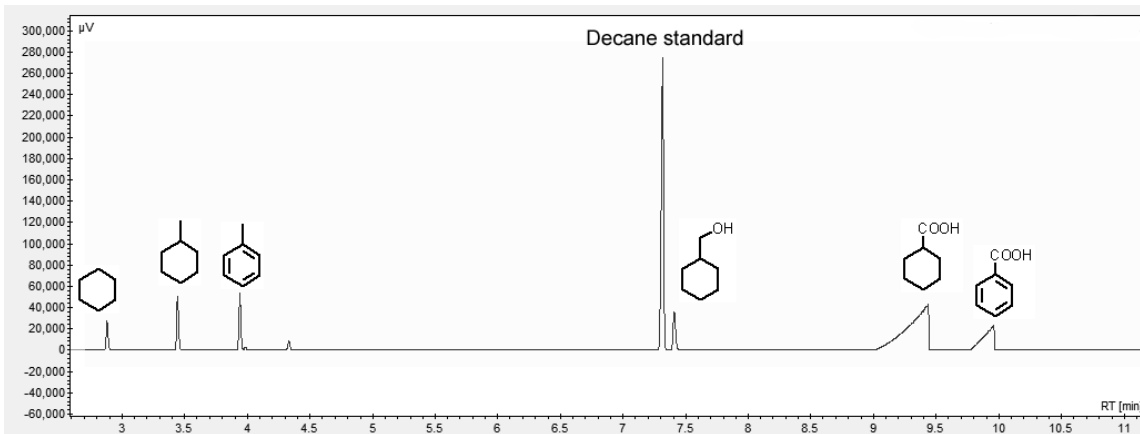


Figure 87. Benzoic acid, 70h Ni+Fe (250°C)

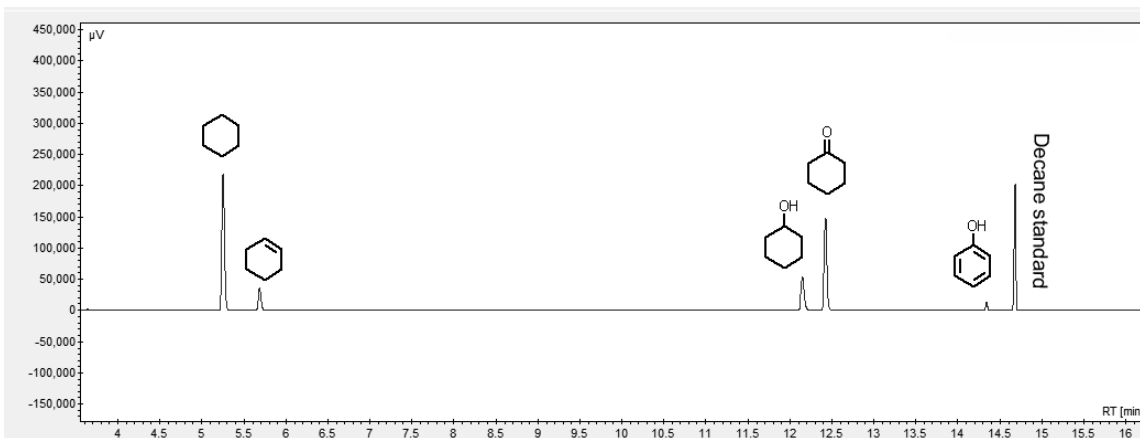


Figure 88. Cyclohexanone, 24h Ni+Fe (250°C)

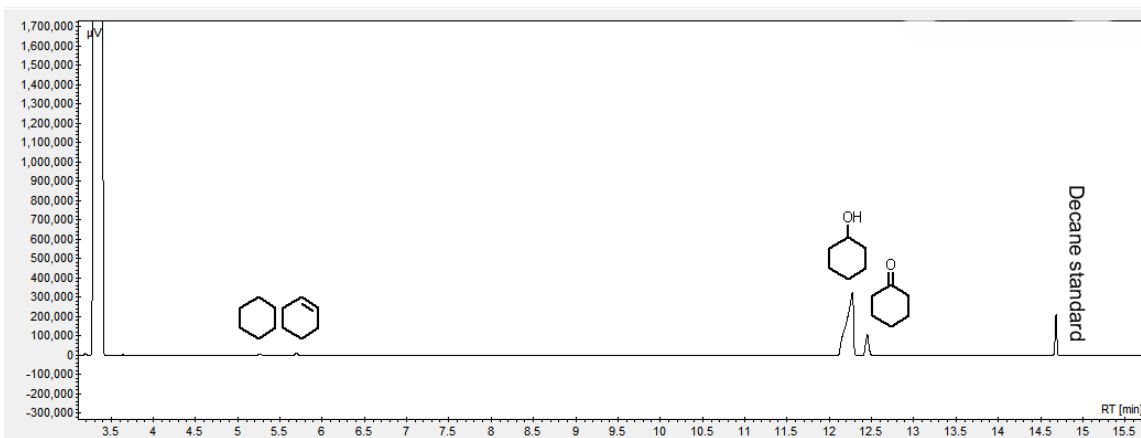


Figure 89. Cyclohexanone, 4h Cu-Zn+Fe (250°C)

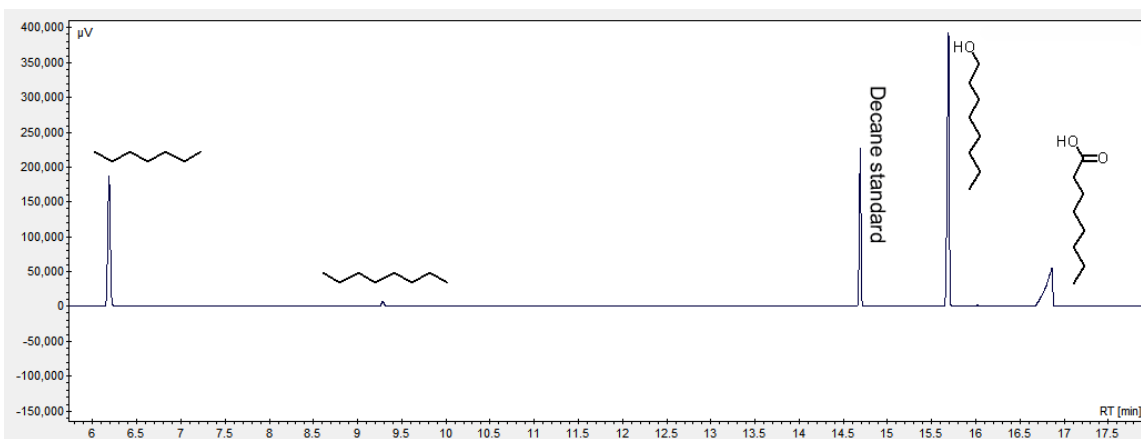


Figure 90. Octanoic Acid, 24h Ni+Fe (250°C)

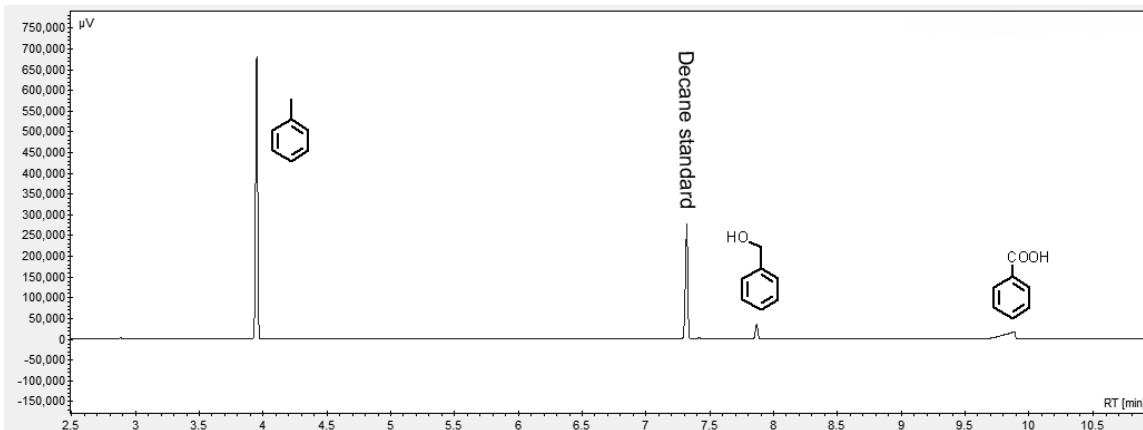


Figure 91. Benzoic Acid 24h Cu-Zn+Fe (250°C)

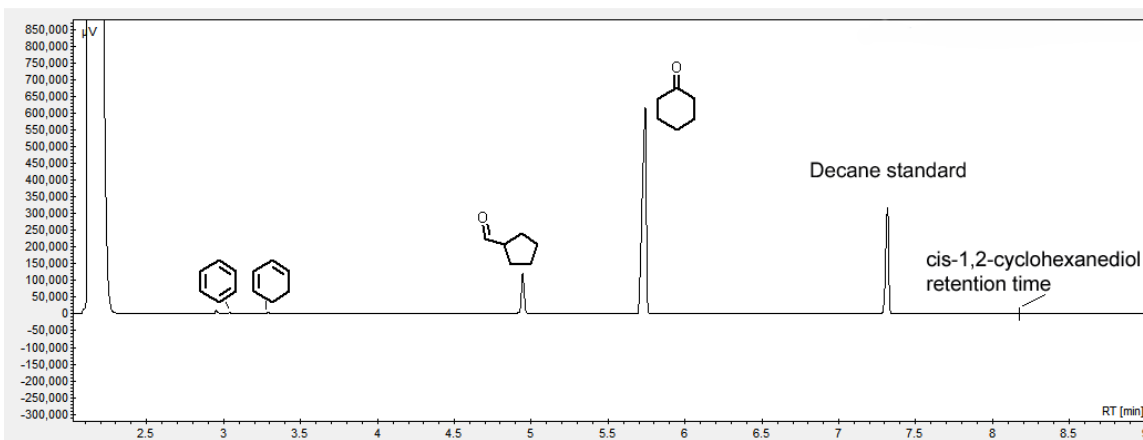


Figure 92. *Cis*-1,2-cyclohexanediol 24h (250°C)



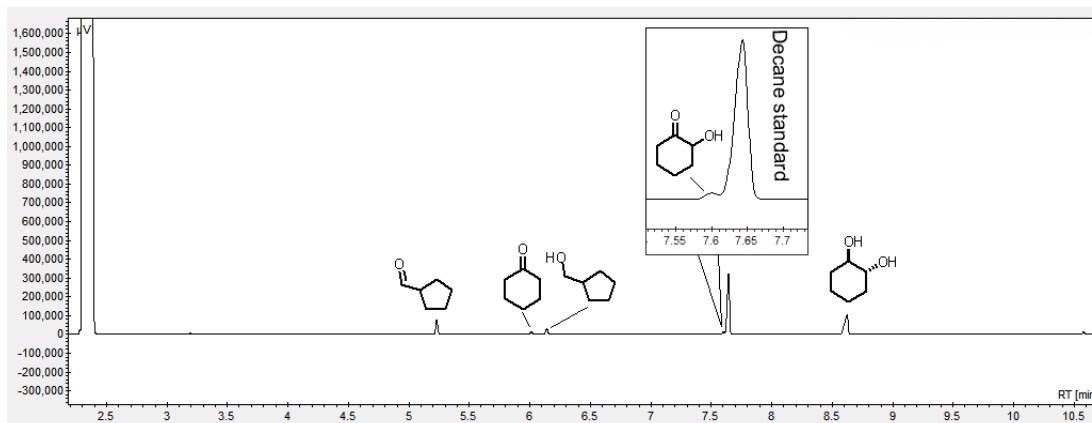


Figure 93. *Trans*-1,2-cyclohexanediol 480h (250°C)

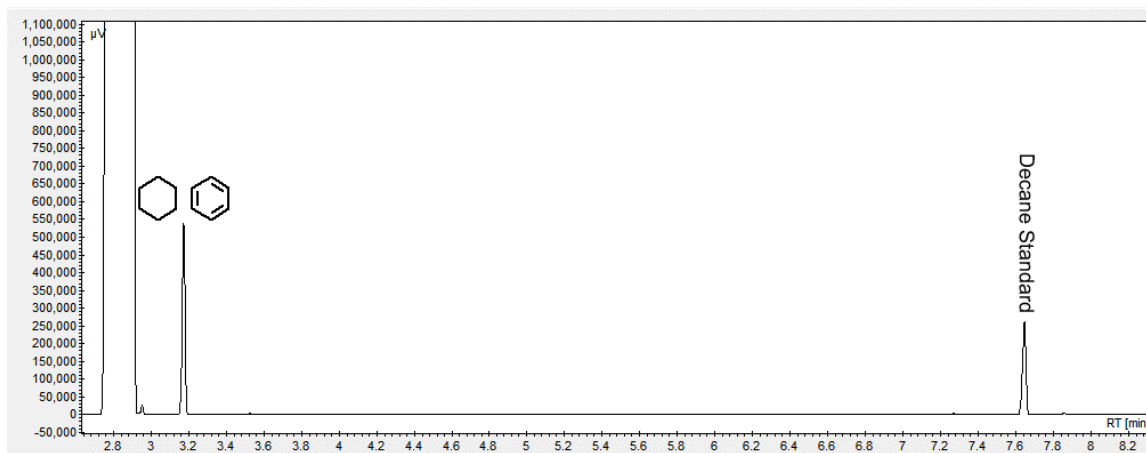


Figure 94. *Cis*-1,2-cyclohexanediol 72h Ni+Fe (250°C)

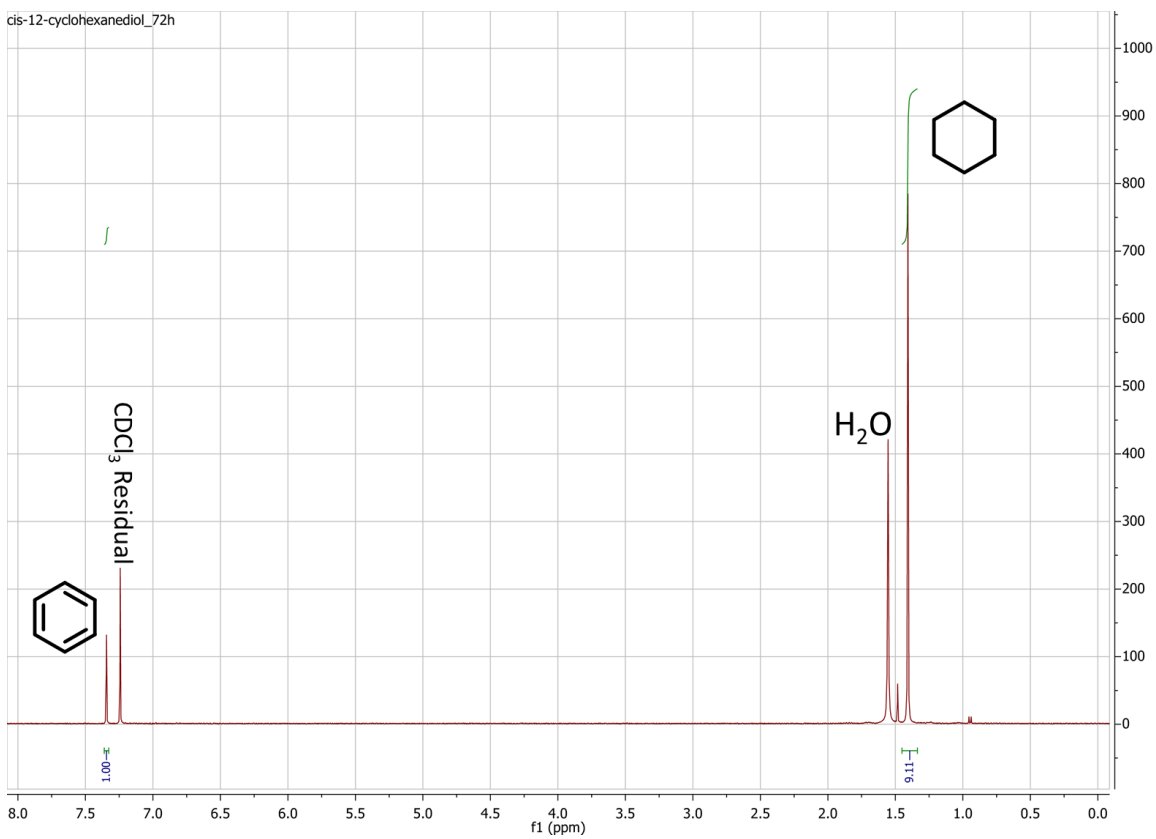


Figure 95.  $^1\text{H}$  NMR spectrum of the *cis*-1,2-cyclohexanediol reaction mixture, in  $\text{CDCl}_3$ . (72h, 250°C, Ni+Fe)

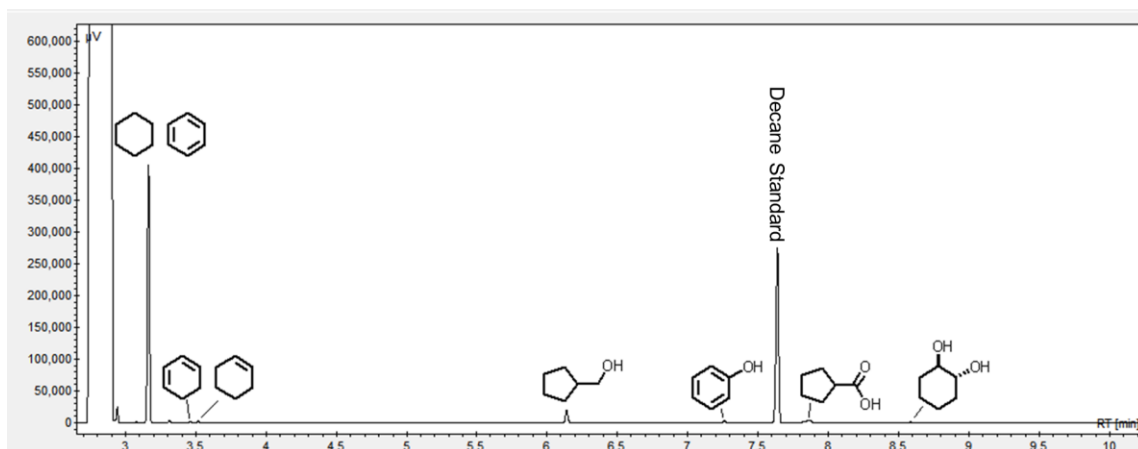


Figure 96. *Trans*-1,2-cyclohexanediol Ni+Fe 70h (250°C)

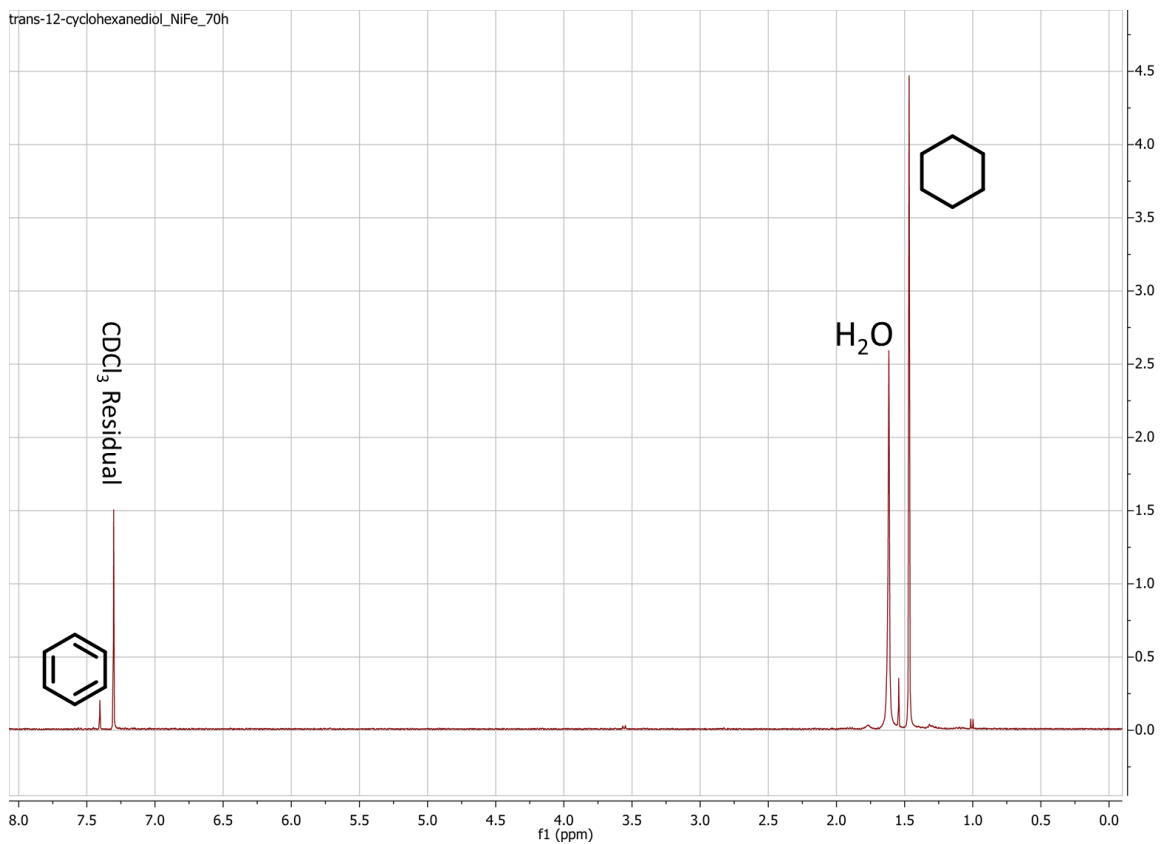


Figure 97. <sup>1</sup>H NMR spectrum of the *trans*-1,2-cyclohexanediol reaction mixture, in CDCl<sub>3</sub>. (70h, 250°C, Ni+Fe)

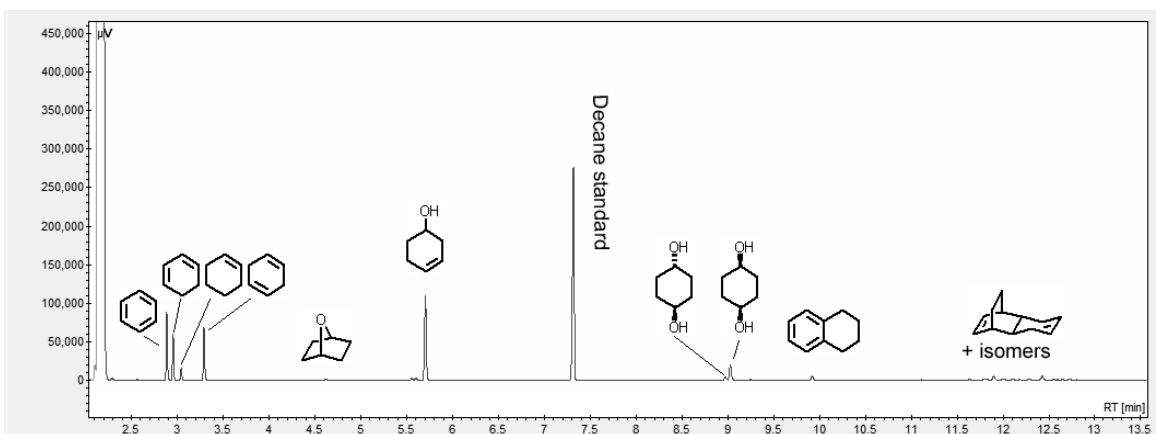


Figure 98. *Cis*-1,4-cyclohexanediol 1 week (250°C), H<sub>2</sub>O.

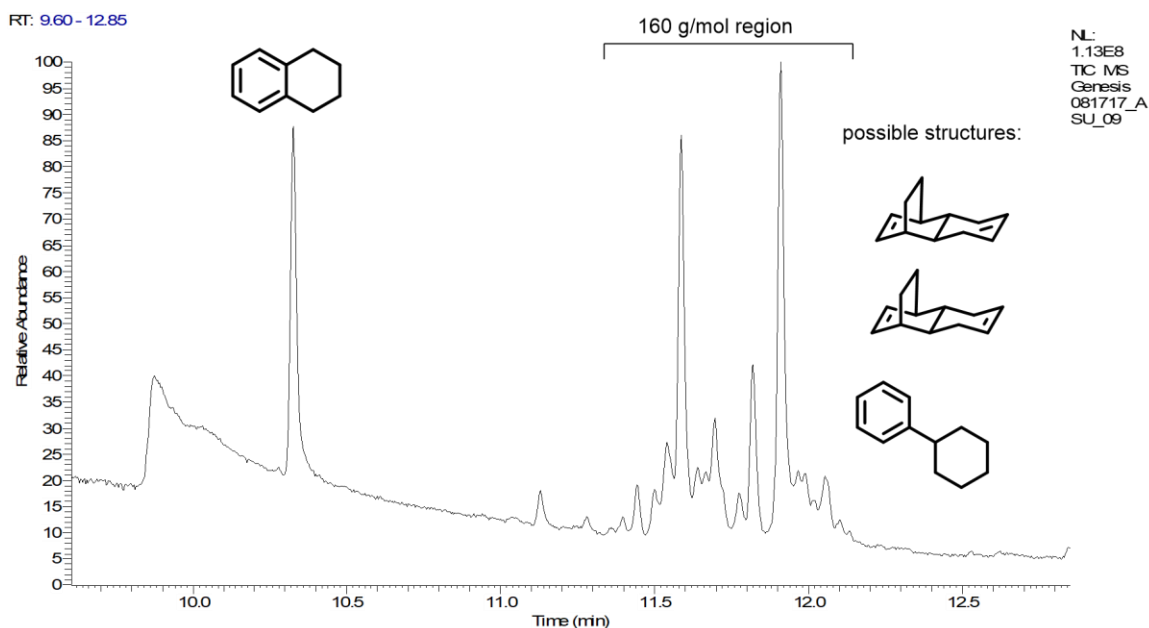


Figure 99. Partial chromatogram from GC/MS analysis of cis-1,4-cyclohexanediol (1 week, 250°C) The region from about 11.4-12.2 minutes are all structural isomers with molecular weight 160 g/mol. This is twice the molecular weight of 1,3 or 1,4-cyclohexadiene. 1,3-cyclohexadiene can undergo a [4+2] cyclization with another alkene, so it is likely that some of these isomers in the region are Diels-Alder products. Others could be EAS products, like cyclohexylbenzene. Example spectra are provided in Figures 100 and 101.

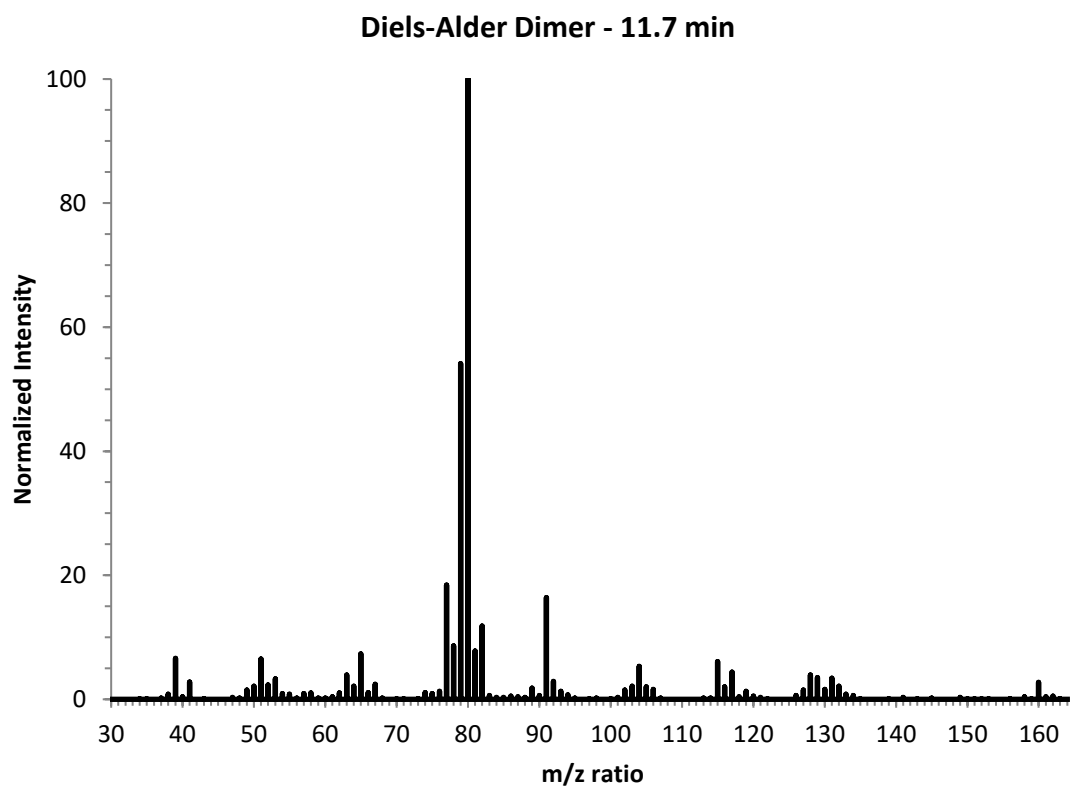


Figure 100. Mass spectrum of the largest Diels-Alder product, from *cis*-1,4-cyclohexanediol. The largest ion peak is 80 m/z, which matches the molecular weight of cyclohexadiene. This is suggestive of retro-Diels-Alder in the mass spectrometer.

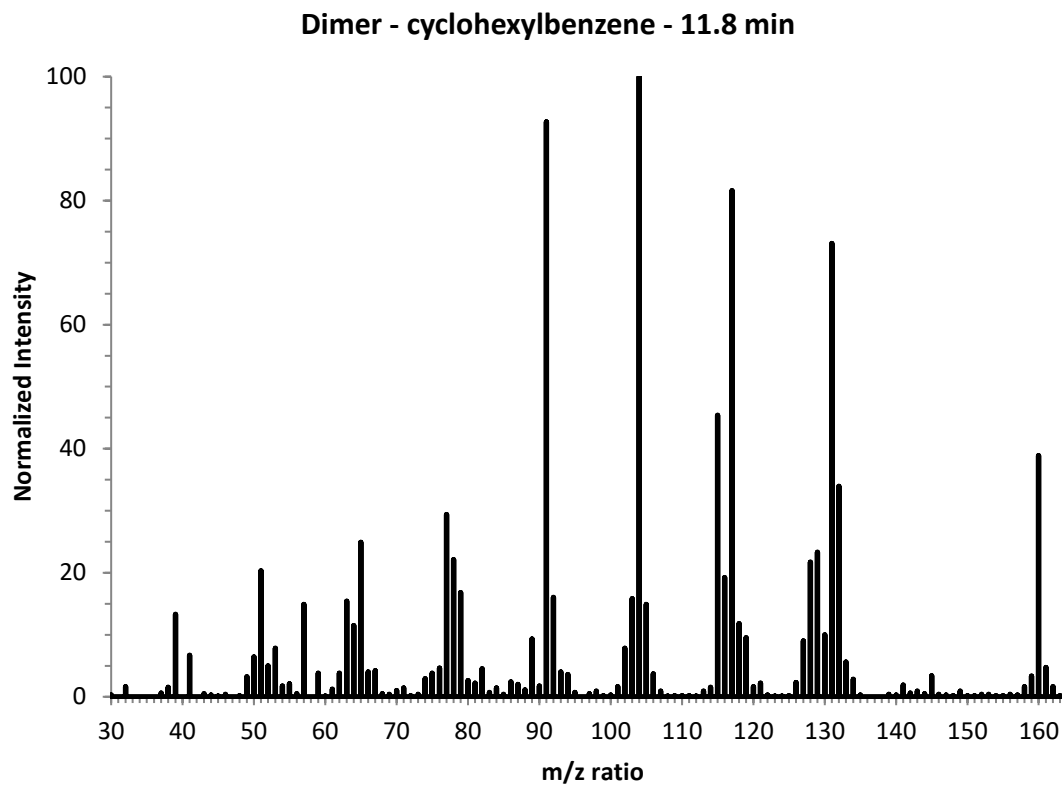


Figure 101. Mass spectrum of cyclohexylbenzene, the result of EAS between benzene and cyclohexene in the reaction of *cis*-1,4-cyclohexanediol.

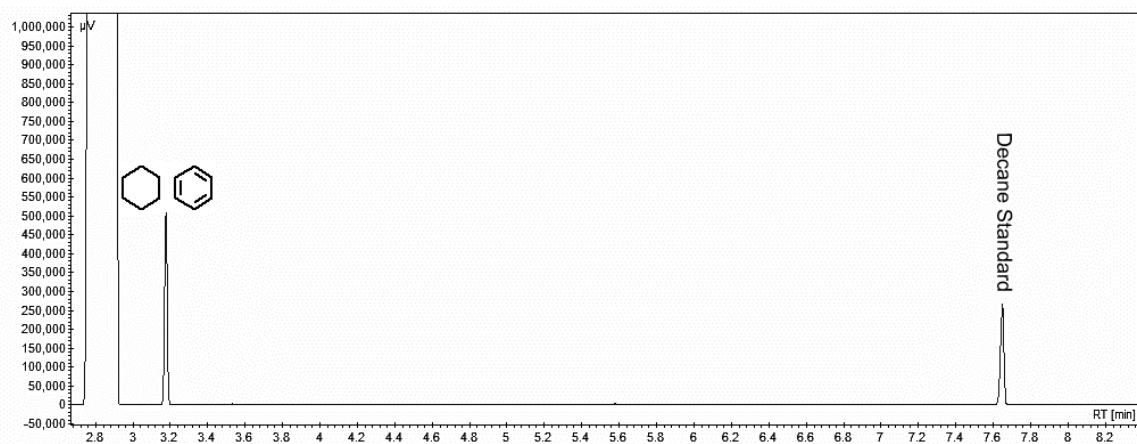


Figure 102. *Cis*-1,4-cyclohexanediol 24h Ni+Fe (250°C)

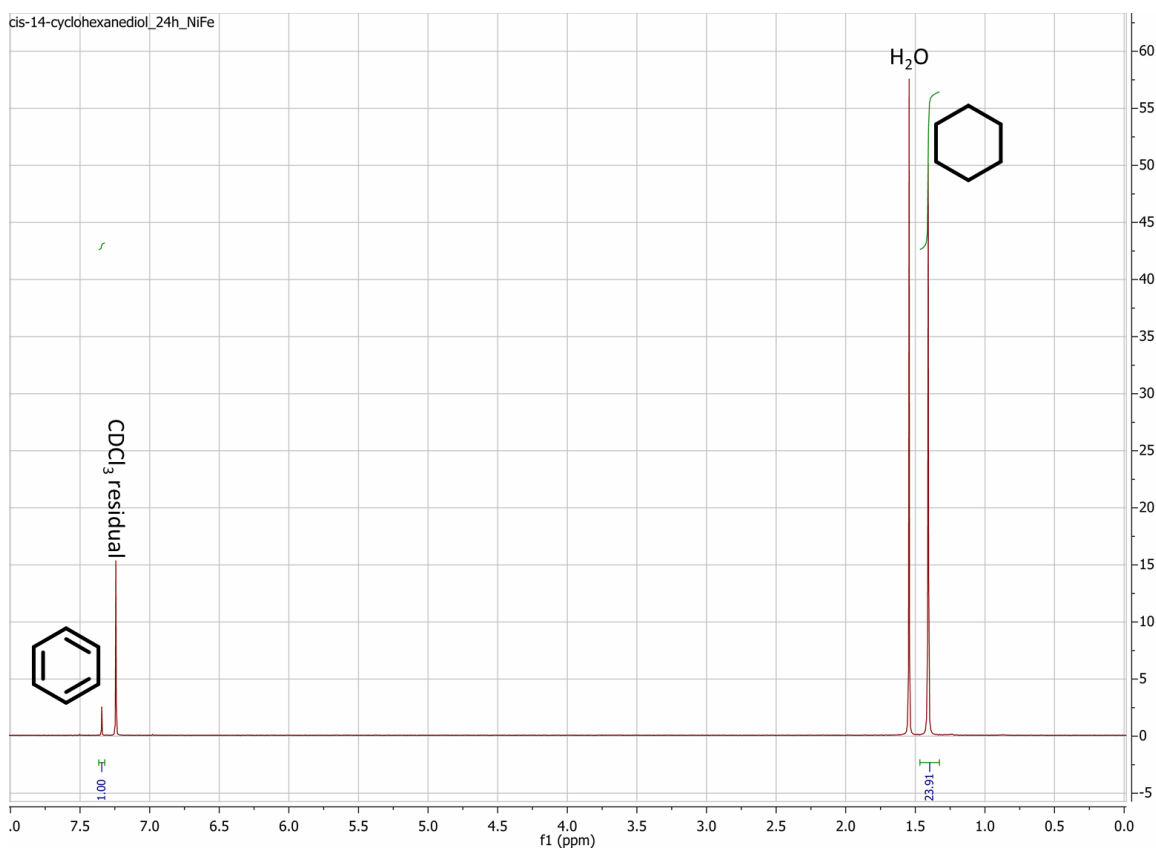


Figure 103. <sup>1</sup>H NMR spectrum of the *cis*-1,4-cyclohexanediol reaction mixture, in CDCl<sub>3</sub>. (24h, 250°C, Ni+Fe)

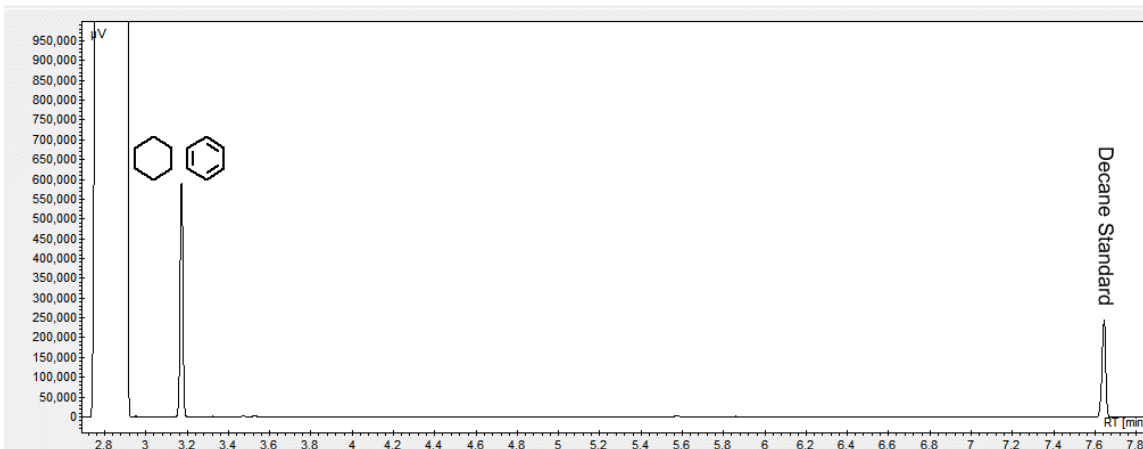


Figure 104. *Trans*-1,4-cyclohexanediol 24h Ni+Fe (250°C)

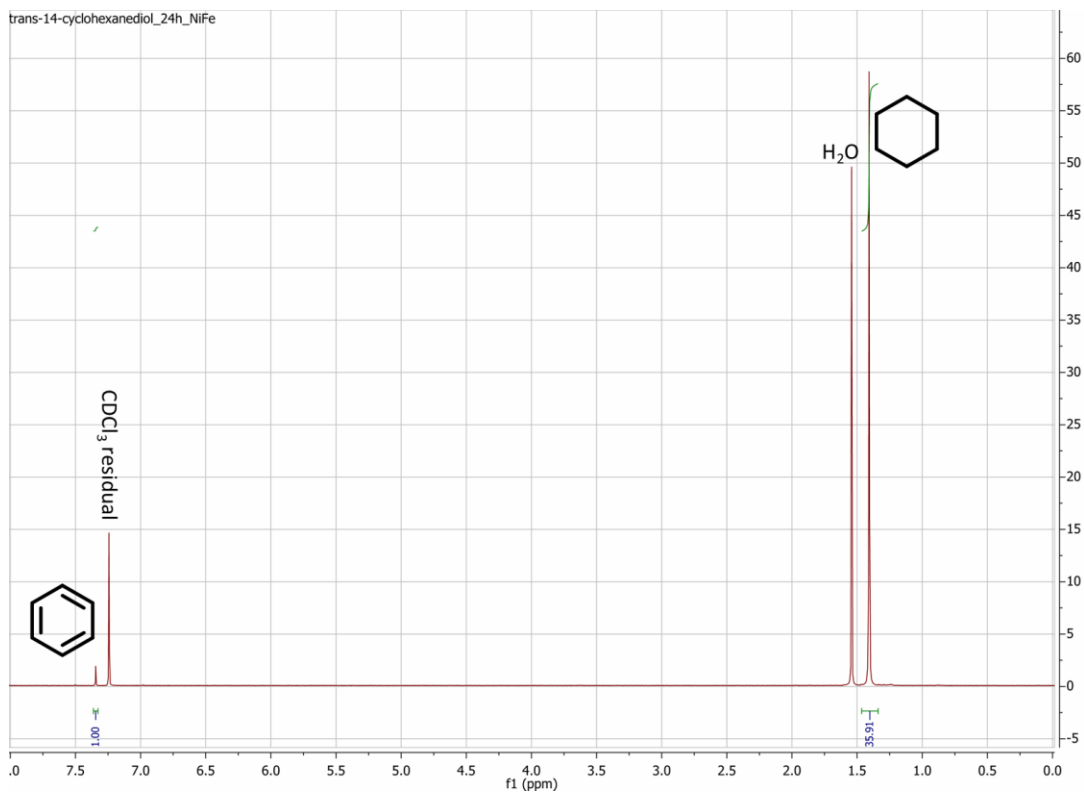


Figure 105. <sup>1</sup>H NMR spectrum of the *trans*-1,4-cyclohexanediol reaction mixture, in CDCl<sub>3</sub>. (24h, 250°C, Ni+Fe)



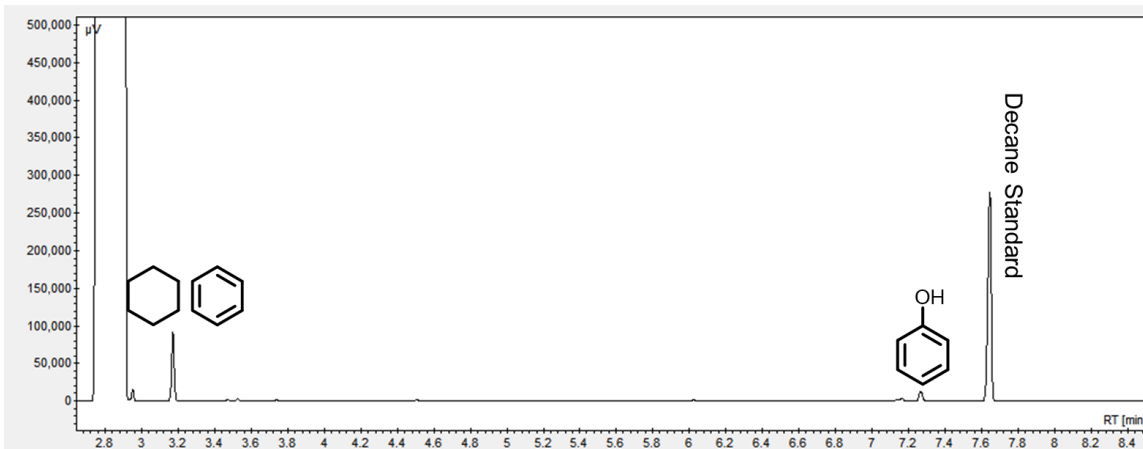


Figure 106. *Myo*-inositol 24h Ni+Fe (350°C)

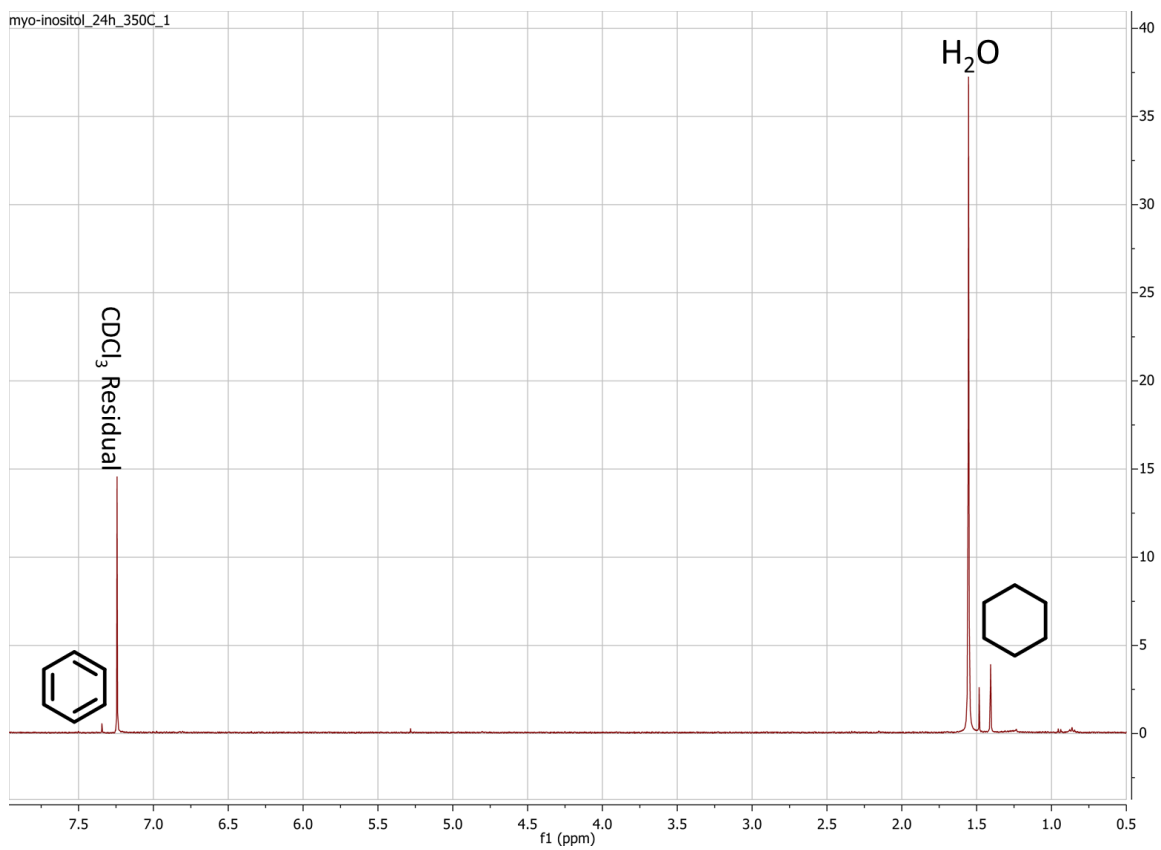


Figure 107.  $^1\text{H}$  NMR spectrum of the *myo*-inositol reaction mixture, in  $\text{CDCl}_3$ . (24h,  $350^\circ\text{C}$ , Ni+Fe)

APPENDIX C.  
DATA TABLES

Table 14. Cyclohexanol conversion at 250°C and 40 bar in water.

Time (h)	% Conversion
0.53	16
1	13
2	25
4.02	64
7.83	74
16	89
24.07	82
47.03	87

Table 15. Abundances of products with time starting with *cis*-4-*tBu*-cyclohexanol at 250°C and 40 bar in water.

Time (h)	Mol% <i>cis</i> -4- <i>tbu</i> -cyclohexanol	Mol% <i>trans</i> -4- <i>tbu</i> -cyclohexanol	Mol% <i>trans</i> -3- <i>tbu</i> -cyclohexanol	Mol% <i>cis</i> -3- <i>tbu</i> -cyclohexanol	Mol% 4- <i>tbu</i> -cyclohexene	Mol% 3- <i>tbu</i> -cyclohexene
0.5	97.7	0.4	0.0	0.0	1.8	0.04
1	90.3	1.3	0.5	0.0	7.3	0.7
2	92.2	1.1	0.4	0.0	5.7	0.5
2	93.0	1.0	0.3	0.0	5.2	0.5
3	47.3	4.5	2.4	0.0	40.9	4.8
4	42.7	4.7	2.5	0.0	44.8	5.2
8	31.6	5.5	3.2	0.0	52.5	7.1
24	5.5	5.0	3.4	1.1	72.4	12.4
48	0.9	3.6	0.8	3.0	76.4	17.4
96	0.7	2.7	2.6	0.7	74.0	23.2

Table 16. Abundances of products with time starting with *trans*-4-*t*Bu-cyclohexanol at 250°C and 40 bar in water.

Time (h)	Mol% cis-4-tbu-cyclohexanol	Mol% trans-4-tbu-cyclohexanol	Mol% trans-3-tbu-cyclohexanol	Mol% cis-3-tbu-cyclohexanol	Mol% 4-tbu-cyclohexene	Mol% 3-tbu-cyclohexene
1	2.4	96.9	0.0	0.0	0.6	0.1
2	1.5	98.0	0.0	0.0	0.5	0.1
3	1.6	96.1	0.0	0.0	2.0	0.3
6	2.5	85.2	0.0	0.8	9.8	1.6
8	1.9	27.9	2.6	1.3	46.1	13.6
16	1.6	22.3	1.3	1.0	58.5	15.0
24	2.4	45.1	1.1	2.0	41.0	8.3
30	1.5	20.6	1.2	2.9	56.4	16.9
40	1.9	43.3	1.2	1.8	43.2	8.6
54	0.4	1.2	0.6	1.9	61.2	33.7
72	0.5	2.6	0.7	2.4	59.3	27.3

Table 17. Conversion of benzene to cyclohexane with time at 250°C and 40 bar in the presence of nickel and iron. Measured by NMR, as a ratio of the benzene and cyclohexane signals, normalized to the number of protons. No other products were detected.

Time (hours)	Mol% Cyclohexane
0	0
24	41.3
120	68.8
168	99.8
216	92.0
360	99.7

Table 18. Abundances of products from starting with diphenylacetylene at 250°C and 40 bar in the presence of nickel and iron.

Time (min)	Mol% DPA	Mol% Cis Stilbene	Mol% Trans Stilbene	Mol% Bibenzyl
0	100	0	0	0
5	87.2	4.7	1.1	6.7
15	53.7	22.9	3.2	19.8
23	45.8	14.3	2.2	36.2
30	1.7	16.9	3.6	74.3
60	0.1	4.3	1.4	91.9

Table 19. Abundances of styrene with time, 250°C and 40 bar in the presence of nickel and iron.

Time (min)	Mol% styrene
0	100
2	42.2
5	9.3
10	1.8
30	1.6

Table 20. Abundances of 4-OCH<sub>3</sub>-styrene with time, 250°C and 40 bar in the presence of nickel and iron.

Time (min)	Mol% 4-OCH <sub>3</sub> -styrene
0	100
1	47.4
3	9.3
5	4.3
15	10.5
35	1.0

Table 21. Abundances of 3-CF<sub>3</sub>-styrene with time, 250°C and 40 bar in the presence of nickel and iron.

Time (min)	Mol% 3-CF <sub>3</sub> -styrene
0	100
1	49.8
3	21.4
5	15.2
5	14.8
10	3.2
15	11.1
20	7.2
30	7.3

Table 22. Abundances of products from cyclohexanone with time, 250°C and 40 bar in the presence of nickel and iron.

Time (h)	Mol% Cyclohexanone	Mol% Cyclohexanol	Mol% Cyclohexene	Mol% Cyclohexane
0	100	0	0	0
1	84.5	11.3	0.1	0.6
4.1	36.7	45.7	6.8	9.9
7	35.4	46.7	4.5	13.5
8	44.7	24.0	5.3	19.2
14.6	30.4	27.9	7.5	30.1
15.2	38.8	17.3	10.2	31.1
24.1	31.3	13.6	7.7	45.4
48.5	14.2	17.2	7.6	58.9
94	1.5	0.4	0.9	96.2

Table 23. Abundances of products from cyclohexanone with time, 250°C and 40 bar in the presence of Cu-Zn and iron.

Time (h)	Mol% Cyclohexanone	Mol% Cyclohexanol	Mol% Cyclohexene	Mol% Cyclohexane
0	100	0	0	0
1	24.8	73.9	1.0	0.4
4	12.8	85.6	1.0	0.6
9.5	12.7	77.0	7.5	2.8
17.2	4.9	48.0	32.9	14.2
23.5	0.2	12.9	34.1	52.9
46.5	0.4	11.4	42.9	45.3
124.4	0.0	0.4	0.8	98.7

Table 24. Abundances of products from octanoic acid with time, 250°C and 40 bar in the presence of nickel and iron.

Time (h)	Mol% octanoic acid	Mol% octanol	Mol% octane	Mol% heptane
0	100	0	0	0
8	83.8	15.6	0.2	0.1
15.2	40.5	53.7	0.8	2.1
20	36.0	56.6	0.6	4.6
24	22.5	48.0	1.1	27.0
24	24.5	49.4	1.1	22.5
48.1	28.3	14.3	1.2	54.6
71.7	4.4	5.9	2.1	87.0
164.3	6.5	10.2	3.3	79.6
192	0.2	0.2	4.5	94.7

Table 25. Abundances of products from octanoic acid with time, 250°C and 40 bar in the presence of Cu-Zn and iron.

Time (h)	Mol% octanoic acid	Mol% octanol	Mol% octyl octanoate
0	100	0	0
0.5	99.2	0.8	0
4	76.4	18.7	4.9
16.8	34.3	62.8	2.9
47.9	9.5	89.8	0.7

Table 26. Abundances of products from acetophenone with time, 250°C and 40 bar in the presence of nickel and iron.

Time (h)	Mol% acetophenone	Mol% 1-phenylethanol	Mol% styrene	Mol% ethylbenzene
0	100	0	0	0
4	44.9	2.2	0.2	50.1
9.1	21.2	2.1	0.1	73.5
16.4	17.8	0.4	0.1	80.9
26.1	0.1	0	0	96.5



Table 27. Abundances of products from 4-OCH<sub>3</sub>-acetophenone with time, 250°C and 40 bar in the presence of nickel and iron.

Time (h)	Mol% 4-OCH <sub>3</sub> -acetophenone	Mol% (4-OCH <sub>3</sub> )-1-phenylethanol	Mol% 4-OCH <sub>3</sub> -styrene	Mol% 4-OCH <sub>3</sub> -ethylbenzene
0	100	0	0	0
4	56.8	0.1	0.4	42.8
7	53.5	0.2	0.8	45.5
18.1	24.3	0	3.2	72.5
24.3	12.1	0	5.9	82.0

Table 28. Abundances of products from 3-CF<sub>3</sub>-acetophenone with time, 250°C and 40 bar in the presence of nickel and iron.

Time (h)	Mol% 3-CF <sub>3</sub> -acetophenone	Mol% (3-CF <sub>3</sub> )-1-phenylethanol	Mol% 3-CF <sub>3</sub> -styrene	Mol% 3-CF <sub>3</sub> -ethylbenzene
0	100	0	0	0
4	62	28	0.3	10
8.3	34	30	0.4	35
16.4	4	24	0.1	72
24.1	0.83	3	0	96

Table 29. Abundances of products from 3,5-di-CF<sub>3</sub>-acetophenone with time, 250°C and 40 bar in the presence of nickel and iron.

Time (h)	Mol% 3,5-di-CF <sub>3</sub> -acetophenone	Mol% (3,5-di-CF <sub>3</sub> )-1-phenylethanol	Mol% 3,5-di-CF <sub>3</sub> -styrene	Mol% 3,5-di-CF <sub>3</sub> -ethylbenzene
0	100	0	0	0
4	49.5	49.9	0.0	0.6
8	44.2	54.3	0.3	1.2
24	6.5	78.7	0.7	14.0

Table 30. Abundances of products from the dehydration of *cis*-1,2-cyclohexanediol with time, 250°C and 40 bar in water.

Time (h)	Mol% <i>Cis</i> -1,2-cyclohexanediol	Mol% Cyclohexanone	Mol% Cyclopentylformaldehyde
0	100	0	0
1	89.3	9.2	1.4
4	54.0	38.8	6.5
5	20.6	66.9	10.8
8	2.0	81.6	12.7
24	0.3	84.3	11.8

Table 31. Abundances of products from the dehydration of *trans*-1,2-cyclohexanediol with time, 250°C and 40 bar in water.

Time (h)	Mol% <i>Trans</i> -1,2-cyclohexanediol	Mol% Cyclohexanone	Mol% Cyclopentylformaldehyde
0	100	0	0
72	94.9	0.6	4.1
126	93.1	0.6	4.2
138	92.4	0.6	5.5
263	76.5	2.0	18.1
480	70.5	2.3	14.1

Table 32. Abundances of products from the disproportionation of *trans*-1,2-cyclohexanediol and cyclopentylformaldehyde with time, 250°C and 40 bar in water.

Time (h)	Mol% Cyclopentanemethanol	Mol% 2-hydroxycyclohexanone	Mol% Cyclopentyl-CO <sub>2</sub> H
0	0	0	0
72	0.2	0	0
126	1.2	0.9	0
138	0.6	0.7	0
263	1.0	1.4	0
480	5.2	5.2	0.1

Table 33. Abundances of *cis*-1,2-cyclohexanediol and cyclohexane/benzene in the presence of nickel and iron, 250°C and 40 bar. Cyclohexane and benzene elute together on the GC, but benzene was only measured at the 72h timepoint.

Time (h)	Mol% <i>cis</i> -1,2-cyclohexanediol	Mol% cyclohexane/benzene
0	100	0
1	83.1	1.1
2	79.8	2.8
4	69.6	4.1
8	59.0	15.2
16	61.0	17.7
24	40.3	29.9
48	16.7	72.8
72	3.3	91.4
96	1.4	88.3

Table 34. Abundances of minor products from the reduction of *cis*-1,2-cyclohexanediol with time, in the presence of nickel and iron, 250°C and 40 bar.

Time (h)	mol% cyclopentane-MeOH	Mol% cyclohexanone	Mol% cyclohexanol	Mol% 2-hydroxy cyclohexanone	Mol% phenol	Mol% Me-cyclopentane
0	0	0	0	0	0	0
1	0.1	2.3	2.4	9.7	1.3	0
2	0.5	2.5	3.3	10.3	0.9	0
4	0.7	3.7	5.3	14.2	2.4	0
8	2.3	6.4	7.8	4.3	3.6	0
16	3.4	3.8	8.6	2.6	1.6	0
24	5.9	7.3	8.4	2.2	2.0	0
48	6.8	0	1.6	0.1	0.9	0.9
72	6.4	0	0	0	1.1	1.9
96	5.0	0.1	0.3	0	0	4.8

Table 35. Summary of yields of cyclohexane and benzene from polyols reduced with nickel and iron.

Starting Material	Conditions	% Yield Cyclohexane	% Yield Benzene
cis-1,2-cyclohexanediol	72h, Ni+Fe, 250°C	83	16
trans-1,2-cyclohexanediol	70h, Ni+Fe, 250°C	59	5
cis-1,4-cyclohexanediol	24h, Ni+Fe 250°C	80	7
trans-1,4-cyclohexanediol	24h, Ni+Fe 250°C	85	5
myo-inositol	24h, Ni+Fe 350°C	23	5

Table 36. Mol% of  $^{13}\text{C}$  labeled methanol with time, measured by  $^{13}\text{C}$  NMR.

Time (h)	Mol% MeOH
0	100
7	54.5
22	60.5
49	17.2
91	5.7